IL
NUOVO CIMENTO
ORGANO DELLA SOCIETÀ ITALIANA DI FISICA
SOTTO GLI AUSPICI DEL CONSIGLIO NAZIONALE DELLE RICERCHE

VOL. IX, N. 10 *Serie nona* 1 Ottobre 1952

Étude de la composante molle du rayonnement cosmique au Pic du Midi.

G. BARONI, G. CORTINI
Istituto di Fisica dell'Università, Centro di Studio per la Fisica Nucleare del C.N.R. - Roma

A. MILONE, L. SCARSI
Istituto di Fisica dell'Università - Genova

G. VANDERHAEGHE (*)
Centre de Physique Nucléaire de l'Université - Bruxelles

(ricevuto il 19 Giugno 1952)

Resumé. — Cet article traite d'une étude de la composante molle du rayonnement cosmique au Pic du Midi (43° lat. N, 2860 m), faite au moyen de plaques photographiques sensibles au minimum d'ionisation. L'étude est basée sur l'examen systématique des traces isolées et des traces de paires d'électrons dans l'émulsion. Les spectres différentiels d'énergie des photons et des électrons sont établis par la mesure du scattering et normalisés suivant les intensités intégrales mesurées; ils sont confrontés avec les spectres calculés par RICHARDS et NORDHEIM suivant la théorie des cascades. L'accord est satisfaisant tant pour la forme des spectres que pour les rapports d'intensités. Les distributions angulaires trouvées pour la composante molle (photons + électrons) et pour la composante dure (mésons) coincident à peu près entre elles et peuvent être representées, en première approximation, par une loi de la forme $I(\theta)\,\mathrm{d}\Omega = I_v \cos^{3.5}\theta\,\mathrm{d}\Omega$.

(*) Chercheur qualifié du Fonds National Belge de la Recherche Scientifique.

1. – Introduction.

Les données sur les spectres d'énergie, les intensités et les distributions angulaires des électrons et des photons de la composante molle sont encore peu nombreuses. Ceci tient en grande partie aux difficultés rencontrées avec les techniques les plus utilisées jusqu'à présent (compteurs de Geiger et Müller, chambre à ionisation et chambre de Wilson), pour séparer les effets de la composante molle de ceux de la composante dure.

Le spectre différentiel d'énergie des électrons a été étudié au moyen de la chambre de Wilson par BLACKETT [1], WILLIAMS [2], GREISEN [3], LOMBARDO et HAZEN [4], au niveau de la mer, et par HAZEN [5], à 2 900 m. Il a aussi été étudié au moyen de la chambre à ionisation, à diverses altitudes, par BRIDGE et ROSSI [6].

La distribution angulaire et l'intensité des électrons ont été étudiées au moyen de compteurs montés en télescope, à différentes altitudes, notamment par GREISEN [7], AUGER et ses collaborateurs [8], COCCONI et TONGIORGI [9], SANDS [10] et BERNARDINI [11]. Une synthèse partielle des résultats obtenus par cette méthode a été faite par ROSSI [12] et par MONTGOMERY [13].

Quant aux études faites au moyen de compteurs sur les gerbes électrophotoniques, elles donnent des renseignements sur différents types de gerbes sélectionnés par divers arrangements de compteurs, mais ne fournissent généralement pas de données quantitatives valables pour l'ensemble de la composante molle.

Contrairement aux autres techniques, les plaques photographiques permettent, dans un certain domaine d'énergie, de discerner assez facilement les deux composantes, mais elles n'ont encore été que très peu utilisées pour

---

(1) P. M. S. BLACKETT: *Proc. Roy. Soc.*, A **165**, 11 (1938).
(2) E. J. WILLIAMS: *Proc. Roy .Soc.*, A **172**, 194 (1939).
(3) K. GREISEN: *Phys. Rev.*, **63**, 74 (1945).
(4) B. LOMBARDO et W. E. HAZEN: *Phys. Rev.*, **68**, 74 (1945).
(5) W. E. HAZEN: *Phys. Rev.*, **65**, 67 (1944).
(6) H. BRIDGE et B. ROSSI: *Phys. Rev.*, **71**, 379 (1947).
(7) K. GREISEN: *Phys. Rev.*, **61**, 212 (1942).
(8) P. AUGER, P. EHRENFEST Jr., A. FREON et A. FOURNIER: *Compt. Rend.*, **204**, 257 (1937).
(9) G. COCCONI et V. TONGIORGI: *Phys. Rev.*, **70**, 850 (1946).
(10) M. S. SANDS: *Phys. Rev.*, **73**, 1338 (1948).
(11) G. BERNARDINI: *Nature*, **129**, 518 (1932).
(12) B. ROSSI: *Rev. Mod. Phys.*, **20**, 537 (1948).
(13) D. J. X. MONTGOMERY: *Cosmic Ray Physics* (Princeton, 1949), p. 131.

l'étude de la composante molle. Notons seulements que le spectre différentiel d'énergie et la distribution angulaire des photons à 20 000 m ont été étudiés au moyen de plaques photographiques exposées en ballons sondes, par CARLSON, HOOPER et KING [14].

Dans le présent travail, nous étudions les spectres différentiels d'énergie, les intensités et les distributions angulaires des photons et des électrons à 2 860 m. Les données relatives aux photons sont obtenues par l'examen des paires d'électrons créees dans l'émulsion; les données relatives aux électrons sont obtenues par l'examen des traces isolées.

2. – Méthode expérimentale.

Des plaques Ilford G 5 de 400 microns d'épaisseur ont été exposées verticalement, pendant 15 jours, au Pic du Midi (43° lat. N, 2 860 m). Elles étaient placées sous un toit de protection léger représentant, avec la couche de neige qui le recouvrait, environ une demi-unité de radiation. Les plaques ont été développées suivant la méthode à variations de température établie par DILWORTH et al. [15,16].

Examen des paires d'électrons. – Un volume total de 36 mm^3 d'émulsion a été exploré systématiquement pour y trouver les paires d'électrons créées par les photons. Les paires ont été repérées de différentes manières (notamment par rapport à un réseau quadrillé de 100 microns d'intervalle, gravé au diamant sur une lamelle couvre-objet fixée sur la plaque).

Les paires ne sont pas toutes également faciles à observer, pour différentes raisons. En premier lieu, une paire est d'autant plus difficile à observer que ses branches sont plus inclinées par rapport au plan de la plaque. La perte qui en résulte peut être déterminée par des considérations géométriques sur lesquelles nous reviendrons plus loin.

En second lieu, une paire est d'autant plus facile à observer que ses branches sont voisines l'une de l'autre sur un plus long parcours, ce qui nécessite que l'angle entre les deux branches soit initialement petit et que les deux branches ne subissent pas un trop grand scattering. Ces deux conditions sont d'autant mieux remplies que l'énergie du photon incident est plus élévée. Il en résulte qu'on perd plus facilement les paires de basse énergie. Pour mettre cette perte en évidence, certaines portions d'émulsions ont été explorées deux fois, par des observateurs différents. L'analyse de leurs résultats permet de tirer les conclusions suivantes:

---

[14] A. CARLSON, J. HOOPER et D. KING: *Phil. Mag.*, **41**, 701 (1950).

[15] C. DILWORTH, G. OCCHIALINI et R. PAYNE: *Nature*, **162**, 102 (1948).

[16] C. DILWORTH, G. OCCHIALINI et L. VERMAESEN: *Bull. Centre Phys. Nucl. de l'Univ. Libre de Bruxelles*, n. 13 (1950).

a) Un certain nombre de paires notées comme « paires douteuses » par les observateurs, ont été écartées d'office. Les branches de ces paires sont des électrons d'énergie inférieure à 2,5 MeV et il se peut qu'il ne s'agisse en réalité que d'un seul électron subissant un scattering simple à grand angle.

b) Aux énergies inférieures à 50 MeV, le pourcentage de perte augmente rapidement lorsque l'énergie décroit; la perte totale peut dépasser 20%.

c) Aux énergies supérieures à 50 MeV, la perte totale ne dépasse pas 10% et le pourcentage de perte est pratiquemment indépendant de l'énergie. En nous basant sur cette dernière conclusion, nous avons procédé à quelques explorations rapides en vue de préciser la distribution des paires aux grandes énergies.

En troisième lieu, on constate dans certaines plaques une perte sensible près de la surface, Pour cette raison, nous avons fait abstraction dans toutes les plaques d'une couche superficielle de 50 microns d'épaisseur. Le volume utile d'émulsion exploré, calculé en considérant seulement une épaisseur de 350 microns, a donc été ramené à 31,5 mm³.

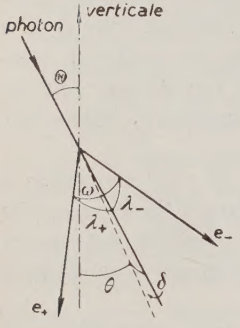

Fig. 1.

Pour chaque branche de paire, nous avons mesuré l'angle d'inclinaison par rapport au plan de la plaque et l'angle entre sa projection sur le plan de la plaque et la direction correspondant à la verticale durant l'exposition. Nous en avons déduit graphiquement l'angle d'ouverture ω de chaque paire et l'angle θ entre la bissectrice de cet angle et la direction de la verticale (fig. 1).

La distribution angulaire des photons incidents doit différer peu de la distribution angulaire des bissectrices des paires. En effet, suivant BETHE ([17]), la distribution des angles d'émission λ_+ et λ_- des électrons par rapport à la direction du photon incident obéit approximativement à la loi de probabilité suivante

$$p(\lambda)\,\mathrm{d}\lambda = \frac{2\lambda_0\lambda\,\mathrm{d}\lambda}{(\lambda_0^2+\lambda^2)^2},$$

expression dans laquelle $\lambda_0 = m_0c^2/(m_0c^2 + E)$, m_0c^2 étant l'énergie propre de l'électron et E son énergie cinétique. La médiane et les quartiles inférieur et supérieur de cette distribution valent respectivement: λ_0, $\lambda_0/\sqrt{3}$ et $\lambda_0\cdot\sqrt{3}$. Il en résulte qu'aux énergies que nous considérons ($E > 2{,}5$ MeV; $\lambda_0 < 10°$) les angles λ_+ et λ_- sont généralement petits de même que l'angle δ entre la bissectrice de l'angle d'ouverture ω et la direction du photon incident. Dans

([17]) H. A. BETHE: *Proc. Cambr. Phil. Soc.*, **30**, 524 (1934).

ces conditions, l'angle θ est généralement assez voisin de l'angle zénithal Θ du photon incident (fig. 1).

Nous avons déterminé l'énergie cinétique des électrons par la mesure de leur scattering multiple, suivant la méthode angulaire établie par GOLDSCHMIDT [18]. Nous avons effectué cette mesure sur toutes les traces inclinées de moins que 30° par rapport au plan de la plaque, en adoptant une cellule de mesure de 50 ou de 100 microns selon l'énergie et en nous limitant à 22 cellules au maximum. Le tableau I indique les marges d'erreur probable sur l'énergie dans ces conditions.

TABLEAU I.

Energie (MeV)	Erreur probable
$6 \leqslant E < 100$	de 17 à 21 %
$100 \leqslant E < 500$	de 17 à 39 %

Nous avons mesuré la distorsion des émulsions à 10% près, par la méthode de COSYNS et VANDERHAEGHE [19], et nous avons corrigé les mesures de scattering en conséquence.

Examen des traces isolées. – Pour l'examen des traces isolées, nous avons utilisé des plaques bien développées dans toute leur épaisseur. Dans chaque plaque, la région à explorer a été recouverte d'une lamelle couvre-objet sur laquelle est gravé un réseau quadrillé de 100 microns d'intervalle. Nous avons noté toutes les traces isolées traversant latéralement, de part en part, des cylindres d'émulsion d'axes perpendiculaires au plan de la plaque, engendrés par des champs circulaires repérés par rapport au réseau de la lamelle couvre-objet. Le diamètre de ces champs (~ 40 μ) a été choisi de manière à ce qu'il y ait, en moyenne, entre 5 et 10 traces par cylindre.

Nous avons mesuré d'abord l'angle d'inclinaison φ de chaque trace notée (fig. 2) et nous n'avons retenu pour les mesures de scattering que les traces d'inclinaison inférieure à 24°. Nous avons ensuite mesuré l'angle α entre la projection de la trace sur le plan de la plaque et la direction correspondant à la verticale durant l'exposition. A partir des angles α et φ nous avons déduit graphiquement l'angle zénithal θ de la trace.

Nous avons mesuré le scattering des traces retenues suivant la même méthode que celle suivie pour les paires d'électrons, sauf pour les traces ayant

---

[18] Y. GOLDSCHMIDT: *Nuovo Cimento*, **7**, 331 (1950).

[19] M. COSYNS et G. VANDERHAEGHE: *Bull. Centre Phys. Nucl. de l'Univ. Libre de Bruxelles*, n. 15 (1950).

un angle moyen de scattering par 100 microns inférieur à 0°,20 pour lesquelles nous n'avons mesuré que 6 cellules. Dans ce cas, en calculant l'angle moyen de scattering d'après les angles entre cellules successives, l'erreur probable sur l'énergie est de l'ordre de 30%.

Indiquons ici que les traces d'ionisation minimum ou voisine du minimum comprennent environ 30% d'électrons d'énergie comprise entre 6 et 70 MeV, et 70% de particules de trop grande énergie pour pouvoir être identifiées par leur scattering, comprenant vraisemblablement encore environ 20% de électrons et 50% de mésons. Les traces d'ionisation supérieure à 1,5 fois le minimum, comprenant des mésons et des protons lents, constituent moins que 5% du total des traces.

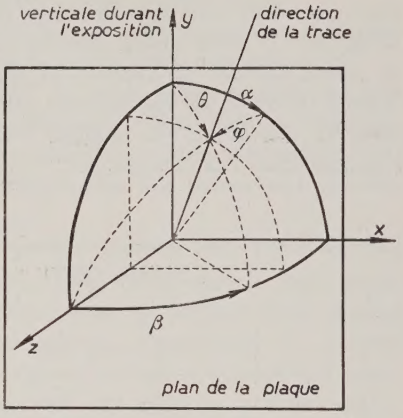

Fig. 2.

3. – Spectre différéntiel d'énergie et intensité des photons.

Au total, 213 paires d'électrons ont été trouvées dans le volume utile d'émulsion exploré systématiquement. Par la mesure du scattering des deux branches, nous avons déterminé l'énergie totale de 140 de ces paires. Nous avons en outre déterminé l'énergie de 37 paires d'énergie supérieure à 50 MeV, trouvées au cours des explorations rapides dont nous avons parlé précédemment (cfr. n. 2). Les 2^e et 3^e colonnes du tableau II donnent les distributions des paires dans les intervalles d'énergie totale indiqués dans la 1ère colonne ($K = E_1 + E_2 + 2m_0c^2$). La 4^e colonne donne la distribution générale obtenue de la manière suivante: aux énergies supérieures à 50 MeV, on a additionné dans chaque intervalle les nombres de paires des 2^e et 3^e colonnes; aux énergies inférieures à 50 MeV, on a multiplié les nombres de paires de la 2^e colonne par le rapport du nombre total de paires d'énergie supérieure à 50 MeV des 2^e et 3^e colonnes au nombre de paires d'énergie supérieure à 50 MeV de la 2^e colonne seulement. La 5^e colonne donne les valeurs moyennes de la fonction de la distribution d'énergie des paires, soit $s(K)$, obtenues en faisant les rapports entre les nombres de paires de la 4^e colonne et la largeur des intervalles d'énergie indiqués dans la 1ère colonne. La fonction de distribution d'énergie normalisée, soit $S(K)$ s'obtient à partir de la fonction $s(K)$ en imposant la condition que l'intégrale $\int_6^\infty S(K)\,dK$ soit égale au nombre total de paires

d'énergie supérieure à 6 MeV créées par cm³ d'émulsion; ce qui donne

$$S(K) = \frac{N_p C_p}{V \int_6^\infty s(K)\,\mathrm{d}K}\, s(K) \text{ cm}^{-3}\,\text{MeV}^{-1}. \tag{1}$$

Tableau II. – $\sigma_0 = 2{,}6 \cdot 10^{-25}$ cm².

K (MeV)	Nombre de paires		Distrib. générale	$s(K)$	$\sigma(K)/\sigma_0$	$q(K)$ (10^{-4} cm^{-2} s^{-1} MeV^{-1})
	expl. complètes	expl. rapides				
6– 10	5	—	7	1,75	3,3	8,70
10– 20	15	—	21	2,10	4,9	7,05
20– 30	20	—	28	2,80	6,2	7,40
30– 50	25	—	35	1,75	7,5	3,85
50– 70	16	9	25	1,25	8,5	2,40
70–100	22	7	29	0,97	9,3	1,70
100–150	16	5	21	0,42	10,1	0,68
150–200	8	3	11	0,22	10,8	0,33
200–400	11	5	16	0,08	11,6	0,11
> 400	2	1	3	—	12,5	—

Dans cette expression, N_p est le nombre total de paires trouvées, soit 213, V est le volume exploré, soit $3{,}15 \cdot 10^{-2}$ cm³, et C_p est un facteur de correction géométrique tenant compte de la perte de paires de grande inclinaison. Pour évaluer ce facteur, nous avons distribué les paires suivant l'angle θ entre leur bissectrice et la verticale, dans des intervalles correspondant à des angles solides égaux. Nous avons compté dans chaque intervalle le nombre de paires dont la bissectrice est inclinée de moins que 30° par rapport au plan de la plaque (pour lesquelles la perte est négligeable) et nous avons multiplié ce nombre par le rapport entre l'angle solide correspondant à l'intervalle entier et la partie de cet angle solide limitée aux angles inferieurs à 30°. En additionnant les nombres ainsi calculés, nous avons obtenu un nombre total de 265 paires au lieu des 213 paires effectivement trouvées. Le facteur C_p vaut donc $265/213 = 1{,}24$. Cette manière de faire la correction est justifiée du fait qu'il n'y a pas de corrélation appréciable entre l'angle θ et l'énergie des paires, comme l'indique le tableau III. Celui-ci donne les valeurs de l'angle médian $\bar{\theta}$ de la distribution angulaire des bissectrices des paires d'énergie comprise dans différents intervalles. On voit, en effet, que ces valeurs sont concordantes dans les limites des erreurs statistiques.

Tableau III.

$\overline{K}$ (MeV)	5 – 50	50 – 100	100 – 200	> 200
$\overline{\theta}$ (degrés)	22 ± 2	19 ± 3	22 ± 4	20 ± 5

De la distribution d'énergie des paires, on peut remonter au spectre différentiel d'énergie des photons. Soit $q(K)\,\mathrm{d}(K)$ le flux omnidirectionnel des photons d'énergie comprise entre K et $K+\mathrm{d}K$. La fonction de distribution d'énergie normalisée des photons, $q(K)$, peut être retrouvée à partir de la fonction de distribution d'énergie normalisée des paires, $S(K)$. En effet, soit n_i le nombre d'atomes par cm³ d'émulsion de l'élément de nombre atomique Z_i et soit $\sigma_i(K)$ la section efficace de création d'une paire dans cet élément par un photon d'énergie K. La section efficace moyenne de matérialisation des photons d'énergie K dans l'émulsion vaut alors

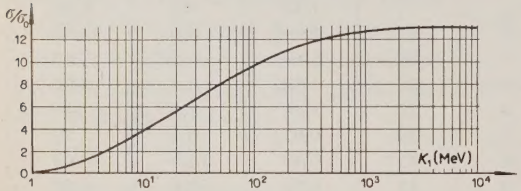

Fig. 3. – Section efficace moyenne de l'émulsion Ilford G 5 pour la matérialisation des photons en fonction de l'énergie. $\sigma_0 = 2{,}6\cdot10^{-25}$ cm².

$$(2)\qquad \sigma(K) = \frac{\sum_i \sigma_i n_i(K)}{\sum_i n_i}\ \mathrm{cm}^2\,,$$

la somme étant étendue à tous les éléments contenus dans l'émulsion. La fig. 3, établie d'après la théorie de Bethe et Heitler ([20]), représente la variation de cette section efficace en fonction de l'énergie.

Les fonctions $S(K)$et $q(K)$ sont liées par la relation suivante

$$(3)\qquad S(K) = T\sigma(K)q(K)\sum_i n_i\ \ \mathrm{cm}^{-3}\ \mathrm{MeV}^{-1}\,,$$

dans laquelle T est le temps d'exposition des plaques, soit $1{,}2\cdot10^6$ s, et $\sum_i n_i$ le nombre total d'atomes par cm³ d'émulsion, soit $83{,}6\cdot10^{21}$. Utilisant la relation (1), nous obtenons finalement la fonction de distribution d'énergie normalisée des photons

$$(4)\qquad q(K) = \frac{N_p C_p}{VT\sum_i n_i \int_6^\infty s(K)\,\mathrm{d}K}\,\frac{s(K)}{\sigma(K)}\ \mathrm{cm}^{-2}\ \mathrm{s}^{-1}\ \mathrm{MeV}^{-1}\,.$$

([20]) W. Heitler: *The Quantum theory of radiation* (Oxford, 1944).

La dernière colonne du tableau II donne les valeurs moyennes de cette fonction dans les intervalles d'énergie indiqués dans la 1ère colonne. La distribution d'énergie des photons ainsi déterminée est représentée par l'histogramme A de la figure 4, établi en coordonnées logarithmiques.

A partir de $q(K)$, on obtient immédiatement l'intensité intégrale des photons d'énergie supérieure à K'

$$(5) \qquad Q_{K'}^{\infty} = \int_{K'}^{\infty} q(K)\,\mathrm{d}K \quad \mathrm{cm^{-2}\,s^{-1}}.$$

Notons la valeur correspondante à $K' = 50$ MeV, qui n'est pas influencée par la perte de paires de basse énergie

$$(6) \quad Q_{50}^{\infty} = \\ = (1{,}76 \pm 0{,}12)\cdot 10^{-2} \ \mathrm{cm^{-2}\,s^{-1}}.$$

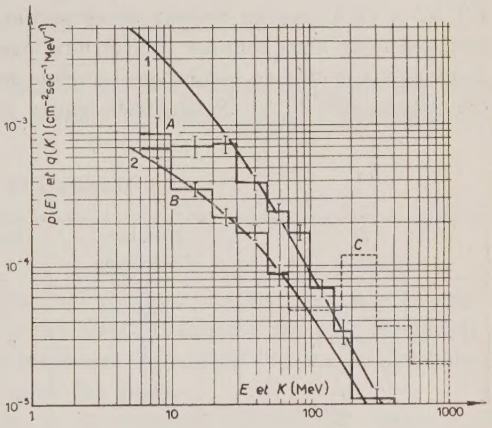

Fig. 4. – Distributions expérimentales des photons (A), des électrons (B) et des particules de grande énergie (C). Spectres différentiels théoriques des photons (1) et des électrons (2), selon Richards et Nordheim.

4. – Spectre différentiel d'énergie et intensité des électrons.

Pour l'étude des traces isolées, 80 cylindres d'émulsion (cfr. n. 2) ont été explorés. Par la mesure du scattering, nous avons identifié 129 électrons d'énergie comprise entre 6 et 70 MeV. La 2e colonne du tableau IV donne la distribution d'énergie de ces électrons, dans les intervalles d'énergie indiqués dans la 1ère colonne. La 3e colonne donne les valeurs moyennes de la fonction de distribution d'énergie des électrons, soit $r(E)$, obtenues en faisant les rapports entre les nombre d'électrons de la 2e colonne et la largeur des intervalles d'énergie indiqués dans la 1ère colonne.

Soit $p(E)\,\mathrm{d}E$ le flux omnidirectionnel des électrons d'énergie comprise entre E et $E + \mathrm{d}E$. La fonction de distribution d'énergie normalisée des électrons, $p(E)$, s'obtient à partir de la fonction $r(E)$ en imposant la condition que l'integrale $\int_6^{70} p(E)\,\mathrm{d}E$ soit égale à l'intensité intégrale des électrons d'énergie comprise entre 6 et 70 MeV; ce qui donne

$$(7) \qquad p(E) = \frac{N_e C_e}{nAT \int_6^{70} r(E)\,\mathrm{d}E}\, r(E) \ \mathrm{cm^{-2}\,s^{-1}\,MeV^{-1}}.$$

Dans cette expression, N_e est le nombre d'électrons observés, soit 129, n est le nombre de cylindres explorés, soit 80, A est la section méridienne des cylindres, soit $1{,}52 \cdot 10^{-4}$ cm^2, T est le temps d'exposition des plaques, soit $1{,}2 \cdot 10^6$ s, et C_e est un facteur de correction géométrique tenant compte du fait que nous nous sommes limités aux traces d'inclinaision inférieure à 24°. Nous avons évalué ce facteur de la même manière que dans le cas des paires d'électrons (cfr. n. 3). Nous avons trouvé $C_e = 1{,}52$. (Remarquons qu'en réalité la section utile des cylindres d'émulsion explorés varie avec l'angle d'inclinaison. Mais comme le diamètre des cylindres vaut environ le dixième de leur hauteur, et comme nous nous sommes limités à des angles d'inclinaison inférieurs à 24°, on vérifie facilement que la correction qui en résulte est seulement de l'ordre de 1%, ce qui est négligeable devant les erreurs statistiques).

Tableau IV.

E (MeV)	Nombre d'électrons	$r(E)$	$p(E)$ (10^{-4} cm^{-2} s^{-1} MeV^{-1})
6 – 10	26	6,50	6,75
10 – 20	33	3,30	3,45
20 – 30	21	2,10	2,20
30 – 50	33	1,65	1,70
50 – 70	16	0,80	0,85

La dernière colonne du tableau IV donne les valeurs moyennes de la fonction $p(E)$ dans les intervalles d'énergie indiqués dans la 1ère colonne. La distribution d'énergie des électrons ainsi déterminée est représentée par l'histogramme B de la fig. 4, établi en coordonnées logarithmiques. Notons la valeur de l'intensité intégrale des électrons d'énergie comprise entre 6 et 70 MeV

$$(8) \qquad P_6^{70} = \int_6^{70} p(E)\,\mathrm{d}E = (1{,}34 \pm 0{,}08) \cdot 10^2 \ \text{cm}^{-2}\,\text{s}^{-1}.$$

Un calcul tout à fait analogue à celui qui vient d'être exposé pour les électrons d'énergie inférieure à 70 MeV à été fait pour les particules de grande énergie, comprenant essentiellement des électrons d'énergie supérieure à 70 MeV et des mésons d'énergie supérieure à 40 MeV. L'histogramme C (en pointillé) de la fig. 4 représente la distribution d'énergie normalisée obtenue en supposant que toutes ces traces correspondent à des électrons. On voit immédiatement qu'au dessus de 150 MeV une grande proportion de mésons doit intervenir, vu que rien ne justifierait une telle discontinuité dans le spectre des électrons.

L'intensité intégrale totale des particules de grande énergie, calculée d'après 264 traces notées, vaut

$$P_{70}^{\infty} + R_{40}^{\infty} = (3{,}55 \pm 0{,}15)\cdot 10^{-2} \text{ cm}^{-2}\,\text{s}^{-1}, \tag{9}$$

P_{70}^{∞} représentant l'intensité intégrale des électrons et R_{40}^{∞} celle des mésons (à l'altitude du Pic du Midi, la plupart de ceux-ci sont vraisemblablement des mésons μ).

5. – Confrontation avec la théorie.

Il est intéressant de confronter nos résultats sur les spectres d'énergie des électrons et des photons avec les résultats théoriques les plus récents et les plus complets, obtenus par RICHARDS et NORDHEIM [21] par la méthode des traces électroniques et photoniques des gerbes.

La *trace électronique* d'énergie E d'une gerbe, $f(E)\,\mathrm{d}E$, est définie comme étant la somme des parcours de tous les électrons de la gerbe dont l'énergie est comprise entre E et $E + \mathrm{d}E$. On définit de manière analogue la *trace photonique* d'énergie K de la gerbe, $g(K)\,\mathrm{d}K$. Les spectres des traces électroniques et photoniques d'une gerbe sont beaucoup plus faciles à calculer que les spectres d'énergie des électrons et des photons en fonction de la distance à l'origine de la gerbe; ils coïncident avec ces derniers au maximum de la gerbe et n'en diffèrent pas sensiblement sur la plus grande partie de son parcours après le maximum [22]. De plus, des calculs effectués par divers auteurs [21,23,24,25] montrent que si l'énergie E_p de la particule primaire de la gerbe est supérieure à trois fois l'énergie critique ($E_c \sim 86$ MeV dans l'air normal) les spectres des traces photoniques et électroniques ne dépendent pas sensiblement de E_p aux énergies petites devant E_p.

Les spectres d'énergie des électrons et des photons observés à une certaine altitude dans l'atmosphère résultent de la superposition des spectres de plusieurs gerbes, amorcées à des altitudes supérieures. Mais, d'après ce qui vient d'être rappelé, si à cette altitude la plupart des électrons et des photons appartiennent à des gerbes qui ne sont pas très au-delà de leur maximum et si

[21] J. A. RICHARDS et L. W. NORDHEIM: *Phys. Rev.*, **74**, 1106 (1948).
[22] B. ROSSI: *Lezioni sui Raggi Cosmici*, cap. V.
[23] I. TAMM et S. BELENKY: *Journ. Phys. U.R.S.S.*, **1**, 177 (1939).
[24] I. TAMM et S. BELENKY: *Phys. Rev.*, **70**, 660 (1946).
[25] B. ROSSI et S. J. KLAPMAN: *Phys. Rev.*, **61**, 414 (1942).
[26] B. ROSSI: *Rev. Mod. Phys.*, **21**, 104 (1949).
[27] P. CALDIROLA et P. GULMANELLI: *Nuovo Cimento*, **8**, 229 (1951).

celles-ci ont été produites par des primaires d'énergie supérieure à trois fois l'énergie critique, les spectres d'énergie de chacune de ces gerbes ne doivent pas différer sensiblement des spectres des traces électroniques et photoniques, et ne doivent pas différer sensiblement entre eux. On peut donc s'attendre, dans ce cas, à ce que les spectres d'énergie totaux observés à cette altitude coïncident à peu près avec les spectres des traces calculés pour une gerbe produite par un primaire d'énergie grande devant l'énergie critique. Il est vraisemblable que ces conditions sont assez bien remplies à l'altitude du Pic du Midi. En effet, d'une part, environ 75% de la composante molle à cette altitude dérive des mésons [26,27] dont le spectre d'énergie [28] est tel que la grande majorité des électrons et photons semblent bien pouvoir être attribués à des gerbes produites par des primaires d'énergie supérieure à 300 MeV. Les gerbes produites par des primaires d'énergie inférieure à 300 MeV sont d'ailleurs pratiquemment absorbées après 3 unités de radiation et ne comportent qu'une dizaine de particules à leur maximum. D'autre part, étant donné que les spectres que nous observons s'étendent principalement aux énergies inférieures à l'énergie critique, il semble bien que les électrons et photons appartiennent à des gerbes qui sont au-delà de leur maximum. Il semble donc assez raisonnable de comparer nos résultats expérimentaux sur les spectres d'énergie des photons et des électrons avec les spectres des traces photoniques et électroniques calculés pour $E_p \gg E_e$.

Les courbes 1 et 2 de la fig. 4 représentent les spectres différentiels des traces photoniques et électroniques repris de l'article de Richards et Nordheim [21]. Ils sont normalisés d'après les résultats expérimentaux, tous les deux avec le même facteur, de manière à conserver les rapports d'intensités théoriques. L'accord entre ces courbes et les histogrammes expérimentaux A et B est bon, sauf pour les photons de basse énergie. Entre 10 et 20 MeV, l'intensité expérimentale est inférieure à l'intensité théorique de plus qu'un facteur 2; entre 6 et 10 MeV le désaccord est encore plus important. Ce désaccord, portant uniquement sur les photons de basse énergie, semble pouvoir être attribué, au moins en grande partie, à la perte de paires de basse énergie au cours des explorations. En effet, nous avons vu (cf. n. 2) qu'un certain nombre de paires avaient été écartées d'office comme douteuses, celles-ci étant certainement d'énergie inférieure à 10 MeV, et que la perte totale sur les paires non douteuses d'énergie inférieure à 50 MeV pouvait dépasser 20%. En conclusion, on peut dire que les spectres théoriques de Richards et Nordheim représentent bien les spectres différentiels d'énergie ainsi que les rapports d'intensités des photons et des électrons à l'altitude du Pic du Midi et dans les domaines d'énergie considérés.

[28] D. B. Hall: *Phys. Rev.*, **66**, 324 (1944).

6. – Intensités intégrales.

Vu les résultats précedents, nous pouvons à présent utiliser les spectres théoriques pour déterminer les intensités intégrales des photons et des électrons. Avant cela, revenons un moment sur la normalisation des courbes 1 et 2 de la fig. 4. Rappelons les valeurs particulières des intensités intégrales expérimentales des photons et des électrons, obtenues aux nn. 3 et 4:

$$Q_{50}^{\infty} = (1{,}76 \pm 0{,}12)\cdot 10^{-2} \text{ cm}^{-2}\,\text{s}^{-1}, \tag{6}$$

$$P_{6}^{70} = (1{,}34 \pm 0{,}08)\cdot 10^{-2} \text{ cm}^{-2}\,\text{s}^{-1}. \tag{8}$$

Dans les mêmes intervalles, les spectres théoriques donnent respectivement les valeurs suivantes, en unités arbitraires:

$$Q'^{\infty}_{50} = 1{,}58, \tag{10}$$

$$P'^{70}_{6} = 1{,}07. \tag{11}$$

En comparant ces valeurs aux valeurs expérimentales, on trouve les rapports suivants:

$$\frac{Q_{50}^{\infty}}{Q'^{\infty}_{50}} = (1{,}12 \pm 0{,}08)\cdot 10^{-2} \quad \text{et} \quad \frac{P_{6}^{70}}{P'^{70}_{6}} = (1{,}25 \pm 0{,}08)\cdot 10^{-2},$$

qui coïncident dans les limites des erreurs.

Pour tracer les courbes 1 et 2 de la fig. 4, nous avons pris la valeur moyenne $1{,}18\cdot 10^{-2}$ comme facteur de normalisation. Utilisant les spectres théoriques ainsi normalisés, nous trouvons pour les intensités intégrales des photons et des électrons d'énergie supérieure à 10 MeV, les valeurs suivantes:

$$Q_{10}^{\infty} = (5{,}55 \pm 0{,}38)\cdot 10^{-2} \text{ cm}^{-2}\,\text{s}^{-1}, \tag{12}$$

$$P_{10}^{\infty} = (1{,}84 \pm 0{,}11)\cdot 10^{-2} \text{ cm}^{-2}\,\text{s}^{-1}. \tag{13}$$

Nous pouvons calculer aussi l'intensité intégrale des mésons d'énergie supérieure à 40 MeV. Il nous suffit pour cela de soustraire de la valeur expérimentale (9) de l'intensité intégrale des traces de grande énergie, la valeur de l'intensité intégrale des électrons d'énergie supérieure à 70 MeV, calculée à l'aide du spectre théorique:

$$P_{70}^{\infty} = 0{,}70\cdot 10^{-2} \text{ cm}^{-2}\,\text{s}^{-1}, \tag{14}$$

d'où:

$$R_{40}^{\infty} = (2{,}85 \pm 0{,}12) \cdot 10^{-2} \text{ cm}^{-2} \text{ s}^{-1} . \tag{15}$$

Les erreurs probables indiquées pour les différentes intensités intégrales sont d'origine purement statistique. Il n'a pas été tenu compte de l'incertitude des extrapolations basées sur les spectres théoriques.

7. – Distributions angulaires et intensités verticales.

Les distributions angulaires des composantes dure et molle ont été étudiées au moyen de compteurs montés en télescope par divers auteurs ([7,8,9,10,11]). Ceux-ci ont cherché à répresenter ces distributions par des lois de la forme suivante

$$I(\theta)\,\mathrm{d}\Omega = I_v \cos^n \theta\,\mathrm{d}\Omega = 2\pi I_v \cos^n \theta \sin\theta\,\mathrm{d}\theta , \tag{16}$$

dans laquelle I_v est l'intensité dans la direction verticale et $I(\theta)$ est l'intensité dans une direction d'angle zénithal θ.

Pour la composante dure, tous les auteurs cités ci-dessus s'accordent pour assigner à l'exposant n du cosinus la valeur 2, à toutes les altitudes, sauf éventuellement aux plus grandes. Pour la composante molle, par contre, il y a des divergences. Les uns ([7,8]) trouvent pour n la valeur 3,5 (ce qui correspond à une distribution plus étroite que celle de la composante dure) les autres ([9,10,11]) trouvent pour n la valeur 2, comme pour la composante dure.

Les mesures angulaires que nous avons effectuées sur les paires et sur les traces isolées nous permettent d'établir les distributions angulaires des photons, des électrons et des particules de grande énergie. Ici, l'avantage de plaques photographiques sur les compteurs est qu'elles donnent directement les distributions angulaires dans l'espace et qu'il n'y a pas lieu de faire de corrections tenant compte d'effets secondaires; il y a donc moins de risques d'erreurs systématiques. Mais, par contre, les erreurs statistiques sur nos résultats actuels sont beaucoup plus grandes que les erreurs statistiques sur les résultats cités ci-dessus, qui sont basés sur le comptage de plusieurs milliers de particules.

Les 2^{e} et 5^{e} colonnes du tableau V donnent les distributions expérimentales des photons et des électrons dans les intervalles d'angle zénithal indiqués dans la 1ère colonne. Les 3^{e} et 6^{e} colonnes donnent, en pour-cent, les distributions obtenues en effectuant les corrections géométriques indiquées aux nn. 3 et 4. Enfin, les 4^{e} et 7^{e} colonnes donnent les mêmes distributions, normalisées de manière à ce que les totaux correspondent respectivement aux intensités intégrales (12) et (13) données au n. 6.

Tableau V.

	Photons			Electrons			Particules de grande énergie		
θ (degrés)	Distrib. expér.	Distrib. corrigée (%)	Distrib. normalisée (10^{-4}cm^{-2}s^{-1}stér^{-1})	Distrib. expér.	Distrib. corrigée (%)	Distrib. normalisée (10^{-4}cm^{-2}s^{-1}stér^{-1})	Distrib. expér.	Distrib. corrigée (%)	Distrib. normalisée (10^{-4}cm^{-2}s^{-1}stér^{-1})
0–17	64	26,6	541,0	38	24,5	166,0	62	18,2	190,0
17–24	45	18,8	382,0	18	11,6	79,0	54	15,8	166,0
24–34	42	19,2	197,0	23	22,0	75,0	54	23,2	121,0
34–42	19	13,4	138,0	8	11,6	39,5	28	18,0	94,0
42–49	11	9,1	93,5	5	8,3	28,4	14	10,3	54,0
49–55	5	5,0	51,5	2	3,9	13,4	4	3,4	17,8
55–61	4	4,2	43,0	3	5,8	19,8	3	2,6	13,6
61–66,5	1	1,3	13,4	3	6,4	21,8	5	5,0	26,0
66,5–72	1	1,3	13,4	1	2,2	7,5	2	2,1	11,0
72–77	1	1,3	13,4	2	4,5	15,4	1	1,2	6,3
>77	0	0	0	0	0	0	0	0	0

Pour déterminer la distribution générale de la composante molle, nous avons réuni les distributions des photons et des électrons. La distribution ainsi obtenue est basées sur 296 événements. Ceci est justifié par les deux raisons suivantes: *a*) Les électrons et les photons sont angulairement liés entre eux dans le développement des gerbes et les deux distributions sont essentiellement liées au scattering multiple des électrons le long de leur parcours. *b*) Les deux distributions exprimées en pour-cent, coïncident à peu près dans les limites des erreurs statistiques. L'histogramme de la fig. 5*a* représente cette distribution générale de la composante molle. Il a été établi en coordonnées logarithmiques, en portant en abscisses les logarithmes de cos θ et en ordonnées des nombres proportionnels aux logarithmes des nombres d'évenements dans les différents intervalles angulaires. Sur ce graphique, les lois de la forme (16) sont représentées par des droites de coefficient angulaire $-n$. On voit que la distribution peut effectivement être représentée, en première approximation, par une loi de la forme (16) avec $n = 3{,}5 \pm 0{,}5$, en accord avec certains des résultats obtenus au moyen de compteurs [7,8]. Cependant, il semble que la distribution puisse être mieux représentée par une ligne courbe, correspondant à une loi plus compliquée. On voit également que l'on peut exclure la valeur 2 pour l'exposant n.

Les histogrammes des fig. 5 *b* et *c*, établis également en coordonnées loga-

rithmiques, représentent les distributions angulaires normalisées des photons et des électrons d'énergie supérieure à 10 MeV. Nous avons reporté sur ces figures les droites de coefficient angulaire — 2 et — 3,5, ainsi que la courbe tracée sur la fig. 5 *a*. Nous pouvons maintenant tâcher d'établir, en utilisant

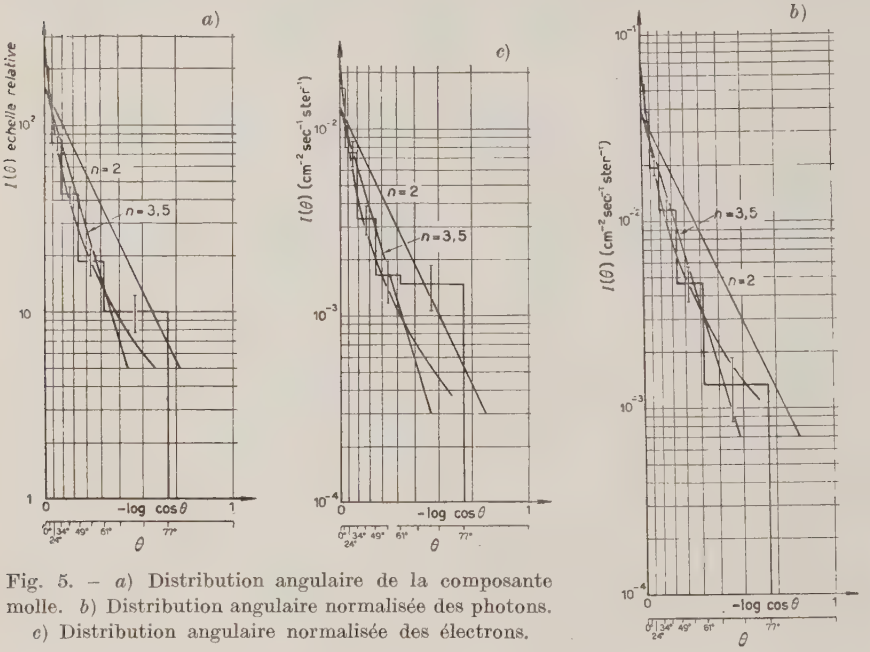

Fig. 5. — *a*) Distribution angulaire de la composante molle. *b*) Distribution angulaire normalisée des photons. *c*) Distribution angulaire normalisée des électrons.

ces données, quelle est l'intensité verticale des composantes que nous avons examinées. Cela nous donne la possibilité de confronter nos résultats avec ceux des mesures faites au moyen de compteurs.

Pour déterminer les intensités verticales, il suffit d'extrapoler les distributions angulaires jusqu'aux abscisses nulles. Si nous extrapolons les courbes des fig. 5 *b* et *c*, nous obtenons les valeurs des intensités verticales indiquées dans la première colonne du tableau VI. D'autre part, en extrapolant la droite de coefficient angulaire — 3,5, nous obtenons les valeurs indiquées dans la 2e colonne du tableau. Ces valeurs sont presque deux fois plus petites que les précédentes. Cette grande différence met en évidence l'incertitude de cette méthode. Des données plus directes du point de vue expérimental peuvent être tirées du rapport entre le nombre des particules comprises dans un petit angle solide (d'axe vertical) et l'amplitude de cet angle lui-même. En réalité, pour obtenir la valeur théorique de l'intensité verticale, cet angle solide devrait

TABLEAU VI.

	Intensités verticales (10^{-2} cm^{-2} s^{-1} stérad^{-1})			
	extrapol. suivant courbe	extrapol. suivant droite $n = 3,5$	cône $\theta = 17°$	ROSSI
Photons ($K > 10$ MeV)	$7.0 \pm 0,5$	$3,8 \pm 0,3$	$5.4 \pm 0,5$	—
Electrons ($E > 10$ MeV)	$2.3 \pm 0,2$	$1,3 \pm 0,1$	$1,7 \pm 0,2$	0,8
Mésons				
($E > 40$ MeV)	—	$1,6 \pm 0,3$	$1,5 \pm 0,2$	—
($E > 220$ MeV)	—	$1,3 \pm 0,3$	$1,2 \pm 0,2$	1,5

être infiniment petit, ce qui naturellement n'est pas possible. Mais on pourrait faire la même remarque à propos des mesures de l'intensité verticale faites au moyen de compteurs. En prenant le cône de demi-ouverture $\theta = 17°$ on obtient les données de la 3^e colonne du tableau VI. La 4^e colonne donne la valeur de l'intensité verticale des électrons obtenue au moyen de compteurs, tirée d'un article de ROSSI [12]. On voit qu'il y a un désaccord assez grand entre les valeurs que nous avons obtenues et celle-ci. Cette différence nous semble pouvoir être due à l'incertitude de l'évaluation de la limite inférieure de l'énergie dans les mesures faites au moyen de compteurs, vu qu'aux environs de 10 MeV la pente du spectre intégral d'énergie est très raide.

Les trois dernières colonnes du tableau V donnent, pour les particules de grande énergie, la distribution expérimentale, la distribution corrigée et la distribution normalisée, obtenues de manière tout à fait analogue que les distributions correspondantes des électrons. L'histogramme de la fig. 6 représente, en coordonnées logarithmiques, la distribution normalisée. On voit que cette distribution peut être représentée assez correctement par une loi de la forme (16) avec un exposant $n = 3,5$, tandis que l'on peut exclure l'exposant 2. Ce résultat est en désaccord avec celui des auteurs cités plus haut,

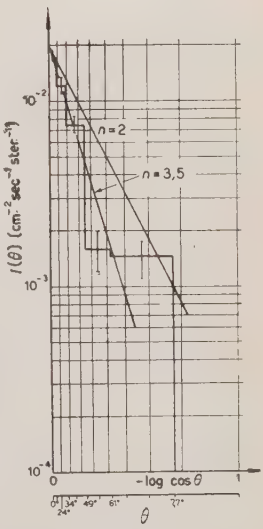

Fig. 6. – Distribution angulaire des particules de grande énergie, normalisée pour les mésons d'énergie supérieure à 40 MeV.

qui trouvent tous un exposant 2, mais il est évidemment délicat de comparer des résultats obtenus par des méthodes si différentes. En extrapolant la droite de coefficient angulaire -3,5, nous obtenons la valeur suivante de l'intensité verticale des particules de grande énergie:

$$I_v = (2{,}0 \pm 0{,}4)\cdot 10^{-2} \text{ cm}^{-2}\,\text{s}^{-1}\,\text{stérad}^{-1}\,. \tag{17}$$

Comme la distribution angulaire des électrons peut être également représentée, en première approximation, par une droite de coefficient angulaire $-3{,}5$, nous pouvons déduire de la valeur (17) l'intensité verticale des mésons d'énergie supérieure à 40 MeV, en utilisant les valeurs (14) et (15) des intensités intégrales des électrons et des mésons compris dans les particules de grande énergie. Nous obtenons ainsi la valeur indiquée dans la 2^e colonne du tableau VI. Dans la 3^e colonne est indiquée la valeur obtenue par la méthode directe citée plus haut. On voit que dans ce cas-ci, les deux méthodes donnent à peu près le même résultat. Nous avons aussi calculé l'intensité verticale des mésons d'énergie supérieure à 220 MeV, pour pouvoir faire la comparaison avec la valeur tirée de l'article déja cité de ROSSI et indiquée dans la 4^e colonne du tableau VI. On voit que l'accord est satisfaisant.

Remerciements.

Ce travail résulte d'une collaboration entre le Centre de Physique Nucléaire de l'Université de Bruxelles et les Instituts de Physique des Universités de Gênes et de Rome.

Nous exprimons notre gratitude envers les Professeurs E. AMALDI, M. COSYNS et G. P. S. OCCHIALINI pour l'aide constante qu'ils nous ont prodiguée au cours de ce travail et pour l'accueil généreux qu'ils ont réservé à ceux d'entre nous qui ont assuré la liaison entre leurs laboratoires. Nous remercions vivement les Professeurs A. BORSELLINO et M. SCHÖNBERG pour l'intérêt qu'ils ont bien voulu porter à nos recherches, et nos collègues C. DILWORTH, A. MANFREDINI et L. VERMASEN, qui nous ont accordé leur précieux concours à maintes reprises. Nous remercions particulièrement le Professeur J. RÖSCH, Directeur de l'Observatoir du Pic du Midi, qui nous a donné toutes les facilités pour exposer les plaques et M. C. WALLER, de Ilford Ltd, qui nous a aimablement fourni les émulsions spéciales. Nous tenons enfin à remercier les microscopistes qui se sont dévoués à la recherche des paires d'électrons dans les émulsions.

L'un de nous (G. C.) est redevable envers le Ministère des Affaires Etrangères de Belgique d'une bourse d'études qui lui a été octroyée dans le cadre des échanges culturels belgo-italiens.

RIASSUNTO (*)

Il lavoro è uno studio della componente molle della radiazione cosmica al Pic du Midi (43° lat. N, 2860 m s.l.m.) condotto per mezzo di lastre fotografiche sensibili alla ionizzazione minima. Lo studio si basa sull'esame sistematico delle tracce isolate e delle tracce di coppie d'elettroni create nell'emulsione. Gli spettri differenziali dell'energia dei fotoni e degli elettroni si identificano misurandone lo scattering e si normalizzano in base alle intensità integrate misurate; si confrontano con gli spettri calcolati da Richards e Nordheim secondo la teoria delle cascate. L'accordo è soddisfacente sia per la forma degli spettri che per il rapporto delle intensità. Le distribuzioni angolari trovate per la componente molle (fotoni – elettroni) e per la componente dura (mesoni) coincidono approssimativamente fra di loro e possono essere rappresentate in prima approssimazione da una legge della forma $I(\theta)\,\mathrm{d}\Omega = I_{\nu}\cos^{3,5}\theta\,\mathrm{d}\Omega$.

(*) *Traduzione a cura della Redazione.*

IL NUOVO CIMENTO Vol. IX, N. 10 1 Ottobre 1952

Conformal relativity.

L. Ingraham

Institute for Advanced Study - Princeton, New Jersey, U.S.A.

(ricevuto l'11 Luglio 1952)

Summary. — If one keeps angle but drops an invariant (four-dimensional) length from an essentially Einstenian description of the world, one gets Conformal Relativity. (The invariance of angle is all that is required by the « invariance of the light cone » for physically equivalent observers). The Special Theory of Conformal Relativity studies the conformal geometry, which replaces the Lorentz geometry of special relativity, from the kinematical point of view, in a world free of force fields. The General Theory treats a world with a curvilinear conformal gometry subjected to the one condition of minimum « total » curvature. The extremal equations describe force fields which comprise, along with the familiar gravitational and electromagnetic fields, several « mesons ». The General Theory is thus a unified field theory, which, because it is modelled on Einstenian relativity, is completely free from arbitrary elements. The mathematical language allows interpretation in terms of exclusively four-dimensional geometric notions.

1. – Introduction.

If the invariance of light velocity alone, without the requirement of an invariant length in space-time, be made to define the class of « physically equivalent observers » then we ought to search for laws exhibiting not only Lorentz but full conformal *invariance in form* (i.e., which maintain their « simplest » form under the whole conformal group). If furthermore, we conjecture that these laws do not form a heterogeneous collection but fit together into a geometric whole, then we are committed to search for a « unified field » theory in whose local spaces (the spaces of physical experience) a geometric structure defining the conformal geometry of local space-time continua is given. The final requirement that this should be the « simplest possible »,

such unified theory, taking general relativity with its freedom from arbitrary elements as the criterion of that « simplest possible structure », then uniquely fixes the theory as will be shown.

The study of the ordinary conformal (« conformal flat ») geometry of an X_4 interpreted as space-time with angle-defining form of signature $(+\ +\ +\ -)$ from the kinematical point of view forms the subject matter of the Special Theory of Conformal Relativity. The main feature is that the class of physically equivalent observers is widenend from that of Special Relativity embracing all those in relative uniforme velocity to all those in relative *uniform* acceleration. Length (i.e., « interval ») and at the same time rest mass go out as invariants against the physical group (group of coordinate transformations between equivalent observers). The study of the « general » (curvilinear) conformal geometry of an X_4 interpreted as space-time with angle-definining tensor of signature $(+\ +\ +\ -)$ which is subjected to the one global condition of *minimum total curvature* forms the subject matter of the General Theory of Conformal Relativity. In addition to the kinematical results holding in each local space known from the Special Theory, one gets as extremal equations a set of nature laws describing various « force » fields.

It is important to emphasize that this unified field theory can be phrased completely in four-dimensional language using only geometrical notions proper to four-dimensional space, or equally well in terms of a larger space and geometry. By this we mean also to imply that there are no arbitrary restrictions on symmetry (e.g., cylinder-condition) geometrically inexplicable in the former interpretation. That is, the two descriptions are completely equivalent in every sense. The description actually adopted in this article is the five-dimensional projective one.

In many ways projective relativity (or the Kaluza theory) reveals itself as a provisional stage on the way to Conformal Relativity in that features which were anomalous or arbitrary in the former are only explained when we come to the latter. We will mention the more important ones, using first the four-dimensional conformal language followed by the equivalent five-dimensional projective version in brackets. First, the mysterious » fifth dimension « of the projective relativity — Kaluza theory (objectionable especially to those who were not willing to give up the affine for the projective language) when extended to the « sixth dimension » of this theory again takes on direct physical meaning with respect to the four dimensions of space-time. For six is the number of supernumerary (« hexaspherical ») coordinates necessary to handle the ordinary conformal geometry of four dimensions by means of *constant* linear transformations. When an ordinary conformal geometry is then put at each point of the manifold of six general supernumerary coordinates, these transformations become the non-constant linear transformations of the *general* (curvilinear) conformal geometry of four dimensions. [Six is

the number of homogeneous coordinates necessary to represent four-dimensional conformal transformations as a group of linear transformations in a bigger, *flat* space (five-dimensional projective space) by means of stereographic projection of a quadric. These ordinary projective spaces then become the local spaces of a *general* (curvilinear) five-dimensional projective space]. Second, the anomalous quadric of projective relativity forms part of the quadratic identity satisfied by local hexaspheric coordinates which represent points of space-time in this theory. [It forms part of the quadric of this theory whose well defined geometric rôle is to define local four dimensional conformal-flat geometries by means of stereographic projection]. Third, a priori criteria were lacking to define completely the quadric's signature in projective relativity, whereas in this theory the quadric's signature is fixed by the « signature of space-time » plus the demand that the preferred systems of the ordinary conformal geometry (hexaspherical coordinates) be real. [The quadric's signature is fixed by the signature of « space-time » plus the demand that the local five-dimensional projective spaces be real]. In other words, Conformal Relativity is to be a theory of real quantities only.

Fundamental for mechanics is the fact that only in Conformal Relativity we do get the optimum relation between the class of all observers « indistinguishable » with respect to the light cone (those connected by conformal coordinate transformations) and the class of all observers for whom the nature laws are « in their simplest form ». Calling the defining groups of coordinate transformations of these classes G_1 and G_2 resp., for the moment, one has in fact in Conformal Relativity $G_1 \subset G_2$ and $G_2 \subset G_1$, or $G_1 = G_2$. In projective relativity one has $G_1 \not\subset G_2$ and $G_2 \not\subset G_1$. In affine (« general ») relativity one has $G_2 \subset G_1$ but $G_1 \not\subset G_2$. In both latter relativities $G_1 \cap G_2 =$ the orthogonal group; i.e., an invariant length figures.

The field equations of the General Theory of Conformal Relativity describe Einsteinian gravitation, Maxwellian electromagnetism, and several mesons (tentatively interpreted); i.e., particles of integral spin and non-zero rest mass (a posteriori defined here) in the language of particle theory. That is, a *unified* theory of force fields necessarily results from dropping invariant length from an essentially Einsteinian description of the world. These field equations are all conformally invariant in form of course, and show covariance against various other important groups. They are nearly linear in regions of tenuous energy, becoming essentially non-linear where energy is dense.

Matter itself is finally geometrized in the generalization to Spinor Relativity, sketched at the end of the article. « Geometrized » here is meant in the literal sense of *complete* unification with the fields occurring already in Conformal Relativity.

2. – Notation and Some Definitions.

The space we start with is a five-dimensional curvilinear projective space H_5; i.e., a five dimensional manifold X_5 described by six homogeneous coordinates X^μ ($\mu = 0, 1, ..., 5$) (X^μ and ϱX^μ describe the same point) which undergo coordinate transformations $X^{\mu'} \quad F^{\mu'}(X^\tau)$ homogeneous of degree $+1$. The motivation for this choice of geometry is to get local ordinary five dimensional projective spaces $P_5(X^\mu)$ at each point X^μ, which will serve as the geometrical frame-work of the conformal geometry of four dimensions. In general we will use the differential geometry notation of SCHOUTEN, VAN DANTZIG *et al.*, a concise summary of which can be found in [1]. Central in its notational philosophy is the designation of a kernel letter T, say, for each geometrical object, which is never changed, and the use of different alphabets: (ϱ), (ϱ'), ... (a), ..., etc. for the indices to indicate the sets of components $T^{\varrho\cdots}_{\cdots}$, $T^{\varrho'\cdots}_{\cdots}$, $T^{a\cdots}_{\cdots}$, etc. wrt (« with respect to ») the different reference systems. Five inhomogeneous manifold coordinates can be introduced by five independent functions, homogeneous of degree zero in the X^μ:

$$x^\alpha = f^\alpha(X^\mu) , \qquad (\alpha = 1, ..., 5)$$

We recall explicitly a few important features: that all geometrical objects of H_5 are homogeneous of various degrees in the X^μ; that we can restrict ourselves to those of *excess zero* (which means, e.g. for tensors that the degree of homogeneity equals the difference of the contravariant and covariant valences); that in addition to $\boldsymbol{H}_6$, the coordinate transformation group above defined, we consider non-holonomic transformations defined by any set of homogeneous functions A^a_ϱ ($a = 0, 1, . ., 5$) and inverses with $\mathrm{Det}\, A^a_\varrho \neq 0$. The kernel A always denotes the unit tensor, defined, $A^a_b \quad \delta^a_b$ in any system (a). The introduction of non-holonomic systems is necessary for the decomposition of field laws into forms familiar from previous theories — e.g., general relativity. (The transformation $T^{\mu\cdots}_{\varrho\cdots} \to T^{a\cdots}_{b\cdots}$ has gone by various names in the literature, e.g., «projecting» a projective tensor into its affine components [2]). For the definitions of further objects and symbols to be used, please see the cited work. The following alphabet conventions will be observed

$\varkappa, \lambda, \mu, \nu, ... \Gamma = 0, 1, . . 5$	homogeneous coordinates of H_5.
$\alpha, \beta, \gamma, \quad ... \varepsilon = 1, ... 5$	inhomogeneous coordinates of H_5.
$a, b, c, ... g$ / $A, B, C, ... G$ $= 0, 1, . . 5$	(in general) non-holonomic systems in H_5.
h, i, j, k / H, I, J, K $= 1, ... 5$	inhomogeneous local coordinates in the $P_5(X^\mu)$'s.
$m, n, p, q, ... s$ / $M, N, P, Q, ... S$ $= 1, ... 4$	coordinates of an X_4 (def.: four-dimensional manifold).

These conventions are to hold always except where a new convention is explicitly introduced, as is necessary only in the last two sections (1).

We are given a symmetric tensor $S_{\mu\varrho}$ (signature $(- + + + - +)1$) and general projective connection $\Gamma_{\mu\varrho}^{\ \ k}$ of excess zero (homogeneous of degrees -2 and -1 resp.) in H_5 and will let the variational equations of one «most natural» Lagrangian decide how they are connected and what are their dependences on X^μ. Simultaneously these equations will reduce the undesirable richness of differential invariants available for Lagrangian building material with which we are confronted ab initio. From $\Gamma_{\mu\varrho}^{\ \ k}$ its curvature tensor can be formed (2):

$$N_{abc}^{\ \ \ d} \equiv -2\partial_{[a}\Gamma_{b]c}^{\ \ \ d} - 2\Gamma_{[a|f|}^{\ \ \ d}\Gamma_{b]c}^{\ \ \ f} - 2\Omega_{ab}^{\ \ f}\Gamma_{fc}^{\ \ d}\,, \tag{2.1}$$

where $\Omega_{ab}^{\ \ f}$ is the non-holonomicity object which vanishes for (a) holonomic:

$$\Omega_{ab}^{\ \ f} \equiv A_{ab}^{\varrho\tau}\partial_{[\varrho}A_{\tau]}^{f}\,. \tag{2.2}$$

When this is contracted to the Ricci tensor $N_{bc} = N_{abc}^{\ \ \ a}$, the Gaussian curvature $N = S^{ab}N_{ab}$ can be formed by means of S_{ab}. Then we define the Lagrangian:

$$L \equiv \int N\sqrt{S}\,(\mathrm{d}X)\ (3)\,, \qquad [(\mathrm{d}X) \equiv \mathrm{d}X^0\,\mathrm{d}X^1 \ldots \mathrm{d}X^5,\ S \equiv \mathrm{Det}\,S_{\mu\varrho}]\,. \tag{2.3}$$

The equations $\delta L = 0$ will then express a minimum total (i.e., integrated) curvature property. This condition gave both general and projective relativity [3] and here is required to give Conformal Relativity. Indeed, the giving of an appropriate manifold geometry, plus an a priori independent linear connection and quadric in the local spaces, subjected to the minimum curvature principle (2.3) is used to define a generic class of «relativities» which are investigated comparatively in Section 6.

(1) To be strictly orthodox, one should introduce a new set of numbers for each new alphabet, e.g., 0, 1, ...; *0*, *1*, ...; 1, 0, ...; but we will in general drop this usage, trusting to the context to make clear to what alphabet a numerical index belongs.

(2) [ ] or ( ) around any set of p indices indicates the alternating or symmetric part, resp. Thus, e.g., for $p = 2$, $P_{[ab]} \equiv 1/2(P_{ab} - P_{ba})$, $P_{(ba)} \equiv 1/2(P_{ba} + P_{ab})$. The mark $|\,|$ around an index indicates it is not to be included in the permutation, e.g., $P_{|a|b|c|} = -1/2(P_{abc} - P_{cba})$. $\partial_a = A_a^{\varrho}\partial_\varrho$, $\partial_\varrho \equiv \partial/\partial X^\varrho$, which defines ∂_a for (a) holonomic or non-holonomic.

(3) $\sqrt{S}\,(\mathrm{d}X)$ is unaffected by the «point transformation» $X^\mu \to \varrho X^\mu$ (i.e., is a projective quantity of H_5). Cf. Pauli, [2], for the proof for four dimensions.

3. – The Variation of the Lagrangian and the Field Equations.

In our Lagrangian, the connection and the quadric (i.e., $S_{\mu\varrho}$) are independently variable quantities. We seek first the connection between them imposed by the minimum curvature principle $\delta L = 0$. Consider first, therefore, the variation wrt the connection Γ. The details are given in Appendix I; it is not essentially different from the Palatini analysis generalized to non-symmetric connections given by SCHRÖDINGER for the case of the four-dimensional affine geometry. This gives

$$\overline{\nabla}_{\varrho} S_{\underset{-}{\nu}\ \underset{+}{\lambda}} = \partial_{\varrho} S_{\nu\lambda} - S_{\tau\lambda}\overline{\Gamma}_{\nu\varrho}{}^{\tau} - S_{\nu\tau}\overline{\Gamma}_{\nu\lambda}{}^{\tau} = 0 \qquad [(\varrho)\ \text{hol.}] \tag{3.1}$$

in terms of the connections $\overline{\Gamma}$ defined by

$$\overline{\Gamma}_{\nu\lambda}{}^{\varrho} \equiv \Gamma_{\nu\lambda}{}^{\varrho} + {}^{2}/_{5}\, A^{\varrho}\Gamma_{[\xi\nu]}{}^{\xi} \qquad [(\varrho)\ \text{hol.}]$$

which satisfies $\overline{\Gamma}_{[\varrho\lambda]}{}^{\varrho} = 0$. Note the crucial index order switch in $\overline{\Gamma}_{\nu\varrho}{}^{\tau}$ in the second term of the middle member of (3.1). Indeed, this small change from the usual covariant derivative equation $\overline{\nabla}_{\varrho} S_{\nu\lambda} = 0$ provides the out from the vexing circumstance that the latter equation does not uniquely determine a connection. For (3.1) *does* uniquely determine $\overline{\Gamma}$ [5]. This explicit solution for $\overline{\Gamma}$ in terms of $S_{\nu\lambda}$ and its first derivatives is quite complicated for the general $S_{\nu\lambda}$. However, for our case of a symmetric $S_{\nu\lambda}$ it is simple, see Appendix I). In fact,

$$\overline{\Gamma}_{\mu\varkappa}{}^{\varrho} = \left\{ \begin{matrix} \varrho \\ \mu\varkappa \end{matrix} \right\}_{S} \qquad [(\mu)\ \text{hol.}];$$

that is, $\overline{\Gamma}$ is not only symmetric, but must be the Christoffel symbols of the $S_{\mu\varkappa}$. We shall need the general form of this equation wrt non-holonomic systems as well, which is well known to be

$$\overline{\Gamma}_{cb}{}^{a} = \left\{ \begin{matrix} a \\ cb \end{matrix} \right\}_{S} - \Omega_{cb}{}^{a} - 2\Omega^{a}(cb)\,, \tag{3.2}$$

where $\left\{ \begin{matrix} a \\ cb \end{matrix} \right\}_{S}$ is the Christoffel differential symbol $\frac{1}{2}S^{ad}(\partial_{c}S_{bd} + \partial_{b}S_{cd} - \partial_{d}S_{cb})$ (no linear connection!).

Remarks: 1) It is characteristic for the « generalized Palatini » variation that the connection we determine, $\overline{\Gamma}$, is not the one, Γ, with which we started. The undetermined vector $\Gamma_{[\xi\nu]}{}^{\xi}$ $[(\nu)\ \text{hol.}]$ occurs in the definitions of $\overline{\Gamma}$. This makes absolutely no difference to the physics of the situation, for it drops

entirely out of the final field equations, cf. in fra. 2) Unlike certain four dimensional affine theories [6], [4], we definitely do *not* envisage drawing further physical fields out of an assumed non-vanishing skew part of $S_{\nu\lambda}$. The rôle of $S_{\nu\lambda}$ is to define quadrics in the local spaces, which then give rise to a conformal geometry there (Section 6). Thus the presence of a skew part, while perhaps physically attractive at first view, would be geometrically meaningless.

The variation of L wrt $S^{\nu\lambda}$ gives easily

$$\delta L = \int G_{\nu\lambda}\delta S^{\nu\lambda}\sqrt{S}\,(\mathrm{d}X)\ ; \tag{3.3}$$

$G_{\nu\lambda}$ the « Einstein » symmetric linear tensor function of $N^{\nu\lambda}$ defined by

$$G_{\nu\lambda} \equiv N_{(\nu\lambda)} - \tfrac{1}{2}S_{\nu\lambda}N \qquad (N \equiv S^{\sigma\tau}N_{\sigma\tau}).$$

From the relation of $\bar{\Gamma}$ and Γ, a simple lemma gives at once that $\bar{N}_{\nu\xi}$ (Ricci tensor of $\bar{\Gamma}$) and $N_{\lambda\xi}$ differ only by a tensor skew in λ, ξ. Therefore

$$\bar{N}_{(\lambda\xi)} = N_{(\lambda\xi)}\ ,$$

and since this is covariantly expressed, it holds in any system (a). Hence we can write the field equations $\delta L = 0$ from (3.3) completely in terms of the well-defined $\bar{\Gamma}$:

$$\bar{G}_{ab} = 0\ , \tag{3.5}$$

where $\bar{G}_{ab}$ is formed with $\bar{N}_{ab}$: Eqs. (3.2) and (3.5) are the field equations.

The field equations thus obtained assume that each component of $S_{\nu\lambda}$ is freely variable; i.e., that this fundamental tensor contains no superfluous lumber in the way of physical fields. In projective relativity the constraint $S_{\mu\varrho}X^{\mu}X^{\varrho} = \pm 1$ is usual, eliminating a scalar field. When we choose the non-holonomic system judiciously for physical interpretation in the next section, we will assume successively one and then a second such constraint. The justification therefore is mainly analytic simplicity — it is to be emphasized that the fields thus discarded may actyually exist in nature.

If the constraints take the form

$$S_{\mu\varrho}v^{\mu}v^{\varrho} = \pm 1\ , \qquad S_{\mu\varrho}w^{\mu}w^{\varrho} = \pm 1\ , \qquad S_{\mu\varrho}v^{\mu}w^{\varrho} = 0\ , \quad \text{etc.}$$

then by the usual Lagrange undetermined multiplier method, eqs. (3.5) are replaced by

$$\bar{G}_{ab} - v_a v_b(\bar{G}_{cd}v^c v^d) - w_a w_b(\bar{G}_{cd}w^c w^d) - \ldots \text{etc.} = 0\ . \tag{3.5$'$}$$

It remains to substitute (3.2) in (3.5). This is laborious but straightforward (4). One ends up with

$$\bar{N}_{(cd)} = R_{(cd)}(\{\}_s) + 2\overset{s}{\nabla}_a \Omega^a{}_{(cd)} + 2\overset{s}{\nabla}_{(c}\Omega_{d)a}{}^a - 4\Omega_{ab}{}^a\Omega^b{}_{(cd)} - \tag{3.6}$$
$$- \Omega_{bc}{}^a \left\{ {b \atop ad} \right\}_s - \Omega_{bd}{}^a \left\{ {b \atop ac} \right\}_s + \Omega^a{}_{bc}\Omega^b{}_{ad} + 4\Omega^{(a}{}_c{}^{b)}\Omega_{(a|d|b)} ,$$

wrt to the general non-holonomic system (a), from which (3.5) can be written down immediately. Thereby we define for any symmetric expressions $\Gamma_{fg}{}^e = \Gamma_{(fg)}{}^e$

$$R_{abc}{}^e(\Gamma_{fg}{}^e) \equiv -2\partial_{[a}\Gamma_{bc]}{}^d - 2\Gamma_{[a|e|}{}^d\Gamma_{b]c}{}^e , \qquad R_{bc}(\Gamma) \equiv R_{abc}{}^a(\Gamma) , \tag{3.7}$$

and $\overset{s}{\nabla}_a$ is *formal* covariant differentiation wrt the $\left\{ {e \atop fg} \right\}_s$ e.g.,

$$\overset{s}{\nabla}_a T^b \equiv \partial_a T^b + T^c \left\{ {b \atop ac} \right\}_s .$$

The expressions on the right of (3.6) are thus differential expressions with fixed meanings defined as just above. They are *not* tensorial taken individually of course, but are the non-tensorial parts encountered in the breakdown of a larger differential expression, $\bar{N}_{(cd)}$, which itself *is* a tensor. We now turn to the question of making a physically interesting choice of reference frame (a), one which in particular introduces the four variables of the space-time continuum.

4. – The Special Reference System.

To investigate the physical content of the field equations, we must now choose the non-holonomic system (A) so as to introduce inhomogeneous coordinates chosen in a way to facilitate the interpretation of the fields occurring therein. It goes without saying that nothing is changed thereby — the field equations in their symmetrical form embodying the physical fields in unfamiliar combinations and employing the unfamiliar projective manifold coordinates, are merely replaced by an equivalent, unsymmetrical set in which the phy-

(4) Certain decompositions of the Ricci tensor given in the author's paper *Ann. of Math.*, **52**, 743 (1950), for the four dimensional affine case are useful here.

sical laws assume the heterogeneous forms more or less familiar from previous un-unified theories.

Consider the field equations then first in the system (a) defined as follows [5]: we introduce five inhomogeneous coordinates by $x^a = f^a(X^\mu)$, f^a homogeneous of degree 0, $\partial_\mu x^a$ of rank 5. By Euler's theorem $X^\mu \partial_\mu x^a = 0$, so that if we define $A^a_\varrho = \partial_\varrho x^a$, we must have $A^\varrho_0 \propto X^\varrho$. Introduce the A^ϱ_a such that

$$A^\varrho_a \partial_\varrho x^\beta = \delta^\beta_a ,$$

made unique by the condition $S_{\mu\varrho} X^\mu A^\varrho_a = 0$. Now we will assume the constraint

$$S_{\mu\varrho} X^\mu X^\varrho = -1 .$$

Hence $A^0_\varrho = -X_\varrho$. So we have defined the non-holonomic transformation $(\varrho) \to (a)$ $(a = 0, 1, \ldots 5)$ given by

$$A^a_\varrho = \partial_\varrho x^a , \qquad A^0_\varrho = -X_\varrho , \tag{4.1}$$

in which the S_{ab} (homogeneous of degree zero, that is, functions of x^a alone) have the form

$$S_{a\beta} \equiv \gamma_{a\beta} , \qquad S_{0a} = 0 , \qquad S_{00} = -1 . \tag{4.2}$$

The non-holonomicity object Ω for (a) is particularly simple since $\partial_{[\varrho} A^a_{\tau]} \equiv \equiv \partial^2_{[\varrho\tau]} x^a = 0$. Thus

$$\Omega_{ab}{}^a = 0 ; \qquad \Omega_{ab}{}^0 = -A^\varrho_a{}^\tau_b \partial_{[\varrho} X_{\tau]} \equiv f_{ab} . \tag{4.3}$$

First note that $f_{a0} = 0$. For

$$X^\tau(\partial_\varrho X_\tau - \partial_\tau X_\varrho) = X^\tau X^\lambda(\partial_\varrho S_{\tau\lambda} - \partial_\tau S_{\varrho\lambda}) = \partial_\varrho(-1) - 2X^\lambda S_{\varrho\lambda} + 2X^\lambda S_{\varrho\lambda} = 0 ,$$

since $S_{\varrho\lambda}$ is homogeneous of degree -2. It now follows that $f_{a\beta}$ is the curl of a vector. Proof: first, by (4.3) since $f_{a0} = 0$,

$$\partial_{[\varrho} X_{\tau]} = -A^{a\,\beta}_{\varrho\,\tau} f_{a\beta} . \tag{4.4}$$

Where the simbol $\langle\ \rangle$ bracketing several indices means the sum of the expres-

[5] This transformation and the resulting form (4.7) of the field equations is familiar from projective relativity, the extra dimension here making no difference in the derivation. Cf. PAULI, [2].

sion with cyclically permuted indices note that $\partial_{<\lambda}\partial_{[\varrho}X_{\tau]>} = 0$. With the aid of the lemma (in which we simply write indices and omit the objects to which they append)

$$\langle\lambda[\varrho\tau]\rangle = \langle[\lambda\varrho]\tau\rangle = 3[\lambda\varrho\tau],$$

this latter, applied to (4.4), gives

$$-2\partial_{<[\lambda}A^{\alpha}_{\varrho]}A^{\beta}_{\tau>}f_{\alpha\beta} - A^{\alpha\beta\gamma}_{<\varrho\tau\lambda>}\partial_{\gamma}f_{\alpha\beta} = 0,$$

using (4.5)*a* (infra) in the last term.

First, $\partial_{[\lambda}A^{\alpha}_{\varrho]} = 0$; second, for any function F homogeneous of degree zero, that is, a function only of the x^{α},

$$(4.5)\qquad \begin{cases} a) & \partial_{\varrho}F \equiv A^{\varrho}_{\theta}\partial_{\varrho}F = A^{\varrho}_{\theta}A^{\alpha}_{\varrho}\partial/\partial x^{\alpha}F = 0, \\ b) & \partial_{\gamma}F \equiv A^{\varrho}_{\gamma}\partial_{\varrho}F = A^{\varrho}_{\gamma}A^{\alpha}_{\varrho}\partial/\partial x^{\alpha}F = \partial/\partial x^{\gamma}F, \end{cases}$$

hence ∂_{θ} is a zero operator and ∂_{γ} the derivative wrt the variable x^{γ}. Hence we get

$$\partial_{<\gamma}f_{\alpha\beta>} = 0 \quad \text{or} \quad f_{\alpha\beta} \equiv \partial_{[\alpha}f_{\beta]},$$

(f_{β} is thereby defined up to a gradient) which was to be proved.

The field equations are very simple in this system (*a*). From (4.2) and (4.5) it is seen that

$$\left\{\begin{matrix}\alpha\\ \beta\gamma\end{matrix}\right\}_{s} = \left\{\begin{matrix}\alpha\\ \beta\gamma\end{matrix}\right\}_{\gamma}; \qquad \text{other} \quad \left\{\begin{matrix}a\\ bc\end{matrix}\right\}_{s} = 0,$$

the $\left\{\begin{matrix}\alpha\\ \beta\gamma\end{matrix}\right\}_{\gamma}$ being the ordinary Christoffel symbols of $\gamma_{\alpha\beta}$. Consequently

$$R_{(\alpha\beta)}(\{\}_{s}) = R_{\alpha\beta} \quad \text{other} \quad R_{(ab)}(\{\}_{s}) = 0,$$

$R_{\alpha\beta} \equiv R_{\alpha\beta}(\{\}_{\gamma})$, the ordinary Ricci tensor of $\left\{\begin{matrix}\alpha\\ \beta\gamma\end{matrix}\right\}_{\gamma}$. From (3.6)

$$\begin{aligned} \overline{N}_{(\alpha\beta)} &= R_{\alpha\beta} - 2f^{\gamma}{}_{\alpha}f_{\gamma\beta}, \\ \overline{N}_{(0\alpha)} &= -\overset{\gamma}{\nabla}_{\beta}f^{\beta}{}_{\alpha}, \\ \overline{N}_{(00)} &= -f^{\gamma}{}_{\delta}f_{\gamma}{}^{\delta} \equiv -(f)^{2}, \\ \overline{N} &= R - (f)^{2}, \end{aligned}$$

where $\overset{\gamma}{\nabla}_\beta$ means the covariant derivative wrt the $\left\{ \begin{matrix} \alpha \\ \beta\gamma \end{matrix} \right\}_\gamma$, and $R = \gamma^{\alpha\beta} R_{\alpha\beta}$. Because of (4.2) all raised indices here are effectively raised with $\gamma^{\alpha\beta}$, the normalized cofactors of $\gamma_{\alpha\beta}$. In (a), $X_0 = -1$, $X_a = 0$; hence the field equations (3.5)′ run

$$\bar{G}_{ab} = 0\,, \qquad (ab \neq 00). \tag{4.6}$$

Using the above decomposition of $\overline{N}_{(ab)}$,

$$\boxed{\begin{aligned} \bar{G}_{\alpha\beta} &= G_{\alpha\beta} - 2E_{\alpha\beta} = 0 \\ \bar{G}_{0\alpha} &= -\overset{\gamma}{\nabla}_\beta f^\beta{}_\alpha \qquad = 0 \end{aligned}}\,. \tag{4.7}$$

where $G_{\alpha\beta}$ is the Einstein tensor function of $R_{\alpha\beta}$ and $E_{\alpha\beta}$ is a traceless tensor defined by

$$E_{\alpha\beta} = f'_\alpha f_{\gamma\beta} - \tfrac{1}{4}\gamma_{\alpha\beta}(f)^2\,, \qquad f_{\alpha\beta} \equiv \partial_{[\alpha} f_{\beta]}\,.$$

Equations (4.7) are our equations in the form in which the fields occurring are tensors against $\boldsymbol{G}_5$, the full group of all non-singular transformations of the five x^α [6]. They are still too unified, however, to permit interpretation in terms of previous theories, in which only covariance against a subgroup of $\boldsymbol{G}_5$ transforming four position variables was considered. The gravitation-characterizing tensor and the EM potential vector still occur in unfamiliar combinations with several new fields in (4.7). To the end of separating the fields further, we introduce the change $(a) \to (A)$ to a further non-holonomic system (A) $(A = 0, 1, \ldots, 5)$. Let

$$\varphi_\alpha \varphi_5 = \gamma_{\alpha 5}\,; \qquad \text{therefore} \quad \varphi^\alpha = \varphi_\beta \gamma^{\beta\alpha} = \delta^\alpha_5/\varphi_5\,,$$

(φ_α is thus no vector against $\boldsymbol{G}_5$). Then define the transformation

$$\left\{ \begin{aligned} &A^\alpha_0 = \delta^\alpha_0\,; \quad A^\alpha_M = \delta^\alpha_M - \delta^\alpha_5 \varphi_M/\varphi_5\,, \quad A^0_M = 0\,; \\ &A^\alpha_5 = \varphi^\alpha = \delta^\alpha_5/\varphi_5\,, \quad A^0_5 = 0\,, \qquad (M = 1, \ldots, 4), \end{aligned} \right. \tag{4.8}$$

where φ_M and φ_5 have been written for φ_m $(M = m)$ and φ_δ resp. to spare un-

[6] The fifth dimension here has a good « four-dimensional » meaning in the new gauge geometry introduced by this theory, cf. end of Section 6.

necessary complication of notation. The A^a_A are homogeneous of degree zero (functions of x^a); Det $A^a_A \neq 0$; therefore they define an admissible transformation. $S_{\varrho\tau}$ has the component in (A):

$$(4.9) \qquad S_{MN} = \gamma_{mn} - \varphi_M \varphi_N \equiv g_{MN}\ ; \qquad S_{55} = -S_{00} = 1\ , \quad \text{other } S_{AB} \text{ zero}\ .$$

$(M, N = m, n \text{ resp.})$ [7].

Instead of studying the field equations in (A) in full generality, we will now make some special assumptions limiting generality for the sake of analytical simplicity and physical suggestiveness. Assume that there is an inhomogeneous coordinate system x^a in which $\gamma_{55} = +1$, hence $\varphi_5 = +1$. This means that we subject the admissible $S_{\mu\varrho}$ to the further constraint

$$S_{\mu\varrho} A^\mu_5 A^\varrho_5 = +1\ ,$$

for the fixed vector A^μ_5 defined by this coordinate system x^a. Also we have $S_{\mu\varrho} A^\mu_5 X^\varrho = S_{50} = 0$ cf. (4.2). Hence there is an extra term in the field equations according to $(3.5)'$ due to this further constraint.

Let the coordinate system (α), occurring in the A^a_A, (4.8), be the special one defined just above; furthermore, consider the case when the fields φ_M and g_{MN} are functions only of the $x^1, \ldots, x^4$. (This amounts to studying only a subclass of all possible solutions). We will write down the field equations wrt system (A) under these limiting assumptions.

The field equations run $\bar{G}_{AB} - \bar{G}_{00}\delta^0_A\delta^0_B - \bar{G}_{55}\delta^5_A\delta^5_B = 0$ where $\bar{G}_{00} = \bar{G}_{\mu\varrho} A^\mu_0 A^\varrho_0$, $\bar{G}_{55} = \bar{G}_{\mu\varrho} A^{\mu\varrho}_{55}$, or

$$(4.10) \qquad \bar{G}_{AB} = 0\ , \qquad (AB \neq 00 \text{ or } 55),$$

in view of (4.6), (4.8), and (4.9). Writing (4.10)

$$0 = \bar{G}_{AB} = A^{a\ b}_{A\ B}\, \bar{G}_{ab}\ , \qquad (AB \neq 00 \text{ or } 55),$$

we can use the decomposition of the $\bar{G}_{ab}$ already made, (4.7). In these expressions we make the substitutions

$$(4.11) \qquad \gamma_{mn} = g_{MN} + \varphi_M \varphi_N\ , \quad \gamma_{m5} = \varphi_m\ , \quad \gamma_{55} = +1\ .$$

The calculations which are lengthy but straightforward are given in Appendix II.

[7] For the time being, $M, N, P, \ldots$ and $m, n, p, \ldots$ shall refer to the same integer without explicit mention.

We write here an equivalent set, after slight rearrangements given in the appendix:

$$(4.10)'\qquad \left|\begin{array}{ll} a) & G_{MN} - 2T_{MN} - 2U_{MN} - 2P_{MN} - 4\Sigma_{MN} + 4\Lambda_{MN} = 0\,. \\ b) & \overset{g}{\nabla}_P \Phi^P{}_M + 2(\varrho)^2\varphi_M - 2\varrho_M(\varrho\varphi) = 2\varrho_P F^P{}_M\,, \\ c) & \overset{g}{\nabla}_P F^P{}_M = 2\overset{g}{\nabla}^P(\varrho_{[P}\varphi_{M]}) + (\varphi)^2\Phi_M{}^P\varrho_P\,, \\ d) & \overset{g}{\nabla}_P{}^P\varrho + 2(\varrho\varphi\Phi) = (F\Phi)\,, \end{array}\right.$$

with the following notation and definitions:

G_{MN} and R here mean the Einstein tensor function and invariant ($g^{MN}R_{MN}$) of R_{MN}, the Ricci tensor of the $\left\{\begin{matrix} P \\ QR \end{matrix}\right\}_g$, Christoffel symbols of the g_{MN}, resp.; $\overset{g}{\nabla}_P$ means covariant differentiation wrt the $\left\{\begin{matrix} P \\ QR \end{matrix}\right\}_g$; $\overset{g}{\nabla}_P{}^P\varrho \equiv \overset{g}{\nabla}_P(g^{PQ}\partial_Q\varrho)$, the Laplacian of ϱ.

For any t_Q, t^P denotes the index raised by means of the g^{MN}: $t^P = t_Q g^{QP}$.

The various fields occurring in (4.10)′ are defined $\Phi_{MN} \equiv \partial_{[M}\varphi_{N]}$, $F_{MN}(\equiv f_{mn}) \equiv \equiv \partial_{[M}F_{N]}$, $\varrho_M \equiv \partial_M\varrho \equiv f_{m5}(\equiv \tfrac{1}{2}\,\partial_m f_5)$; and

$$\begin{aligned} T_{MN} &\equiv \Phi^P{}_M\Phi_{PN} - \tfrac{1}{4}g_{MN}(\Phi)^2\,, \\ U_{MN} &\equiv F^P{}_M F_{PN} - \tfrac{1}{4}g_{MN}(F)^2\,, \\ P_{MN} &\equiv \varrho_M\varrho_N - \tfrac{1}{4}g_{MN}(\varrho)^2\,, \\ \Sigma_{MN} &\equiv \varphi_{(M}\varphi_{N)}(\varrho\varphi) - \tfrac{1}{2}\varphi_M\varphi_N(\varrho)^2 - \tfrac{1}{4}g_{MN}(\varrho\varphi)^2\,, \\ \Lambda_{MN} &\equiv \varrho_P F^P{}_{(M}\varphi_{N)} - \varphi_P F^P{}_{(M}\varrho_{N)} - \tfrac{1}{2}g_{MN}(\varrho\varphi F)\,, \end{aligned}$$

with the notation

$$\begin{aligned} &(F)^2 \equiv F^{PQ}F_{PQ}\,, \quad (\Phi)^2 \equiv \Phi^{PQ}\Phi_{PQ}\,, \quad (\varrho)^2 \equiv \varrho^P\varrho_P\,, \quad (\varphi)^2 \equiv \varphi^P\varphi_P\,, \\ &(F\Phi) \equiv F^{PQ}\Phi_{PQ}\,, \quad (\varrho\varphi) \equiv \varrho^P\varphi_P\,, \quad (\varrho\varphi F) \equiv \varrho^P\varphi^Q F_{PQ}\,, \quad (\varrho\varphi\Phi) \equiv \varrho^P\varphi^Q\Phi_{PQ}\,. \end{aligned}$$

Remark.: All these symmetric tensors $T_{MN}, \ldots, \Lambda_{MN}$ are traceless with the exception of P_{MN} and Σ_{MN}.

These then are the field equations in their « four-dimensional » form in which they are perhaps most physically suggestive. They will be interpreted in the next section. Before interpretation we must remark some important mathematical features.

The precise characterization of the « four-dimensional » form is the following: The equations (4.10)′ are covariant against the subgroup $\boldsymbol{M}_4$ of $\boldsymbol{G}_5$ defined

as the direct product of the two groups

$$x^{M'} = f^{M'}(x^N) : \boldsymbol{G}_4 \quad \text{and} \quad x^{5'} = x^5 - \lambda(x^N) : \boldsymbol{J},$$

under which the fields occurring in them transform like affine 4-tensors under $\boldsymbol{G}_4$ and according to

$$(4.12) \qquad g_{MN} \to g_{MN}, \quad \varphi_M \to \varphi_M - \partial_M \lambda, \quad F_M \to F_M - 2\varrho \partial_M \lambda, \quad \varrho \to \varrho,$$

under $\boldsymbol{J}$. The proof that the group of (4.10)′ is $\boldsymbol{M}_4$ can be inferred in generality from the fact that the field equations are tensorial plus the fact that the two special assumptions 1) all fields are functions of four variables only, and 2) $\varphi_5 = 1$, are invariant assumptions under $\boldsymbol{M}_4$.

This invariance is interesting enough to check by direct calculation in a simple case, to see, e.g., how a « vector meson » equation *b*) (anticipating an interpretation) with a « mass term » linear in φ_M can be invariant under $\boldsymbol{J}$. Making the substitutions (4.11), Φ_{MN} is invariant and $F_{MN} \to F_{MN} - 2\varrho_{\cdot M} \partial_{N]} \lambda$. Hence writing only the « extra » terms which arise on each side of the equation, one must have

$$2(\varrho)^2(-\partial_M \lambda) + 2\varrho_M \varrho^P \partial_P \lambda = -4\varrho^P \varrho_{[P} \partial_{M]} \lambda,$$

which is true. Hence *b*) is invariant under $\boldsymbol{J}$ without use of the other field equations. On the other hand, the invariance of *c*) under $\boldsymbol{J}$ uses the equation *d*).

The general field equations (3.5) (or (3.5)′) referred to any system (*a*) will be shown in Section **6** to satisfy a special invariance property called *invariance in form* under the group of all conformal transformations in local X_4's. *Invariance in form* is the generalization to the whole conformal group of Lorentz-invariance.

The field equations (4.7) or the less general (4.10)′ satisfy a number of conservation (differential) laws which hold *in virtue of these undifferentiated field laws themselves*. The proof of this property is fairly trivial for (4.7) — it is no different from the same proof in projective relativity. The proof for (4.10)′ will not be given here.

5. – Interpretation.

Now, in the light of former physical theories, some interpretations are fairly easy, others are more tentative. First for the field laws (4.10)′.

The tensor [8] g_{MN} has signature $(+ + + -)1$ by (4.9), since $S_{\mu\varrho}$ is as-

[8] « Tensor », « vector » in this section refer to the group $\boldsymbol{G}_4$.

sumed to have signature $(- + + + - +)1$. It corresponds to the gravitation-characterizing metric of general relativity. Equation *a*) is the new «law of gravitation» in which, as sources of the g_{MN} field appear the symmetric energy tensors, T_{MN}, U_{MN}, traceless energy tensors of the potentials φ_M and F_M resp., P_{MN} $(P \neq 0)$ the energy tensor of the field ϱ, and Σ_{MN}, Λ_{MN} interaction energy tensors. The tensor g_{MN} then is determined as a function of *all* the energy present. (This was of course true already in projective relativity). As will emerge in Section **6**, g_{MN}'s geometric rôle is to define angle in the space of physical experience. Length as an invariant concept is absent there.

With the identification of F_M as the electromagnetic potentials, equation *c*) (along with $F_{MN} \equiv \partial_{[M} F_{N]}$) are the Maxwell laws with source terms depending on the fields φ_P and ϱ. Since matter (Dirac field) is not in this unified field theory (see Section **7**, Generalization), this is a contribution to the effective current which will be superimposed on the electric current.

ϱ and φ_M will be called «mesons» in a tentative interpretation, for by $(4.10)'$ *b*) and *d*) they are, in the language of particle theory, particles of integral spin and non-zero rest mass. They are scalar and vector mesons resp., (under $\boldsymbol{G}_4$) and transform under $\boldsymbol{J}$ as indicated in (4.11). A third scalar meson φ_5 has been suppressed by assuming this field constant (but occurs in (4.7). Equation *d*), the scalar meson equation, says that the Laplacian of ϱ plus a «mass-like» term which however involves the gradient of ϱ instead of ϱ itself, equals a certain source strength. Since $\varrho \equiv \frac{1}{2} f_5$, it is seen that this meson is connected geometrically with the EM potentials rather than with the vector meson φ_M.

Equation *b*) is a vector meson equation of form which recalls those that have been studied [7], [8]. A mass term $\varphi_P(2(\varrho)^2\delta^P_M - 2\varrho_M\varrho)^P$ is included. This is of course compatible with the inclusion of general relativity in the theory since mass here is not represented by a number m, the «gravitational mass», but by certain tensors which depend on *all* the energy present. (Take trace of *a*). One gets $R/(1-(\varphi)^2)$; and g_{MN}, hence R is a function of all energy present as remarked above). The mass term is also compatible with the invariance under $\boldsymbol{J}$ («gauge invariance») as shown explicitly in the last section. A source term depending on ϱ and F_M is present. Remark: a meson theory starting from *b*) with these latter two terms omitted would, besides losing all geometrical meaning, prove unsatisfactory practically on the grounds that it would thereby lose «gauge invariance». When the theory is generalized to Spinor Relativity, a Dirac-type current term occurs here also (as well as providing extra terms in all the other field equations of course).

Perhaps the most obvious success of this theory from the physical point of view is this demonstration that unified field theory can produce meson equations, scalar and vector, automatically gauge invariant and compatible with the representation of mass à la general relativity, alongside the gravi-

tational and electromagnetic laws. And it is philosophically satisfying to know that their appearance is due to the introduction of the conformal geometry into the local spaces, for that it being necessary to enlarge the matrix of quadric coefficients (the 4×4 g_{MN} and 5×5 $\gamma_{\alpha\beta}$ of general and projective Relativity, resp.) to the 6×6 $\delta_{\mu\varrho}$ of conformal Relativity.

The field laws, which must be considered as a whole, thus provide a suggested non-linear theory of gravitation, electro-magnetism, and several «mesons». The non-linearity manifests itself not only in bi-linear coupling terms between fields but also, more subtly, in the presence of the g_{MN} and their first derivatives in the covariant differentiation in *b*), *c*), and *d*). For by *a*), g_{MN} is in turn a function of these other fields.

The more general field equations (4.7) describe, besides the previously discussed fields (recognized by the identifications of last section), the extra scalar meson φ_5. In general all fields are functions of position *and* gauge. The additions brought the field equations by φ_5 are complicated. The question of whether φ_5 occurs in nature or should be definitely eliminated by a constraint is here left open.

With the present interpretations of the fields, two conjectures of a general nature can be made. First, if these equations do describe one or more kinds of meson, since the EM and gravitational fields admit classical field interpretations, the equations suggest that the mesons described equally should admit classical field interpretation. Conversely, if the mesons described admit satisfactory interpretation when the corresponding theories given by (4.10)′ are quantized, gravitation should admit a corresponding statistical interpretation, (the quantum interpretation of the Maxwell theory being well known). *That is, may be both classical and statistical meanings are simultaneously possible for all fields involved, the observational interpretation of the field symbol being of course different in the two cases.* These remarks are necessarily vague, in the absence of much extra work. The quantization of non-linear theories has been investigated by Bergmann [9].

The second conjecture is an explanation of the inadequacy of flat-space (linear) theories, of the kind encountered in quantum field theories, in the domain of the nucleus or, precisely, in regions of great energy density. Ever since general relativity, there has been no doubt that gravitational energy bends space. As an inevitable extension of this idea, this and other unified field theories predict that *all* kinds of energy, irrespective of «kind», bend space. Eq. (4.10)′ *a*) is the quantitative formulation of this, associating a curvature with any given energy distribution. Now according to *b*), *c*), *d*), the *EM* and meson equations will have more or less classical form where the energy is tenuous and thus the g_{MN} are approximately constant in suitable cartesian coordinates. But in regions of violent potential gradients, the g_{MN} will not be even approximately constant; terms in the covariant derivatives in

(4.10)′ *b*), *c*), and *d*) which were neglected in the flat approximation will no longer be negligible, in fact may become the leading terms (9). The theories become essentially non-linear. For this reason it seems that the hope that linear theories can finally be found which will be valid in all domains is completely untenable optimism. Moreover, if one admits that non-linear terms must be added, these field equations give the unique form of that non-linearity which is geometrically meaningful. Alternatively, proceeding ad hoc, one is confronted with a bewildering array of possible non-linearities to try. A remark which may be interesting physically is that due to the characteristic quadratic form of the energy source terms in *a*), the non-linear terms occurring in the covariant derivatives in, e.g., the vector meson equation contain cubic terms in the potential vector.

Another remark which may have light to shed on the apparent multiplicity of elementary particle masses observed in nature is that rest mass (once suitably defined a posteriori as in general relativity) [10] is *no* invariant wrt the class of physically equivalent observers of this theory. See remark in the kinematical discussion of the Principal Theorem of Section **6**.

One final remark: no interesting pure number constants of nature are produced at this stage in unified field theory. But it is a fact that on going to Spinor Relativity (introduction of matter), an array of pure (rational) numbers is produced, which occur as coupling coefficients between the matter terms and these occurring already in Conformal Relativity. These occur as linear combinations of certain coefficients which generalize the combination coefficients ${}_pC_q$ of ordinary probability theory and arise on solving for the linear connection in spin space in terms of the quantities of Conformal Relativity. If numbers such as ${}^1{}_{137}$ can be produced by unified field theory, they should probably be looked for at this stage.

6. – The Geometry.

A) *The Local Geometry.*

In any geometric field theory, the *geometry in the large* (def.: the manifold (curvilinear) geometry) implies the corresponding flat geometry in the local spaces at each manifold point. In this theory, we start with a curvilinear five-dimensional projective geometry H_5 with homogeneous coordinates X^μ as geometry in the large; thus at every point X^μ there is a local flat five-dimen-

(9) This suggests that the discrete, quantum effects, which are today taken care of as eigenvalues of an operator, might be explainable here as due to « bumps » of sharp curvature in the manifold.

sional projective geometry $P_5(X^\mu)$ with homogeneous coordinate Z^a, say, $(a = 0, 1, \ldots, 5)$. The group against which all our formalism is covariant is that of arbitrary (allowable) coordinate transformations $Z^{a'} = A^{a'}_b(X^\mu)Z^b$ in the local P_5's. In the case that both (a') and (b) are holonomic systems (say (μ') and (ν) resp.) then the transformation $A^{\mu'}_\nu = \partial_\nu X^{\mu'}$ can be induced by a coordinate transformation in the manifold; in all other cases the $A^{a'}_b(X^\mu)$ are local transformations which are non-holonomic, defined by any homogeneous $A^{a'}_b(X^\mu)$, with inverse. Because the local spaces are projective, $A^{a'}_b$ and $\tau(X^\mu)A^{a'}_b$ are the *same* transformation since τZ^a and Z^a are considered the same projective vector (« point ») in the same coordinates, (more generally, $T^{a\cdots}_{b\cdots}$ and $\tau^d T^{a\cdots}_{b\cdots}$ for any integer d are the same projective tensor in the same coordinates). Combining these statements, we can say that the group against which our formalism is covariant is that of all (non-singular) *collineations* in the local P_5's, conceived as coordinate transformations.

Accordingly, the field equations $H_{ab} = 0$ (eq. (3.5) or (3.5)′) under any collineation $A^{a'}_b$ obey

$$H_{a'b'} = A^{a,b}_{a'b'}H_{ab} = 0\,. \tag{6.1}$$

H_{ab}, as a fixed differential expression in tensors, S_{ab}, A^c_e, (cf. eq. (3.6)) *is itself a tensor*, so that $H_{a'b'}$ is the same function of the tensors $S_{a'b'}$, $A^c_{e'}$ in the new system (a') as H_{ab} is of the tensors S_{ab}, A^c_e in the old system (a). [This remarkable property is of course common to all the tensorial differential forms of tensors which define the various laws of physics]. Emphasizing this fact, we rewrite (6.1)

$$H_{a'b'}(S_{c'd'}, A^e_{f'}) = A^{a,b}_{a'b'}H_{ab}(S_{cd}, A^e_f) = 0\,, \tag{6.1}'$$

where the kernel H thereby denotes the fixed differential expression in the indicated tensor arguments defined by the field laws (3.5) (or (3.5)′) together with the decomposition (3.6). We are insisting on this obvious fact because of its fundamental importance for the theorem which follows shortly.

Superimposed on H_5, we are given the symmetric tensor $S_{\mu\varrho}$ which determines a quadric Q

$$S_{ab}Z^aZ^b = 0\,, \qquad : Q \tag{6.2}$$

in each local P_5. This is the geometric meaning of $S_{\mu\varrho}$ and the reason for its appearance in the theory; let it be emphasized that therefore any skew part would be geometrically meaningless. Now whenever a quadric exists, the group of (real) point transformations $Z^a = P^a{}_b\bar{Z}^b$ taking the quadric into

itself is immediately singled out for special attention. The condition for that is that $\bar{Z}^b$ be on Q if Z^a is on Q, or

$$S_{ab}P^a{}_cP^b{}_d = hS_{cd} \qquad \text{(for some } h\text{)}. \tag{6.3}$$

(It follows that $h > 0$ and $h^6 = (\mathrm{Det}\, P^a{}_c)^2$). The $P^a{}_b$ form the group of *quadric collineations* in P_5 wrt the quadric Q: obviously from (6.3) they form a $6^2 - \frac{1}{2}6(6+1) = 15$ parameter group. Since S_{ab} is a function of the manifold point: $S_{ab}(X^\mu)$, so is $P^a{}_b$: $P^a{}_b(X^\mu)$. The significance for physics of this group is that under $P^a{}_b$, conceived as a local coordinate transformation $(a)\to(\bar{a})$: $A^{\bar{a}}_b \equiv P^a{}_b$ (for the time being let a, b, c.... and $\bar{a}$, $\bar{b}$, $\bar{c}$, resp. denote the same integer), the field equations (6.1) have an extra invariance property in addition to the tensorial invariance, guaranted for *all* collineations, expressed by (6.1). For by (6.3) (in which the $P^a{}_b$ have been normalized so that $h=1$ without destroying generality, since they are collineations) the components of $S_{\mu\varrho}$ in the new system $(\bar{a})$ are equal, component by component, to the components in the old, (a)

$$S_{\bar{a}\bar{b}} = S_{ab} \ ;$$

hence substituting for $S_{\bar{a}\bar{b}}$ in (6.1)′ we get

$$H_{\bar{a}\bar{b}}(S_{c\bar{d}}, A^{\bar{e}}_{\bar{e}}) = P^f{}_aP^g{}_bH_{fg}(S_{ad}, A^e{}_e) = 0. \tag{6.4}$$

That is, if we restrict transformations to the quadric collineation group in each local space, the field equations transform tensorially by means of the $P^a{}_b$ but the components of the fundamental tensor S_{cd} figuring in them remain numerically unaltered throughout the whole group. [To be remarked here: if (a) is chosen so that S_{ab} reduces to constant values, e.g.

$$-S_{00} = S_{11} = S_{22} = S_{33} = -S_{44} = S_{55} = +1 \ ; \qquad S_{ab} = 0 \ , \quad (a \neq b),$$

then all physical fields are comprised in the $\Omega_{ab}{}^c$. These geometrical objects, functions of the A^ϱ_e defined by (2.2) have the transformation rule

$$\Omega_{\bar{a}\bar{b}}{}^{\bar{c}} = A^{\bar{c}}_h(A^{f\,g}_{\bar{a}\bar{b}}\Omega_{fg}{}^h - \partial_{\bar{a}}A^h_{\bar{b}}), \tag{6.5}$$

and so the transformation $A^\varrho_e \to A^{\bar{\varrho}}_{\bar{e}} = P^f{}_eA^\varrho_f$ indicated explicitly in (6.4) induces the transformation of the physical fields Ω (6.5) in which $A^{\bar{a}}_{\bar{b}} \equiv P^a{}_b$. It is worth noting that if the S_{ab} are constants over the manifold, then so are the $P^a{}_b$; hence by (6.5) the physical fields $\Omega_{ab}{}^c$ transform like tensors under quadric collineations]:

Let the special invariance property expressed by (6.4) be called *invariance in form* because of the invariability of S_{cd}. It is of course no different in

principle from the Lorentz invariance of special relativistic theories. It means that the systems (a), (a), (a), ... connected by quadric collineations are indistinguishable as far as criteria of distinguishability furnished by the quadric are concerned. How far this is the same as physical equivalence, what this has to do with the relative motion of physically equivalent observers, is settled by the Principal Theorem of this section.

Before we state this theorem, we must define what we mean by the *physical group* and *physical geometry* of any relativity. (In this section the generic class of relativities comprising affine (or «general»), projective, conformal, and Spinor relativities will be studied, and the concepts introduced will apply equally well to all of them).

In defining the physical geometry of any relativity, we depart from the fundamental principle that the velocity of light must *be the same* for all physically equivalent observers. In each relativity we will define the local (space-time) X_4 — provided with angle defining constant form, g_{mn}, defined up to a non-constant factor — imbedded in each local space. Then the analytical expression of the above principle is that only point transformations which are conformal i.e., carry the null curves $ds^2 = 0$ into themselves, will be allowed in defining transformations between physically equivalent observers. In the local space of each relativity, we are given a quadric. Then the group of quadric collineations (point transformations) in the local space induces a group of point transformations in its local X_4 via the imbedding equations. Let the *physical group* of the relativity denote the intersection of this group with the group of conformal point transformations in X_4. [This will be *the* group of local point transformations which both preserve light velocity and the *invariance in form* of the field equations]. The physical group so defined will later be interpreted as a *coordinate* transformation group. And, in the sense of F. KLEIN [11], let the *quadric geometry* and *physical geometry* denote the set of all geometric definitions and properties invariant under and under only the quadric group and physical group, resp.

Principal Theorem of Conformal Relativity.

The quadric geometry and physical geometry of Conformal Relativity coincide, and the physical geometry is the conformal-flat metric geometry C_4 of signature $(+\,+\,+\,-)$1.

To prove the first part of the theorem, all we must show is that every quadric collineation in P_5 is a conformal point transformation of X_4 (and thus belongs to the physical group). The second part asserts [10] that *every* con-

[10] This in view of the fact that the conformal-flat (metric) geometry of an X_n is by definition the Klein geometry defined by the group of conformal point transformations in X_n.

formal transformation of X_4 belongs to the physical group and thus is a quadric collineation. Thus together they say that the quadric group in P_5 *is* (i.e., is isomorphic to) the conformal group of X_4. This is a well known result, first stated by F. KLEIN [12]; we will merely sketch a variant proof below.

Choose coordinates (a) in P_5 such that the quadric becomes

$$S_{ab}Z^aZ^b \equiv S_{mn}Z^mZ^n - 2Z^0Z^5 = 0\,. \tag{6.6}$$

We will now make a 1–1 correspondence between Z^a on Q and points θ^m of a certain four-dimensional manifold. Define

$$\theta^m = Z^m/Z_0\,, \tag{6.7}$$

with inverse

$$\tau Z^0 = 1\,, \quad \tau Z^m = \theta^m, \quad \tau Z^5 = \tfrac{1}{2}\, g_{mn}\theta^m\theta^n = \tfrac{1}{2}(\theta)^2\,, \tag{6.7$'$}$$

(τ a proportional factor)

where $g_{mn} \equiv S_{mn}$ will be the angle-defining tensor in X_4. [Geometrically these formulae represent stereographic projection of Q from the point Φ^a on Q which is $(0, 0, 0, 0, 0, \varrho)$ in these coordinates onto the hyperplane H_6 tangent to Q which is $Z^5 = 0$ in these coordinates. The stereographic correspondence can be viewed in various inhomogeneous coordinates in P_5 by taking sections of the quadric cone with the corresponding hyperplanes. The inhomogeneous coordinates employed above use the polar hyperplane of Φ^a as hyperplane at infinity — hence the quadric is the paraboloid

$$g_{mn}\xi^m\xi^n - 2\xi^5 = 0 \qquad (\xi^a \equiv Z^a/Z^0)$$

wrt the five rectilinear affine coordinates ξ^a of the five dimensional manifold X_5 of P_5, and X_4 is simply the hyperplane $\xi^5 = 0$ in X_5]. Then a (normalized) quadric collineation $Z^c = P^c{}_a\bar{Z}^a$, where

$$S_{cd}P^c{}_aP^d{}_b = S_{ab}\,, \tag{6.8}$$

induces the transformation of X_4 given by

$$\theta^m \equiv Z^m/Z^0 = \frac{P^m{}_a\bar{Z}^a}{P^0{}_a\bar{Z}^a} = \frac{P^m{}_0 + P^m{}_n\bar{\theta}^n + \tfrac{1}{2}P^m{}_5\,(\bar{\theta})^2}{P^0{}_0 + P^0{}_n\bar{\theta}^n + \tfrac{1}{2}P^0{}_5\,(\bar{\theta})^2}\,, \tag{6.9}$$

where $(\bar{\theta})^2 \equiv g_{mn}\bar{\theta}^m\bar{\theta}^n$. The coefficients in (6.9) are restricted by (6.8) so that

these transformations of X_4 are a 15-parameter group, as remarked above. But now if $\partial\theta^m/\partial\bar{\theta}^n$ be computed from (6.9), it can be verified [13] that

$$g_{mn}\frac{\partial\theta^m}{\partial\bar{\theta}^p}\frac{\partial\theta^n}{\partial\bar{\theta}^q} = \lambda g_{pq} \qquad [\lambda(\bar{\theta}^p) > 0]\,, \tag{6.10}$$

hence every transformation (6.9) *is conformal* when angle is defined in the usual way with the g_{mn}. But since there are ∞^{15} of them, we get all conformal transformations of X_4 this way ([11]). Since « quadric collineation », « stereographic projection of Q onto X_3 » and « conformality of a transformation in X_4 » are coordinate-free notions, it follows that we have proved the theorem, except for verifying the signature.

X_4 is thus proved to have a conformal-flat metric geometry C_4 under the physical group, which means that only angle is invariant under its defining group of point transformations (and under no larger group). Equivalently stated, the physical geometry C_4 is a four dimensional manifold X_4 with angle-defining tensor $\varrho(\theta^p)g_{mn}$ defined only up to a non-constant multiple $\varrho(\theta^p)$ of the g_{mn} (constant in each local X_4) provided by a solution of field equations. By (6.6) and the assumed signature $(-+++-)1$ of $S_{\mu\varrho}$, it follows that $g_{mn} \equiv S_{mn}$ has signature $(+++-)1$. This completes the proof.

Remark: The stereographic projection defined by (6.7), (6.7)′ maps *all* points Z^a of P_5 1-1 onto hyperspheres of X_4 with centers θ^m and radii R via

$$\theta^m = Z^m/Z^0\,, \qquad R^2 = S_{ab}Z^aZ^b/(Z^0)^2, \quad \text{inverse}$$
$$\tau Z^0 = 1\,, \qquad \tau Z^m = \theta^m, \qquad \tau Z^5 = \tfrac{1}{2}[(\theta)^2 - R^2]\,.$$

[Geometrically, the polar hyperplane of Z^a cuts Q in a circle which is projected into a hypersphere of X_4. (6.7), (6.7)′, considered a map onto spheres instead of points of X_4, maps the Z^a on Q onto the degenerate spheres (« light cones ») of X_4 with centers (vertices) θ^m and $R = 0$. The importance of the above extended map is then that it shows the physical meaning of the five independent coordinates of our manifold X_5 of Conformal Relativity. The generalized event in the local space, (θ^m, R^2) is a *sphere*, or point in space-time *plus some standard reference length* R, chosen arbitrarily. (A conformal transformation in X_4 takes this sphere into another sphere with an in general different radius $R' \neq R$ (if $R \neq 0$). Hence the new reference length is different. Time-like and space-like « spheres » occur (R imaginary and real, resp.). The introduction of general affine or projective coordinates, x^a or X^μ resp., mixes these (θ^m and R^2) in a general way. Conformal Relativity is thus a « gauge

([11]) The conformal group in X_n is a $\frac{1}{2}(n+1)(n+2)$ parameter group.

theory » with length absent as an invariant concept. Therefore it should be emphasized that in this theory there is no need for arbitrary fiats like the cylinder-condition to eliminate the fifth dimension — the fifth dimension with its perfectly good « four-dimensional » meaning is an essential part of it.

Now the important question must be answered: what are the preferred coordinate systems of the conformal-flat metric geometry C_4 — that is, what is the class of coordinate systems connected by conformal point transformations *interpreted as coordinate transformations in* C_4? [E.g., this preferred class for R_4 is that of all (say right-angled) cartesian coordinate systems — we seek the corresponding answer here]. Now since the stereographic projection (6.7), (6.7)′ provides 1–1 correspondence between certain rectilinear affine coordinate systems (m) in X_4 and certain other (a) in P_5, we can define this class equally well in either space. Most simply we can say that the preferred class of coordinate systems is all systems in $P_5(X^a)$ in which the $S_{ab}(X^a)$ have some arbitrary but fixed set of values. For this is just the class of coordinate systems connected by quadric collineations interpreted as coordinate changes in P_5: $A^{a'}_{b} = P^a{}_b$ $(b' = b)$, and we know that the quadric collineation is the representation in P_5 of a conformal transformation in X_4.

However, if one has prejudices against talking about bigger spaces and bigger geometries, the above can be stated completely equivalently in four-dimensional language using only geometric notions proper to four dimensions, as follows. Make the simple coordinate change

$$Z^{5^*} = \tfrac{1}{2}(Z^0 - 2Z^5), \quad Z^{0^*} = \tfrac{1}{2}(Z^0 + 2Z^5), \quad Z^{m^*} = Z^m, \quad (m^* = m)$$

from the coordinates of (6.6) so that the quadric becomes

$$(6.6)' \qquad S_{a^*b^*}Z^{a^*}Z^{b^*} \equiv g_{mn}Z^{m^*}Z^{n^*} + (Z^{5^*})^2 - (Z^{0^*})^2 = 0 \qquad (m, n = m^*, n^* \text{ resp.}).$$

Then these Z^a (dropping the * henceforth) are *hexaspherical coordinates* of X_4 defined by the above transformation together with (6.7), (6.7)′; that is, coordinates referring points of X_4 to six coordinate real hyperspheres in X_4. (Each set of rectilinear affine coordinates θ^m is assigned an auxiliary R_4: $(m) \to R_4[(m)]$, in which it is interpreted as a cartesian coordinate system for which the metric is g_{mn}. Thus length, hence spheres, and thus the hexaspherical coordinates $(a) \longleftrightarrow (m)$ for each (m) are definable). There are six coordinates for an X_4 because they are homogeneous and also satisfy a quadratic homogeneous identity: (6.6)′. Z^a has the geometrical meaning of the ratio of the *power* of the point θ^m wrt the a-th coordinate sphere to its radius (when g_{mn} is diagonal). The exigencies of space forbid a complete exposition; for the details on polyspherical coordinates, the reader is referred to F. Klein, *Vorlesungen über Höhere Geometrie*, 3rd ed., p. 19. Then the importance of

hexaspherical coordinates for C_4 is contained in the following statement:

Hexaspherical coordinate systems are the preferred systems of a C_4,

by which we mean, to repeat, that a conformal point transformation $\bar{\theta}^m = f^m(\theta^p)$ interpreted as a coordinate transformation $\theta^{m'} = f^{m'}(\theta^p)$ in C_4 carries [12] one such system into another. The proof will not be given here for reasons of space; the following remarks will have to suffice:

1) The reason is of course that while hyperplanes, say, are not carried into hyperplanes by a general conformal transformation and hence would not serve as coordinate surfaces for C_4, nevertheless hyperspheres do go into hyperspheres and therefore serve as coordinate surfaces.

2) A hypersphere in X_4 wrt hexaspheric coordinates Z^a is simply a linear locus $\overset{a}{\Sigma}_a Z^a = 0$. That is, the tensor $\overset{a}{\Sigma}_a$, transforming cogrediently to Z^a, represents a hypersphere. In the hexaspheric coordinates (a), the six *coordinate* spheres $\overset{a}{\Sigma}_b$ (a labels the sphere) have the form $\overset{a}{\Sigma}_b = \delta^a_b$ (these are the six spheres $\theta^m = 0$ $(m = 1, \ldots, 4)$, $(\theta)^2 = 1$, $(\theta)^2 = -1$). The conformal coordinate transformation of the θ^m is represented by the linear coordinate transformation of Z^a defined by $A^{a'}_b = P^a{}_b$. Then the coordinate hyperspheres $\overset{a'}{\Sigma}_{b'}$ $(= \delta^{a'}_{b'})$ of the coordinates (a') have the components in (a): $\overset{a'}{\Sigma}_b = \overset{a'}{\Sigma}_{c'} A^{c'}_b = \delta^{a'}_{c'} P^c{}_b = P^a{}_b$ $(a = a')$. Summarizing, the conformal point transformation $\bar{\theta}^m = f^m(\theta^p)$ defined by $P^a{}_b$ can be interpreted as the conformal coordinate transformation $\theta^{m'} = f^{m'}(\theta^p)$ in C_4 from spheres $Z^a = 0$ to the spheres $P^a{}_b Z^b = 0$ as coordinate spheres resp. of (a) and (a'), $((a)$ and (a') corresponding to (m) and (m'), resp.). This is what the underlined statement supra asserts.

Fine points: in the preferred coordinate systems defined, we always have $\tau Z^m = \theta^m$, which means that four coordinate spheres have degenerated into hyperplanes, so that Z^m are simply the cartesian coordinates wrt these coordinate hyperplanes in $R_4[(m)]$ up to a proportionality factor.

Note that the general conformal coordinate transformation, although a coordinate transformation of C_4 as just shown, is *no* coordinate transformation in any one R_4. For θ^m and $\theta^{m'}$ are cartesian systems in *different* R_4's: $R_4[(m)]$ and $R_4[(m')]$ resp. Relative to $R_4[(m)]$, $\theta^{m'}$ are *not* cartesian — in fact by (6.10)

$$(6.10)' \qquad g_{m'n'} = \lambda g_{mn} \qquad (m'n' = m, n \text{ resp.})$$

and $\lambda = |\mathrm{Det}\, \partial\theta^p/\partial\theta^{p'}|^{1/2}$ is non-constant.

[12] This means by definition that referring points to the coordinate surfaces, transformed by the inverse transformation has the same effect as referring the transformed points to the untransformed coordinate surfaces.

The requirement that only real fields and coordinates appear in the theory together with the known space-time signature sig g_{mn} *uniquely* fixes the signature of S_{ab} as (sig g_{mn}, $+1$, -1). For the sign difference in the last two entries is necessary for the reality of the hexaspheric coordinates — equivalently, for the reality of the P_5 [12].

The discussion of the conformal group from the kinematical point of view will be briefly postponed until after the analogous theorems are proved for the previous two relativities. Since they together with Conformal and the later-to-be introduced Spinor Relativity form a generic class, the same definitions apply and the line of attack is the same.

In projective relativity we have a curvilinear projective geometry H_4 in the large, local P_4's at each manifold point; and a superimposed symmetric tensor $\gamma_{\mu\nu}$ of signature $(- + + + -)1$ which gives a quadric

$$\gamma_{ab} Y^a Y^b = 0 \,, \tag{6.11}$$

in each local P_4. [in this part, let $\mu, \nu, \xi, \ldots, \tau = 0, 1, \ldots, 4$ denote holonomic systems, for which the homogeneous coordinates X^μ exist, and $a, b, c \ldots, g = 0, 1, \ldots, 4$ denote general holonomic or non-holonomic systems. Y^a will be coordinates in local P_4's]. But here, the presence of a quadric is geometrically somewhat anomalous. The field equations express the same minimum curvature property (L given by (2.3)). The unspecified projective connection Γ turns out to be necessarily the Christoffel symbols of $\gamma_{\mu\nu}$ via the field equations (3.2), and the final field equations have the form (3.5)′ with (3.6).

The field equations are covariant against the group of all (non-singular) collineations in the local P_4's. The subgroup of *quadric collineations* $Q^a{}_b$ taking (6.11) into itself:

$$\gamma_{cd} Q^c{}_a Q^d{}_b = k \gamma_{ab} \qquad \text{(follows } k > 0\text{)}, \tag{6.12}$$

are again singled out for special attention. Under this *quadric group* the field equations are *invariant in form* ((6.4)), the γ_{ab} remaining numerically fixed throughout the group.

The physical group of projective relativity has been defined. Now we can state the corresponding:

Principal Theorem of Projective Relativity.

The quadric geometry and physical geometry of Projective Relativity do *not* coincide, and the physical geometry is the flat metric geometry R_4 of signature $(+ + + -)1$.

We must show first that there exist quadric collineations of P_4 which are not conformal point transformations of X_4, and second that the physical group is the whole orthogonal group in an R_4 of signature $(+ + + -)1$.

Choose coordinates (a) in P_4 such that the quadric becomes

$$\gamma_{ab}Y^aY^b \equiv \gamma_{mn}Y^mY^n - (Y^0)^2 = 0\,. \tag{6.13}$$

Define the X_4 of rectilinear affine coordinates θ^m by $\theta^m = Y^m/Y^0$; inverse $\tau Y^0 = 1$, $\tau Y^m = \theta^m$. [In this case X_4 is of course the whole manifold of P_4]. Let $g_{mn} \equiv \gamma_{mn}$ be the angle-defining tensor of X_4 in the coordinates θ^m.

Then a quadric collineation $Y' = Q^c_a \overline{Y}^a$ induces the transformations of X_4 given by

$$\theta^m = Y^m/Y^0 = \frac{Q^m{}_0 + Q^m{}_n\bar{\theta}^n}{Q^0{}_0 + Q^0{}_n\bar{\theta}^n}\,. \tag{6.14}$$

These form a $5^2 - \frac{1}{2}5(5+1) = 10$ parameter group by (6.12). But these transformations are conformal only if $Q^0{}_n = 0$, (geometrically speaking, only if the hyperplane at infinity for the inhomogeneous coordinates θ^m: $Y^0 = 0$ is fixed). But then it follows from (6.12) that these reduce to the orthogonal group in an R_4

$$\theta^m = Q^m{}_n\bar{\theta}^n\,, \qquad g_{mn}Q^m{}_pQ^n{}_q = g_{pq} \qquad (Q \text{ normalized}),$$

which is certainly conformal. The orthogonal group in R_4 is only 6-parameter; hence there are quadric collineations which are not conformal, which was to be proved. [This fact is the substance of A. EINSTEIN's objections to projective relativity as I understand them; he objects that the projective formalism is superfluously big since there exist transformations under which the field equations are invariant in form, but which correspond to no transformation between physically equivalent observers]. Since the physical group has been shown to be the *whole* orthogonal group, the physical geometry is R_4 with metric g_{mn} of signature $(+\,+\,+\,-)1$, as one sees by comparing the assumed signature of $\gamma_{\mu\nu}$ with (6.13). Viewing the physical group as coordinate instead of point transformations, one now asks what are the preferred coordinate systems of an R_4? These are the cartesian systems as is well known.

Fine point: One of the objectionable features inherent in projective relativity was the arbitrariness of signature of $\gamma_{\mu\nu}$. It was proposed to choose between $(\pm\,+\,+\,+\,-)1$ on physical grounds, since a priori criteria were lacking [2]. On the other hand, in Conformal Relativity as previously remarked the signature of $S_{\mu\varrho}$: (sig g_{mn}, $+1$, -1) is completely determined by the signature of g_{mn}. Of course, the greatest such arbitrary element in projective relativity was the appearance of the quadric itself; for by the above theorem, the quadric group is anomalously *too big* for the physics of the si-

tuation. In Conformal Relativity, where the quadric has the sole meaning of defining the conformal geometry of X_4, the quadric group is *just big enough* to embrace all physically equivalent observers.

In affine («general») relativity, one starts with a curvilinear affine four-dimensional geometry A_4 in the large; local E_4's (def.: flat four-dimensional affine geometry) at each manifold point; and a superimposed symmetric tensor g_{MN} (metric) of signature $(+\,+\,+\,-)1$, which gives a quadric

$$g_{mn}\theta^m\theta^n - 1 = 0\,, \tag{6.15}$$

in each local E_4. [In this part $M, N, P, \ldots, R = 1, \ldots, 4$ denote holonomic systems, for which the coordinates x^M exist, and $m, n, p, q, \ldots, r = 1, \ldots, 4$ denote general (holonomic or non-holonomic) systems. Let θ^m denote rectilinear affine coordinates in local E_4's]. The field equations express the minimum curvature property (Lagrangian of form (2.3)). Thereby the affine connection Γ, a priori independent of g_{MN}, is fixed as the Christoffel symbols of the metric ((3.2)). The final field equations have the form [13] (3.5) with (3.6).

The field equations are covariant against the group of all (non-singular) *affinities* (i.e., affine transformations) in the local E_4's [13]. The subgroup of *quadric affinities* $\theta^m = a^m_n\bar{\theta}^n$ taking the quadric (6.15) into itself;

$$g_{mn}a^m{}_p a^n{}_q = g_{pq}\,, \tag{6.16}$$

forms the *quadric group* under which the field equations are *invariant in form*. The physical group being defined, one can state:

The Principal Theorem of Affine Relativity.

The quadric geometry and physical geometry of Affine Relativity coincide, and the physical geometry is the flat metric geometry R_4 of signature $(+\,+\,+\,-)1$.

The proof is obvious. Here the local X_4 is the whole manifold of the corresponding local E_4. The quadric group by (6.16) is the whole orthogonal group in an R_4, hence the quadric and physical geometries are the same. Length is thus definable and invariant under the physical group and no larger group, so the physical geometry is by definition R_4 with metric g_{mn}. Last, g_{MN} is of signature $(+\,+\,+\,-)1$ by assumption, which completes the proof.

The physical group, viewed as coordinate transformation group, again has cartesian systems as preferred coordinate systems.

[13] The field equations of general relativity are usually written in a form covariant only against holonomic transformations.

Remark: Thus affine relativity, having just the same physical geometry as projective relativity, avoids the anomalous relation between the quadric and physical geometries of the latter. But their common physical group is not big enough to embrace all physically equivalent observers (according to our definition).

Now for the physical interpretation of the foregoing theorems: Lorentz covariant theories were originally introduced to be consistent with the notion of an invariant *light cone* (cone with null-generators); of course they went beyond this requirement in bringing in also an invariant length. As we have seen, this invariant length has been retained in the physical geometries of both general and projective relativity. The physical group of Conformal Relativity, however, requires only the invariant light cone and dispenses with the length.

The kinematical interpretation of the general conformal coordinate transformation is as important for this theory as is the well-known interpretation of the (proper) orthogonal subgroup in terms of observers moving with constant relative velocity for special relativity. It was known to J. HAANTJES in 1940 [14] that the conformal coordinate transformations corresponding to inversions in hyperspheres represented observers moving with constant relative acceleration, and that every constant relative acceleration could be so obtained (uniquely, when natural restrictions were imposed). Since now all the rest of the conformal transformations are similarity transformations (orthogonal transformations, dilatations, and translations), which correspond to constant relative velocities of observers, we see that *the whole conformal group represents changes of system between observers (Cartesian reference frames) moving relative to one another with uniform accelerations, and every uniform acceleration is so represented.* The formerly considered Lorentz transformations in particular form a subgroup of *zero* relative accelerations.

The conformal transformations representing changes between systems in uniform relative acceleration along one direction build a one parameter Abelian group in which the relative acceleration is very simply read off from the formulae in much the way that this is done for the relative velocity in the usual analogous treatment of the proper Lorentz group. Precisely ([14]),

$$\theta^{1'} = \frac{\theta^1 + \tfrac{1}{2}\,\alpha(\theta)^2}{1 + \alpha\theta^1 + \tfrac{1}{4}\,\alpha^2(\theta)^2}, \qquad \theta^{i'} = \frac{\theta^i}{1 + \alpha\theta^1 + \tfrac{1}{4}\,\alpha(\theta)^2}, \qquad (\theta)^2 = g_{mn}\theta^m\theta^n,$$

$$(i', i = 2, 3, 4),$$

represents a uniform acceleration α (units: $c = 1$) of the system (m') wrt

([14]) HAANTJES [14], eq. (2.18). A sign difference is due to the fact that he takes the signature of g_{mn} to be $(- - - +)$1.

the system (m) along the θ^1 axis. The world lines of physical observers wrt the R_4 of any one of them are circles (with imaginary time) or hyperbolae with real time. These hyperbolae have *null* asymptotic directions i.e., their associated (relative) velocities are always bounded above by light velocity (which is of course the same for all observers by the invariance of the ligth cone). For other details, especially on the « gauge » trasformation of rest mass connected with a conformal transformation, see the cited work of HAANTJES. (Non zero) length is no longer an invariant, by which we mean the following: since each observer (m) has his private $R_4[(m)]$ in which θ^m are cartesian coordinates, two observers in relative acceleration will not agree on the metric. Given the vector $\xi^{m'}$, (m') computes the (length)^2 as $g_{mn}\xi^{m'}\xi^{n'}$ (m', $n' = m$, n resp.) whereas (m) computes it as $g_{m'n'}\xi^{m'}\xi^{n'} = \lambda g_{mn}\xi^{m'}\xi^{n'}$($m'$, $n' = = m$, n resp.) by (6.10)′. For (m) considers (m') a non-cartesian system in $R_4[(m)]$ wrt to which a constant gravitational field, reflected by the non-constant metric $g_{m'n'} = \lambda g_{mn}$, exists. This is all just to say that an invariant length does not exist for C_4. Therefore it should be possible theoretically to test this theory by observing one of the supposed fundamental constant lengths of nature from two systems which are in sufficiently high relative acceleration to predict an observable difference of measured length.

HAANTJES states that as far as *EM* phenomena go, the physical geometry is C_4, not R_4. *In Conformal Relativity where all field equations (including gravitation!) are conformally invariant in form, the statement that the physical geometry is C_4 can be made without any qualification — it is the Principal Theorem.* (Nor is this statement invalidated when the transition to the relativity containing matter (section 7) is made, the physical geometry there is still C_4). In view of the kinematic interpretation above, the principle here which corresponds to the Principle of Relativity in special relativity states: The nature laws « look the same » (i.e., are *invariant in form*) for all observers in uniform relative acceleration. With respect to the preferred class of hexaspherical coordinates in C_4 they take on their « simplest form ».

In the light of the foregoing theorems it will be seen that the physical fields described in any of the relativities have essentially the same geometric rôle, which is given by the following characterization:

The rôle of physical fields in a relativity is to determine a quadric in each local space which defines the class of physically equivalent observers associated with the relativity as those systems which are indistinguishable with respect to the quadric. Indistinguishable here means that the quadric is carried into itself by any transformation between systems viewed as a point transformation. One needs only to add the footnote that in the anomalous case of projective relativity, the non-conformal transformations must be deleted. It is worth remarking that this principle is still valid in the bigger relativity which includes matter (section 7) due essentially to the (1–1) isomorphism which exists between

transformations in spin space carrying the linear family of involutions $\eta_\varrho{}^a{}_b$ (η_ϱ in matrix nôtation), such that

$$\eta_{(\varrho}\eta_{\tau)} = S_{\varrho\tau} \qquad \text{(matrix multiplication)}$$

into itself and the group of quadric collineations considered in this theory [15].

This must suffice for the analysis of the local geometry — the exigencies of space do not permit a full treatment of the details, of which only the most important have been treated above.

As the final sub-section of this section, we append the following, which may be of some mathematical interest.

This theory has necessarily introduced the notion of a conformal geometry *in the large* which we will now formalize by some definitions. It bears some resemblance to O. VEBLEN's geometry of «conformal tangent spaces» [13], but then there are essential differences.

Recall that an *ordinary* conformal space C_n is an ordinary (real) $n-1$-dimensional projective space P_{n+1} together with all its points Z^a which lie on a given quadric

$$S_{ab}Z^aZ^b = 0 \qquad : Q.$$

Furthermore we make the 1–1 coordinate free correspondence $\overset{A}{T}_b$ [16], inverse $\underset{A}{T}{}^b$, (stereographic projection) of Q onto the X_n with rectilinear affine coordinates θ^m

$$\theta^m = \overset{m}{T}_aZ^a/\overset{0}{T}_aZ^a\,,$$

with inverse

$$\tau\overset{0}{T}_aZ^a = 1\,, \quad \tau\overset{m}{T}_aZ^a = \theta^m, \quad \tau\overset{n+1}{T}_aZ^a = \tfrac{1}{2}\,(\theta)^2 \qquad [(\theta)^2 \equiv g_{mn}\theta^m\theta^n]\,,$$

where

$$S_{ab}\underset{A}{T}{}^a\underset{B}{T}{}^b \equiv G_{AB}\,; \quad G_{mn} \equiv g_{mn}\,, \quad G_{0n+1} = -1\,, \quad \text{others zero,}$$

and g_{mn} is the angle-defining symmetric form of C_n in the coordinates θ^m. The signature of S_{ab} must be chosen, by these equations, (sig g_{mn}, $+1, \cdots -1$). [Other stereographic projections work equally well, of course; the one above is the one actually used before in this section]. Remark: The stereographic projection gives a 1–1 map of all points of P_{n+1} onto hyperspheres of C_n,

[15] This is described in more detail in Section 7.

[16] The indices A, B, ... directly above and below the kernel T are not subjected to transformations.

the points on Q going into hyperspheres with $R = 0$, as remarked before Thus the whole of P_{n+1} is « used » in defining C_n.

Then an allowable transformation of P_{n+1} (collineation) taking Q into itself, $P^a{}_b$, is a conformal point transformation in C_n via the stereographic projection.

This said, we can simply define a curvilinear (or « general ») conformal space K_n, say, as follows:

A curvilinear conformal space K_n is nothing more than an $n+1$-dimensional manifold X_{n+1} with the corresponding ordinary conformal gometry C_n at each manifold point.

Thus it is defined by replacing P_{n+1} by H_{n+1} ($n+1$-dimensional curvilinear projective space, homogeneous manifold coordinates X^μ) in the former definition, and noting that Z^a, S_{ab}, $\overset{A}{T}_b$ and G_{AB} there are now in general non-constant functions of the manifold point X^μ. Corresponding, the θ^m become the coordinates of the *local* X_n of the *local* C_n.

The allowable transformations of H_{n+1} taking Q into itself are all quadric collineations $P^a{}_b(X^\mu)$. These may or may not, depending on S_{ab}, contain *holonomic* quadric collineations — namely those for which there exist functions $\overline{X}^\mu(X^\varrho)$ (homogeneous of degree $+1$) such that $P^\mu{}_\nu \equiv \partial_\nu \overline{X}^\mu$.

The study of the C_4 with g_{mn} of signature $(+\ +\ +\ -)1$ from the physical point of view (the identification of θ^m as space-time, the sphere (θ^m, R^2) as generalized event, observers as cartesian reference frames, the conformal transformation as uniform acceleration of observer, etc.) forms the subject matter of the Special Theory of Conformal Relativity. The study of the corresponding K_4 subjected to the minimum curvature requirement is the subject matter of the General Theory of Conformal Relativity. In the latter theory, in addition to kinematical results in each local C_4 already from the Special Theory, one gets laws governing various « force » fields.

7. – Generalization.

This theory has allowed generalization to a yet bigger relativity, called Spinor Relativity because of its characteristic local spaces, which actually introduces matter in the form of a generalized Dirac theory. Let it be emphasized at the outset that it is actually a « relativity », belonging to the generic class already defined, whose members are built upon the model of general relativity with its essential simplicity and freedom from arbitrary elements. Former theories of the electron in conjunction with gravitation etc. all without exception had the common feature that they did *not* geometrize the electron. By that I mean that there was no geometrical unification of all fields treated — the ordinary dynamically suggested Dirac Lagrangian, covariantized against

various groups, was simply, added to the Lagrangian of the other fields (which itself sometimes has a simple geometric meaning). Clearly, this or that covariantization of the Dirac theory is far short of unification; the application of the word «unified» to such theories, which was sometimes made, is certainly an inadmissibly loose usage of the term.

Spinor Relativity is a *unified* theory with matter, and moreover, as a *relativity*, is the simplest possible such unified theory, taking general relativity to be the criterion of this simplicity. Because unified, it enjoys the freedom from arbitrary elements with which non-unified theories are plagued. First we will characterize it in skeletonized form from the strictly mathematical point of view just as the former relativities were characterized, then examine in a few remarks the more important physical implications. Unfortunately the theory cannot be adequately summarized in the space allowed here.

Conformal Relativity must be properly included. In addition, the description of matter requires the introduction of particles of half-integral spin; that is, the local spaces whose quantities go to build the Lagrangian must be spin-spaces (of some dimension). These two requirements uniquely fix the relativity as the following.

We start with a curvilinear projective geometry H_5 in the large, local P_5's at each manifold point. Superimposed on this we are given a set of six (normalized) anticommuting involutions $\eta_a{}^\alpha{}_\beta$ ($a = 0, 1, \ldots, 5$) in local complex seven-dimensional projective spaces $P_7{}^*$ ($\alpha, \beta \quad 1, \ldots, 8$) with squares $(- + + + - +)1$ when (a) in P_5 is chosen to put the quadric of Conformal Relativity S_{ab} in principal axes form. They thus obey

$$\eta_{(a}\eta_{b)} = S_{ab}A\,, \qquad \text{(matrix notation; matrix multiplication)}$$

$A(\equiv A^\alpha{}_\beta)$ the identity tensor in $P_7{}^*$, for (a) any system in P_5. The $2^{6/2}=8$-dimensional spin space S_8 of P_5 is simply this $P_7{}^*$ provided with the set η_a. In addition to the η_a, a particular point (vector) ψ^α in $P_7{}^*$ is singled out. The η_a define a linear family of involutions $\Lambda(\equiv \Lambda^\alpha{}_\beta)$

$$\Lambda = Z^a\eta_a \qquad \cdot\ (Z^a \text{ in } P_5),$$

in each local S_8 (the locus here corresponding to the quadric in the former relativities).

A projective connection $\Gamma_{\alpha\beta}{}^\gamma$ of the S_8's can be defined *which is essentially different from all those previously considered in that it arises from a generalized notion of covariant differentiation in spin spaces and effectively treats the differentiation index on an equal footing with the others* (see remark later). Γ is *uniquely* determined as a function of S_{ab} *and* ψ. Also the η_a bring with them

an array of fundamental tensors in S_8 [17] one of which can be used as metric. With Γ and this metric, the curvature invariant $\mathcal{R}$ is formed and the «total» curvature over the manifold is formed:

$$L \equiv \int \mathcal{R}\sqrt{g}\,(\mathrm{d}X)\,.$$

The field equations $\delta L = 0$ express the minimum curvature property. They have the characteristic form for a relativity already given ((3.5) or (3.5)′ with (3.6)).

The field equations are covariant against the group of all (non-singular) collineations in local S_8's («changes of representation»), and all(non-singular, real) collineations in local P_5's. The subgroup (of collineations in S_8) formed by those $T(=T^{\alpha}{}_{\beta})$ which take the linear family of involutions into itself

$$T(Z^{\alpha}\eta_{\alpha})\bar{T}^{-1} = \bar{Z}^{\alpha}\eta_{\alpha} \qquad \text{(for some } \bar{Z}^{\alpha} \text{ in } P_5),$$

whence follows

$$T\eta_{\alpha}\bar{T}^{-1}P^{\alpha}{}_{b} = \eta_{b} \qquad \text{(for some real } P^{\alpha}{}_{b}), \tag{7.1}$$

is singled out for special attention. Call this the «involution group» for convenience, and let the «involution geometry» designate the Klein geometry of this group, as usual. By the above equation, each $T \to P^{\alpha}{}_{b}$, $P^{\alpha}{}_{b}$ a collineation in P_5, which in turn induces a transformation in the local X_4's of Conformal Relativity. This correspondence then defines the physical group and physical geometry of Spinor Relativity. But now by what might be called the fundamental theorem of spin space [18], the correspondence $T \longleftrightarrow P^{\alpha}{}_{b}$ given by (7.1) is a (1–1) isomorphism between the involution group of T's and *the group of* (*normalized*) *quadric collineations* $P^{\alpha}{}_{b}$

$$S_{ab}P^{a}{}_{c}P^{b}{}_{d} = S_{cd}\,.$$

Thus the physical group of Spinor Relativity is no bigger than that of Conformal Relativity (as was desired), namely all conformal transformations in the local X_4's. We infer first that the field equations of this theory are *invariant in form* under the involution group (S_{ab} numerically invariant, or equivalently, the $\eta_{\alpha}{}^{\alpha}{}_{\beta}$ numerically invariant if T and the corresponding $P^{\alpha}{}_{b}$ are simultaneously performed, cf. (7.1)) and second the:

[17] See say Schouten [16], II.
[18] See say Veblen and Givens [15], chap. V.

Principal Theorem of Spinor Relativity.

The involution geometry and the physical geometry of Spinor Relativity coincide, and the physical geometry is the conformal-flat metric geometry C_4 of signature $(+ + + -)$1.

The preferred coordinate systems of X_4 are hexaspherical; of P_5, those allowable systems connected by quadric collineations; of S_8, those allowable systems connected by collineations of the involution group. This finishes the mathematical skeletonization of the theory.

From the physical point of view:

1) The most remarkable fact then to emerge is that these field equations actually give a (generalized) Dirac equation and the Conformal Relativity field equations modified by the addition of Dirac-type terms (energy, current, etc.) all with the correct reality properties and occurring in the expected places. Here is the place to note that the heart of the matter is the generalized linear connection Γ in spin space. It can be shown that the Dirac equation *cannot* occur in a theory built around the curvature tensor of a conventional spin-connection of the kind used heretofore.

2) The interpretation of the fields in the field equations is of course left open for the moment. In particular the question of whether they must all be quantized, all classical fields, or something else again. One knows a good classical field interpretation of g_{mn} and a good quantum field interpretation of the Dirac ψ. These field equations then assert that *at least* one interpretation must serve for all fields.

3) Since matter is now in a unified field theory via the vector ψ (interpretation not yet certain), one can hope at last to dispense with the representation of matter as singularities which was necessary in all relativities up to this one.

4) The most striking formal difference with the classical Dirac theory is that here we have an eight rather than four dimensional spin space. It is conjectured that this is an advantage for the physics of the situation, for it will allow ψ to represent particle and anti-particle as parts of one entity. Another point: the group theoretical paradox of an energy of indefinite sign under the complete Lorentz group in the c-number Dirac theory is avoided in this theory.

5) An array of (« non-trivial ») pure (rational) numbers occurs in coupling positions between matter terms and the others. When these are determined, there is good hope that the pure number constants of nature which occur here will be found.

6) The physical geometry is C_4: an invariant length does not exist, the invariance of the light cone is the sole criterion of physical equivalence. All field equations, in particular the generalized Dirac equation, are invariant in form against the whole conformal group; kinematically, they are in their « simplest form » with respect to the class of all observers in uniformly accelerated relative motion.

Appendix I.

The variation of the Lagrangian (2.3) is much simplified if we perform it for N expressed in terms of a holonomic system (μ); the resulting equations can then be written in terms of any system (a) by expressing them in covariant form.

Consider first $\delta\Gamma_{\mu\lambda}{}^{k}$ satisfying the usual boundary conditions:

$$\text{(A1.1)} \qquad \delta L = \int S^{\nu\lambda}\delta N_{\nu\lambda}\sqrt{S}\,(\mathrm{d}X) = \\ = \int S^{\nu\lambda}\sqrt{S}\,[\nabla_{\nu}(\delta\Gamma_{\varrho\lambda}{}^{\varrho}) - \nabla_{\varrho}(\delta\Gamma_{\nu\lambda}{}^{\varrho}) + 2\delta\Gamma_{\xi\lambda}{}^{\varrho}\Gamma_{[\nu\varrho]}{}^{\xi}]\,(\mathrm{d}X)\,.$$

(Note that $\delta\Gamma_{\mu\lambda}{}^{k}$ is a tensor, so that this variation will yield tensor laws). We have used the more general identity

$$\delta N_{\mu\nu\lambda}{}^{k} = \nabla_{\nu}(\delta\Gamma_{\mu\lambda}{}^{k}) - \nabla_{\mu}(\delta\Gamma_{\nu\lambda}{}^{k}) + 2\delta\Gamma_{\xi\lambda}{}^{k}\Gamma_{[\nu\mu]}{}^{\xi}\,.$$

Manipulating (A1.1) by partial differentiation,

$$\text{(A1.2)} \qquad \delta L = \int [\nabla_{\nu}(S^{\nu\lambda}\delta\Gamma_{\varrho\lambda}{}^{\varrho}) - \nabla_{\varrho}(S^{\nu\lambda}\delta\Gamma_{\nu\lambda}{}^{\varrho}) - \\ - \nabla_{\nu}S^{\nu\lambda}\,\delta\Gamma_{\varrho\lambda}{}^{\varrho} + \nabla_{\varrho}S^{\nu\lambda}\,\delta\Gamma_{\nu\lambda}{}^{\varrho} + 2S^{\nu\lambda}\,\delta\Gamma_{\xi\lambda}{}^{\varrho}\Gamma_{[\nu\varrho]}{}^{\xi}]\sqrt{S}\,(\mathrm{d}X)\,.$$

To transform the first two terms, we make use of the easily proved lemma where V^{k} is a vector such that it vanishes on the boundary:

$$\int \nabla_{\mu}V^{\mu}\sqrt{S}\,(\mathrm{d}X) = \int - V^{\mu}H_{\mu}\sqrt{S}\,(\mathrm{d}X)\,, \qquad H_{\mu} \equiv \partial_{\mu}\log\sqrt{S} - \Gamma_{\lambda\mu}{}^{\lambda}\,.$$

Then (A1.2) becomes

$$\text{(A1.3)} \qquad \delta L = \int \delta\Gamma_{\nu\lambda}{}^{\varrho}[\nabla_{\varrho}S^{\nu\lambda} - A^{\nu}_{\varrho}\nabla_{\xi}S^{\xi\nu} + S^{\nu\lambda}H_{\varrho} - A^{\nu}_{\varrho}S^{\xi\lambda}H_{\xi} + 2S^{\xi\lambda}\Gamma_{[\xi\varrho]}{}^{\nu}]\,V\sqrt{S}\,(\mathrm{d}X).$$

Introduce the tensor $H^{\nu\lambda}{}_{\varrho}$ defined by

$$\text{(A1.4)} \qquad H^{\nu\lambda}{}_{\varrho} \equiv \nabla_{\varrho}S^{\nu\lambda} + S^{\nu\lambda}H_{\varrho} + 2S^{\xi\lambda}\Gamma_{[\xi\varrho]}{}^{\nu} - {}^{2}/_{5}A^{\nu}_{\varrho}S^{\xi\lambda}\Gamma_{[\xi\tau]}{}^{\tau}\,.$$

Then (A1.3) can be written

$$\delta L = \int \delta\Gamma_{\nu\lambda}{}^{\varrho}[H^{\nu\lambda}{}_{\varrho} - A^{\nu}_{\varrho}H^{\xi\lambda}{}_{\xi}]\sqrt{S}\,(\mathrm{d}X)\,. \tag{A1.5}$$

Before writing down the field equations it is convenient to transform $H^{\nu\lambda}{}_{\varrho}$ by making the substitution

$$\bar{\Gamma}_{\nu\lambda}{}^{\varrho} \equiv \Gamma_{\nu\lambda}{}^{\varrho} + {}^{2}/_{5}A^{\varrho}_{\lambda}\Gamma_{[\xi\nu]}{}^{\xi}.$$

To note that $\bar{\Gamma}$ *is* a connection ((*k*) holonomic) and that in addition it satisfies

$$\bar{\Gamma}_{[\tau\lambda]}{}^{\tau} = 0\,.$$

Then from (A1.4) (after combining the first and third terms on the right):

$$H^{\nu\lambda}{}_{\varrho} = \partial_{\varrho}S^{\nu\lambda} + S^{\xi\lambda}\bar{\Gamma}_{\xi\varrho}{}^{\nu} + S^{\nu\xi}\bar{\Gamma}_{\varrho\xi}{}^{\lambda} -$$
$$- {}^{2}/_{5}S^{\xi\lambda}A^{\nu}_{\varrho}\Gamma_{[\tau\xi]}{}^{\tau} - {}^{2}/_{5}S^{\nu\xi}A^{\lambda}_{\xi}\Gamma_{[\tau\varrho]}{}^{\tau} - {}^{2}/_{5}A^{\nu}_{\varrho}S^{\xi\lambda}\Gamma_{[\xi\tau]}{}^{\tau} + S^{\nu\lambda}H_{\varrho} = \bar{\nabla}S^{\nu\lambda}_{-+} + S^{\nu\lambda}H_{\varrho}\,,$$

where [19]

$$\bar{\nabla}_{\varrho}S^{\nu\lambda}_{-+} \equiv \partial_{\varrho}S^{\nu\lambda} + S^{\xi\lambda}\bar{\Gamma}_{\xi\varrho}{}^{\nu} + S^{\nu\xi}\bar{\Gamma}_{\varrho\xi}{}^{\lambda}\,,$$

and [20]

$$\bar{H}_{\varrho} \equiv H_{\varrho} - {}^{2}/_{5}\Gamma_{[\tau\varrho]}{}^{\tau} = \partial_{\varrho}\log\sqrt{S} - \bar{\Gamma}_{\tau\varrho}{}^{\tau}\,.$$

Therefore the field equations $\delta L = 0$ are, referring to (A1.5):

$$0 = H^{\nu\lambda}{}_{\varrho} = \bar{\nabla}_{\varrho}S^{\nu\lambda}_{-+} + S^{\nu\lambda}\bar{H}_{\varrho}\,.$$

These can be given the equivalent form

$$0 = \bar{\nabla}_{\varrho}S_{\nu\lambda}{}^{\nu\lambda}_{-+} - S_{\nu\lambda}H_{\varrho}, \tag{A1.6}$$

using $S_{\nu\lambda}S^{\lambda k} = S^{k\lambda}S_{\lambda\nu} = A^{k}_{\nu}$ (i.e., in which no use is made of the assumed symmetry of $S_{\nu\lambda}$).

Expanding $\bar{\nabla}_{\varrho}S_{\nu\lambda}{}^{\nu\lambda}_{-+}$ and multiplying (A1.6) by $S^{\nu\lambda}$, one derives

$$\bar{H}_{\varrho} = 0\,,$$

[19] The (+ −) differentiation notation is that of EINSTEIN for the four-dimensional affine case. The index with a minus subscript has the two covariant indices of the connection transposed in the term where the quantity is contracted with the connection in this index.

[20] Note $\bar{H}_{\varrho}$ is a vector due to $\bar{\Gamma}_{\tau\lambda}{}^{\tau} = \bar{\Gamma}_{\lambda\tau}{}^{\tau}$ ((λ) hol.), although H_{ϱ} was not.

where use has been made of $\Gamma_{\tau\varrho}{}^{\varrho} = \bar{\Gamma}_{\varrho\tau}{}^{\tau}$. Therefore finally

$$\bar{\nabla}_{\varrho} S_{\nu\lambda} = 0 . \tag{A1.7}$$

An equivalent form of (A1.7), sufficient for our purposes, is given by ([21])

$$a) \qquad \bar{\Gamma}_{[\nu\lambda]}{}^{k} = h^{k\varrho}[\overset{(\ )}{\nabla}_{\varrho} S_{[\nu\lambda]} - \tfrac{1}{2}\, \partial_{<\varrho} S_{[\nu\lambda]>}] ,$$

$$b) \qquad \bar{\Gamma}_{(\nu\lambda)}{}^{k} = \left\{ \begin{matrix} k \\ \nu\lambda \end{matrix} \right\}_{h} + I_{\nu\lambda}{}^{k} ,$$

where

$$c) \qquad I_{\nu\lambda k} = S_{[\nu\xi]} \bar{\Gamma}_{[k\lambda]}{}^{\xi} + S_{[\lambda\xi]} \bar{\Gamma}_{[k\nu]}{}^{\xi} ,$$

and $\left\{ \begin{matrix} k \\ \nu\lambda \end{matrix} \right\}_{h}$ denotes the Christoffel symbols of $h_{\lambda\xi} = S_{(\lambda\xi)}$, $h^{k\varrho}$ $(= h^{(k\varrho)})$ are the normalized cofactors of $h_{\lambda\xi}$; all indices are raised with $h^{k\varrho}$; the symbol $\langle\ \rangle$ bracketing several indices means that the sum of all the cyclic permutations is to be taken; and $\overset{(\ )}{\nabla}_{\varrho}$ denotes covariant differentiation wrt $\bar{\Gamma}_{(\varrho\lambda)}{}^{k}$. Then the solution of $\nabla_{\varrho} S_{\nu\lambda} = 0$ is reduced to solving the implicit equation c) for the tensor $I_{\nu\lambda}{}^{k}$. In our case of symmetric $S_{\mu\lambda}$, the solution is very simple:

$$\bar{\Gamma}_{[\nu\lambda]}{}^{k} = 0 , \qquad \bar{\Gamma}_{(\nu\lambda)}{}^{k} = \left\{ \begin{matrix} k \\ \nu\lambda \end{matrix} \right\}_{S} .$$

Appendix II.

First we compute a series of necessary expressions, starting with the Christoffel symbols of the first kind of the $\gamma_{\alpha\beta}$:

$$[mn, 5]_{\gamma} = \partial_{[M} \varphi_{N)} \equiv \Pi_{MN} ,$$

$$[5m, n]_{\gamma} = \partial_{[M} \varphi_{N]} \equiv \Phi_{MN} ,$$

$$[mn, p]_{\gamma} = [MN, P]_{g} + 2\varphi_{(M} \Phi_{NP)} + \varphi_{P} \Pi_{MN} ,$$

other $$[\alpha\beta, \gamma]_{\gamma} = 0 ,$$

([21]) Cf. Ingraham: *Ann. of Math.*, **52**, 743, eq. (2) and (4).

where $[MN, P]_g$ are the Christoffel symbols of the first kind of the g_{MN}. Then

$$\left\{ \begin{matrix} p \\ mn \end{matrix} \right\}_\gamma = \left\{ \begin{matrix} P \\ MN \end{matrix} \right\}_g + 2\varphi_{(M}\Pi_{N)}^{\ P},$$

$$\left\{ \begin{matrix} 5 \\ mn \end{matrix} \right\}_\gamma = -\varphi_P \left\{ \begin{matrix} P \\ MN \end{matrix} \right\}_g - 2\varphi_P\varphi_{(M}\Phi_{N)}^{\ P} + \Pi_{MN},$$

$$\left\{ \begin{matrix} n \\ 5m \end{matrix} \right\}_\gamma = \Phi_M^{\ N}, \qquad \left\{ \begin{matrix} 5 \\ 5m \end{matrix} \right\}_\gamma = \varphi_P \Phi^P_{\ M}, \qquad \left\{ \begin{matrix} 5 \\ 55 \end{matrix} \right\}_\gamma = 0.$$

$\left\{ \begin{matrix} P \\ MN \end{matrix} \right\}_g$ are the Christoffel symbols (of the second kind) of the g_{MN}; where for any t_P, $t^Q = t_P g^{PQ}$, g^{PQ} the normalized cofactors of g_{PQ}. The relations of φ^P and g^{PQ} to $\gamma_{\alpha\beta}$,

$$g^{pq} = \gamma^{pq}, \qquad \varphi^P = -\gamma^{pj},$$

which follow from (4.11), have been used.

Another useful relation is γ (def.: Det $\gamma_{\alpha\beta}$) $= g$ (def.: Det g_{MN}) as follows easily from (4.11).

Then

$$R_{mn}(\{\}_\gamma) = R_{MN}(\{\}_g) + 2\Phi^P_{\ M}\Phi_{PN} - 2\varphi_{(M}\overset{g}{\nabla}_{|P|}\Phi_{N)}^{\ P} - \varphi_N\varphi_M(\Phi)^2,$$

$$R_{5m}(\{\}_\gamma) = \overset{g}{\nabla}_P \Phi^P_{\ M} - \varphi_M(\Phi)^2,$$

$$R_{55}(\{\}_\gamma) = -(\Phi)^2, \qquad [(\Phi)^2 \equiv \Phi^P_{\ Q}\Phi_P^{\ Q}],$$

$$R\ \ (\{\}_\gamma) = R(\{\}_g) + (\Phi)^2,$$

where we note that $R_{MN}(\{\}_g)$ is the ordinary Ricci tensor of $\left\{ \begin{matrix} P \\ QR \end{matrix} \right\}_g$. $R(\{\}_g) = g^{PQ}R_{PQ}(\{\}_g)$, and $\overset{g}{\nabla}_P$ means covariant differentiation wrt the $\left\{ \begin{matrix} P \\ QR \end{matrix} \right\}_g$. Hence

$$\text{(A2.1)} \qquad G_{mn}(\{\}_\gamma) = G_{MN}(\{\}_g) + 2T_{MN} - 2\varphi_{(M}\overset{g}{\nabla}_{|P|}\Phi_{N)}^{\ P} - \\ - \tfrac{1}{2}\varphi_M\varphi_N R(\{\}_g) - \tfrac{3}{2}\varphi_M\varphi_N(\Phi)^2,$$

$$G_{m5}(\{\}_\gamma) = \overset{g}{\nabla}_P \Phi^P_{\ M} - \tfrac{1}{2}\varphi_M[3(\Phi)^2 + R(\{\}_g)],$$

$$G_{55}(\{\}_\gamma) = -\tfrac{3}{2}(\Phi)^2 - \tfrac{1}{2}R(\{\}_g),$$

where $G_{MN}(\{\}_g)$is the Einstein tensor fnuction or $R_{MN}(\{\}_g)$ and T_{MN} is a traceless expression given by

$$T_{MN} \equiv \Phi^P_{\ M}\Phi_{PN} - \tfrac{1}{4}g_{MN}(\Phi)^2.$$

Now it remains to break up the tensor $E_{\alpha\beta}$ with the followingi identifications

$$\partial_{[M}F_{N]} \equiv F_{MN} \equiv f_{mn}\,, \qquad \partial_M \varrho \equiv \varrho_M \equiv f_{m5} \quad (= \tfrac{1}{2}\,\partial_m f_5)\,,$$

which define F_N and ϱ,

$$\begin{aligned} f^{mn} &= F^{\underline{M}\underline{N}} - 2\varrho^{[\underline{M}}\varphi^{\underline{N}]}\,,\\ f^{m5} &= -F^{\underline{M}}{}_{\underline{P}}\varphi^{\underline{P}} + \varrho^{\underline{M}} - \varphi^{\underline{M}}(\varrho\varphi)\,,\\ (f)^2 &= (F)^2 + 2(\varrho)^2 - 2(\varrho\varphi)^2 - 4(\varrho\varphi F)\,, \end{aligned}$$

with the notation

$$\begin{aligned} (f)^2 \equiv f^{\alpha\beta}f_{\alpha\beta}\,, \qquad (F)^2 \equiv F^{\underline{P}\,\underline{Q}}F_{PQ}\,,\\ (\varrho^2) \equiv \varrho_P\varrho^{\underline{P}}\,, \qquad (\varrho\varphi) = \varrho_P\varphi^{\underline{P}}\,, \qquad (\varrho\varphi F) \equiv \varrho^{\underline{P}}\varphi^{\underline{Q}}F_{PQ}\,. \end{aligned}$$

With these we compute

$$\text{(A2.2)} \qquad \left\{ \begin{aligned} E_{mn} &= U_{MN} + P_{MN} + 2F_{P(M}\varrho_{N)}\varphi^{\underline{P}} + \tfrac{1}{2}g_{MN}(\varrho\varphi)^2 + \\ &\quad + g_{MN}(\varrho\varphi F) - \tfrac{1}{4}\,\varphi_M\varphi_N\big[(F)^2 + 2(\varrho^2) - 2(\varrho\varphi)^2 - 4(\varrho\varphi F)\big]\,,\\ E_{m5} &= \varrho_P F^{\underline{P}}{}_M + \varrho_M(\varrho\varphi) - \tfrac{1}{4}\,\varphi_M\big[(F)^2 + 2(\varrho)^2 - 2(\varrho\varphi)^2 - 4(\varrho\varphi F)\big]\,,\\ E_{55} &= \tfrac{1}{2}(\varrho)^2 + \tfrac{1}{2}(\varrho\varphi)^2 - \tfrac{1}{4}(F)^2 + (\varrho\varphi F)\,, \end{aligned} \right.$$

where U_{MN} is a traceless expression and P_{MN} one with nonvanishing trace given by

$$\begin{aligned} U_{MN} &\equiv F^{\underline{P}}{}_M F_{PN} - \tfrac{1}{4}\,g_{MN}(F)^2\,,\\ P_{MN} &= \varrho_M\varrho_N - \tfrac{1}{2}\,g_{MN}(\varrho)^2\,. \end{aligned}$$

With (A2.1) and (A2.2), the expressions $\bar{G}_{\alpha\beta} = G_{\alpha\beta} - 2E_{\alpha\beta}$ can be decomposed.
Decomposing

$$G_{0\alpha} = -\overset{\gamma}{\nabla}_\beta f^\beta{}_\alpha = -\frac{1}{\sqrt{-\gamma}}\,\partial_\beta\,(\sqrt{-\gamma}f^\beta{}_\alpha) + f^{\beta\lambda}\partial_\beta\gamma_{\lambda\alpha}\,,$$

the same way, using $\gamma = g$ and identifications already introduced, yields for for the components $\bar{G}_{0P}$ and $\bar{G}_{05}$ wrt (A) of (4.10)

$$\left\{ \begin{aligned} \bar{G}_{0P} &\equiv \bar{G}_{0P} - \varphi_P\bar{G}_{05} = -\overset{g}{\nabla}_\varrho F^{\underline{Q}}{}_P + 2\overset{g}{\nabla}_\varrho(g^{QR}\varrho_{[R}\varphi_{P]})\,,\\ \bar{G}_{05} &= \bar{G}_{05} = -\overset{g}{\nabla}_P{}^{\underline{P}}\varrho + (F\Phi) - 2(\varrho\varphi\Phi)\,, \end{aligned} \right.$$

where $\overset{g}{\nabla}_P \overset{P}{-}_Q \varrho \equiv \overset{g}{\nabla}_P (g^{PQ} \partial_Q \varrho)$ is the Laplacian and

$$(\varphi)^2 \quad \varphi_P \varphi^P \,, \qquad (F\Phi) \quad F^{PQ} \Phi_{PQ} \,, \qquad (\varrho\varphi\Phi) \quad \varrho^P \varphi^Q \Phi_{PQ} \,.$$

With these, the field equations wrt the system (A), (4.10), become

$$a) \qquad G_{MN}(\{\}_g) + 2T_{MN} - 2U_{MN} - 2P_{MN} +$$
$$+ 4[\varphi_{(M}\varrho_{N)}(\varrho\varphi) - \tfrac{1}{2}\varphi_M\varphi_N(\varrho)^2 - \tfrac{1}{4} g_{MN}(\varrho\varphi)^2] +$$
$$+ 4[\varrho_P F^P{}_{(M}\varphi_{N)} - \varphi_P F^P{}_{(M}\varrho_{N)} - \tfrac{1}{2} g_{MN}(\varrho\varphi F)] \,,$$

$$b) \qquad \overset{g}{\nabla}_P \Phi^P{}_M + 2\varphi_M(\varrho)^2 - 2\varrho_M(\varrho\varphi) - 2\varrho_P F^P{}_M = 0 \,,$$

$$c) \qquad -\overset{g}{\nabla}_P F^P{}_M + 2\overset{g}{\nabla}_P(g^{PR}\varrho_{[R}\varphi_{M]}) + (\varphi)^2 \Phi_M \overset{P}{-}_P \varrho_P = 0 \,,$$

$$d) \qquad -\overset{g}{\nabla}_P \overset{P}{-}_Q \varrho + (F\Phi) - 2(\varrho\varphi\Phi) = 0 \,.$$

[Remark: take the trace of a), noting that all expressions there are traceless except $G_{MN}(\{\}_g)$, Σ_{MN}, P_{MN} This evaluates $(\varrho)^2$ in terms of $(\varphi)^2$ and $R(\{\}_g)$ as $(\varrho)^2 = \tfrac{1}{2} R(\{\}_g)/1 - (\varphi)^2]$.

RIASSUNTO (*)

Se si conservano gli angoli, ma si elimina una lunghezza (quadridimensionale) invariante da una descrizione essenzialmente einsteniana dell'universo, si ottiene la Relatività conforme. (L'invarianza degli angoli è la sola condizione richiesta per l'« invarianza del cono di luce », da parte di osservatori fisicamente equivalenti). La teoria speciale della relatività conforme studia la geometria conforme, che sostituisce la geometria di Lorentz della Relatività ristretta, dal punto di vista cinematico in un universo libero da campi di forze. La teoria generale tratta un universo dotato di geometria conforme curvilinea soggetta all'unica condizione di possedere curvatura « totale » minima. Le equazioni estremanti descrivono campi di forze che comprendono assieme ai soliti campi gravitazionali ed elettromagnetici, alcuni « mesoni ». La teoria generale è pertanto una teoria dei campi unificata, che, essendo modellata sulla relatività einsteniana, è completamente esente da elementi arbitrari. Il linguaggio matematico consente l'interpretazione in termini di concetti geometrici esclusivamente quadridimensionali.

(*) *Traduzione a cura della Redazione.*

BIBLIOGRAPHY

[1] J. A. Schouten: *Ann. Inst. H. Poincaré*, **5**, 51 (1935).
[2] W. Pauli: *Ann. der Phys.*, **18**, 305 (1933).
[3] O. Veblen and B. Hoffmann: *Phys. Rev.*, **36**, 810 (1930).
[4] E. Schrödinger: *Proc. Roy. Ir. Acad.*, **51** A, 63 (1947).
[5] E. Straus: *Rev. Mod. Phys.*, **21**, 414 (1949).
[6] A. Einstein: *Sitz. ber. d. Preuss. Akad. d. Wiss.*, **414** (1925).
[7] G. Wentzel: *Quantentheorie der Wellenfelder*, Chap. III.
[8] J. K. Lubanski and L. Rosenfeld: *Physica*, **9**, 117 (1942).
[9] P. G. Bergmann: *Phys. Rev.*, **75**, 680 (1949); P. G. Bergmann and J. H. M. Brunings: *Rev. Mod. Phys.*, **21**, 480 (1949).
[10] A. Einstein, L. Infeld and B. Hoffmann: *Ann. of Math.*, **39**, 65 (1938).
[11] O. Veblen and J. H. C. Whitehead: *Foundations of Differential Geometry* (Cambridge, 1932).
[12] F. Klein: *Math. Ann.*, **5**, 257 (1872).
[13] O. Veblen: *Proc. Nat'l. Acad. Sci.*, **14**, 725 (1928); **21**, 168 (1935).
[14] J. Haantjes: *Proc. Ned. Akad. v. Wet.*, **43**, 3 (1940).
[15] O. Veblen and W. Givens.: *Geometry of Complex Domains*, lectures given at the Inst. for Adv. Study, 1935-36.
[16] J. A. Schouten: *Proc. Kon. Akad. v. Wet.*, I, **52**, 178 (1949); II, **52**, 217 (1949); III, **52**, 336 (1949); IV, **53**, 41 (1950).

Sui livelli energetici dei nuclei pesanti.

F. Ferrari

Istituto di Fisica dell'Università, Istituto Nazionale di Fisica Nucleare - Sezione di Padova

C. Villi

Istituto di Fisica dell'Università - Trieste

(ricevuto il 16 Luglio 1952)

Riassunto. — Si calcola la densità dei livelli energetici dei nuclei pesanti tenendo conto delle interazioni nucleari e del loro effetto sulla dipendenza dell'energia di eccitazione dalla temperatura del nucleo.

1. – Da molteplici esperienze con neutroni lenti [1] è noto che i nuclei pesanti presentano un grande numero di livelli energetici, la cui densità aumenta fortemente con l'energia di eccitazione E del nucleo. Le ragioni teoriche per la loro esistenza sono state discusse da Bohr [2] e vari tentativi sono stati fatti per calcolare in base alle ipotesi estreme di debole [3] e forte [4] interazione nucleone-nucleone, la loro distanza media $D(E)$.

[1] R. Frisch e G. Placzek: *Nature*, **137**, 357 (1936); F. D. Weekes, M. S. Livingston e A. H. Bethe: *Phys. Rev.*, **49**, 471 (1936); F. Rasetti, C. Fink, H. H. Goldsmith e G. A. Mitchell: *Phys. Rev.*, **49**, 869 (1936); E. Amaldi e E. Fermi: *Ric. Sci.*, **1**, vol. 7-8 (1936); G. H. Collie: *Nature*, **137**, 614 (1936); R. H. Peck: *Phys. Rev.*, **76**, 1279 (1949); E. C. Pollard, P. L. Sailor e L. D. Wyly: *Phys. Rev.*, **75**, 725 (1949); H. L. Bradt e D. J. Tendam: *Phys. Rev.*, **72**, 1177 (1947); L. W. Seagondollar e H. H. Barshall: *Phys. Rev.*, **72**, 439 (1947); F. C. Shoemaker, J. E. Fawlkner, S. G. Kaufman e D. M. Bouricius: *Phys. Rev.*, **79**, 228 (1950).

[2] N. Bohr: *Nature*, **137**, 344 (1936); G. Breit e E. Wigner: *Phys. Rev.*, **49**, 519 (1936).

[3] H. A. Bethe: *Phys. Rev.*, **50**, 332 (1936); J. R. Oppenheimer e E. Serber: *Phys. Rev.*, **50**, 391 (1936).

[4] N. Bohr e F. Kalkar: *Dans. Akad.* (1939).

Le varie teorie prevedono una dipendenza di $D(E)$ da E regolata essenzialmente dalla funzione $\exp[E^m]$ ($m = 3/4$ per il modello reticolare e per quello a goccia in bassa energia; $m = 1/2$ per il modello a gas di Fermi). I risultati, in generale poco soddisfacenti, presentano solo accordo qualitativo con l'esperienza.

Anche trattazioni più elaborate [5], fondate sulla ipotesi che la profondità della buca di potenziale vari con la velocità della particella o che l'interazione tra due nucleoni sia rappresentabile nella forma $((1-g)P_M + gP_B)J(r)$, in cui P_B e P_M sono rispettivamente gli operatori di Heisemberg e Majorana e r la distanza tra due particelle, conducono ad una densità di stati al top della distribuzione di Fermi non atta a rendere conto delle evidenze sperimentali.

Una soluzione di compromesso è fornita dalla formula semi-empirica di Weisskopf [6] in cui la dipendenza della densità dei livelli $\varrho(E)$ da E è data da $\varrho(E) = C \cdot \exp[kE]^{1/2}$, dove $C = 0{,}2$ e $K = 26$ MeV^{-1} sono determinati in base ai livelli di risonanza dei neutroni. Questa relazione che è in discreto accordo con l'esperienza sino ad energie di eccitazione inferiori a 2 MeV, presenta uno scarto molto marcato per energie di eccitazione prossime all'energia di legame del neutrone.

In generale si può osservare che le previsioni basate sul modello di Fermi presentano un disaccordo molto più rilevante di quello ottenuto con il modello a goccia [7]. Quest'ultimo fornisce una densità di livelli intorno ai 9 MeV di eccitazione in buon accordo con le osservazioni eseguite sul Rh^{103}, mentre per basse energie l'accordo peggiora sensibilmente, pur essendo ancora rispettato l'ordine di grandezza.

I risultati negativi ottenuti con l'applicazione del modello a gas sono da imputarsi essenzialmente alla legge $E = bT^2$, valida per un gas ideale, ma non adeguata a descrivere il comportamento del nucleo eccitato a causa delle forti interazioni che sussistono tra i nucleoni. Una indicazione in questo senso è del resto fornita dalla stessa relazione di Weisskopf; infatti, tenendo conto del valore sperimentale di k e osservando che l'esponente $(kE)^{1/2}$ ha il ruolo di un'entropia, si ottiene per b il valore 6,5 MeV^{-1} ($A = 100$) invece di ~ 11 MeV^{-1}, come previsto dalla statistica di Fermi per un nucleo pesante standard. Una ulteriore conferma di questa insufficienza è data dal valore $b \sim 5$ MeV^{-1} trovato da Bardeen [5], in quanto, a causa delle interazioni nucleari, l'energia totale di una particella individuale nel nucleo dipende dal numero d'onda più fortemente dell'energia cinetica stessa.

---

[5] J. Bardeen: *Phys. Rev.*, **51**, 799 (1937).

[6] V. F. Weisskopf e D. H. Ewing: *Phys. Rev.*, **57**, 472 (1940); V. F. Weisskopf: *Lectures Series in Nuclear Physics* (Washington, D.C., 1947).

[7] H. Wergeland: *Fysik Verden*, 223 (1945).

Scopo della presente nota è il calcolo della densità dei livelli energetici dei nuclei pesanti in base al modello di Fermi, nel quale le interazioni tra i nucleoni che lo compongono sono interpretate come agitazione termica della materia nucleonica, secondo i criteri già elaborati in un precedente lavoro [8].

2. – A causa delle transizioni tra stati occupati e non occupati dovute alle interazioni tra i nucleoni, la funzione di distribuzione di Fermi risulta perturbata già per $T = 0$. Si può tener conto dell'effetto di queste interazioni individuando, secondo una legge opportuna, una temperatura equivalente τ, alla quale il nucleo può ancora riguardarsi come gas ideale ed essere trattato con la solita statistica. Il conseguente stato di agitazione termica della materia nucleonica comporta una energia latente di eccitazione del nucleo, la cui entità può essere valutata nel modo seguente.

Poichè l'energia cinetica media di un nucleone nel nucleo è $K^{(0)} = (3/5)\psi_0$ ($\psi_0 = 21$ MeV), segue dai calcoli di WATANABE [9] che l'eccesso di energia cinetica dovuto alle interazioni nucleari è, in seconda approssimazione, $K^{(2)}/K^{(0)} = 0{,}34$; quindi, in media, un nucleone possiede un eccesso di energia cinetica uguale a 4,2 MeV. Detto A il numero di massa, l'energia latente di eccitazione termica risulta $4{,}2A$ MeV. Per i nuclei pesanti ($A \geqslant 100$) l'entità di questa energia è tale che non appare lecito applicare le formule approssimate della statistica di Fermi vincolate alla condizione restrittiva $y = \tau/\psi(\tau) \ll 1$. In conseguenza, è più corretto discostarsi dal procedimento di WATANABE e individuare il valore del parametro descrittivo del gas relativo alla minima temperatura equivalente $(y)_{\tau=\tau_0} = a$ in base al risultato che l'energia latente termonucleare $E(\tau_0) = 4{,}2A$ è data dalla seguente relazione esatta della statistica di Fermi (cfr. I, 5):

$$E(\tau_0) = \frac{6C}{5}\left(\frac{A}{2C}\right)^{5/3}\{\mu^{-5/3}(a)\nu(a) - 1\}\,. \tag{1}$$

Nella (1) le funzioni $\mu(y)$ e $\nu(y)$ sono espresse dalle

$$\mu(y) = \int_{-1/y}^{\infty} \frac{(1+xy)^{3/2}e^x}{(1+e^x)^2}\,\mathrm{d}x\,; \qquad \nu(y) = \int_{-1/y}^{\infty} \frac{(1+xy)^{5/2}e^x}{(1+e^x)^2}\,\mathrm{d}x\,,$$

le quali, moltiplicate per $C\psi^{3/2}(\tau)$ e, rispettivamente, per $(3/5)C\psi^{5/2}(\tau)$ esprimono il numero di particelle e la loro energia totale. Risolvendo l'equazione (1),

[8] F. FERRARI e C. VILLI: *Nuovo Cimento*, **9**, 487 (1952). Questo lavoro verrà in seguito indicato con (I).

[9] S. WATANABE: *Zeits. f. Phys.*, **113**, 482 (1939).

invece del valore 0,29, cui conduce il procedimento di WATANABE [10], si trova, per un nucleo standard con $A = 100$, $a = 0{,}35$.

Estendendo il risultato di WATANABE, valido solo per $T = 0$, faremo l'ipotesi (I, 6) che la dipendenza fra la temperatura equivalente τ e quella effettiva T sia rappresentabile mediante la funzione-tentativo.

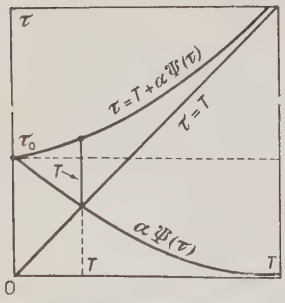

Fig. 1. – Andamento indicativo della funzione $\tau = T + a\psi(\tau)$.

$$\tau = T + a\psi(\tau)\,, \tag{2}$$

dalla quale, per $T = 0$, si ottiene $\tau_0 = a\psi(\tau_0) = 6{,}6583$ MeV, temperatura che corrisponde all'energia latente di eccitazione nucleare $E(\tau_0)$ precedentemente calcolata. La (2) è rappresentata, in modo puramente indicativo, nella fig. 1. La funzione $a\psi(\tau)$ decresce lentamente con l'aumentare della temperatura e ciò esprime il fatto fisico che l'effetto di perturbazione delle interazioni nucleari sulla funzione di distribuzione di Fermi diminuisce con l'aumentare di τ. Allo scopo di evitare la risoluzione grafica della (2), è conveniente assumere come unica variabile indipendente il parametro $y = \tau/\psi(\tau) \geqslant a$, tramite il quale si può descrivere il comportamento del gas nucleonico nella regione delle temperature equivalenti; dalla (2) si ottiene:

$$T = (y - a)\psi(\tau)\,. \tag{2a}$$

Infine, tenendo conto che il parametro descrittivo del gas reale alla temperatura effettiva T è $\eta = T/\psi(T)$, si trova immediatamente che y è legato a η dalla relazione:

$$\eta = (y - a)\cdot\frac{\tau}{T}\,\frac{\ln(1/\Lambda)}{\ln(1/\lambda)}\,, \tag{2b}$$

in cui Λ è il grado di degenerazione del gas nella regione delle temperature equivalenti ($\Lambda_0 = \exp[-1/a] = 0{,}0578 \leqslant \Lambda < 1$) e λ è il grado di degenerazione del gas reale alla temperatura T ($0 \leqslant \lambda = \exp[-1/\eta]$).

In vista del successivo calcolo della densità dei livelli energetici, limiteremo ogni considerazione a valori dell'energia di eccitazione E variabili tra $0 \leqslant E < 10$ MeV. Se i nucleoni del gas di Fermi non interagissero fra di loro ($a = 0$, $\tau_0 = 0$; $E(\tau_0) = 0$) in questo intervallo energetico sarebbe valida la

[10] L. ROSENFELD: *Nuclear Physics* (Amsterdam, 1948).

legge $E = bT^2$ con $b \sim 11$ MeV^{-1}. Siccome l'esistenza delle interazioni nucleari ($a \neq 0$) equivale ad un aumento di temperatura esso limita l'applicabilità dell'usuale procedimento deduttivo della suddetta relazione, il problema da risolvere consiste quindi nello stabilire, in base alla (2) e al valore calcolato nell'energia latente $E(\tau_0)$, quale relazione debba essere sostituita alla $E = bT^2$ per un gas reale obbediente alla statistica di Fermi.

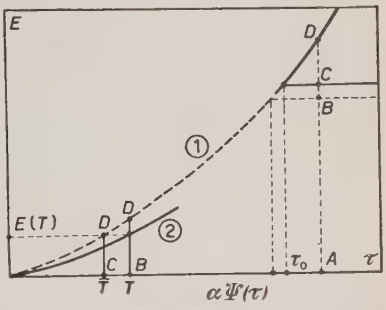

Fig. 2. – Trasformazione dell'equazione di stato di un gas di Fermi dalla regione delle temperature equivalenti a quella delle temperature effettive. Le curve indicative (1) e (2) si riferiscono rispettivamente al gas ideale e al gas reale con interazioni nucleari.

Una elementare considerazione fisica permette di prevedere che anche per il gas reale nella regione delle basse energie di eccitazione si avrà una dipendenza di E dal quadrato della temperatura T, ma non secondo una legge di semplice proporzionalità come nel caso del gas ideale. Infatti l'ipotesi del nucleo « caldo » porta come conseguenza che a parità di energia di eccitazione E, il gas reale (con interazioni) si trova ad una temperatura effettiva T maggiore della temperatura $\bar{T}$ alla quale si troverebbe lo stesso gas considerato come ideale (senza interazioni) (fig. 3). Siccome la statistica di Fermi è applicabile solamente ad un gas ideale, per quest'ultimo si potrà sempre scrivere la relazione $E = b\bar{T}^2$. Segue che per stabilire la nuova legge tra E e T basterà individuare la relazione che intercede tra $\bar{T}$ e T. Detta $\bar{T} = f(T) < T$ la relazione da determinare, si avrà:

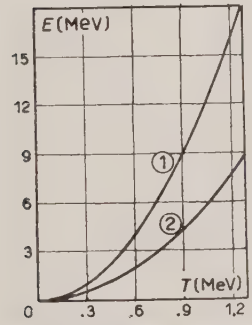

Fig. 3. – Curva energia-temperatura calcolata mediante la relazione $E = bT^2$ (curva 1) e le relazioni equivalenti (5) e (7) (curva 2).

$$E = b\bar{T}^2 = bf^2(T) = B(T)T^2 , \tag{3}$$

da cui risulta che la presenza della funzione $B(T)$, in luogo della costante b, elimina, nel caso del gas reale, la dipendenza lineare dell'energia di eccitazione dal quadrato della temperatura del nucleo.

In definitiva, si può concludere che per tener conto delle interazioni nucleari, interpretate come agitazione termica della materia nucleonica, è sufficiente associare alla temperatura effettiva T del gas reale, calcolata in base alla ($2a$) per un dato valore di $y \geqslant a$, l'energia $E = b\bar{T}^2$ del gas ideale alla temperatura $\bar{T}$, univocamente determinata da T. Immediata conse-

guenza di queste considerazioni è che l'effetto delle interazioni nucleari tende a ridurre lo stato di degenerazione del gas reale: infatti, detto $\bar{\eta} = \bar{T}/\psi(\bar{T})$ il parametro che descrive il gas ideale, si ha $0 \leqslant \bar{\lambda} = \exp[-1/\bar{\eta}] < \lambda$.

Tenendo conto del concetto di temperatura equivalente, per risolvere il problema si può procedere secondo due criteri sostanzialmente analoghi: *a*) individuando direttamente la funzione $B(T)$, che compare nella (3), dopo aver trasformato, in base ad opportune considerazioni energetiche, l'equazione di stato del gas dalla regione delle temperature equivalenti a quella delle temperature effettive; *b*) ricercando direttamente la relazione che intercede tra T e $\bar{T}$ e quindi applicando la (3).

3. – Il criterio *a*) si collega al risultato (I, 8*ab*) valevole per un nucleo pesante standard:

$$(4) \qquad E(T) = E(\tau) - E(\tau_0) = \frac{6C}{5}\left(\frac{A}{2C}\right)^{5/3}[\mu^{-5/3}(y)\nu(y) - \mu^{-5/3}(a)\nu(a)] ,$$

in cui l'energia di eccitazione $B(T)$, funzione della temperatura effettiva T, è espressa come differenza tra l'energia di eccitazione del nucleo $E(\tau)$ e quella latente termonucleare $E(\tau_0)$. Per mettere in evidenza la dipendenza di E dalla temperatura T è preferibile scrivere la (4) in forma diversa, in modo, fra l'altro, di indicare esplicitamente il fatto che nella regione delle basse energie di eccitazione considerate, il termine $a\psi(\tau)$ che compare nella (2) è predominante rispetto a T.

Per modificare la forma della (4) basta osservare che l'energia totale di eccitazione del gas nella regione delle temperature equivalenti AD (fig. 2) è somma dell'energia di perturbazione $\overline{AB}$, corrispondente alla temperatura $a\psi(\tau)$ e dell'energia $\overline{DB}$ del gas senza interazioni alla temperatura T: $\overline{AD} = AB + B\bar{D}$. Essendo AC l'energia di eccitazione termonucleare alla temperatura τ_0 ($T = 0$), segue che l'energia di eccitazione di un gas reale di Fermi avente temperatura effettiva T e temperatura equivalente τ è: $\overline{AD} - \overline{AC} = AB + B\bar{D} - \overline{AC} = DC < BD$, la quale, ammessa valida per le ragioni dette (n. 2) la normale relazione di Fermi, corrisponderà ad una temperatura $\bar{T} < T$. Tenendo presenti le espressioni esatte della statistica di Fermi (I, 4), il primo termine dell'ultimo membro della (4), interpretato come funzione additiva dell'energia del gas senza interazioni e dell'energia di perturbazione, diviene:

$$(4a) \qquad \frac{6C}{5}\left(\frac{A}{2C}\right)^{5/3}\mu^{-5/3}(y)\nu(y) = \frac{6C}{5}\left(\frac{A}{2C}\right)^{5/3}[\mu^{-5/3}(\eta)\nu(\eta) + \mu^{-5/3}(\omega)\nu(\omega)] ,$$

in cui $\omega \quad a\psi(\tau)/\psi[a\psi(\tau)] \leqslant a$. Siccome il parametro che descrive il gas reale

è $\eta = T/\psi(T) \ll 1$, la (4*a*) può scriversi nella forma:

$$(4b) \qquad \frac{6C}{5}\left(\frac{A}{2C}\right)^{5/3}\mu^{-5/3}(y)\nu(y) = bT^2 + \frac{6C}{5}\left(\frac{A}{2C}\right)^{5/3}\mu^{-5/3}(\omega)\nu(\omega)\,,^{(*)}$$

e, quindi, tenendo conto della (4), si ha:

$$(5) \qquad E(T) = b\left[1 - \frac{6C}{5b}\left(\frac{A}{2C}\right)^{5/3}\frac{\mu^{-5/3}(a)\nu(a) - \mu^{5/3}(\omega)\nu(\omega)}{T^2}\right]\cdot T^2\,.$$

Si mette in evidenza, così, la dipendenza formale di $E(T)$ dal quadrato della temperatura effettiva T, caratteristica per gas di Fermi fortemente degeneri; è da notare tuttavia la notevole differenza della (5) rispetto alla legge $E = bT^2$ in quanto in luogo della costante $b \sim 11$ MeV^{-1} si trova

$$B(T) = b\left[1 - \frac{6C}{5b}\left(\frac{A}{2C}\right)^{5/3}\frac{\mu^{-5/3}(a)\nu(a) - \mu^{-5/3}(\omega)\nu(\omega)}{T^2}\right] < b\,.$$

La funzione $B(T)$ è lentamente decrescente con T (tabella I) ed acquista valori che sono in accordo con quelli previsti da altri Autori in base a considerazioni sostanzialmente diverse.

La curva energia-temperatura, calcolata secondo la (4) è confrontata in fig. 3 con la curva di Fermi $E = bT^2$; l'introduzione delle interazioni nucleari si riflette sul fatto che, a parità di eccitazione, ad una determinata temperatura effettiva T del nucleo corrisponde una temperatura $\bar{T} < T$ del gas privo di interazioni, come diretta conseguenza della circostanza $B(T) < b$.

Tabella I.

y	$\mu(y)$	$\nu(y)$	T	$E(T)$	$B(T)$
0,35	1,1608	1,7201	0	0	9,02
0,351	1,1618	1,7239	0,511	1,386	5,31
0,352	1,1628	1,7277	0,693	2,520	5,24
0,354	1.1648	1,7352	1,005	5,160	5,11
0,356	1,1667	1,7428	1,24	7,810	5,07
0,358	1,1686	1,7503	1,47	10,710	4,96
0,36	1,1705	1,7579	1,65	13,230	4,86

(*) Osserviamo che, assumendo $y \geqslant a$ come variabile indipendente, resta definito il parametro ω e quindi la (4*b*) esprime l'equazione di condizione per la temperatura T.

4. – La relazione (5) presenta lo svantaggio di richiedere delle delicate integrazioni numeriche, in quanto, per i valori di E che interessano agli effetti del confronto con i dati sperimentali relativi alla densità dei livelli energetici ($0 \leqslant E < 10$ MeV), il parametro y che compare nelle funzioni integrali $\mu(y)$ e $\nu(y)$ e che soddisfa alla (4a), varia nel ristretto intervallo $0{,}35 \leqslant y < 0{,}36$. Inoltre, in previsione dei successivi sviluppi del calcolo, è conveniente ricercare una espressione più semplice per la funzione $B(T)$ a causa della sua complicata dipendenza da T tramite la funzione di funzione $\mu^{-5/3}(\omega)\nu(\omega)$. Per queste ragioni è preferibile riferirsi al criterio (b) del n. **2** e cioè individuare direttamente la funzione $\bar{T} = f(T)$ e calcolare l'energia di eccitazione applicando la (3). Il modo più semplice per procedere consiste nel ricercare quale temperatura $\bar{T}$ deve essere attribuita ad un gas ideale di Fermi che abbia la stessa energia di eccitazione di un gas reale alla temperatura effettiva T legata, tramite la relazione (2), alla temperatura equivalente τ.

A tale scopo si osservi che, siccome $\psi(\tau) \leqslant \psi(\tau_0)$, risulta $\tau - \tau_0 < T$. La corrispondenza biunivoca fra le temperature e i parametri che descrivono il gas nella regione delle temperature effettive ed equivalenti è fissata dalle seguenti inequazioni:

$$0 \leqslant \frac{\tau - \tau_0}{\psi(\tau - \tau_0)} < y - a \; ; \qquad 0 \leqslant \eta \; < \eta \; .$$

Siccome nel limitato intervallo energetico considerato i parametri che descrivono il gas approssimativamente sono funzioni lineari della temperatura ad essi corrispondente, e inoltre $\psi(\tau - \tau_0) \sim \psi(T)$ si ha:

$$\bar{T} = f(T) = \frac{(\tau - \tau_0)\eta}{y - a} < T \; . \tag{6}$$

In definitiva, limitando per le ragioni dette il calcolo all'intervallo $0 \leqslant E < 10$ MeV, si verifica agevolmente che $\bar{\eta} = \bar{T}/\psi(\bar{T}) \ll 1$ e quindi, essendo soddisfatta la condizione restrittiva, si può applicare per questa temperatura il procedimento risolutivo valido per gas fortemente degeneri e si ritrova la (3). Infine, tenute conto della (3), (2b) e (6), si trova che per un gas reale di Fermi nella regione delle basse energie di eccitazione esiste fra E e T la relazione

$$E(T) = b \left\{ \frac{\tau \; \ln(1/A)}{T \; \ln(1/\lambda)} \right\}^2 \left\{ 1 - \frac{\tau_0 - \tau + T}{\bar{T}} \right\}^2 \cdot T^2 = B(a, T) \cdot T^2 \; . \tag{7}$$

Nella (7) la funzione $B(T)$ è stata indicata con la scrittura $B(a, T)$ per mettere in evidenza che i valori da essa assunti nell'intervallo energetico considerato dipendono in maniera sensibile dal parametro a. La funzione $B(a, T)$

Tabella II.

y	$\mu(y)$	$\mu'(y)$	$\nu(y)$	T	$B(a, T)$
0,35	1,1608	0,9342	1,7201	0	9,02
0,36	1,1705	0,9591	1,7579	0,189	5,43
0,37	1,1800	0,9836	1,7992	0,376	5,37
0,38	1,1902	1,0071	1,8409	0,561	5,30
0,39	1,2001	1,0277	1,8849	0,744	5,24
0,40	1,2063	1,0485	1,9310	0,924	5,18
0,41	1,2209	1,0679	1,9753	1,10	5,12
0,42	1,2316	1,0868	2,0232	1,28	5,06
0,45	1,2649	1,1394	2,1717	—	—
0,60	1,4540	1,3722	3,0429	—	—

è decrescente con la temperatura (tabella II). La relazione (7) si converte nella usuale di Fermi, valida per un gas ideale, quando si escludano le interazioni nucleari e si ponga $E(\tau_0) = 0$, cioè $a = 0$ ($\tau_0 = 0$; $B(0, T) = b =$ costante).

Il fatto che per una determinata temperatura effettiva T si ottenga la stessa energia sia valutandola in un intorno di $T = 0$ oppure di τ_0, cioè in corrispondenza di due intervalli in cui la curva energia-temperatura possiede pendenze molto diverse, si giustifica osservando che nel primo caso all'intervallo energetico $0 \leqslant E < 10$ MeV corrisponde il parametro y variabile tra 0,35 $\vdash$ 0,36 (tabella I), mentre nel secondo caso, all'intervallo di temperatura limitato fra $T = 0$ ($E = 0$) e $T = 1{,}4$ ($E = 10$ MeV) corrispondono per y valori variabili tra 0,35 $\vdash$ 0,42 (tabella II).

5. – Il calcolo dei livelli energetici $\varrho(E)$ posseduti da un nucleo di numero di massa A eccitato all'energia E può essere eseguito o considerando i neutroni e i protoni che lo costituiscono semplicemente come variabili termodinamiche o come parametri che intervengono nella definizione del potenziale termodinamico. Il primo criterio conduce alla relazione di Bethe [11]

$$\frac{1}{\varrho(E)} = D(E) = T\left(2\pi \frac{\mathrm{d}E}{\mathrm{d}T}\right)^{1/2} \cdot \exp\left[-S\right], \tag{8}$$

che è valida indipendentemente dal legame che esiste tra energia di eccitazione e temperatura del nucleo. Il secondo criterio [12] invece, si può appli-

[11] H. A. Bethe: *Rev. of Mod. Phys.*, **9**, 81 (1937).
[12] I. N. Sneddon e B. F. Touschek: *Proc. Camb. Phil. Soc.*, **44**, 391 (1948).

care osservando che una volta definita l'energia libera del sistema

$$F = -T\int_0^T E\,\mathrm{d}E/T^2\,,$$

la funzione $\exp[-F/T]$ risulta essere la trasformata di Laplace della densità dei livelli energetici

$$\exp[-F/T] = \int_0^\infty \varrho(E)\exp[-E/T]\,\mathrm{d}E\,,$$

da cui si ottiene mediante antitrasformazione

$$\varrho(E) = \frac{1}{2\pi i}\int_{\gamma-i\infty}^{\gamma+i\infty}\exp\{zE - zF(1/z)\}\,\mathrm{d}z\,, \qquad \gamma > 0\,.$$

Questo secondo metodo comporta delle maggiori difficoltà di ordine matematico non compensate dai risultati che consente di ottenere; per esempio la sua applicazione quando si ammetta valida la legge $E = bT^2$ porta alla espressione

$$D(E) = T\left(2\pi\frac{\mathrm{d}E}{\mathrm{d}T}\right)^{1/2}\cdot\exp[-S]\left\{1 - \frac{3}{16b^{1/2}E^{1/2}} + \ldots\right\}^{-1},$$

praticamente coincidente con quella di Bethe.

Per questa ragione abbiamo senz'altro applicato la (8) dopo aver calcolato il calore specifico e l'entropia del gas nucleonico tramite la (7), in modo da evitare le espressioni più complicate che richiederebbero lunghe valutazioni numeriche qualora si fosse considerata l'energia nella forma (4).

Eseguiti i calcoli elementari assumendo come unica variabile indipendente la y, si può tracciare il seguente quadro di confronto tra il gas nucleonico con e senza interazioni:

(9)

	con interazioni	*senza interazioni*
Energia	$E(T) = B(a,T)\cdot T^2\,,$	$E(T) = bT^2\,,$
Calore specifico	$\dfrac{\mathrm{d}E}{\mathrm{d}T} = 2B(a,T)\cdot T[1 - T\varepsilon(a,y)]\,,$	$\dfrac{\mathrm{d}E}{\mathrm{d}T} = 2bT\,,$
Entropia	$S = 2[B(a,T)\cdot E]^{1/2}\cdot\sigma(a,y)\,,$	$S = 2(bE)^{1/2},$

in cui

$$\left\{\begin{array}{l} B(a,T) = b\left\{\dfrac{\tau}{T}\,\dfrac{\ln(1/\Lambda)}{\ln(1/\lambda)}\right\}^2\left\{1-\dfrac{\tau_0-\tau+T}{T}\right\}^2, \\ \varepsilon(a,y) = \dfrac{2}{3\sqrt[3]{\gamma_0^2}}\,\dfrac{\mu^{-1/3}(y)\mu'(y)}{1-\dfrac{2}{3}(y-a)\dfrac{\mu'(y)}{\mu(y)}}, \qquad \dfrac{\mathrm{d}\mu}{\mathrm{d}y} = \mu'(y), \\ \sigma(a,y) = \dfrac{2}{3}\,\dfrac{\mu^2(y)}{y-a}\cdot\displaystyle\int_0^y \mu^{-2}(y)\left[\frac{3}{2}-2(y-a)\frac{\mu'(y)}{\mu(y)}\right]\mathrm{d}y\,. \end{array}\right.$$

È di immediata verifica che le nuove espressioni si convertono nelle solite espressioni di Fermi quando nella descrizione del comportamento del nucleo si prescinde dalle interazioni nucleari e si elimina la condizione $y \geqslant a$ che vincola ogni considerazione al campo delle temperature equivalenti:

$$B(0,T) = b\,,$$

$$\lim_{y\to 0}\varepsilon(0,y) = 0\,, \qquad \lim_{y\to 0}\sigma(0,y) = 1\,.$$

Tenendo conto della (9) la (8) diviene

$$10) \qquad \varrho(E) = \left(\frac{1}{2\pi}\right)^{1/2}\left[\frac{B(a,T)}{E^3}\right]^{1/4}\times \times \frac{\exp\{2[B(a,T)\cdot E]^{1/2}\sigma(a,y)\}}{[2-2T\varepsilon(a,y)]^{1/2}}\,.$$

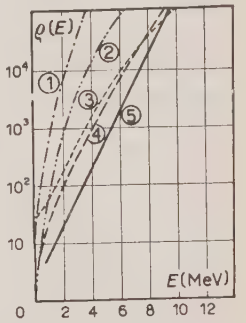

Fig. 4. – Densità dei livelli energetici di un nucleo pesante standard in funzione dell'energia di eccitazione.

La (10) è confrontata nella fig. 4 (curva 4) con le curve teoriche di Lier e Uhlembeck [13] (curva 1), di Wergeland [7] (curva 3), ricavata in base al modello a goccia, e con la formula di Weisskopf (curva 2). I dati sperimentali [4] (curva 5) si riferiscono all'elemento Pd^{103} normalizzati all'energia di legame del neutrone in base ai dati sperimentali [15] ricavati per il Rh^{103}. L'attendibilità di questi dati deriva dal

[13] C. V. Lier e G. E. Uhlembeck: *Physica*, **4**, 531 (1937).
[14] D. C. Gugelot: *Phys. Rev.*, **81**, 51 (1951).
[15] L. B. Borst, A. J. Ulrich, C. L. Osborne e B. Hasbrouck: *Phys. Rev.*, **70**, 557 (1946); R. R. Mayer: *Phys. Rev.*, **75**, 773 (1949).

fatto che per quest'ultimo elemento la larghezza naturale del livello è certamente molto maggiore della larghezza Doppler.

In conclusione, l'ipotesi del nucleo « caldo », e la relazione (7) che ne deriva conduce, rispetto alle altre previsioni basate sul modello di Fermi, ad un accordo abbastanza soddisfacente con i dati sperimentali. Il fatto che la curva teorica calcolata con la (10) abbia l'andamento di quella prevista dal modello a goccia si può in parte giustificare pensando che l'introduzione nel modello di Fermi delle interazioni nucleari dell'entità considerata descrive il nucleo in uno stato più condensato di quello previsto dal modello a particelle libere. Infine, per migliorare l'accordo, sembra legittimo pensare piuttosto che ad una insufficienza della relazione (2) al fatto che il valore di $a = 0{,}35$ dal quale dipendono fortemente tutti i risultati del calcolo, è stato ricavato in base al rapporto di WATANABE $K^{(2)}/K^{(0)} = 0{,}34$ a proposito del quale si hanno sufficienti dati sperimentali che lo fanno ritenere approssimato per difetto. Questo argomento, insieme alla giustificazione teorica della legge (2), verrà discusso in un successivo lavoro.

Ringraziamo i proff. N. DALLAPORTA e E. CLEMENTEL per alcune discussioni sull'argomento e la dott. S. CHERSI che ha eseguito i calcoli numerici.

SUMMARY

The level density of a standard heavy nucleus is calculated taking into account the modifications brought about by nuclear interactions in the Fermi gas model. Their effect on the energy-temperature dependence is evaluated by the aid of the following relation:

(2) $$\tau = T + a\psi(\tau)$$

between the equivalent temperature τ and the true temperature T. The energy-temperature relation may be derived either on the basis of the exact Fermi expressions for the number of particles and their total energy (Eqs. 4-5) or modifying the coefficient b of the law $E - bT^2$ (Eqs. 7), which may be written in the form $E = B(a, T)T^2$. The function $B(a, T)$ depends strongly on the parameter a and is slowly varying with temperature (Table I and II) in the energy range $0 \leqslant E < 10$ MeV, whereabout calculations are referred. The parameter a is closely related to the thermonuclear energy as expected from Watanabe's ratio $K^{(2)}/K^{(0)} = 0{,}34$. Its value was found to be 0,35 instead of 0,29 as given by this Author; such difference is due to the fact that exact expressions of Fermi statistics have been throughout used instead of the approx-

imated ones in the equivalent temperature region. The energy levels have been calculated with Bethe's formula taking into account modified expressions for the nuclear specific heat and entropy (Eqs. (9)). The mean value of $B(a, T)$ in the considered energy region is fairly well fitted with Bardeen's previsions, although derived on substancially different assumptions. In Fig. 4 the energy levels calculated with formula (10) are compared with other theoretical predictions (curves 1, 2, 3) and with the experimental values (curve 5) observed for Pd^{103}. The agreement between our previsions and those obtained with the liquid drop model is briefly discussed.

Evalutation of Integrals in the Theory of Atomic Scattering of Electrons.

E. Corinaldesi (*) and L. Trainor (*)

Division of Physics, National Research Council - Ottawa, Canada

(ricevuto il 21 Luglio 1952)

Summary (**). — It is shown how using methods recently developed in field theory, one may exactly evaluate some integrals appearing in the calculation of the differential cross section for the scattering of electrons by atoms.

The problem of the scattering of electrons by atoms is still of considerable interest (1). The literature (2, 3, 4, 5) appears to agree on the one point, that the use of the Born or of the Oppenheimer approximation is likely to lead to unsatisfactory results at low energies of the incident electron. First of all, both approximations can be invalidated by the requirement of convergence. Moreover, the very consistency of the Oppenheimer approximation has been questioned. In this connection it was shown in a previous letter (6) that the Oppenheimer method is based on the single assumption that, if the scalar product of the initial and final wave functions is different from zero, one of them may still be « approximated » by a linear combination of functions all

(*) National Research Laboratories Postdoctorate Fellow.

(**) *Editor's summary.*

(1) We thank Dr. Ta-You Wu for many stimulating discussions.

(2) G. Wentzel: *Handbuch der Physik*, **24**/1, p. 726.

(3) N. F. Mott and H. S. W. Massey: *The Theory of Atomic Collisions* (Oxford, New York, 1933).

(4) D. R. Bates, A. Fundaminsky and H. S. W. Massey: *Trans. Roy. Soc.* (London), **243**, 93 (1950).

(5) D. Layzer: *Phys. Rev.*, **84**, 1221 (1951).

(6) E. Corinaldesi, L. Trainor and Ta-Yoy Wu: *Nuovo Cimento*, **9**, 436 (1952).

orthogonal to the other. Thus before reaching any conclusion the precise meaning of « approximated » should be defined.

The numerical values of total cross sections yielded by the Born and by the Oppenheimer approximation were checked, by BATES and co-workers [1], against an upper limit which can be exactly derived from the theory of collisions. The result of this comparison was that, of the two, the Born approximation seemed to give more credible results. It may be pointed out that one might question the accuracy of the numerical values of such cross sections [4] [7], which were obtained by making drastic approximations in the evaluation of certain integrals. This note purposes to reduce this difficulty by showing how the integrations occurring in the differential cross sections for the scattering by a hydrogenic system (nuclear charge Z) can be carried out exactly. Use is made of methods recently developed in the theory of fields [9].

Departing somewhat from the notation used in [6], consider the matrix elements

$$T_{ba}^{(i)} = f\left\{\frac{1}{r_{12}} - \frac{Z}{r_1}\right\} \pm g\left\{\frac{1}{r_{12}} - \frac{Z}{r_i}\right\} \qquad (i = 1, 2), \tag{1}$$

where f and g are the functionals

$$f\{\zeta\} = \int \zeta \exp\left[i\boldsymbol{s}\cdot\boldsymbol{r}_1\right] \varphi_b^*(\boldsymbol{r}_2)\varphi_a(\boldsymbol{r}_2)\,\mathrm{d}\boldsymbol{r}_1\,\mathrm{d}\boldsymbol{r}_2\,, \tag{2a}$$

$$g\{\zeta\} = \int \zeta \exp\left[i(\boldsymbol{p}\cdot\boldsymbol{r}_2 + \boldsymbol{q}\cdot\boldsymbol{r}_1)\right]\varphi_b^*(\boldsymbol{r}_2)\varphi_a(\boldsymbol{r}_1)\,\mathrm{d}\boldsymbol{r}_1\,\mathrm{d}\boldsymbol{r}_2\,. \tag{2b}$$

Here $\boldsymbol{s} = \boldsymbol{p} + \boldsymbol{q}$, $\boldsymbol{p}$ denoting the momentum of the impinging electron (expressed in atomic units), $-\boldsymbol{q}$ that of the outgoing electron, while φ_a and φ_b are the hydrogenic eigenfunctions representing the initial and final states of the bound electron (energy eigenvalues ε_a and ε_b). $T_{ba}^{(1)}$ and $T_{ba}^{(2)}$ are the « prior » and « post » matrix elements. However, from the equation [8]

$$g\left\{\frac{1}{r_2}\right\} = (\boldsymbol{p}^2 - \varepsilon_b)g\{1\} = (\boldsymbol{q}^2 - \varepsilon_a)g\{1\} = g\left\{\frac{1}{r_1}\right\}, \tag{3}$$

it is apparent that $T_{ba}^{(1)} = T_{ba}^{(2)}$. Therefore no « prior-post discrepancy » occurs in the present problem; the values 1 and 2 of the index i may be used indifferently in eq. (1).

[7] H. S. W. MASSEY and C. B. O. MOHR: *Proc. Roy. Soc.*, A **132**, 605 (1931).

[8] Obtained by using the wave equations obeyed by φ_a and φ_b and the conservation of energy between initial and final states.

The f's and g's are the so-called Coulomb and exchange terms respectively. In this note only the **1s-1s**, **1s-2s**, and **1s-2p** transitions will be considered. In order to distinguish them, the symbols (f, g) will hereafter refer only to the **1s-1s** transition, while (f', g') will refer to the **1s-2s**, and (f'', g'') to the **1s-2p** transition.

Angular integration of $|T_{ba}|^2$ are now in progress for the calculation of the total cross sections.

Repeated use will be made of differentiation with respect to parameters, particularly those occurring in the exponentials of the hydrogenic wave functions. Some formulae will be included only for completeness, being alternative derivations of those obtained by previous authors.

Coulomb integrals.

It is convenient to define the functions

$$F_{lm}(\alpha, \boldsymbol{s}) = \int \frac{1}{r_{12}} \exp\left[i\boldsymbol{s}\cdot\boldsymbol{r}_1 - \alpha r_2\right] Y_{lm}((\vartheta_2, \varphi_2)\, \mathrm{d}\boldsymbol{r}_1\, \mathrm{d}\boldsymbol{r}_2\,, \tag{4}$$

where r_2, ϑ_2, φ_2 are the spherical coordinates of $\boldsymbol{r}_2$, and Y_{lm} is a spherical harmonic. Thus we have

$$f\left\{\frac{1}{r_{12}}\right\} = \frac{2Z^3}{\sqrt{\pi}} F_{00}(2Z, \boldsymbol{s})\,, \tag{5a}$$

$$f'\left\{\frac{1}{r_{12}}\right\} = \frac{Z^3}{\sqrt{8\pi}}\left[\left(2 + Z\frac{\partial}{\partial\alpha}\right) F_{00}(\alpha, \boldsymbol{s})\right]_{\alpha = 3Z/2}\,, \tag{5b}$$

$$f''\left\{\frac{1}{r_{12}}\right\} = \frac{(-1)^{m+1} Z^4}{\sqrt{24\pi}}\left[\frac{\partial}{\partial\alpha} F_{1m}(\alpha, \boldsymbol{s})\right]_{\alpha = 3Z/2} \qquad (m = 0, \pm 1)\,. \tag{5c}$$

Let $s = |\boldsymbol{s}|$, ϑ, φ be the spherical coordinates of $\boldsymbol{s}$. The integral $F_{lm}(\alpha, \boldsymbol{s})$ can be easily expressed as the product of the spherical harmonic $Y_{lm}(\vartheta, \varphi)$ by an elementary, one-dimensional integral depending on the parameters α and s. The final results are given at the end of the paper.

Coulomb integrals of the type $f\{1/r_1\}$ vanish except in the case of elastic scattering, for which

$$f\left\{\frac{1}{r_1}\right\} = \int \frac{1}{r_1} \exp\left[i\boldsymbol{s}\cdot\boldsymbol{r}_1\right] \mathrm{d}\boldsymbol{r}_1 = \frac{4\pi}{s^2}\,. \tag{6}$$

Exchange integrals.

Introducing the function

$$A=\int \frac{1}{r_{12}} \exp\left[-\alpha r_1-\beta r_2+i(\boldsymbol{p}\cdot\boldsymbol{r}_2+\boldsymbol{q}\cdot\boldsymbol{r}_1)\right] \mathrm{d}\boldsymbol{r}_1\,\mathrm{d}\boldsymbol{r}_2\,, \tag{7}$$

one can write

$$g\left\{\frac{1}{r_{12}}\right\}=\frac{Z^3}{\pi}\,[A]_{\alpha=z,\,\beta=z}\,, \tag{8a}$$

$$g'\left\{\frac{1}{r_{12}}\right\}=\frac{Z^3}{4\pi\sqrt{2}}\left[\left(2+Z\frac{\partial}{\partial\beta}\right)A\right]_{\alpha=z,\,\beta=z/2}\,, \tag{8b}$$

$$g''\left\{\frac{1}{r_{12}}\right\}=\frac{Z^4}{8\pi i}\begin{pmatrix}\dfrac{\partial}{\partial p_x}-i\dfrac{\partial}{\partial p_y}\\ \sqrt{2}\,\dfrac{\partial}{\partial p_z}\\ -\dfrac{\partial}{\partial p_x}-i\dfrac{\partial}{\partial p_y}\end{pmatrix}[A]_{\alpha=z,\,\beta=z/2}\,. \tag{8c}$$

The three variants of (8*c*) refer to final **2*p*** states with magnetic quantum number $m=1,\,0,\,-1$ respectively.

Using the momentum representation of $(r_{12})^{-1}$, and integrating over $\boldsymbol{r}_1$ ans $\boldsymbol{r}_2$, (7) becomes

$$A=8\,\frac{\partial}{\partial\alpha}\,\frac{\partial}{\partial\beta}\int \frac{\mathrm{d}\boldsymbol{k}}{\boldsymbol{k}^2[\alpha^2+(\boldsymbol{k}+\boldsymbol{q})^2][\beta^2+(\boldsymbol{k}-\boldsymbol{p})^2]}\,. \tag{9}$$

Using the parametrization method [9], A can be given the form

$$A=384\pi\alpha\beta\int_0^1 x(1-x)\,\mathrm{d}x\int_0^1 y^3\,\mathrm{d}y\int_0^\infty [z^2+(v-\boldsymbol{u}^2)]^{-4}\,\mathrm{d}z\,, \tag{10}$$

where

$$v=y[x(\alpha^2+\boldsymbol{q}^2)+(1-x)(\beta^2+\boldsymbol{p}^2)]\,,\qquad \boldsymbol{u}=y(x\boldsymbol{s}-\boldsymbol{p})\,. \tag{11}$$

By this method one is left with elementary integrations only.

The remaining exchange integrals can be evaluated in a straightforward manner by making use of equation (3).

[9] R. P. Feynmann: *Phys. Rev.*, **76**, 769 (1949).

Tabulation of results.

Hereinafter p, q, s will *not* denote $|\boldsymbol{p}|$, $|\boldsymbol{q}|$, $|\boldsymbol{s}| = |\boldsymbol{p} + \boldsymbol{q}|$ as formerly, but rather these quantities divided by Z. The adoption of this convention will simplify the formulae considerably. The scattering angle will be denoted by Θ and the azimuth by Φ.

Elastic scattering (**1s-1s**). With $P = p \sin \Theta/2$ we have

$$Z^2 f\left\{\frac{1}{r_{12}}\right\} = \pi[P(1+P^2)]^{-2}\,; \qquad Z^2 f\left\{\frac{1}{r_2}\right\} = \pi P^{-2}\,;$$

$$Z^2 g\left\{\frac{1}{r_{12}}\right\} = 4\pi[P(1+p^2)]^{-3}\big[P(1+P^2)^{-2}(2P^4 + P^2[3+p^4] - 2p^2) + \\ + 2(p^2+P^2)\sin^{-1}(P/\sqrt{1+P^2})\big]\,;$$

$$Z^2 g\left\{\frac{1}{r_2}\right\} = 32\pi(1+p^2)^{-3}.$$

1s-2s and **1s-2p** transitions. It is convenient to introduce the variable $t^2 = 4s^2$, the substitution $\varkappa = 1 + 4p^2$, and the functions

$$X = \sin^{-1}\left(\frac{t^2+3}{\sqrt{(t^2+9)(t^2+1)}}\right) + \sin^{-1}\left(\frac{t^2-3}{\sqrt{(t^2+9)(t^2+1)}}\right);$$

$$B_1 = 64(t^2+9)^{-2}, \qquad B_2 = -48t^{-2}(t^2+9)^{-1} + 8t^{-3}X\,,$$

$$B_3 = 6t^{-1}(t^2+3) + t^{-5}(t^4 - 10t^2 - 27)X\,;$$

$$C_1 = \frac{512}{3}(t^2+27)(t^2+9)^{-3}, \qquad C_2 = 128(t^2+9)^{-2},$$

$$C_3 = -8t^{-1}(t^2-27)(t^2+9)^{-1} + 4t^{-5}(t^2-9)X\,,$$

$$C_4 = \frac{1}{3}t^{-6}(9t^4 - 58t^2 - 135) + \frac{1}{2}t^{-7}(t^5 - 7t^4 + 63t^2 + 135)X\,;$$

$$D_1 = \frac{1024}{5}(t^2+9)^{-3}, \qquad D_2 = -64t^{-4}(t^2+9)^{-2}(5t^2+27) + 32t^{-5}X\,,$$

$$D_3 = 6t^{-5}(t^2+9)^{-1}(t^4 + 40t^2 + 135) + t^{-7}(t^4 - 30t^2 - 135)X\,.$$

With this notation we have, for the **1s-2s** transition,

$$Z^2 f' \left\{ \frac{1}{r_{12}} \right\} = 1\,024\sqrt{2}\,\pi(t^2+9)^{-3}\,; \qquad Z^2 g' \left\{ \frac{1}{r_2} \right\} = 512\sqrt{2}\,\pi(\varkappa-2)\varkappa^{-1}\,;$$

$$Z^2 g' \left\{ \frac{1}{r_{12}} \right\} = 8\sqrt{2}\,\pi\varkappa^{-3}(3\varkappa^2 B_1 + 16\varkappa B_2 + 32 B_3) - \\ - 3\sqrt{2}\pi\varkappa^{-1}(\varkappa^3 C_1 + 8\varkappa^2 C_2 + 128\varkappa C_3 + 256 C_4)\,.$$

For the **1s-2p** transition, with the polar axis along the direction of the incident electron, we have

$$Z^2 f'' \left\{ \frac{1}{r_{12}} \right\} = 6\,144\pi i \sqrt{\frac{8\pi}{3}} \left(\sqrt{\frac{3}{4\pi}}\, p\,\delta_{0m} - q\, Y_{1m}(\Theta, \Phi) \right) t^{-2}(t^2+9)^{-3}\,;$$

$$Z^2 g'' \left\{ \frac{1}{r_2} \right\} = 2\,048\sqrt{2}\,\pi i \varkappa^{-1} p\,\delta_{0m}\,;$$

$$Z^2 g'' \left\{ \frac{1}{r_{12}} \right\} = 16\sqrt{2}\pi i p\,\delta_{0m}\varkappa^{-1}(\varkappa^2 C_2 + 32\varkappa C_3 + 96 C_4) + \\ + 2\sqrt{2}\pi i(p - q\cos\Theta)\delta_{0m}\varkappa^{-3}(15\varkappa^2 D_1 + 48\varkappa D_2 + 128 D_3)\,;$$

where δ_{ik} is the Kronecker symbol and $m = 0, \pm 1$.

RIASSUNTO (*)

Si mostra come, facendo uso di metodi recentemente sviluppati nella teoria dei campi, si possano valutare esattamente alcuni integrali che compaiono nel calcolo delle sezioni d'urto differenziali per il processo di diffusione di elettroni da parte di atomi.

(*) *Traduzione a cura della Redazione.*

IL NUOVO CIMENTO Vol. IX, N. 10 1 Ottobre 1952

A Cloud Chamber Analysis of Cosmic Rays at 3500 Metres.

Part A: The Electronic Component from Nuclear Disintegrations in Lead.

A. Lovati, A. Mura, G. Tagliaferri and S. Terrani

Istituto di Scienze Fisiche dell'Università - Milano

(ricevuto il 21 Luglio 1952)

Summary. — A multiplate cloud chamber has been operated at mountain altitude, yielding 16000 photographs of random expansions. This paper is intended to study the production of electronic component in nuclear disintegrations induced in lead by cosmic ray particles of moderately high energy. Assuming the neutral meson hypothesis, the ratio of the numbers of neutral to charged π-mesons forming in these disintegrations is derived to be $0.42 \pm 40\%$. The probability of production of electron-photon component in nucleon-Pb nucleus collisions is suggestively reported for two energy intervals: the indicative values are about 0.3 and 0.6 times the geometrical cross-section, for incident particle-energies centered, respectively, around 2 and 6 GeV. It is remarked that the results obtained, though rather poor statistically, are believed to be unaffected by instrumental selections.

We intended to carry out an unbiased analysis on some aspects of cosmic radiation at mountain altitude. In particular, we planned to collect, using a cloud chamber containing several lead plates and randomly operated, some of the data which can be obtained with a greater difficulty by means of the photographic emulsion technique: say, on the hard and soft components; on some peculiarities of nuclear disintegrations occurring in materials of high atomic number (e.g., the ratio of the numbers of neutral to charged mesons); on the associated events (especially the development of the nucleon cascade).

To this purpose we gathered from October 1951 to May 1952 at the Laboratorio della Testa Grigia (3500 m a.s.l., geomagn. lat. 47°7′ N) 16000 photographs of random expansions of a large cloud chamber (1) containing 9 lead plates 18 g cm^{-2} thick each.

(1) The instrument employed has been described by A. Lovati, A. Mura, G. Tagliaferri and L. Terra: *Nuovo Cimento*, **8**, 713 (1951).

Our experimental conditions were rather similar to the ones of HAZEN [2] and POWELL [3] who, a few years ago, performed analyses of cosmic rays at mountain altitude with random operating cloud chambers. The overmentioned authors had already noticed the advantages of an unbiased picture of the cosmic ray particles and their interactions. Later on, as the study of cosmic ray nuclear interactions aimed to become more quantitative, remarkable difficulties have arisen from the imperfect knowledge of the effects deriving from the control systems employed to select the *interesting* events. The troubles of such *a priori* selections can be completely removed, obviously, giving up any control. Thus, using a chamber with a large collection volume and with a great deal of material distributed in plates, the removal of the counter control may be found convenient at mountain altitude notwithstanding the severe limitation in the rate of collecting the data.

PART A: The electronic component from nuclear disintegrations in lead.

1. – Introduction.

The presence of electronic component among the products of the nuclear disintegrations induced by high energy cosmic ray particles is nowadays currently attributed to the creation of neutral π-mesons in these interactions, and to their successive γ decay. Though a conclusive proof of the creation of neutral mesons in cosmic ray disintegrations has not yet been reported, the hypothesis of the neutral mesons—whose existence has however been proved by the results of the artificial accelerators—can be considered reliable since it has never been contradicted by the experimental evidence so far available.

Accepting the neutral meson hypothesis, a multiplate cloud chamber allows to reveal the presence of these particles by observing the electronic cascades originated by their decay γ rays. Once that the *a priori* selection of the controlling devices has been avoided, as we did, this technique can be favourably compared to the photographic emulsion one.

A comprehensive discussion about the possibilities of the cloud chamber method for the study of neutral meson production has been recently carried out by SALVINI and KIM [4], who have also laid once more stress upon the importance of avoiding the instrumental selections. It is worth to remark

(2) W. E. HAZEN: *Phys. Rev.*, **65**, 67 (1944).
(3) W. M. POWELL: *Phys. Rev.*, **69**, 385 (1946).
(4) G. SALVINI and Y. KIM: in course of publication.

that SALVINI (5) has devised an elegant solution to reconcile the opposite requirements of observing with a cloud chamber practically unbiased nuclear disintegrations and of taking the well-known advantage of a controlling device. He used, in fact, a control system consisting of a scintillation counter by means of which he could reveal, basing on the evaporation particles, the disintegrations induced in the crystal placed within the chamber itself.

2. – Size-frequency distribution of the nuclear disintegrations.

We searched on the photographs the disintegrations happened in the lead plates, requiring for acceptance the convergence in a point of the plate of (i) at least two tracks of ionizing particles, one of which should appear four times more ionizing than the minimum, or of (ii) two or more particles traversing at least one plate without multiplying. Considering only the disintegrations occurred in the first eight plates downwards, and taking into account exclusively the events showing with sharp, well defined tracks, that is the events photographed *at the due time*, we observed 660 disintegrations in total.

In the works with photographic emulsions the disintegrations are classified according to the number of *shower particles*, which are known to be mostly protons of kinetic energy > 500 MeV and π-mesons of kinetic energy > 80 MeV. In order to enable a comparison with the emulsion work, we too adopted a similar classification: we defined as *penetrating shower particle* (p.s.p.) a penetrating particle which could be seen to ionize near the minimum ($\leqslant$ twice the minimum) before and after the traversing of the plate just close to the one where the disintegration took place. This brings to consider protons with > 270 MeV and π-mesons with > 60 MeV kinetic energy. As to the π-mesons our definition does not entail a significant difference from that adopted for the photographic emulsions; as to the protons, which however represent the least part of the shower particles, the difference is more important. Any way, we took time by time into account, if necessary, the effect of our different low energy limits.

Table I refers the numbers of the observed disintegrations distributed according to the number of p.s.p. .

While we can believe to have recognized all the disintegrations containing two or more p.s.p., it is obvious that we could not recognize all the disintegrations with one p.s.p., as the heavily ionizing particles accompanying these disintegrations could have remained completely within the plates. For the same reason, even more disintegrations with 0 p.s.p. were lost. Then, while the disintegrations with $\geqslant 2$ p.s.p. present heavily ionizing particles

(5) G. SALVINI: *Nuovo Cimento*, **8**, 798 (1951).

TABLE I.

Number of p.s.p.	0	1	2	3	4	5	Total:
Number of disintegrations	479 (~1 500) *	115 (195) *	43	18	4	1	660
Kind of the particles producing the disintegrations:							
— ionizing	84	39	13	11	1	1	149
— non ionizing	327	57	24	5	3		416
— unidentified	68	19	6	2			95

(*) This figure represents the corrected number of disintegrations, allowing for the unrevealed events (see text).

in the 57% of the cases, those with 1 p.s.p. which were identified present them, on the contrary, in the 97% of the cases. Whence we deduced that it is possible to correct the number of identified disintegrations with 1 p.s.p. multiplying the experimental figure by the factor $(100/57)\cdot(97/100) = 1.7$. The number thus corrected of disintegrations with 1 p.s.p. (195) is reported between brackets in table I.

The distribution of disintegrations we obtained agrees very well with the recent one by ROSSER and SWIFT [6] resulting from photographic emulsions exposed at mountain altitude. Basing on the data of these authors, we corrected the number of disintegrations with 0 p.s.p., a correction hard to perform utilizing only our own experimental data.

Bearing in mind the relation between the mean energy of the producing particles and the mean shower particle multiplicity [7], from our table it is seen that the disintegrations we detected are mostly of low and medium (about a few GeV) energy, till an upper limit of some 10 GeV.

We want to mention here that among the particles emitted in the 660 disintegrations considered, we identified one particle of the V^0 type. Another particle of the same kind was observed in a group of 260 disintegrations which were not considered in table I since they had not happened at the due time: all together, then, two V^0 particles out of a total of 920 disintegrations. This could be a first rough indication of the order of magnitude of the V^0 particle production cross-section in the foresaid energy interval.

[6] M. G. V. ROSSER and M. W. SWIFT: *Phil. Mag.*, **42**, 856 (1951).

[7] U. CAMERINI, W. O. LOCK and D. H. PERKINS: *Progress in Cosmic Ray Physics* (Amsterdam, 1952), Chapter I.

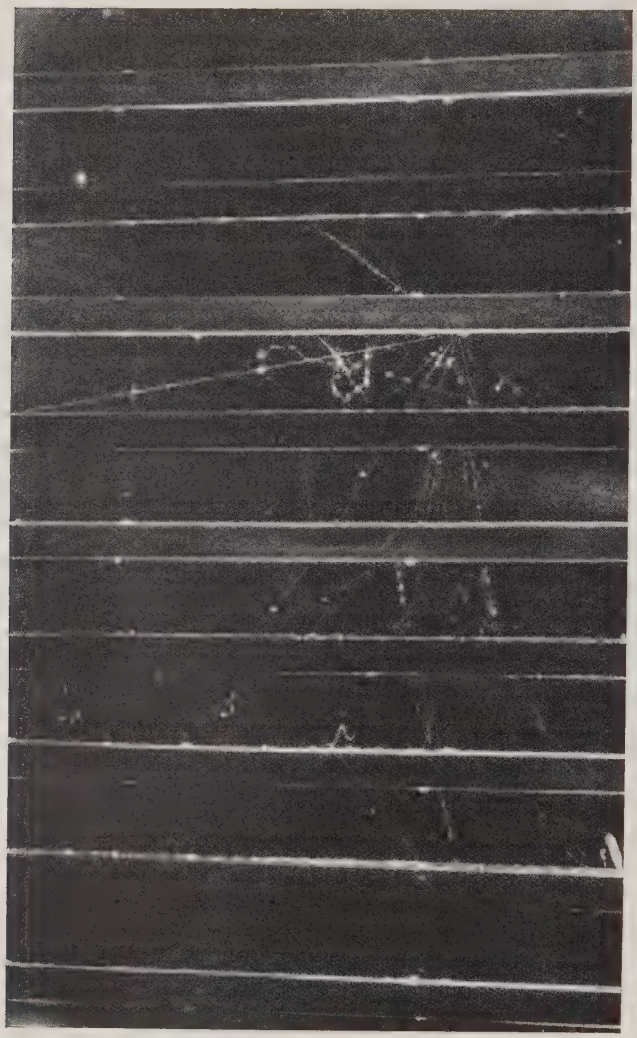

Fig. 1. – A nuclear disintegration produced by a non ionizing particle in the 3rd lead plate. Stereoscopic examination of the event allows to recognize the emission of 4 p.s.p., one of which interacts within the 5th plate originating a secondary disintegration with 2 p.s.p.. There are clearly two electron showers whose axes reproject to the origin of the primary disintegration. The energies of the e.s. are estimated to be ~ 450 and ~ 600 MeV, and the angle between the axes is found to be 18°: these values are in fair agreement with the creation of one neutral π meson (af about 900 MeV energy).

3. – The revealing of the neutral π mesons.

To reveal the presence of the neutral π-mesons, we analyzed the disintegrations by searching for electronic showers (e.s.) with two particles at least, coming from the lead plate close to the one where the disintegration had happened. The axis of the e.s. was to have such a direction that it was likely

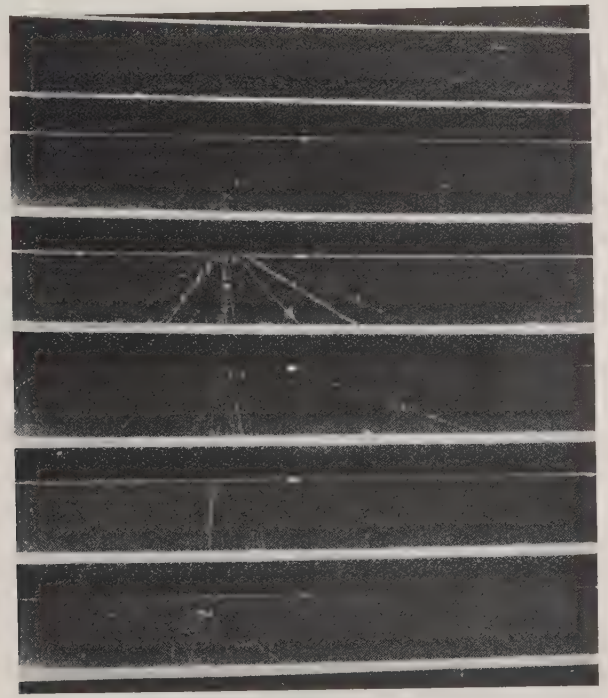

Fig. 2. – A disintegration (containing at least 1 p.s.p.) produced by an ionizing primary. Two e.s. have been identified at the exit from the plate just under the one where the disintegration has occurred. The energy of each e.s. was estimated, perhaps with considerable incertitude, to be about 400 MeV. The neutral meson relation can not, however, be proved in this instance, on account of unreliability also in measuring the angle between the e.s..

associated with the disintegration. Figs. 1, 2 and 3 are reported as typical instances of the available material.

The distribution of the numbers of the nuclear disintegrations with electronic

component according to the number of p.s.p., and the distribution of the numbers of e.s. coming from these disintegrations, are shown in table II.

TABLE II.

Number of p.s.p.	0	1	2	3	4	5	Total:
Number of disintegrations with electronic component . . .	11	8	5	7	2	1	34
Number of e.s.	17	11	12	12	3	1	56

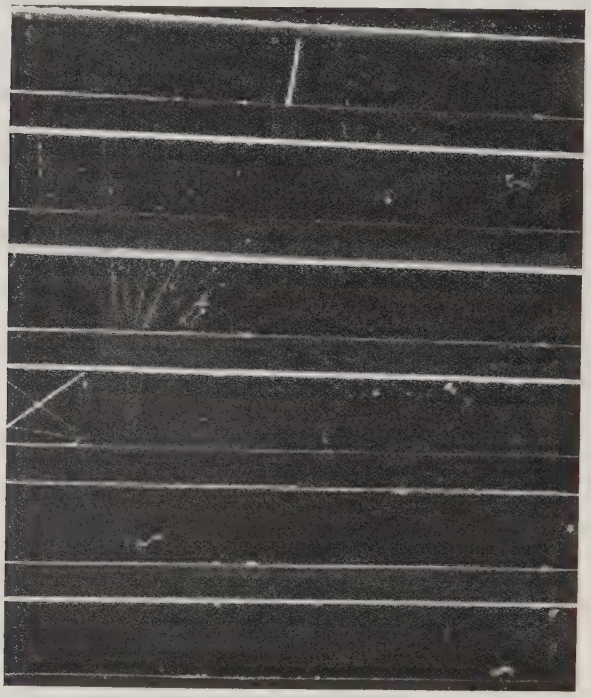

Fig. 3. – A fairly representative example of a disintegration clearly showing electronic component, but difficult to analyze because of poor resolution.

The disintegrations with electronic component showed 1, 2, 3, or at the most 4 e.s.. In table III these events are divided owing to the number of e.s. observed in each disintegration.

We evaluated the number of electrons of every e.s., and then, basing on this and taking into account the traversed thickness of lead from the origin of the

TABLE III.

Number of e.s. per disintegration . . .	1	2	3	4	Total:
Number of disintegrations	18	12	2	2	34

disintegration to the exit from the analyzing plate, we estimated the energy following Wilson's graphs ([8]). The energy distribution of the e.s. can be seen in table IV.

TABLE IV.

Energy interval (MeV)	150-300	300-450	450-600	> 600
Number of e.s.	36	12	5	3

The cut-off of the lowest energies is due to the fact that photons with an energy < 150 MeV are not able to reveal as e.s., because of the thickness and the material of the plates.

To infer from the e.s. energy distribution the π^0 energy spectrum, at least above a certain energy, it would be necessary one could couple the e.s. of the same event, after being assured that every couple of e.s. can be reliably attributed to the decay of a single neutral meson. This should be done by verifying the well-known relation

$$(2 \sin \Phi/2)^2 = (m_{\pi^0} c^2)^2 / E_1 E_2 ,$$

connecting the angle Φ between the axes of the e.s. and their energies E_1 and E_2. The matter is in practice very cumbersome; it is possible only for a part of the collected events, and it is subject to very large incertitude. The same conclusion had been reached also by GREGORY and TINLOT ([9]).

Consequently, it is not possible to draw a rather reliable spectrum of the π^0 issued in our disintegrations. The evaluations we did on the basis of the e.s. energies indicate, however, that the π^0 are distributed in the same energy interval as the charged mesons ([7]).

To estimate from the observed number of e.s. the total number of emitted π^0, we can make use of the hystogram representing the energy distribution of the photons obtained by CARLSON *et al.* ([10]). The fact that such a distribution is relative to the total γ radiation at balloon flight altitude should not entail, in our opinion, an important difference. From the hystogram one can deduce that the photons with energy higher than 150 MeV, that is the ones we re-

([8]) R. R. WILSON: *Phys. Rev.*, **86**, 261 (1952).
([9]) B. P. GREGORY and J. H. TINLOT: *Phys. Rev.*, **81**, 675 (1951).
([10]) A. G. CARLSON, J. E. HOOPER and D. T. KING: *Phil. Mag.*, **41**, 701 (1950).

vealed, are the 45% of the total number of photons. From this we get that the number of neutral mesons emitted in our disintegrations is plainly given by multiplying the number of the observed e.s. by the factor 1.1.

4. – The ratio $R = N_{\pi^0}/(N_{\pi^+} + N_{\pi^-})$.

A remarkable interest is at present attributed to the knowledge of the ratio between the number of π^0-mesons and that of charged π-mesons created in nuclear disintegrations. Shortly, it can be said that this interest is connected with the possibility of getting information on the peculiarities of the nucleon-nucleus interaction and on the energy loss in the nucleon cascade.

The values of the above ratio (hereafter referred to as R), so far published ([9-15]), run about the figure 1/2, though they may be affected by important errors both statistical and systematic. Only the result of CAMERINI *et al.*, who give $R = 1 \pm 0.3$ for disintegrations with at most 4 shower particles ($n_s \leqslant 4$), might be perhaps disagreeing. These authors made an essential criticism to the way of calculating the values of R: when one does not consider all the disintegrations, but one selects classes of nuclear disintegrations containing only low or high values of n_s, one favours or respectively disfavours the neutral mesons.

Besides, the values of R generally depend on the energy spectrum of the particles producing the disintegrations at the altitude where the observations are carried out. To obtain a more significant datum it would be necessary to reckon the energy of each interacting particle, and to derive then the R's for different energy intervals. The determining of the energy of the primary seems hard with the presently available techniques. Moreover one should remember that the number of shower particles is a rather poor index of the energy, as shown by the hystograms of the shower particle multiplicity distributions in function of the energy of the primary ([7]).

We will calculate the value of R for *all* the disintegrations occurred in the chamber plates: withby we should escape the criticism of favouring the charged or respectively neutral mesons. Our values will depend on the energy spectrum of the particles producing the disintegrations at our observation

([11]) A. LOVATI, A. MURA, G. SALVINI and G. TAGLIAFERRI: *Nuovo Cimento*, **7**, 945 (1950).

([12]) U. CAMERINI, J. H. DAVIES, P. H. FOWLER, C. FRANZINETTI, H. MUIRHEAD, W. O. LOCK, D. H. PERKINS and G. YEKUTIELI: *Phil. Mag.*, **42**, 1241 (1951).

([13]) A. LOVATI, A. MURA and G. TAGLIAFERRI: *Nuovo Cimento*, **9**, 205 (1952).

([14]) G. SALVINI and Y. KIM: *Phys. Rev.*, **85**, 921 (1952).

([15]) R. R. DANIEL, J. H. DAVIES, J. H. MULVEY and D. H. PERKINS: *Phil. Mag.*, **43**, 753 (1952).

altitude. We can however notice that most p.s.p. and π^0 (cf. table V) are delivered by the classes of disintegrations with 1, 2, 3 p.s.p. or with 0 p.s.p. but with electronic component; that is disintegrations whose primaries have likely energies within the limits of 1 to 5 GeV.

Before really calculating R we must further observe that it is true that a certain number of p.s.p. and e.s. (and therefore of π^0) is not revealed owing to chamber geometry. Given the dimensions of the plates, their spacing and the angular spread of the p.s.p. and e.s., it is believed that nearly the same amount (estimated about 25%) of the ones and others is lost. It is not however necessary to bear the above correction if one refers, as we do, to the ratio between π^0 and $\pi^\pm$ emitted inside the same solid angle.

In table V, the 3rd and 4th rows show the pertinent numbers of p.s.p. and π^0, shared according to the number of p.s.p. with which the disintegration has appeared.

TABLE V.

Number of p.s.p. per disintegration	0	1	2	3	4	5
Number of disintegrations	~ 1500	195	43	18	4	1
Number of disintegrations with electr. component	34	14	5	7	2	1
Total number of p.s.p.		195	86	54	16	5
Total number of π^0	59	20	13	13	3	1

The figures of the 1st and 2nd columns take into account the disintegrations unrevealed because of the complete absorption of the heavily ionizing particles within the plates.

From the figures of the 3rd row one obtains a total of 356 p.s.p.. From the energy distribution of the protons and charged π-mesons issued from the disintegrations observed at balloon flight altitude ([16]), one can argue that the $\pi^\pm$ of kinetic energy > 60 MeV are about 60% of our p.s.p.. Therefore the $\pi^\pm$-mesons with kinetic energy > 60 MeV are $356 \times 0.60 = 214$. The energy distribution just mentioned allows to calculate the total number of $\pi^\pm$ created in our disintegrations, bearing a correction of $\sim 20\%$ to take into account also the $\pi^\pm$ of kinetic energy < 60 MeV: $\pi^\pm_{tot} = 214 + 43 = 257$.

From the 4th row one gets the total number of π^0 mesons, $\pi^0_{tot} = 109$.

In conclusion, it follows

$$R = 109/257 \approx 0.42 .$$

([16]) See reference ([7]), pag. 24, fig. 10.

We have estimated that this final result may be affected by an error of 40% at the most.

5. – Cross-section for π^0 production in nucleon-nucleus collisions.

The 1st and 2nd rows of table V give respectively the numbers of the nuclear disintegrations occurred in chamber plates and the numbers of those yielding electronic component, both parted after the p.s.p. multiplicity. Dividing the numbers of the 2nd row by the ones of the 1st, the relative frequency of the events with electronic component is obtained.

This frequency can be assumed as an approximative indication of the ratio between the π^0 production cross-section and the corresponding one for production of nuclear disintegrations in the nucleon-Pb nucleus collisions. If we assume that this latter cross-section—for the energy interval here concerned—be practically coincident with the geometrical cross-section of the Pb nucleus, the above ratio will indicate even the value of the π^0 production cross section as a fraction of the geometrical one.

From table V one can observe that the relative frequency of the events with electronic component rises when the p.s.p. multiplicity runs from 0 to 5; that is, it very likely rises when the energy of the producing particle becomes greater.

Due to the limited statistical consistency of the single values, we must confine to deduce the π^0 production cross-section for groups of disintegrations; for instance, as SALVINI and KIM [14] have already done, for the groups containing (*a*) 1 or 2 p.s.p. or 0 p.s.p. but electronic component, and (*b*) at least 3 p.s.p..

The we get:

$$\text{in case } (a) \qquad (\sigma_{\pi^0}/\sigma_{\text{geom}})_{\text{Pb}} = 53/272 \approx 0.20\,,$$

$$\text{in case } (b) \qquad (\sigma_{\pi^0}/\sigma_{\text{geom}})_{\text{Pb}} = 10/23 \approx 0\ 43\,.$$

These figures are however lower limits, since we must consider the effect, of failure in revealing the γ rays due to the chamber geometry (a loss of 25% cf. n. 4) and to the cut-off in the γ energy spectrum (a loss of 55%, cf. n. 3). By utilizing the distribution of the disintegrations according to the number of e.s. (table III), it may be concluded that the number of disintegrations having electronic component must be increased by nearly 50%.

Accordingly, and bearing in mind the primary energy-n_s multiplicity relations [7], we estimate the following indicative values: (*a*) 0.3 and (*b*) 0.6 times the geometrical cross-section, for incident particle energies roughly centered around, respectively, 2 and 6 GeV. The above values are in fair

agreement with the ones derived by SALVINI and KIM [14] for disintegrations produced in sodium iodide.

6. – Conclusion and acknowledgements.

Throughout this paper the appearance of the electronic component from nuclear disintegrations in lead has been examinated, finally coming to the evaluation of the ratio of the number of neutral to charged mesons, and of the relative frequency of production of electromagnetic component. It is realized that there has been a remarkable lot of corrections to obtain the final results; moreover the statistical evidence is, of course, scanty. However, it was cared to minimize undesirable selections: first, by using the random expansion technique; and further by attempting to reconstruct the actual size-frequency distribution of the disintegrations occurred within the plates. Whenever possible, the sharing of the observed events in arbitrary classes was also avoided.

Therefore, the cloud chamber works most conveniently comparable with the present experiment are the ones of SALVINI and KIM [4,14], provided it is noticed that these authors examined an energy interval presumably a little higher than we did; and that they took disintegrations produced mainly by protons, whereas this condition was not imposed by us. Then, all that can be said is that no significant difference appears between our results and those of SALVINI and KIM.

It is a pleasure to acknowledge our indebtedness to Prof. G. POLVANI, Director of this Institute, for his constant interest and encouragement in the course of this work.

We would like further to express our appreciation to Prof. G. SALVINI for the helpful discussions on the subject of this paper, and for letting us read the manuscript of his unpublished work.

Thanks are also due for the use of the facilities of the Laboratorio della Testa Grigia to the Director, Prof. G. BERNARDINI; and to Drs. M. BOSSI, P. CASALE, A. ROSSI and C. SUCCI for their valuable assistance in carrying on the measurements.

The financial helps of the University of Milan, of the Consiglio Nazionale delle Ricerche, of the Associazione Nazionale A.N.I.D.E.L. and of the Gruppo degli Amici dell'Istituto are gratefully acknowledged.

RIASSUNTO

Per compiere un'analisi inselezionata su alcuni aspetti della radiazione cosmica a quota di montagna, sono state raccolte alla quota di 3500 m, con una camera di Wilson contenente 9 setti di piombo dello spessore di 18 g cm^{-2} ciascuno, 16000 fotografie di espansioni a caso. Nel presente lavoro è stata studiata la componente elettronica proveniente dalle esplosioni nucleari di bassa e media energia prodotte dalla radiazione cosmica nel piombo. Accettando l'ipotesi che la componente elettrofotonica provenga dal decadimento di mesoni π neutri, si è ricavato il rapporto fra il numero dei mesoni neutri e quello dei mesoni carichi emessi nelle nostre disintegrazioni. Si è trovato il valore $R = N_{\pi^0}/(N_{\pi^+} + N_{\pi^-}) = 0.42 \pm 40\%$. Si è pure calcolata la probabilità di produzione della componente elettrofotonica nelle collisioni dei nucleoni con i nuclei di piombo: per particelle incidenti di energia intorno a 2 e a 6 GeV si sono ricavati per la sezione di produzione rispettivamente valori di 0.3 e 0.6 volte la sezione geometrica del nucleo di piombo. Nell'analisi dei fotogrammi raccolti, si sono potute riconoscere due particelle V^0 su un totale di 920 disintegrazioni osservate nei setti di piombo.

The disintegration of μ mesons in carbon.

A. Alberigi Quaranta

Istituto di Fisica dell'Università, Centro di Studio per la Fisica Nucleare del C.N.R. - Roma

E. Pancini

Istituto di Fisica dell'Università - Sassari
Centro di Studio per la Fisica Nucleare del C.N.R. - Roma

(ricevuto il 23 Luglio 1952)

Summary. — An experiment is described for the study of some of the properties of μ-mesons stopped in carbon. The μ^+ and μ^- mesons have been studied separately and we have found very precise apparent mean lifetimes in carbon of $\tau^+ = 2.22 \pm 0.06$ μs and $\tau^- = 2.18 \pm 0.07$ μs. The data obtained from these measurements are discussed and compared with those of other experimenters to see if there is a possible difference in the behaviour of the positive and the negative mesons. It is concluded that there are no indications for believing that there is a real difference between the natural mean lives of the μ^+ and μ^- mesons, although one cannot exclude the eventual possibility of a divergence. It is further demonstrated that there are no indications for believing the energy spectra of the disintegration electrons to be greatly different for the + and — mesons.

1. – Introduction.

Recently various authors have indicated the possibility that the negative μ-mesons manifest some differences with respect to the positive mesons, both [1] in the energy spectra of the disintegration electrons and [2] in their natural

[1] For the bibliography see [2].
[2] N. Dallaporta: *Nuovo Cimento*, **9**, 449 (1952).

mean life-times; at least one might expect a difference in the case in which the μ^-meson is captured in the K orbit of the nucleus.

Unfortunately, both types of investigation are difficult with a cosmic ray experiment, in the first place because it is always difficult to obtain a complete separation of the two mesons, and in the second because, the more efficient the separation, the less the intensity obtainable.

Further, if one wishes to determine the energy spectrum of the disintegration electrons with precision, it is necessary to use a thin absorber, and the intensity of the electrons produced is thus further reduced.

As far as regards the possibility of determining with precision the natural mean life τ_0^-, we note that one can deduce it from the following relation ([3]):

$$\tau_0^- = \tau^- \left[\left(\frac{Z_e}{Z_0} \right)^k + 1 \right], \tag{1}$$

where τ^- is the apparent mean life of the negative meson, k is a number close to 4, Z_0 a number close to 10 and Z_e is a function, not known with sufficient certainty, of the atomic number of the absorber. As a result of this, the value of τ_0^- can be deduced from a measurement of τ^- only for elements of low atomic number, for which $(Z_e/Z_0)^k$ is small with respect to 1, so that the uncertainty due to this factor weighs very little in the determination of the relation τ_0^-/τ^-; $[(Z_e/Z_0)^k \cong 0.05$ for Be and 0.1 for C].

On the other hand the measurement of τ^- in the light elements can not be done if the μ^+ and μ^-mesons are not separated. Because of the small difference between the mean lives $\tau^+ = \tau_0^+$ and τ^- it is not possible to determine the mean life τ^- from the composite disintegration curve. If the mesons are however separated with a magnetic field, the hourly intensity is, in the limits of practical possibilities, so low (some few events per hour) that it would require, for a precision on the order of 1%, measurements lasting over a period of several years.

Notwithstanding the practical impossibility of answering definitely the hypothesis posed by DALLAPORTA, we have decided to publish the results obtained thus far relative to the mean lives of the μ^+ and μ^- mesons stopped in carbon. These results have been taken from a series of systematic measurements still being made in the laboratory at Testa Grigia (3 500 meters above sea level) with the purpose of investigating the dependence of the value of τ^- on the atomic number of the absorber, for the light elements.

Up to this moment, our data are the most precise that have been collected, with some probability of not being rapidly improved, and we believe that they are a useful contribution to the discussion of this problem.

([3]) J. A. WHEELER: *Rev. Mod. Phys.*, **21**, 133 (1949).

2. – Experimental Arrangement.

The arrangement used by us, schematically represented in fig. 1, is constructed of telescope counters I and II between which are placed the usual magnetic lenses (4) (thickness 20 cm: $B = 15\,000$ Gauss) used to separate

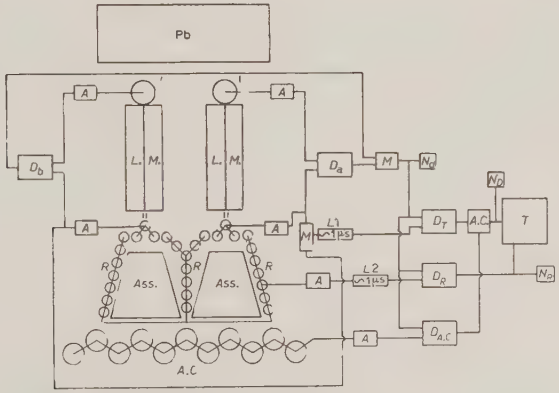

Fig. 1. - Plan of the experimental arrangement: *Pb*: 10 cm of Pb; *Ass*: Graphite absorber; *M.L.*: Magnetic Lenses; *A*: Amplifier; *M*: Mixer (Mixing Circuit); L_1 and L_2: Variable artificial delays ~ 1 μs; N_a; N_D; N_R: Numerator circuits; D_a; D_b; $D_{A.C.}$; D_T; D_R: Double coincidences (Resolving power ~ 10 μs); *A.C.*: Anticoinciednce Circuit; *T*: Time-interval measuring circuit; I: 4×25 cm Counters; II: 2×25 cm Counters; *R*: 2×50 cm Counters; *A.C.*: 4×60 cm Counters.

mesons of different sign before they come to rest in the absorber (Ass.); around this, (for the detection of the disintegration electrons), is placed the group of counters *R* just outside the solid angle determined by the telescopes (I and II). The counters of anti-coincidence (A.C.) (with a total efficiency of about 95%) have the purpose of reducing to a minimum the prompt triple coincidences (I, II, *R*), for the larger part due to showers. For the same purpose lead of 10 cm thickness has been placed above the entire apparatus. Two identical arrangements of telescopes, magnetic lenses and absorbers have been used to double the intensity.

The associated electronics are schematically represented in fig. 1. The pulse from the double-coincidence D_T is always determined from the time point of view, by the group of counters II, while the pulse from the double coincidence D_R is time-determined by the pulses of the counters *R*.

(4) G. Bernardini et *al.*: *Phys. Rev.*, **68**, 109 (1945).

The arrangement indicated with T catalogues the intervals of time which separate each pair of pulses coming from D_T and from D_R into eight contiguous groups, in the k-th of which are summed all of the delays whose durations are between t_k and $t_k + 1$. When the anti-coincidence circuit is not contemporaneously triggered, such pairs of pulses are due in good part to a meson absorbed in the absorber and to its decay electron.

The three numerators N_d, N_R, N_D count, as a control, respectively the double coincidences (I, II) the triples (I, II, R) and the doubles not accompanied by a signal from the anti-coincidence group ((I, II)-A.C.).

The counters used for the Group II and for the Group R are of the ordinary type with radius of 1 cm and one can therefore expect [5] that the response of the counter follows the passage of the particle with a delay of 0 to 0.18 μs. On the other hand it is well known [6] that the lags of the counter do not influence the determination of the mean life provided that one measures only those delays greater than the maximum lags of the counter.

During our measurements the fixed variable delays L_1 and L_2 (equal to about 1 μs) were chosen in such a way that contemporaneous signals of the counters II and R would be registered by T in the second group of delays. In this way, if on the one hand, the fineness of the analysis of the delays diminishes, on the other hand one gains much in the control of the orderly functioning of the arrangement, based on the analysis of the distribution of the lags of the counter proper.

In the measurements for the determination of the mean lives of μ^+ and μ^- in carbon, the following arrangement for the groups of delays has been adopted:

Group	from	to
I	-0.31 μs	-0.10 μs
II	-0.10	$+0.20$
III	$+0.20$	$+0.52$
IV	$+0.52$	$+1.02$
V	$+1.02$	$+1.8$
VI	$+1.8$	$+2.75$
VII	$+2.75$	$+3.85$
VIII	$+3.85$	$+\sim 10$

As it has been already mentioned the time origin is determined as the time of arrival of the signal from D_T and therefore from the Group II counters. This

(5) A. ALBERIGI QUARANTA, L. MEZZETTI, E. PANCINI and G. STOPPINI: *Nuovo Cimento*, **8**, 618 (1951).

(6) B. ROSSI and N. NERESON: *Phys. Rev.*, **62**, 417 (1942).

signal comes after the passage of the particle through the counter in a time which includes the constant delay, and the statistical delay variable from 0 to 0.18 μs (lags of the counter). From this it follows that events physically contemporaneous in I, II, R can be registered as anticipated events or as delays according to the value of the lags of the counters II and R themselves.

With the choice of the limits for the groups of delays as given in the table above, it is easy to calculate that the ratio of the numbers of events in group I and II must be about 1/5. The experimental value of this ratio gives a very precise indication of the regularity of the functioning of the entire apparatus.

The initial point of the delays for Group III has been chosen at $+ 0.2$ μs in order to be certain that all the events registered by this group and by the following ones correspond to the effective physical delays. The results of the numerous control measurements made without absorber confirm the soundness of this criterion.

3. – Experimental Results.

With the arrangement described above measurements were made on the μ^+ and the μ^- mesons which were alternatively selected, both with and without absorber. During the entire series of measurements, the apparatus, conveniently monitored at regular intervals, functioned without trouble.

The results of all measurements are summarized in Table I. For each partial measurement it has been specified that:

1) The number of events N_d, N_R, N_D should not scatter, aside from the barometric effects, from their mean values more than would be compatible with statistical variations.

2) The ratio between the number of events registered in Group I and in Group II be equal to 1/5, again allowing for statistical scattering.

All measurements not corresponding to these criteria were excluded.

a) *Measurements without absorber.* – As to the measurements without absorber, the analysis of Table I shows clearly that the greater part of the delay events, from Group III and those that follow, is due to disintegration electrons emitted by the mesons absorbed in the supports and in the walls of the counters. In fact, the number of delay events from Group III on is much less when the μ^- mesons have been selected than when the μ^+ mesons have been selected. Further, the data for the μ^+ mesons are in agreement with a mean life of about 2 μs, while those of the μ^- mesons indicate with certainty a mean life rather shorter, as one would expect since the walls of the counters and the supports are of brass and aluminium.

TABLE I.

Length of the measurement	Absorber	Sign	N_D/h	N_R/h	N_d/h
70.40 h	no	+	60.8 ± 0.9	150.2 ± 1.5	1164 ± 4
62.40 h	no	—	59.5 ± 1	148.6 ± 1.6	1110 ± 4
88.65 h	graphite	+	92.6 ± 1	152.6 ± 1.5	1153 ± 4
Correction	—		—	—	—
Corrected values . . .	—		—	—	—
96.75 h	graphite	—	84.0 ± 1	153.9 ± 1.3	1089 ± 3
Correction	—		—	—	—
Corrected values . . .	—		—	—	—

As was to be expected, the positive excess is reflected only in the number N_d and does not influence, either the number N_R, which, as we have said, is due in large part to showers, or the number N_D which represents substantially, in this case, the counts missed in the anti-coincidence. The value of the positive excess in N_d is $(5.2 \pm 0.3)\%$, a value perfectly in accord with that which one would expect with magnetic lenses of the type which we have used [7].

b) *Measurements with a carbon absorber.* – In Table I are also listed the results obtained using as an absorber, two blocks of graphite (density 1.6 g/cm³) of trapezoidal cross section and of 12 cm thickness, equivalent to about 20 g/cm³.

With the absorber in place, the number N_D/hour increases by 31.8 ± 1.4/hour for the positive mesons, and for the negative mesons by 24.5 ± 1.5/hour. This corresponds to a mean coefficient of absorption in carbon for this energy region (in our case around 400 MeV), equal to 0.12% per g/cm² of carbon, in good agreement with the values which one can deduce from the energy spectrum of mesons at 4300 meters a.s.l. found by D. B. HALL [8].

This shows that the greater part of the particles which cross the telescope (I, II) is effectively composed of mesons.

This is also confirmed by the fact that the number of particles stopped in the absorber show a positive excess of $28 \pm 5\%$.

It is convenient at this point to note that in order to be certain of the nature of the numerous triple coincidences not accompanied by anti-coincidences ((I, II, *R*)-A.C.), which have been registered in the I and II groups of delay ($N_{\text{I}} + N_{\text{II}}$), and only partially attributable to mesons disintegrating in the absorber, we have made preliminary measurements without the protection of the 10 cm of Pb above the apparatus. Under such conditions we

[7] I. F. QUERCIA, B. RISPOLI and S. SCIUTI: *Nuovo Cimento*, **4**, 283 (1947).
[8] D. B. HALL: *Phys. Rev.*, **66**, 321 (1944).

N_{I}	N_{II}	N_{III}	N_{IV}	N_{V}	N_{VI}	N_{VII}	N_{VIII}
86	596	23	21	12	13	9	12
77	519	7	12	10	1	2	0
183	1025	97	135	171	107	73	140
108	750	29	26	15	16	11	15
75	275	68	109	156	91	62	125
190	1168	74	121	108	92	64	92
119	804	11	19	16	2	3	0
71	364	63	102	92	90	61	92

have established that such events increase by about 100% while the ((I, II, R)-A.C.) registered in Group III and on i.e. ($N_{III} + N_{IV} + \ldots + N_{VIII}$) increase by only 25%. This indicates that:

1) The presence of the 10 cm of Pb shifts the energy band of mesons stopped in the absorber, with respect to the maximum of the energy spectrum, towards higher energies, as was predictable.

2) A good part of the coincidences ((I, II, R)-A.C.) registered in the I and II Group ($N_{I} + N_{II}$) is due to electron showers. This is also confirmed by the fact that neither in the measurements with absorber nor in those without absorber, does the ($N_{I} + N_{II}$) group show a positive excess.

The efficiency of this arrangement for detecting the disintegration electrons from the absorber, calculated with reference only to those with a delay greater than 0.2 μs, is, for the positive sign

$$\varrho^{+} = \frac{(6.9 \pm 0.28)/\text{hour}}{(31.8 \pm 1.4)/\text{hour}} = (21.7 \pm 1.3)\ \%\,.$$

The efficiency for the negative sign is

$$\varrho^{-} = \frac{(5.2 \pm 0.25)/\text{hour}}{(24.5 \pm 1.4)/\text{hour}} = (21.2 \pm 1.6)\ \%\,.$$

The hourly rate of the delay events with the absorber has been calculated from the values under the heading « corrected values ». Such values have been obtained subtracting from the experimental values with absorber those without absorber, normalized to the same number of hours.

Proceding in this way, we have considered the delay events registered without absorber as a background due to mesons disintegrating in the supports and walls of the counters, to casual coincidences, etc., and it is further sup-

posed that this value is independent of the presence of the absorber, which is only approximately true.

On the other hand, the same efficiencies calculated from the uncorrected experimental values are respectively $(25.6 \pm 1.3)\%$ and $(23.5 \pm 1.6)\%$, values which are still practically identical.

For the calculation of the mean life τ, since the precise method of PEIERLS [9] is not applicable in our case, we have used the well known formula

$$\tau = \frac{t - t_0}{\lg r}, \qquad \overline{\delta\tau}^2 = \left(\frac{\tau}{t - t_0}\right)^2 \left(\frac{\tau^2}{N}\right)\left(\exp\left[\frac{t - t_0}{\tau}\right] - 1\right),$$

where r is the ratio of the total number of delay events after time t_0 to the number of delay events after time t.

From our data it is possible to obtain five independent values of the apparent mean life of the μ-mesons as follows:

$$\tau^+ = 2.30 \pm 0.12;\quad 2.15 \pm 0.11;\quad 2.03 \pm 0.11;\quad 2.56 \pm 0.19;\quad 2.46 \pm 0.29\ \mu s,$$

$$\tau^- = 2.15 \pm 0.12;\quad 2.14 \pm 0.12;\quad 2.22 \pm 0.14;\quad 2.20 \pm 0.17;\quad 2.30 \pm 0.3\ \mu s,$$

from which one obtains the average mean lives

$$\tau^+ = 2.22 \pm 0.06\ \mu s,$$

$$\tau^- = 2.18 \pm 0.07\ \mu s.$$

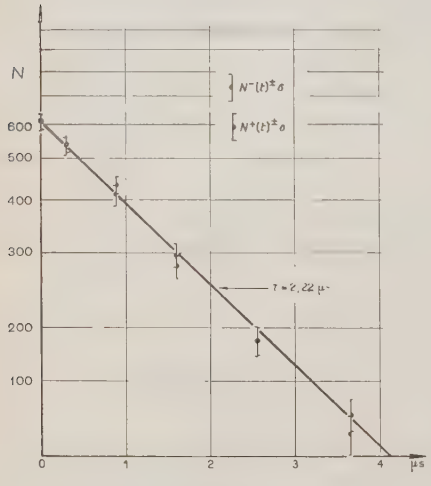

Fig. 2.

The total of the systematic errors, in the measurements of the times, for each group of delays, is on the order of 3% [10].

The complete agreement, therefore, between the value found here and that of BELL and HINCKS [11], which is the most accurate that we have today, can be regarded as fortuitous. It must be remembered, in addition, that the systematic errors do not influence the ratio τ^+/τ^-. In fig. 2 are listed the experimental points with their errors. The values pertaining

[9] R. PEIERLS: *Proc. Roy. Soc.*, **149**, 467 (1937).

[10] A. ALBERIGI QUARANTA, F. LEPRI, L. MEZZETTI and E. PANCINI: *L'Energia Elettrica*, **27**, 561 (1950).

[11] W. E. BELL and E. P. HINCKS: *Phys. Rev.*, **84**, 242 (1951).

to the μ^- mesons have been normalized so that their total number corresponds to that of the μ^+ mesons. In the same figure we have also drawn the line corresponding to a mean life of 2.22 μs.

4. – Conclusions.

From the results that we have obtained for the value of the apparent mean life of the μ^--meson ($\tau^- = 2.18 \pm 0.07$ μs) it is possible to obtain, admitting the validity of (1), a very useful check of the hypothesis advanced by DALLAPORTA concerning a possible difference between the value for τ_0^+ and τ_0^-. One finds, in fact, from (1) placing $Z_0 = 10$, $k = 4$, $Z_e = 5.78$ and $\tau^- = 2.18 \pm 0.07$ μs,

$$\tau_0^- = 2.42 \pm 0.08 \ \mu\text{s}$$

and thus for the ratio τ_0^+/τ_0^- ($\tau_0^+ = \tau^+ = 2.22 \pm 0.06$ μs)

$$\frac{\tau_0^+}{\tau_0^-} = 0.92 \pm 0.04 ,$$

consistent with the value $\tau_0^+/\tau_0^- = 1$. We have preferred to compare with 1 the value of the ratio τ_0^+/τ_0^-, because this is the only ratio we can deduce from our measurements, which is independent of the systematic errors in the time measurements.

Applying the same criterion to the results of all experiments completed up to now in which τ^- and τ_0^+ have been separated and contemporaneously measured, the weighted mean of all the values of τ_0^+/τ_0^- [12] [13] including ours is:

$$\frac{\tau_0^+}{\tau_0^-} = 0.93 \pm 0.03 ,$$

still consistent with $\tau_0^+/\tau_0^- = 1$.

One can further observe that the experimental data obtained up to now are not such as to make completely sure the choice of $Z_0 = 10$ as used in formula (1).

Introducing, then, $Z_0 = 11$ in (1) and repeating the preceeding comparisons one obtains for τ_0^+/τ_0^- values all consistent with 1, and the weighted mean now becomes:

$$\frac{\tau_0^+}{\tau_0^-} = 1.01 \pm 0.03 .$$

One can thus conclude that the interpretation of the data obtained up to now

[12] C. W. KISSINGER and D. COOPER: *Phys. Rev.*, **74**, 349 (1948).
[13] H. K. TICHO: *Phys. Rev.*, **74**, 1337 (1948).

does not require the hypothesis of DALLAPORTA, although the one raised by DALLAPORTA can not be excluded.

With respect to the efficiency values of our arrangement for the detection of disintegration electrons from the μ^+ and μ^- mesons respectively, we note that these efficiencies can be expressed by means of the following:

$$(2) \qquad \varrho^+ = G^+ \exp\left[-\frac{t_{III}}{\tau^+}\right], \qquad \varrho^- = G^- \exp\left[-\frac{t_{III}}{\tau^-}\right] W_z ,$$

where t_{III} represents the initial time of the III group of delays; W_z the probability of decay of the μ^-, and G^+ and G^- are convenient geometrical factors which will differ only if there is a difference in the behaviour of the energy spectra of the disintegration electrons of the mesons of the two signs.

From (2), substituting for t_{III}, τ^-, ϱ^-, τ^+, ϱ^+ their values, and for W_z the value calculated with the formula of WHEELER [3] one obtains for $Z_0 = 10$

$$\frac{G^+}{G^-} = \frac{\varrho^+}{\varrho^-} 0.90 = 0.92 \pm 0.09 ,$$

and for $Z_0 = 11$

$$\frac{G^+}{G^-} = \frac{\varrho^+}{\varrho^-} 0.93 = 0.95 \pm 0.09 .$$

From these results, one may conclude that, as far as the accuracy of our measurements allows judgment, G^+ and G^- must be considered as being equal. Further, in order to decide if this result is, or not consistent with possible differences in the two spectra, it would be necessary to perform a very fastidious calculation to ascertain in what manner such a difference would influence the values of these geometrical factors for our apparatus.

RIASSUNTO

Viene descritta una esperienza per lo studio di alcune proprietà dei mesoni μ condotti a riposo in Carbonio. I mesoni μ^+ e μ^- vengono studiati separatamente e si ricava fra l'altro un valore assai preciso delle loro vite medie apparenti in C $\tau^+ = 2.22 \pm 0.06$ μs e $\tau^- = 2.18 \pm 0.07$ μs. Si discutono i dati ottenuti in queste misurazioni e si confrontano con quelli di altri autori per cercare indicazioni circa una eventuale diversità del comportamento dei mesoni dei due segni. Si conclude che non vi sono indicazioni per ritenere che vi sia diversità tra le vite medie proprie dei mesoni dei due segni, benchè questa eventualità non si possa senz'altro escludere. Si mostra inoltre che non si hanno indicazioni per ritenere diversi gli andamenti degli spettri di energia degli elettroni di disintegrazione.

IL NUOVO CIMENTO Vol. IX, N. 10 1 Ottobre 1952

On the interaction of cosmic rays with matter under 50 metres water equivalent.

E. Amaldi, C. Castagnoli, A. Gigli (*) and S. Sciuti

Istituto di Fisica dell'Università - Roma
Istituto Nazionale di Fisica Nucleare - Sezione di Roma

(ricevuto il 4 Agosto 1952)

Summary. — The production of penetrating secondaries by cosmic rays at 50 m w.e. has been investigated by means of a counter hodoscope. The cross section (in lead) for events which can be interpreted as pairs of associated penetrating particles (*a.p.p.*) is not larger than $(13 \pm 3) \cdot 10^{-30}$ cm^2/nucleon. Such a value is deduced from measurements of the corresponding differential cross section as a function of the penetration of the secondary particles produced (section 4·3 table V). A value of the same order of magnitude is found for the production of *a.p.p.* in rock (section 4·5). Furthermore it is shown that the events that can be interpreted as showers penetrating 15 cm Pb, have a frequency that can be explained, at least in part, as due to purely electromagnetic interaction. Therefore one can establish an upper limit of a few units in 10^{-30} cm^2/nucleon for the cross section for production in Pb of penetrating showers by μ-mesons. Finally we discuss those events which appear to be due to a few penetrating particles coming from the rock and it is shown that they can be accounted for, by considering besides the production of penetrating showers in rock the penetrating particles present in the vicinity of the core of extensive air showers.

(*) Dell'Istituto di Fisica dell'Università di Pavia, attualmente in congedo presso l'Istituto Nazionale di Fisica Nucleare, Sezione di Roma.

1. – Introduction.

Various authors have observed stars (1), neutrons (2), bursts containing penetrating particles (3) and pairs of associated penetrating particles (4), produced by cosmic rays underground at depths of a few tens of m w.e.

All these events are produced in part by μ-mesons and in part by π-mesons and neutrons from the stars directly due to μ-meson collisions with nucleons.

The experimental values of the corresponding cross section of μ-mesons with nucleons and their dependence on the energy of the incoming particles, have been compared with the theoretical values deduced under the assumption that all above mentioned phenomena are due to the interaction of the electromagnetic field of the incoming μ-meson with the mesonic field of the nucleons (5).

Such a comparison throws some light on the possible existence of a specific interaction between μ-mesons and nucleons. From experiments on the capture of slow μ-mesons by light nuclei (6) as well as on the elastic scattering at angles larger than 20° of μ-mesons of about 10^9 eV (7), one would expect that, also for energies of the order of 10^{10} eV, such interactions are not very important.

However the cross sections observed underground by the above mentioned authors for the elastic scattering at angles larger than 25° (8) as well as the cross section for production of bursts containing penetrating particles (3) and of pairs of associated penetrating particles (4), seem to be too large to be explained only by means of the electromagnetic interaction of μ-mesons with the mesonic field of the nucleons.

(1) E. P. George and J. Evans: *Proc. Phys. Soc.*, **63**, 1248 (1950); **64**, 195 (1951).

(2) G. Cocconi and V. Cocconi-Tongiorgi: *Phys. Rev.*, **84**, 29 (1951); M. F. Crouch and R. Sard: *Phys. Rev.*, **85**, 120 (1952); R. D. Sard, M. F. Crouch, D. R. Jones, A. M. Conforto and B. F. Stearns: *Nuovo Cimento*, **8**, 326 (1951). We thank doctor Sard for having communicated his results before publications.

(3) E. P. George and P. Trent: *Nature*, **164**, 839 and 248 (1949).

(4) H. J. Braddick and G. S. Hensby: *Nature*, **44**, 1012 (1939); H. J. Braddick, W. F. Nash and A. W. Wolfendale: *Phil. Mag.*, **42**, 1277 (1951).

(5) S. Hayakawa: *Phys. Rev.*, **84**, 37 (1951).

(6) M. Conversi, E. Pancini and O. Piccioni: *Phys. Rev.*, **68**, 232 (1945) and **71**, 209 (1947); E. Fermi and E. Teller: *Phys. Rev.*, **72**, 399 (1947); E. Fermi, E. Teller and V. Weisskopf: *Phys. Rev.*, **71**, 314 (1947).

(7) E. Amaldi and G. Fidecaro: *Nuovo Cimento*, **7**, 535 (1950); *Phys. Rev.*, **81**, 339 (1951).

(8) F. Nash: Ph. D. Thesis, Manchester; reported in J. G. Wilson: *Progress in Cosmic Rays Physics* (Amsterdam, 1952).

Therefore we thought it worth while to try to do an experiment on the production of penetrating showers from which one could determine the corresponding cross section.

In order to collect statistically significant data in a reasonable time in spite of the low intensity of cosmic rays underground, we have chosen a counter technique and we have drawn the experimental set-up of rather large geometrical dimensions. The information that one can get from such an experiment are rather rough, if compared with that obtained with cloud chamber or nuclear emulsion techniques, but still they can be useful to clarify the very incomplete picture of cosmic rays underground.

In section 2 we describe the experimental set-up; in section 3 we report on the experimental results obtained at a depth of 50 m w.e. from the top of the atmosphere, in section 4 we discuss our experimental results and derive the cross sections of various types of events.

2. – Procedure.

2·1. – The experimental set-up is drawn schematically in fig. 1. Each counter, of 4 cm diameter, is connected to a corresponding neon lamp with the exception of the counters of the set A for which there is a single neon lamp for each group of five counters.

The useful length is 100 cm for the counters of set A, 60 cm for the counters of set B and 80 cm for the counters of sets C, D and E. Therefore the solid angle of the incident particles is defined by the counter-sets B and E.

The rather large geometrical dimensions of our experimental set-up (total sensitive area of counters 3.2 m^2) give a reasonably large intensity and a good angular definition (a few degrees).

Above each one of the counter-sets C, D, E there is a layer of Pb 5 cm thick. The counters of the sets C and E are separated from one another by a layer of Pb 1 cm thick, in order to reduce the number of recorded electronic secondaries.

The master pulse which triggers the hodoscope can be easily changed. During the measurements that we report here, the master pulse used, was for part of the time $B_1C_2D_1E_1$, for part of the time $B_1C_1D_2E_1$ and for the rest of the time $B_1C_2D_1E_2$, the subscript giving the minimum number of counters which must be discharged in each set.

Besides the hodoscope, the experimental set-up includes ordinary coincidence circuits which can be used to count the fourfold coincidences (C_4) between the four sets of counters B, C, D, E (all counters of each set in parallel)

and the fivefold coincidences (C_5) between the four preceeding sets and the counters A all in parallel.

Measurements have been made with and without the layer of Pb (Σ) whose thickness was either 5 or 7.5 cm.

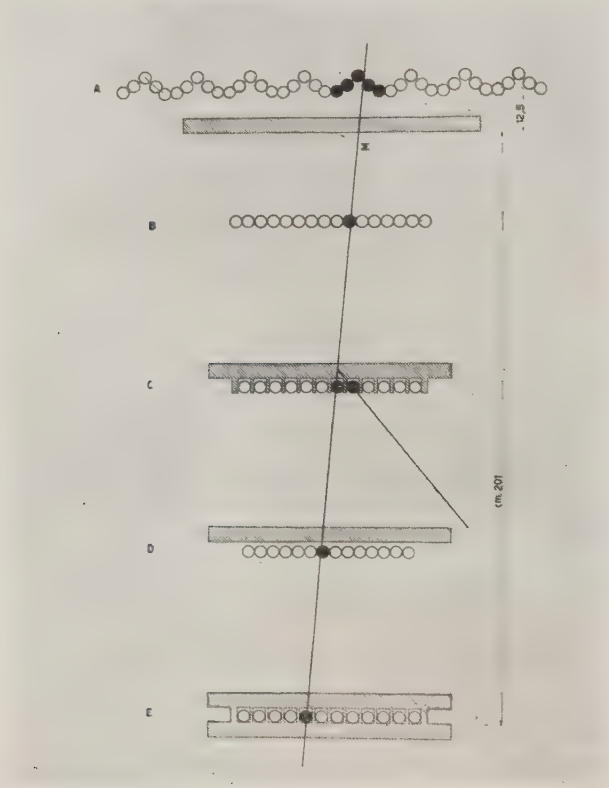

Fig. 1. – Schematical drawing of the experimental set up, with an example of *e.s.* (i.e. photogram interpreted as due to an electronic secondary: an alignment plus one single counter discharged in a single set of counters).

2·2. – Fig. 2 shows a block-diagram of our circuits. Each counter of the sets B, C, D, E is connected to a cathodic multivibrator (*mv*) mounted directly on the counter: for the set A there is a single *mv* for each group of five counters.

The output of each one of the *mv* is connected to a double coincidence circuit (*dc*) which provides the coincidence between the counter and the master

pulse. The output of each *dc* triggers the circuit of the corresponding neon lamp.

The outputs of all the *mv* connected to the counters of one of the sets *B*, *C*, *D*, *E* are added, by means of resistences of 100 kΩ, on the grids of two polarized amplifiers (*ad*) which constitute two pulse discriminators. The polarization of one of these two circuits *ad* is adjusted, for each one of the *B*, *C*, *D*, *E* counter-sets, to transmit single pulses: the corresponding outputs are used for the fourfold (C_4) and fivefold (C_5) coincidences.

The polarization of the other *ad* circuit can be changed in such a way that at least two, three or more counters must be discharged simultaneously in the corresponding set: through two double coincidence circuits they give rise to the master pulse.

All the neon lamps are placed on a panel together with a watch and a mechanical counter which records the number of master pulses.

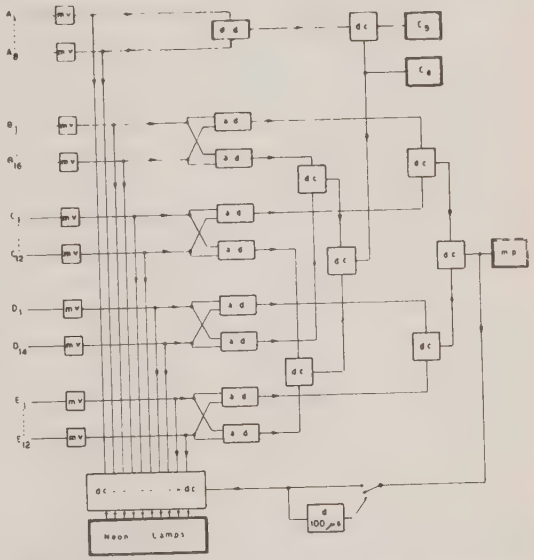

Fig. 2. – Block diagram of the circuits. *mv* — multivibrator; *dc* = double coincidence; *ad* = amplifier-discriminator; *dd* = decoupling diodes; *mp* = master pulse; *d* = delay.

A camera with open objective takes a picture of such a panel, and then the film advances with a 0.1 second delay, anytime that at least one neon lamp lights. This is obtained by triggering the motor of the camera with a pulse taken from a 200 Ω resistance placed in series with the 300 volt supply of the neon lamps.

Such an advancement device allows us to recognize any possible misfunctioning of the neon lamp circuits since the resulting pictures do not correspond to the imposed master pulse. The resolving time of the coincidence circuits *dc* is about 15 μs.

2·3. – A detailed discussion of all the possible chance coincidences which can appear as a production in Σ of 2 or more penetrating particles, shows

that one has to distinguish four types of events in which no counter A is discharged and 5 other types in which a single group of counters A is discharged.

Among all these events clearly the more frequent one consists in two independent μ-mesons which cross the same group of counters A and different counters B, C, D, E.

Considering the resolving time of our circuits and the intensity of the incident particles (~ 12.6 min^{-1}) one gets a frequency of less then $2 \cdot 10^{-5}$ min^{-1}, which is much smaller than the frequency of the events considered in this paper. Furthermore one could remark that in the discussion of our results we will impose the condition that the lighted neon lamps are aligned in such a way to simulate particles arising in Σ. Such a condition reduces the preceding evaluation.

As a rough check of the chance lighting of the neon lamps we have made a few measurements of the following type.

A delay of 100 μs was introduced, by means of a convenient circuit, in the point marked d in the block-diagram of fig. 2.

Under these conditions the camera takes a picture of the hodoscope with a delay of 100 μs with respect to the master pulse. The result of measurements of this type is that out of 821 cases only three pictures showed a single lamp lighted (namely ${}^{8}A$; ${}^{16}B$; ${}^{10}C$). Considering the frequencies of the pulses of the single counters as well as of the above mentioned cases which can simulate a real event, we conclude that the chance coincidences cannot affect our results.

2·4. – The measurements have been made in the access tunnel of the hydroelectric power station S. Giacomo (Abruzzi, magn. lat. $\Phi = 43^{\circ}\,2'$ N; altitude 400 m a.s.l.) of the S. A. Terni.

By displacing the apparatus in the tunnel it is possible to vary the thickness of the intervening rock from a few m w.e. to 1200 m w.e..

Fig. 3. shows the arrangement of our equipment with respect to the walls and ceiling of the tunnel. The rock is argillous chalk whose density is 2.23 g/cm^3.

3. – Results.

3·1. – The measurements that we report here have been performed from September 1, 1951 to February 6, 1952. All the reported data have not been corrected for barometric variations; such a correction has been neglected, because it is rather uncertain and of practically no importance for our conclusions.

Table I contains the total numbers of fourfold (C_4) and fivefold coinci-

dences (C_5) counted simultaneously, as well as the corresponding frequencies (c_4, c_5, min^{-1}). The ratio of these last numbers represents, in the case $\Delta_\Sigma = 0$,

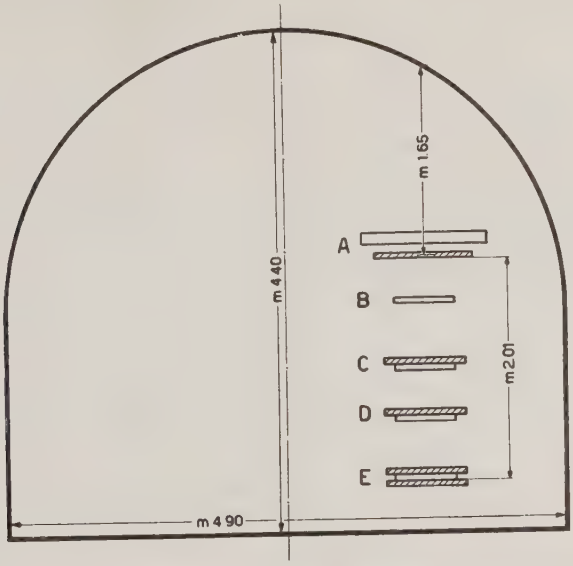

Fig. 3. – Position of the apparatus in the tunnel. The axes of the counters are perpendicular to the plane of the figure.

the efficiency $\eta_A = 0.966 \pm 0.0030$ of the counter-set A and has to be compared with a value of (0.967 ± 0.040) found by inspecting the pictures of the hodoscope obtained under the same experimental conditions.

TABLE I. – *Fourfold and fivefold coincidences.*

Δ_Σ (g/cm^2)	t (min)	C_4	c_4	C_5	c_5	$c_4 - c_5$
1	2	3	4	5	6	7
0	21 803	279 188	12.805 $\pm$ 0.024	269 798	12.374 $\pm$ 0.024	0.431 $\pm$ 0.004
57	21 018	265 458	12.630 $\pm$ 0.024	256 728	12.215 $\pm$ 0.024	0.415 $\pm$ 0.004
85	18 203	226 433	12.439 $\pm$ 0.026	218 786	12.019 $\pm$ 0.026	0.420 $\pm$ 0.005

The high value of η_A is due, at least in part, to the geometry of counters A, and proves their good performance.

TABLE II. – *Repartition of all the observed events according to our classification.*

$n_A \geqslant 2$									$n_A \geqslant 3$	Non-utilized events			Total number of recorded events
e.s. *	*d.e.s.* *	$p \wedge 4$	$p \wedge 3$ *	$p \wedge 2$ *	*p.s.*4	*p.s.*3 *	*p.s.*2 *	*p.p.p.*	all events *	out of angle	non-classified	non-interpretable	
1	2	3	4	5	6	7	8	9	10	11	12	13	14
5882	492	12	185	275	72	266	685	77	531	719	95	135	9426

* These data include events produced in the lead above the counter-sets *C*, *D*, *E*, which are not discussed in the text.

TABLE III. – *Frequencies* ($\times 10^2$ min^{-1}) *of the different classes of events discussed in the test.*

Δ_Σ (g/cm^2)	$f_{e.s.}$		$f_{d.e.s.}$		$f_{p \wedge i}$			$f_{p.s.i.}$			$f_{p.p.p.}$
	C	*D*	*CD*	*CE*	$f_{p \wedge 4}$	$f_{p \wedge 3}$	$f_{p \wedge 2}$	$f_{p.s.4}$	$f_{p.s.3}$	$f_{p.s.2}$	
1	2	3	4	5	6	7	8	9	10	11	12
0	6.99 ± 0.30	—	0.213 ± 0.050	0.085 ± 0.035	0.011 ± 0.009	0.298 ± 0.060	0.820 ± 0.010	0.051 ± 0.020	0.204 ± 0.045	1.45 ± 0.02	0.017 ± 0.010
57	6.28 ± 0.21	23.8 ± 0.4	0.277 ± 0.035	0.123 ± 0.039	0.019 ± 0.008	0.285 ± 0.035	0.516 ± 0.060	0.104 ± 0.020	0.364 ± 0.040	1.22 ± 0.09	0.027 ± 0.009
85	5.73 ± 0.25	—	0.259 ± 0.050	0.061 ± 0.030	0.014 ± 0.010	0.423 ± 0.070	0.518 ± 0.070	0.173 ± 0.040	0.371 ± 0.060	1.27 ± 0.11	0.014 ± 0.010
$\frac{N_{n_A \geqslant 3} \cdot 10^2}{N_{n_A \geqslant 3} + N_{n_A \leqslant 2}}$	1.3	—	7.1	7.4	—	2.5	2.5	47.5	17.6	12.7	—

By means of standard methods, we have measured also the efficiencies $\eta_C = 0.733 \pm 0.026$; $\eta_D = 0.944 \pm 0.043$ and $\eta_{CD} = 0.651 \pm 0.006$ of the counter-sets C, D and both together.

The values correspond to those expected from the efficiency of the single counters and their geometry.

Also the value of the total intensity of the incident ionizing particles agrees with the value calculated from the vertical intensity at 50 m w.e. and the geometry of our set-up.

9 426 events have been recorded in 68 105 minutes. Of these 949 could not be used for different reasons that we will explain in the following. The remaining 8 477 have been divided in two groups according to the number n_A of counter-sets A discharged: the first group corresponds to $n_A \leqslant 2$, while the second one to $n_A \geqslant 3$. Such a separation is based on the fact that the secondaries accompanying a penetrating ionizing particle are distributed on such an area that in the majority of cases they discharge only one or two counter-sets A.

All the 8 477 events belonging to both these two groups have been further classified in 5 typical different classes according to empirical rules given in fig. 1, 5, 6, 7, 10 and 11, which show also the corresponding interpretation in terms of different types of phenomena. Table II contains the repartition of all the recorded photograms in the different classes and table III the frequencies for the various values of Δ_Σ.

In the following we give a detailed discussion of each class of events for $n_A \leqslant 2$; then we compare the events with $n_A \geqslant 3$ with those with $n_A \leqslant 2$ and finally we discuss the 949 non utilized-events.

3·2. – Soft secondaires.

3·2.1. – *Single electronic secondaries* (*e.s.*). – We put in this class all events appearing as an alignment $BCDE$ plus a single counter discharged in a single set.

Columns 2 and 3 of table III contain our results for the *e.s.* for each value of Δ_Σ as measured for the counter-sets C and D.

For counter-set E we get a result equal, within the statistical errors, to that obtained for set C. Furthermore, for each set of measurements, we have classified the observed events according to the number of undischarged counters interposed between the « alignment » due to the « primary » and the extra counter discharged (fig. 4). In the majority of cases, the « secondary particle » discharges a counter close to the alignment due to the « primary » and it is almost certainly an electronic secondary.

In the other cases the « secondary » could be either a low energy photon or a penetrating particle of short range emitted at a rather large angle, or, in the case of the counter sets D and E, an energetic electronic secondary produced in the lead placed above the upper counter set. The probability of this last event for the counter set C is much smaller than for counter sets D

and E on account of the good efficiency of counters B which are discharged by the majority of the particles generated in Σ and reaching C.

The inclusion in the *e.s.* class of these events of doubtful interpretation does not affect appreciably our following discussion and conclusions.

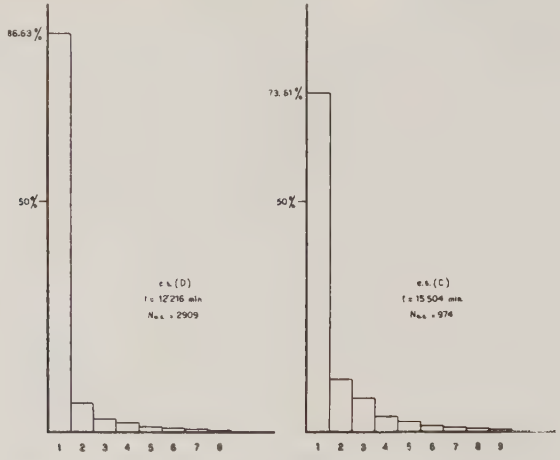

Fig. 4. – Histogram of *e.s.* as a function of the number of undischarged counters between the alignment due to the primary and the counter discharged by the secondary.

Considering the intensity of the incident ionizing particles (table I), we find that the number of *e.s.* recorded by the various counter-sets for incident particle, are

$$(1) \qquad \begin{cases} p_{e.s.}(D) = (1.88 \pm 0.04)\cdot 10^{-2} \\ p_{e.s.}(C) = (0.50 \pm 0.02)\cdot 10^{-2} \\ p_{e.s.}(E) = (0.62 \pm 0.06)\cdot 10^{-2}\,. \end{cases}$$

It is well known that in Pb the number of electronic secondaries in equilibrium with a μ-meson at 50 m w.e. is about 0.1. A value of 2 percent, as obtained for the counter set D, i sreasonable if we consider that a large percentage of the electronic secondaries crosses the same counter as the primary meson.

By comparing $p_{e.s.}(C)$ and $p_{e.s.}(D)$ one recognizes that 1 cm Pb interposed between the counters reduces the frequency of the recorded *e.s.* by about a factor 4.

Until now we have considered, according to the definition of *e.s.* given in fig. 1, only events in which a single counter was discharged in a single set. However it appears to be reasonable to include in this class also cases in which, besides an alignment, there are 2 or more counters discharged in a single set of counters. They are probably due to showers produced by high energy secondary electrons. If we include these events in the class *e.s.* the frequency

of these will increase by about 3 percent in the case of the sets C and E, and by about 10 percent in the case of the set D.

3·2 2. – *Double electronic secondaries* (*d.e.s.*). – To this class belong all events appearing as an alignment plus a single counter in two different sets which can not be interpreted as due to a single secondary particle.

One should remark that an event of this type can be attributed almost

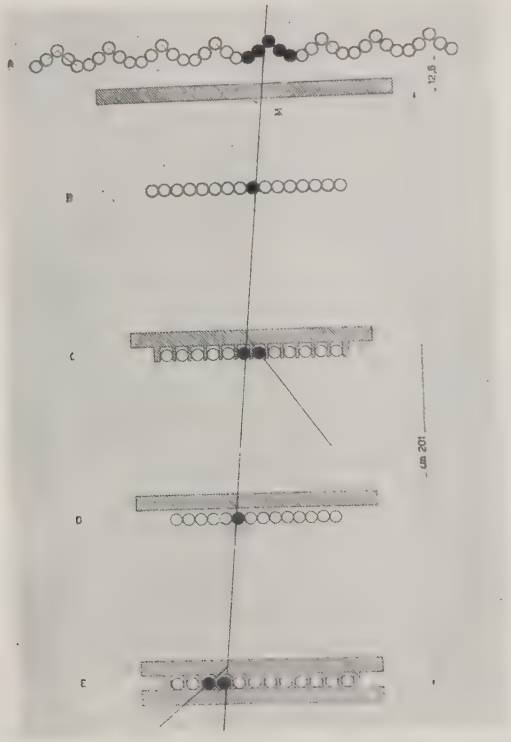

Fig. 5. – *d.e.s.* An alignment plus one single counter discharged in each one of two counter-sets is interpreted as due to a double electronic secondary. In this picture we show a non-ambiguous case.

certainly to a double electronic secondary only when the two counter-sets involved are not contiguous one to the other, for instance C and E (fig. 5). In all other cases the distinction between a *d.e.s.* and a $p \wedge i$ can be ambiguous.

Columns 4 and 5 of table III contain the frequencies of the *d.e.s.* for the CD and CE pairs of counter-sets.

Similar results have been obtained also for BC, BD, BE and DE pairs of counter-sets.

Let us first consider the non ambiguous case CE.

Assuming that the production of two electronic secondaries in two layers of lead are independent events, one can calculate, from the frequencies $f_{e.s.}$ of the *e.s.* given in table III, the expected number, per incident μ-meson, $p_{d.e.s.}$ of double electronic secondaries.

Noting, that under our assumption we have

$$p_{d.e.s.}(CE) = p_{e.s.}(C) \times p_{e.s.}(E) \,, \tag{2}$$

we get, making use of (1),

$$[p_{d.e.s.}(CE)]_{\text{calculated}} = (0.31 \pm 0.04) \cdot 10^{-4} \,, \tag{3}$$

which is to be compared with

$$[p_{d.e.s.}(CE)]_{\text{exp}} = \frac{f_{d.e.s.}(CE)}{e_4} = (0.71 \pm 0.02) \cdot 10^{-4} \,, \tag{4}$$

obtained from the data of table III by averaging with respect to the different values of Δ_Σ.

The ratio of (4) to (3) gives 2.3 ± 0.4. This number does not change appreciably if the $f_{e.s.}$ and $f_{d.e.s.}$ are calculated considering only the secondaries which discharge a counter close to the alignment due to the primary.

By considering the efficiency of counter-set D one can conclude that the high frequency of the *d.e.s.* is due only in small part to showers or penetrating particles generated above counter set C which reach counter set E without triggering counter set D.

Whe think, therefore, that the high value of $f_{d.e.s.}$ is due to the fact that the production of secondaries in two layers of lead by the same incident particle are not independent events. Although a more detailed investigation is needed to clarify this point it seems to us that the value of about 2 is reasonable if one considers the energy dependence of the cross section for the production of *e.s.*.

A similar consideration can be done for the *d.e.s.* involving other pairs of counter-sets, and one obtains similar results.

Let us now consider the ambiguous cases and in particular the case in which the C and D counter-sets are involved.

In this case it is sometimes impossible to decide if a given photogram has to be classified as a *d.e.s.* in C and D or as a $p \wedge 3$ or as a shower produced in the lead above C crossing 5 cm Pb (fig. 6).

In order to avoid underestimating the frequency of the $p \wedge 3$ and $p \wedge 2$ we have used the conservative criteria of classifying as a *d.e.s.* only photograms that can not be $p \wedge 3$ or $p \wedge 2$ as for instance in the case in which the two *e.s.* discharge two counters which lie on opposite sides with respect to the primary. Therefore the frequency $f_{d.e.s.}(CD)$ given in column 4 of table III is certainly underestimated while the frequencies of the $p \wedge i$ are correspondingly overestimated.

One can try to estimate the correct frequency of the *d.e.s.* in C and D, noting that it should be about 4 times larger then the frequency of the *d.e.s.*

in C and E because the frequency of the *e.s.* in D is 4 times larger than that of the *e.s.* in E.

From such a consideration one gets

$$f_{d.e.s.}(CD) \sim 0.0039 \pm 0.0005 ,$$

to be compared with 0.0026 ± 0.0002 (average value of those given in table III).

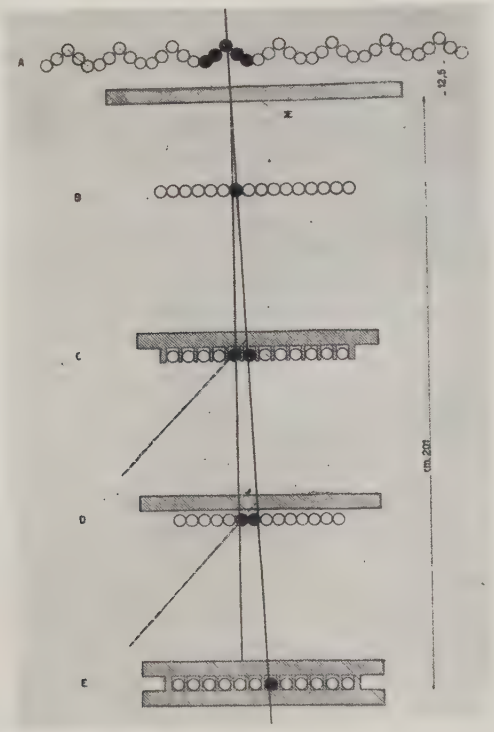

Fig. 6 – This is a typical example of ambiguous interpretation: a double electronic secondary (*d.e.s.*) or a penetrating secondary ($p \wedge 3$) or a small shower generated in the lead above C.

The ratio of these two frequencies (1.5 ± 0.2) can be used in order to correct the numbers of *d.e.s.* and $p \wedge 3$: the first one has to be increased by a factor of 1.5, while the second one has to be decreased by a corresponding amount. We will return to this points in sections 3·3.2 and 4·3.

3·3. – Possible penetrating secondaires.

3·3.1. – Let us now consider those events whose photograms contain, besides an alignment that can be attributed to a primary particle, a certain number

of lighted neon lamps which suggest the existence of at least one secondary particle generated in Σ which crosses i sets of counters:

$i = 2$ if the counter-sets involved are B and C (the secondary has crossed 5 cm Pb).

$i = 3$ if the counter-sets involved are B, C and D (the secondary has crossed 10 cm Pb).

$i = 4$ if the counter-sets involved are B, C, D and E (the secondary particle has crossed 15 cm Pb).

Such a distinction according to the number of counter-sets discharged by the secondaries, aims to classify the considered events according to the penetration of the generated particles: it is more probable that the events with $i = 4$ contain penetrating particles, while the events with $i = 2$ can be quite often electronic showers of energy large enough to discharge some counters after crossing a layer of Pb whose thickness is 10 radiation units: the events with $i = 3$ are obviously an intermediate case.

A further reasonable subdivision is to classify the events, corresponding to a fixed value of i (say for instance $i = 4$), according to the minimum number m of secondaries that have to be produced in Σ in order to justify the corresponding hodoscopic photogram. The dependence of the frequency on the value of m does not suggest that the events with $m = 1$ have to be considered separately from the others as due to a physically well defined phenomenon. However, considering that the hodoscopic technique gives only very rough information on the recorded events and other authors have given some evidence for the existence of pairs of associated penetrating particles ([4]) (*a.p.p.*) we will use the special simbol $p \wedge i$ to indicate the events with $m = 1$ and we will treat them all as due to pairs of associated penetrating particles.

All other events will be indicated as *p.s.i.*.

Before discussing our experimental results about the $p \wedge i$ and *p.s.i.*, we have to note that events of the same type are produced in the rock and that they are included in the above mentioned classes only if their angular opening and distance of production from the experimental set-up, are so small that they can discharge only one or two counter-sets A. But if they discharge more than two counter-sets A, they are put in the group $n_A \geqslant 3$ and considered at a later time.

Finally we have to call attention to the obvious fact that the same phenomena that are produced in Σ are produced also in the layers of Pb placed above the counter-sets C and D.

We will not give details about these events because our hodoscope gives more satisfactory information on what is produced in Σ than in the other layers of Pb. We limit ourselves to state that there is very satisfactory internal consistency among the various experimental observations.

3·3.2. – $p \wedge i$. – Our experimental results on these events (fig. 7) are summarized in table IV about which one can make the following remarks:

a) Of the 10 $p \wedge 4$ observed with $\Delta_\Sigma = 57$ and 85 g/cm², one is certainly produced in rock and not in Σ (*R*), two could be produced as well in rock as

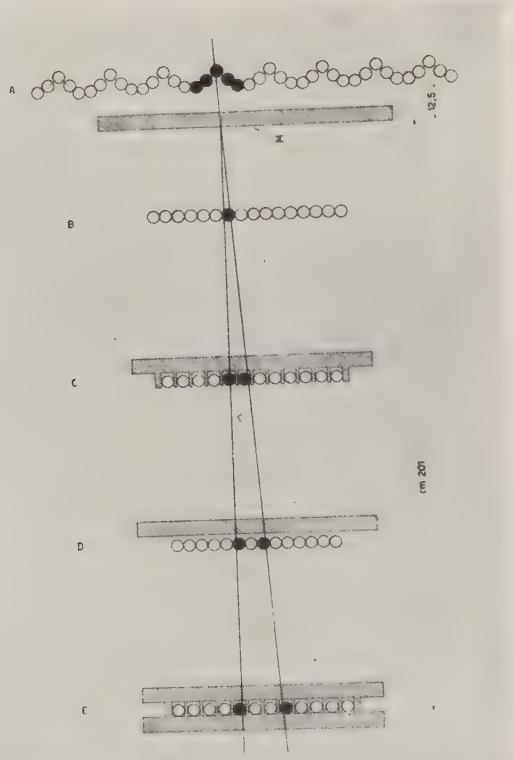

Fig. 7. – $p \wedge 4$, i.e. a photogram which can be interpreted as a pair of associated penetrating particles crossing 15 cm Pb.

in Σ (*r*) and one appears to be produced in air (*a*). Such a photogram can also be interpreted as due to a rather large angle scattering of the secondary particle of an *a.p.p.* produced in rock (or in Σ). Finally of the remaining 6 photograms, three (two with $\Delta_\Sigma = 57$ and one with $\Delta_\Sigma = 85$) show a third neon lamp lighted in the counter-set *D*. These events could be classified as *p.s.*4 (see section 3·3.3) but they can also be interpreted as an *a.p.p.* provided we assume that one of the two particles undergoes an interaction in the lead above the counter-set *C*.

TABLE IV. – *Number of $p \wedge i$ and p.p.p. observed with different Δ_Σ.*

Δ_Σ (g/cm²)	i	t (min.)	$N_{p \wedge i}$					p.p.p.
			Σ	r	R	a	s	
1	2	3	4	5	6	7	8	9
	4	17 591	—	—	2	—	—	3
0	3	10 774	—	28	2	—	4	4
	2	10 774	8	67	10	—	13	26
	4	36 668	2	2	—	1	2	10
57	3	27 720	17	46	1	—	16	6
	2	15 504	22	54	1	—	4	9
	4	13 846	1	—	1	—	1	2
85	3	11 572	16	20	—	—	13	1
	2	11 572	15	41	—	—	4	3

Σ: generated in Σ
R: » » rock
r : » » Σ or in rock
a : » » air
s : accompanied by generation of secondaries in Pb above counters *CDE*.

The remaining 3 cases of $p \wedge 4$ are certainly produced in Σ without any complications.

The fact that with $\Delta_\Sigma = 0$ we have observed two $p \wedge 4$ (marked R) in a rather short time, gives support to the assumption that also the two $p \wedge 4$ observed with $\Delta_\Sigma = 57$ g/cm² (marked r) are produced in rock and not in Σ.

b) The experimental frequency of the events $p \wedge 3$ given in table IV is certainly overestimated on account of the ambiguity of interpretation with the events *d.e.s.* as already discussed in section 3·2.2.

Introducing the corresponding correction, $N_{p \wedge 3}$ decreases, for $\Delta_\Sigma = 57$ g/cm², from 79 to 41 ± 11 (the error is the sum of the statistical error and of the error introduced by the correction) and for $\Delta_\Sigma = 85$ g/cm², from 49 to 34 ± 10.

This means that the values of $N_{p \wedge 3}$ given in table IV should be divided by roughly a factor 1.7.

The fact that the frequency of the $p \wedge 3$ observed with $\Delta_\Sigma \neq 0$ is comparable with that observed with $\Delta_\Sigma = 0$ is a further indication that a good fraction of these events is not produced in Σ: they are either *d.e.s.* or *a.p.p.* generated in rock. The inspection of the photograms confirms this interpretation.

c) The experimental frequencies of the events $p \wedge 2$ are also overestimated for two reasons: an ambiguity of interpretation similar to that met for the $p \wedge 3$ and the non negligible probability that they are produced by electronic

secondaries crossing 5 cm Pb. Although it is very difficult to estimate the error introduced by this fact, we can expect that it is not smaller than that for the events $p \wedge 3$.

We will follow the rather conservative procedure of dividing the values of the $N_{p\wedge 2}$ given in table IV by a factor 2.

Also for the $p \wedge 2$, the frequency observed with $\Delta_\Sigma \neq 0$ is comparable with that observed with $\Delta_\Sigma = 0$. In this case however there are eigth $p \wedge 2$ which appear to be produced in Σ: they are probably electronic secondaries generated in the walls of counters A and their supports. The 67 $p \wedge 2$ marked r correspond to two parallel particles very close to each other so that they discharge in each counter-set two contiguous counters.

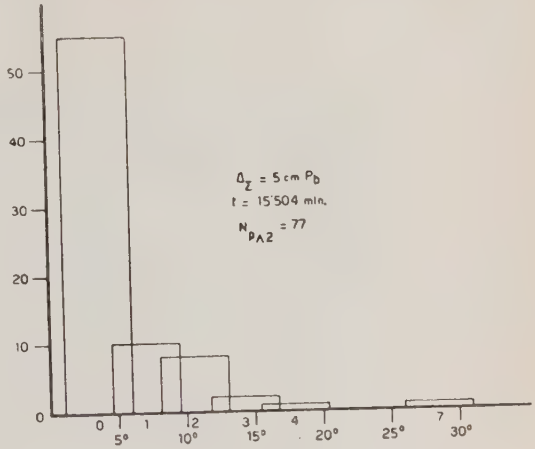

Fig. 8. – Angular distribution of $p \wedge 2$.

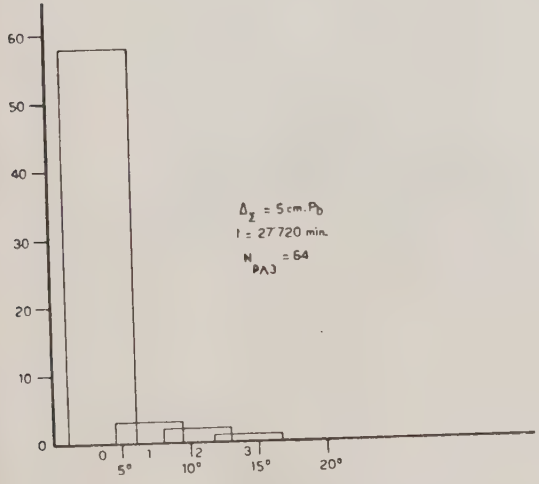

Fig. 9. – Angular distribution of $p \wedge 3$

One can conclude that the total number of $p \wedge 4$ observed with $\Delta_\Sigma \neq 0$ is certainly not larger than 9, probably not larger than 7 $(9 - 2r)$, and possibly equal to 3, and that the numbers of $p \wedge 3$ and $p \wedge 2$ are overestimated by at least a factor 1.7 and 2 respectively.

While for the $p \wedge 4$ the statistics are too poor, the numbers of $p \wedge 3$ and $p \wedge 2$ given in table IV are large enough to attempt to get some information about their angular opening.

As an example we give in fig. 8 and 9 the number of $p \wedge 2$ and $p \wedge 3$ ob-

served with $\Delta_\Sigma = 5$ cm as a function of the number of undischarged counters in set C interposed between the two counters discharged by the two penetrating particles. One can make the following remarks about these figures:

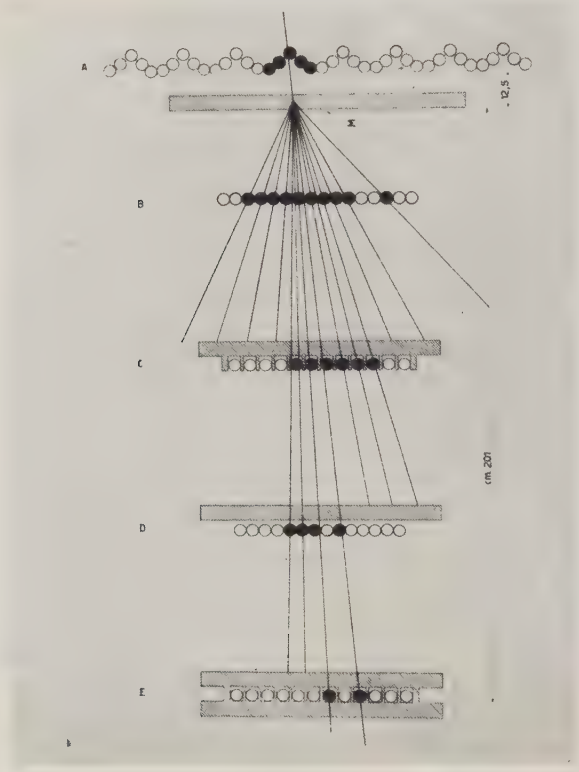

Fig. 10. – *p.s.*4, i.e. a photogram which can be interpreted as due to a shower crossing at least 15 cm Pb.

a) The majority of ambiguous cases ($p \wedge i$ ($i = 2, 3$) or *d.e.s.*) fall in the first block of the histograms.

b) The angular distributions seem to be more narrow than that given by BRADDICK and coworkers ([4]).

These two remarks are in agreement with the fact already discussed, that an appreciable fraction of the events classified as $p \wedge 2$ and $p \wedge 3$, are more probably *d.e.s.*

3·3.3. – *p.s.i.* – In table III columns 9, 10 and 11 are given the frequencies of the *p.s.i.*

The more interesting case is that of the *p.s.*4 (fig.10). These events have been divided in two groups according to the maximum number M of discharged counters in any one of the counter-sets $BCDE$: the first group corresponds to $M = 3$ ($p_3\,s.4$), the second one to $M > 3$ ($p_{>3}.s.4$). The $p_3.s.4$ are very similar to the $p \wedge 4$ considered in the preceding section while the $p_{>3}.s.4$ have the appearance of showers.

We are not sure that such a distinction corresponds to physically different phenomena, but it is justified, from the inspection of our photograms, as well as the distinction of the $p \wedge 4$.

The appearance of the $p_3\,s.4$ suggests the existence of a few penetrating particles moving in a narrow cone whose origin is quite often ambiguous: it could be in the lead Σ as well as in the rock. The average numbers of counters discharged by these events in counters-sets C and E are respectively $\overline{n}_C = 2.1$, $\overline{n}_E = 2.5$.

Such an ambiguity does not exist, usually, for the $p_{>3}.s.4$ whose origin seems to be in Σ. They contain some penetrating particles besides particles that are absorbed by 5 cm Pb; for these events $\overline{n}_C = 4.4$, $\overline{n}_E = 3.7$.

A further possible subdivision of the $p_{>3}.s.4$ can be made according to the fact that the number of discharged counters increases or decreases with increasing depth of lead. Such a distinction probably does not correspond to any physical difference but simply to individual fluctuations from case to case.

The *p.s.*3 could be, at least in part, electronic showers generated by rather high energy electronic secondaries, or gamma rays, produced by the incident μ-meson. Such a generation could happen in Σ or, sometimes in the Pb above C and D.

However in some cases they could be events containing a few penetrating secondaries; in these cases they are different from the *p.s.*4 either because the penetrating secondaries have a shorter range or because they are emitted in such a direction that they can not be recorded by the counter set E. In the majority of cases, the number of counters discharged in B is larger than the number of counters discharged in C. That means that 5 cm Pb produce, at least in most cases, an appreciable absorption of the particles generated in Σ. This remark is in support of the assumption that the considered *p.s.*3 are, in great part electronic showers.

Similar considerations can be made for the *p.s.*2.

3·3.4. *p.p.p.* – We have observed a certain number of pairs of penetrating parallel particles (*p.p.p.*) (fig. 11) whose frequency is given in column 12 table III. This data refer only to *p.p.p.* crossing all counter sets: in table IV we give also the number of *p.p.p.* crossing a smaller number of coun-

ter-sets, probably for geometrical reasons. These events have been given in table IV because they could be $p \wedge i$ produced in rock far away from the

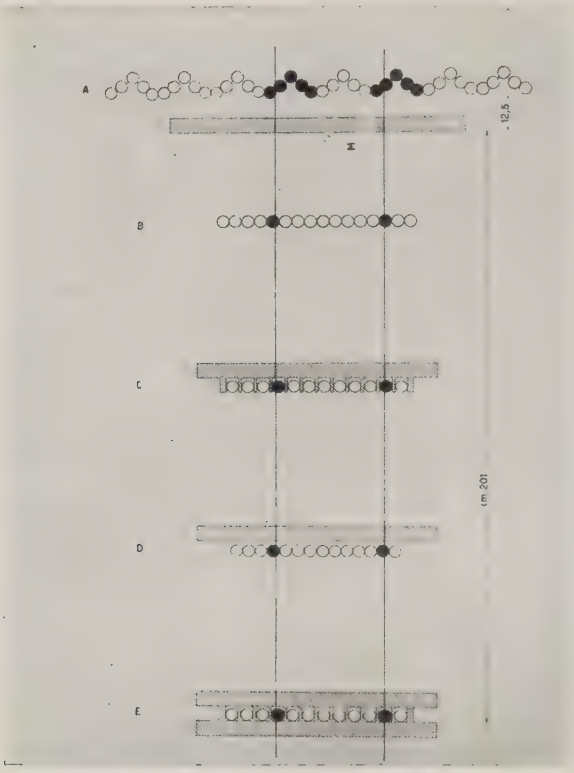

Fig. 11. – Example of a pair of penetrating parallel particles (*p.p.p.*).

experimental set-up. We note that among the $p \wedge 4$ there are a few cases which could be interpreted as *p.p.p.* with a very small distance (a few centimeters) among the two particles.

Besides the above mentioned *p.p.p.* there are 8 events which appear to be *p.p.p.* crossing all sets of counters, in which one or both of the particles produce some secondary effect.

3·3.5. – In the last row of table III we give, as an example, for each class of events the ratio of the number of photograms with $n_A \geqslant 3$ to the total number of photograms with any value of n_A observed with $\Delta_\Sigma = 5$ cm and the master pulse $B_1 C_2 D_1 E_1$.

This ratio is in most cases, a few percent, but for the events *p.s.*4 (Fig. 12) it is about equal to one half.

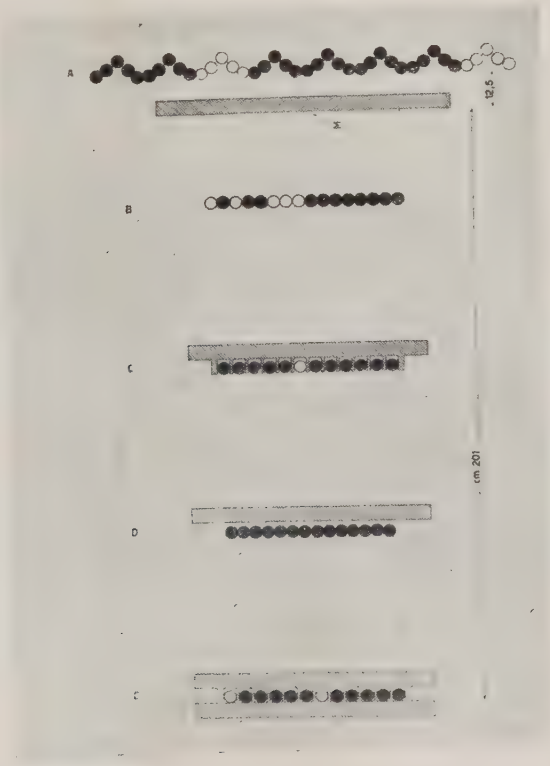

Fig. 12. – Example of *p.s.*4. with $n_A \geqslant 3$.

3·3.6. – The 949 non-used events can be divided in three classes (table II) which, for the sake of simplicity, we will call « out of angle », « non-classified », « non-interpretable ».

The « out of angle » events are 719 and correspond to primaries crossing only 2 or 3 of the 4 sets of counters *BCDE*, giving rise to secondaries which, discharging other counters, provide the formation of the master pulse.

The « non-classified » events are 95 and represent phenomena which do not fit in any one of the different classes considered above: in general they correspond to one of the above considered classes complicated by some secondary effect.

Finally there are 135 « non-interpretable » events which can not be classified at all. Of these 53 correspond to superimposed photograms due to the finite time of displacement of the film in the camera.

The remaining 78 are events whose photograms are complicated by chance coincidences, or scattering of some of the particles etc.

Not one of the 135 non-interpretable events could be a $p \wedge i$.

4. – Discussion.

4·1. – The data collected in table I on the fourfold and fivefold coincidences can be used to discuss the possible existence of a neutral component which could undergo a charge exchange process in Σ. This problem has already been discussed by us in a preceding short publication [9] and therefore it will not be considered here in detail. We will only recall that from the data of table I one can exclude the theory suggested by HAYAKAWA [10], which explains various observations underground as due to the existence of $k^{\pm}$-mesons produced locally by k^0-mesons through a charge exchange process.

4·2. – Little can be said about the electronic secondaries of mesons because the geometry of our experimental set-up does not allow a quantitative comparison between the experimental data on the e.s. and the conventional theories on the production of electronic secondaries by fast μ-mesons. Semiqualitative considerations show that the observed frequencies are of the expected order of magnitude. We can add the following remark on the double electronic secondaries: our measurements indicate the possible existence of a coherence effect in the production of two electronic secondaries in two successive layers of Pb. Such a phenomenon needs further investigation with a more appropriate technique and could be used as a test on the dependence of the electromagnetic interaction on the energy of the primary particles.

4·3. – The principal aim of the present work was to investigate the production underground of penetrating particles; according to our rules, phenomena of this type are put in class $p \wedge i$ and *p.s.*4. Before we distinguish between these different cases, we note that for an experimental set-up like that used in the present work, one can write the two following obvious relations

$$C_4 = N_c G \,, \tag{5}$$

$$N_e = \mathcal{N} \Delta_\Sigma \sigma_e G_e N_c \,. \tag{6}$$

[9] E. AMALDI, C. CASTAGNOLI, S. SCIUTI and A. GIGLI: *Proc. Phys. Soc.*, **65**, 556 (1952).

[10] S. HAYAKAWA: *Proc. Phys. Soc.*, **65**, 215 (1952).

N_c is the number of charged particles (almost all μ-mesons) incident in the vertical direction per cm² and per steradian; $\mathcal{N}$ is Avogadro's number, Δ_Σ the thickness in g/cm² of Σ, σ_e the cross section (averaged on the energy spectrum of the incident particles) for the particular type of event considered, whose number is N_e. G and G_e are geometrical factors with the dimensions of an area depending on the geometry of the apparatus, the angular distribution of the incident particles and the type of event considered (Appendix I).

From (5) and (6) we get

$$N_e = \mathcal{N} \Delta_\Sigma \sigma_e \frac{G_e}{G} C_4. \tag{7}$$

Let us now apply eq. (7) to the *a.p.p.*'s that, with our notations are called $p \wedge i$ $(i = 2, 3, 4)$.

First, however, we note that the cross sections which we will obtain by applying equation (7) to the $p \wedge 2$ and $p \wedge 3$, are differential cross sections in the sense that they correspond to *a.p.p.*'s whose secondaries have a range R respectively between 5 and 10 cm Pb and 10 and 15 cm Pb.

Table V contains our results and is similar to a table published previously [11].

The corrected values of $N_{p \wedge i}$ are obtained by applying to the experimental values given in table IV the remarks *a*) *b*) *c*) of section 3·3.2; the corresponding times of observation and frequencies of the incident particles c_4 are given respectively in table IV column 3 and table I column 4. Column 4 of table V contains the used geometrical factors which depend on the assumed angular distribution of the *a.p.p.*'s (see Appendix I).

TABLE V. – *Cross section for production of pairs of associated penetrating particles.*

Penetration of secondary particle (g/cm²)	i	$N_{p \wedge i}$ (corrected) Δ_Σ(g/cm²) 57	Δ_Σ(g/cm²) 85	$\frac{G_i}{G}$	σ_i (cm²/nucleon)
1		2	3	4	5
57–113	2	40	30	0.79	$(6.3 \pm 1) \cdot 10^{-30}$
113–170	3	41	34	0.87	$(4.6 \pm 1) \cdot 10^{-30}$
>170	4	5	2	0.13	$(2.1 \pm 1) \cdot 10^{-30}$
					$\sigma_{tot} = (13 \pm 3) \cdot 10^{-30}$

(11) E. AMALDI, C. CASTAGNOLI, A. GIGLI and S. SCIUTI: *Nuovo Cimento*, **9**, 453 (1952).

The values reported in table V have been calculated making use of the angular distribution given by BRADDICK and coworkers. In Appendix I we consider also a different assumption which, however, gives a numerical value about 30% lower than the previous one.

We can conclude that, assuming the existence of pairs of *a.p.p.* the corresponding cross section for production in lead by μ-mesons of mean energy $\sim 3.5 \cdot 10^{10}$ eV ([12]), is $(13 \pm 3) \cdot 10^{-30}$ cm^2/nucleon. Such a value corresponds to the production of secondaries of range larger than 5 cm lead, i.e., if they are mesons (π or μ), of energy larger than $\sim 10^8$ eV.

Our cross section is appreciably lower than that given by BRADDICK, NASH and WOLFENDALE ($50 \cdot 10^{-30}$ cm^2/nucleon) ([1]), expecially if one consider that according to these Authors the energy of the secondary meson ought to be of the order of 10^9 eV. If such an evaluation of the energy is correct, one has to compare their cross section at least with our result for $R \geqslant 15$ cm Pb, i.e. $(2 \pm 1) \cdot 10^{-30}$ cm^2/nucleon which, allowing for various errors and uncertainties, could reach, as a maximum value, $5 \cdot 10^{-30}$ cm^2/nucleon.

Furthermore one has to note that our value of σ_{tot} has been obtained including in the $p \wedge i$ a few events of doubtful interpretation: namely the events marked *a* and *s* in table IV. Such a procedure is justified under the assumption that the secondary particles of a pair of *a.p.p.*'s have a strong interaction with matter as would happen for π-mesons. But if the secondary particle has a small interaction, the events mentioned above are not to be included in the *a.p.p.*'s, and the cross section would turn out to be slightly smaller than the value given above.

Finally we suspect that in spite of the applied correction a non negligible fraction of the $p \wedge 2$ and possibly a smaller percentage of the $p \wedge 3$ can be due to electronic secondaries, and that not only with our rough technique, but also with a more refined one, it may be very difficult to establish the nature of secondary particles whose range is of the order of 5 cm Pb. Such a remark is supported by recent work on fluctuations of electronic showers ([13]).

The cross section for production of *a.p.p.*'s can be compared with the cross sections for production of neutrons and stars.

The first one has been measured by COCCONI and COCCONI-TONGIORGI ([2]) and more recently by SARD and coworkers ([2]). The first authors found 10^{-29} cm^2/nucleon and the second ones a few units in 10^{-29} cm^2/nucleon: the statistical errors are so large that no discrepancy exists among the two results. A smaller cross section ($5 \cdot 10^{-30}$ cm^2/nucleon) has been found by GEORGE and EVANS ([1]) for the production of stars by fast μ-mesons while one would expect a value very close to that observed for the production of neutrons.

([12]) M. MANDÒ: *Nuovo Cimento*, **9**, 517 (1952).
([13]) R. R. WILSON: *Phys. Rev.*, **86**, 261 (1952).

Now it is quite evident that if we do not invoke some physically rather unlikely process, we have to expect that the cross section for production of *a.p.p.*'s is smaller than the cross section for production of nuclear evaporation (neutrons and stars).

From this point of view our rather low value of the cross section for production of *a.p.p.*'s fits quite well into the general picture of known facts on the behaviour of penetrating ionizing particles observed underground.

4·4. – Let us now consider the *p.s.*4 (columns 2, 3 and 4 of table VI). These have been divided in a rather arbitrary way (section 3·3.3) in two groups according to the fact that the maximum number M of counters discharged

TABLE VI. – *Number of p.s.*4 *as a function of the number of counter-groups* n_A *discharged in set A.*

Δ_Σ (g/cm²)	t (min.)	Number of counter groups discharged in set A								
		0	1	2	3	4	5	6	7	8
	1	2	3	4	5	6	7	8	9	10
57	36 668	4	27	8	16	13	13	6	9	7
85	13 846	1	19	4	3	2	4	—	1	3

in any one of the counter-sets *BCDE* is 3 or larger than 3. In order to prove the physical significance of such a distinction it would be necessary to perform an experiment giving better statistics and, at the same time, more detailed information on the considered events.

These two requirements are in some way of opposite nature and need special consideration for future investigation.

Apart from this problem we can put the following question: the experimental frequency of these events, taken all together, is so high as to impose the existence of a specific interaction of μ-mesons with nucleons, or it can be explained taking into account only the usual electromagnetic interaction.

The production of electronic showers generated by high energy μ in Σ, and penetrating in lead (mainly by means of low energy photons) until reaching counters *D* and *E*, is considered in Appendix II.

The expected probability per incident ionizing particle obtained with a few simplifying assumptions for this type of events is of the same order of magnitude of that observed for the *p.s.*4 (for $\Delta_\Sigma = 57$, it is $8 \cdot 10^{-5}$ against the experimental value $39/463.117 = 8.4 \cdot 10^{-5}$).

Therefore we cannot exclude that these events are all or at least in great part due to purely electromagnetic phenomena. In order to establish an upper limit for the production of *p.s.*4 by nuclear interaction of μ-mesons with

nucleons, we assume that, in spite of the preceding remark, none of the observed *p.s.*4 is due to electromagnetic interactions and we introduce their total numbers taken from table VI, (39 for $\Delta_\Sigma = 57$, 24 for $\Delta_\Sigma = 85$) in equation (7). If we take $G_{p.s.4}/G \sim 1$ we get

$$\sigma = (2.5 \pm 0.5) \cdot 10^{-30} \text{ cm}^2/\text{nucleon}, \tag{8}$$

which increases to $3 \cdot 10^{-30}$ if we consider also the 8 *p.s.*4 with $n_A \geqslant 3$ (see **4**·6). One could suspect that such a low value is due, in part to the use of a large geometrical factor for all the *p.s.*4, independent of the value of M. But if one treats separately the $p_3.s.4$'s and the $p_{>3}.s.4$'s using the geometrical factors calculated for the $p \wedge 4$ for the first group of events, and again a geometrical factor equal to 1 for the second group, one gets respectively $4 \cdot 10^{-30}$ and $2 \cdot 10^{-30}$ and therefore a total cross section equal to about $6 \cdot 10^{-30}$.

Such a value represents an upper limit and is about 10 times smaller than that given by GEORGE and TRENT [3].

4·5. – In this section we will consider those photograms which can be interpreted as due to *a.p.p.*'s produced in rock and crossing all the lead of our telescope (only $\Delta_\Sigma = 57$ and 85). With our notations the considered events are $p \wedge 4$ produced in rock. There are 11 photograms of this type: 4 are given in table IV ($\Delta_\Sigma = 57$, 2 marked *r*, 1 marked *a*; $\Delta_\Sigma = 85$, 1 marked *R*), and 7 are *p.p.p.* which, on account of the angular indefinition due to the finite dimensions of the counters, could be produced in rock at a minimum distance of half a metre from the ceiling of the tunnel. All the other 7 *p.p.p.* have a minimum distance of production from the ceiling of the tunnel of at least 5 m and therefore they can not contain secondary particles having a strong interaction with matter. They will be considered in the next section. Of the 7 *p.p.p.* that we consider here, 2 produce some secondaries in the lead of our apparatus and are not given in table IV column 9.

Assuming in a rather arbitrary way that the thickness of the useful layer of production is equal to the mean free path of the secondary particles produced in penetrating showers ($\lambda = 160 \pm 50$ g/cm^2) [14] and using the geometrical factor calculated in Appendix I, we find a cross section of about $6 \cdot 10^{-30}$ cm^2/nucleon.

We note that such a value, which we consider more uncertain than that given in table V, is inversely proportional to the thickness of the layer of production.

If, therefore, the secondaries were particles having a weak interaction with matter (μ mesons), the number of events to be considered would increase

[14] B. GREGORY and J. H. TINLOT: *Phys. Rev.*, **81**, 667 (1951).

from 7 to 12 ($= 7 - 2 + 7$) but the thickness of the corresponding layer of production would increase by a much larger factor; the corresponding cross section would turn out to be appreciably smaller than the value given above.

4·6. – Finally we can add a few remarks about the *p.s.*4 with $n_A \geqslant 3$ (table VI, columns from 5 to 10). First we note that their frequency does not decrease appreciably when n_A increases from 3 to 8, and that the average number of counters discharged in counter-sets C and E are both equal to about 5. Of the 64 events observed with $\Delta_\Sigma = 57$ g/cm², 8 have the appearance of a burst produced in Σ and 3 of *p.p.p.* all accompanied by soft particles discharging a few counter-sets A. Adding to all these, 13 other events observed with $\Delta_\Sigma = 85$ g/cm² one gets a total of 77 *p.s.*4 with $n_A \geqslant 3$.

There are three possible interpretations of these events: the first is that they are electronic showers produced in rock, of energy large enough to reach the counters D and E. Such an interpretation can be disregarded because the corresponding calculated frequency (Appendix II) turns out to be ~ 100 times smaller than observed.

The second assumption is that they are phenomena similar to that discussed in section **4·4**.

The corresponding cross-section, assuming a geometrical factor equal to 1, and a layer of production of about 160 g/cm², turns out to be $\sim 1 \cdot 10^{-30}$ cm²/nucleon. Such a value has to be compared with (8): the fact that it seems to be appreciably smaller in rock than in lead could be interpreted as an indication of an appreciable contribution of high energy electromagnetic showers produced locally by μ-mesons.

A third possibility which we have to keep in mind and which could explain in part the events under consideration is that they are due to the penetrating particles, mainly μ-mesons, present in the core of an extensive air shower whose soft particles have been completely absorbed in the rock. A quantitative consideration along this line is rather uncertain for lack of information of the following type: absorption in the earth of the μ-mesons present in an air shower; variation of their density as a function of the distance from the core of the shower. In order to estimate only the order of magnitude we can note that $\bar{n}_c = 5$ corresponds roughly to a density of penetrating particles underground of $5/(4 \times 80 \times 12) \sim 13 \times 10^{-4}$ particles/cm².

Assuming tentatively that the number of penetrating particles of a shower are reduced from sea level to our station of observation by a factor of the order of 2, that their density increases going from 6 to 1 m distance from the core by a factor of the order of 5 ([15]) and taking the ratio of the total number

([15]) G. Cocconi, V. Cocconi-Tongiorgi and K. Greisen: *Phys. Rev.*, **76**, 1020 (1949).

of particles to the penetrating ones equal to 100, one get a frequency for the corresponding air shower of the same order of magnitude of that obtained adding to the 77 considered events the 7 *p.p.p.* of very low convergence.

Such an argument shows that an appreciable fraction of the *p.s.*4 with $n_A \geqslant 3$ could be cores of extensive air showers ([16]).

Our thanks are due to Professors B. FERRETTI, M. MANDÒ and G. SALVINI for valuable discussion and to Dr. E. P. George for criticisms to our manuscript. We also thank the S. A. Terni and in particular Professor A. M. ANGELINI and Engineer E. GIGLI for the hospitality and help we received during our staying at the power station of S. Giacomo.

APPENDIX I.

A1·1. – The direction of motion of the incident μ-meson (fig. 13) is given by the angles θ_0 and φ which are related to the zenital angle θ by

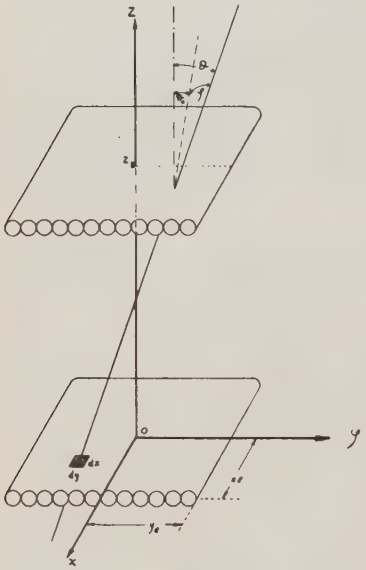

Fig. 13.

$$\cos\theta = \cos\theta_0 \cos\varphi \,. \tag{A1.1}$$

The solid angle is given by the expression

$$\mathrm{d}\omega = \cos\varphi \,\mathrm{d}\varphi \,\mathrm{d}\theta_0 \,, \tag{A1.2}$$

$$0 \leqslant \theta_0 \text{ and } \varphi < \pm \frac{\pi}{2} \,.$$

Let us first calculate the mesonic intensity under the assumption that the whole surface covered by the counter-sets *BCDE* is sensitive to the incident ionizing particles.

Assuming that the intensity of the incident particles is represented correctly by the expression

$$I \,\mathrm{d}\omega = I_0 \cos^n\theta \,\mathrm{d}\omega \,, \tag{A1.3}$$

one gets immediately the following expression for the number of particles re-

([16]) G. COCCONI: *Progress Report n. 1 of Cornell University* (September 1951).

corded by our telescope

$$N = I_v \int_{-Y_E}^{+Y_E} dy \int_{\theta_1}^{\theta_2} \cos\theta_0^{n+1}\, d\theta_0 \int_{-X_E}^{+X_E} dx \int_{\varphi_1}^{\varphi_2} \cos^{n+2}\varphi\, d\varphi\,, \tag{A1.4}$$

$$\theta_1 = -\operatorname{arctg}\frac{Y_B + y}{Z_B}\,, \qquad \theta_2 = \operatorname{arct}\frac{Y_B - y}{Z_B}\,, \tag{A1.5}$$

$$\varphi_1 = -\operatorname{arctg}\frac{X_B + x}{Z_B}\cos\theta_0\,, \qquad \varphi_2 = \operatorname{arctg}\frac{X_B - x}{Z_B}\cos\theta_0\,. \tag{A1.6}$$

If θ_1 and θ_2 are small for all values of y, we can substitute, in the expression of φ_1 and φ_2 to $\cos\theta_0$ a convenient average value, $\overline{\cos\theta_0}$, and write eq. (A1.4) in the more convenient form

$$N = I_v \Theta \Phi = I_v G\,, \tag{A1.7}$$

where

$$\Theta = \frac{2Z_B^2}{3}\left\{\frac{1}{\{Z_B^2 + (Y_B - Y_E)^2\}^{1/2}} - \frac{1}{\{Z_B^2 + (Y_B + Y_E)^2\}^{1/2}}\right\} + \tag{A1.8}$$

$$+ \frac{4}{3}\left[\{Z_B^2 + (Y_B + Y_E)^2\}^{1/2} - \{Z_E + (Y_B - Y_E)^2\}^{1/2}\right],$$

$$\Phi = \frac{1}{4}\frac{1}{\overline{\cos\theta_0}}\left\{\frac{Z_B}{1 + \left(\frac{X_B - X_E}{Z_B}\overline{\cos\theta_0}\right)^2} - \frac{Z_B}{1 + \left(\frac{X_B + X_E}{Z_B}\overline{\cos\theta_0}\right)^2} + \right. \tag{A1.9}$$

$$\left. + 3\,(X_B + X_E)\operatorname{arctg}\frac{X_B + X_E}{Z_B} - 3(X_B - X_E)\operatorname{arctg}\frac{X_B - X_E}{Z_B}\right\}.$$

A1·2. – Let us now consider the case in which between the counters of sets C and E there are insensitive zones Δy^* due to the layers of Pb (1 cm thick).

Equations (A1.7) and (A1.8) still hold while equation (A1.9) can be substituted by the expression

$$\Theta = \sum_1^{12_i} \Delta y_i \sum_{a_i}^{b_i}{}_k \cos^{n+1}\theta_{0ik}\,\Delta\theta_{0ik}\,, \tag{A1.10}$$

which is correct under the assumption that the distance between the planes C and E is large with respect to both the diameter of the counters Δy and the insensitive interval between two successive counters Δ_y^*; a_i and b_i are the

limits of the sum which have to be choosen in such a way that the corresponding directions cross the counter-set B; $\Delta\theta_{0ik}$ is the angle under which counter k of set C is seen from counter i of set E.

With the same approximation one has

$$\Delta\theta_{0ik} = \frac{\Delta y_k}{Z_C} \cos^2 \theta_{0ik} \,. \tag{A1.11}$$

As a conclusion we have

$$\Theta = \Delta y^2 \frac{1}{Z_C} \sum_1^{12_i} \sum_{a_i}^{b_i} \cos^{n+3} \theta_{0ik} \,, \tag{A1.12}$$

$$\begin{cases} \operatorname{tg} \theta_{0ik} = (i-k) \dfrac{\Delta y + \Delta y^*}{Z_C} \,, \\ \cos \theta_{0ik} = \dfrac{Z_C}{\sqrt{Z_C^2 + (i-k)^2 (\Delta y + \Delta y^*)^2}} \end{cases} \tag{A1.13}$$

A1·3. – Let us consider a μ-meson of momentum p in the laboratory system (l.s.) colliding with a nucleon at rest.

The angle of emission of a secondary particle in the l.s., corresponding to 90° in the center of gravity system (c.g.s.) is given by the well known relation

$$\operatorname{tg} \theta_{1/2} = \beta_\pi \frac{1}{p} \sqrt{[\{p^2 + \mu^2 c^2\}^{1/2} + Mc]^2 - p^2} \cong \frac{\beta_\pi}{p} \sqrt{2 Mcp + (Mc)^2} \,, \tag{A1.14}$$

where β_π refers to the emitted particles in the c.g.s..

Under the assumption that the probability of emission of the secondary particle is symmetric with respect to the equatorial plane in the c.g.s. one can write the following expression for the probability that the secondary particle crosses the area $d\xi \cdot d\eta$, placed at distance l from the point of emission in a plane perpendicular to the direction of motion of the incident μ

$$P(\xi, \eta)\, d\xi\, d\eta = P(\xi)\, d\xi \times P(\eta)\, d\eta, \quad P(\xi)\, d\xi = \frac{0{,}693^{1/2}}{\pi^{1/2} r_{1/2}} \exp\left[-0{,}693 \frac{\xi^2}{r_{1/2}^2}\right] d\xi \,, \tag{A1.15}$$

where

$$r_{1/2} = l \operatorname{tg} \theta_{1/2} \,. \tag{A1.16}$$

A1·4. – Making use of the preceding considerations one can calculate the number of events in which are emitted m penetrating particles of which n are detected as n different alignments crossing the telescope $BCDE$.

The simplest case is that of $m = n = 1$, i. e. that of the event $p \wedge 4$.

In this case we have

$$N_{p \wedge 4} = I_v \cdot \mathcal{T} \cdot \sigma_4 \cdot \Delta_\Sigma \Theta^{11} \Phi^{11} = I_v \cdot \mathcal{T} \cdot \sigma_4 \cdot \Delta_\Sigma G_4 \,, \tag{A1.17}$$

where $\mathcal{N}$ is Avogadro's number, σ_4 is the cross section for this event and

$$\Phi^{11} = \int_{-X_E}^{+X_E} \mathrm{d}x \int_{\varphi_1}^{\varphi_2} \cos^{n+1} \varphi \, \mathrm{d}\varphi \, \psi(x, \bar{\theta}_0, \varphi) \,, \tag{A1.18}$$

$$\Theta^{11} = (\Delta y)^2 \frac{1}{Z_c} \sum_1^{12}{}_i \sum_{a_i}^{b_i}{}_k \cos^1 \theta_{0i} \, P_{ik}^{11} \,,$$

with

$$\psi = \int P(\xi) \, \mathrm{d}\xi = \frac{1}{2}\{\varphi(\alpha_1) + \varphi(\alpha_2)\},$$

where φ is the probability integral and

$$\left\{\begin{aligned}
\alpha_1 &= \frac{0.693^{1/2}}{\operatorname{tg} \theta_{1/2}} \frac{\overline{\cos \theta_0} \, (X_E - x)}{Z_\Sigma(1 + \operatorname{tg}^2 \varphi) - (X_E - x) \operatorname{tg} \varphi \, \overline{\cos \theta_0}} \\
\alpha_2 &= \frac{0.693^{1/2}}{\operatorname{tg} \theta_{1/2}} \frac{\overline{\cos \theta_0}(X_E + x)}{Z_\Sigma(1 + \operatorname{tg} \varphi) + (X_E + x)} \\
P_{ik}^{11} &= \frac{0.693^{1/2}}{\pi^{1/2} r_{1/2}} \sum_s \exp\left[-\frac{0.693 \xi_0^2}{r_{1/2}^2}\right] \Delta\xi_s = \sum_s p(ik) \\
\Delta\xi_1 &= \frac{B_s - A_s}{\cos \theta_{0ik}}, \qquad \xi_s = \left\{\frac{A_s + B_s}{2} - c_s\right\} \frac{1}{\cos \theta_{0ik}} \,.
\end{aligned}\right. \tag{A1.19}$$

A_s and B_s represent the extreme of the interval $\Delta\xi_s$ which is effective for the detection in the plane E of the secondary particle generated by the primary incident in the direction ik (see fig. 14).

In general one has

$$N^{mn} = I_v \mathcal{N} \cdot \sigma_m \Delta_\Sigma \cdot G^{mn} \,, \qquad G^{mn} = (\Delta y)^2 \frac{1}{Z_C} \sum_1^{12}{}_i \sum_{a_i}^{b_i}{}_k \cos^1 \theta_{0ik} G_{ik}^{mn} \,, \tag{A1.20}$$

where

$$G_{ik}^{mn} = \Phi^{11} \sum \frac{m!}{a_0! \, a_1! \ldots a_n!} p_0^{a_0} p_1^{a_1} \ldots p_n^{a_n} \quad (a_0 + a_1 + \ldots + a_n = n),$$

and p_0 is defined by the following equation

$$\Phi^{11} p_0(i, k) = \Phi - \sum \Phi^{11} p_s(i, k) \,.$$

Similar equations hold for the events $p \wedge 4$ produced in rock. In this case assuming that the layer of generation

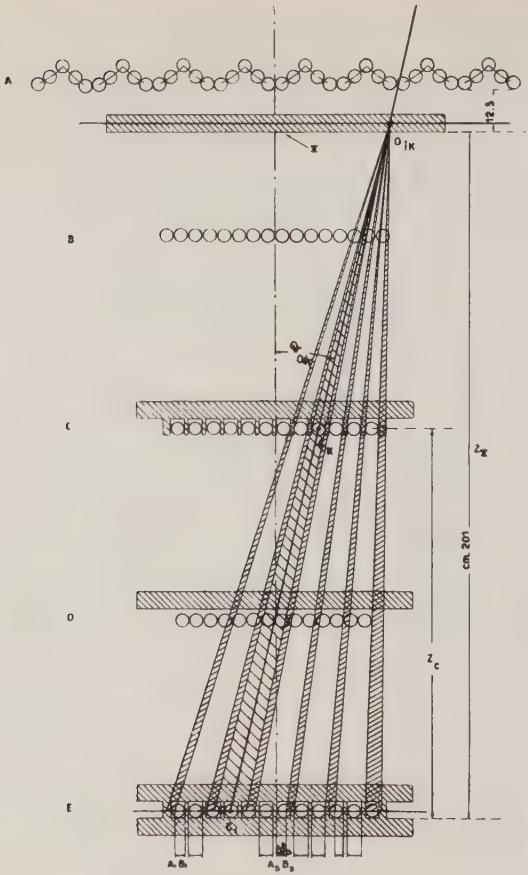

Fig. 14.

was one m inside the rock, we found $G_{4\text{in }R}/G = 0.03$. We give in table A1.1 the results of our numerical calculation for various energies of the primary ($n = 2$). One can see that, under our assumption the experimental set up shows its maximum sensitivity for energies of the incident μ-mesons between 10^{10} and 10^{12} eV. In the last row we give the values of the quantity

$$\frac{\int G_4 F(E)\,\mathrm{d}E}{\int F(E)\,\mathrm{d}E},$$

where $F(E)$ is the meson spectrum underground

(A1.21) $$F(E) = \frac{2E_0^2}{(E + E_0)^3}\,\mathrm{d}E\,, \qquad (E_0 = 1.14 \cdot 10^{10}\ \text{eV}).\ (12)$$

TABLE A1.1. – *Geometrical factors for the events* $p \wedge 4$ *produced in* Σ *or in rock* (R).

E (eV)	G_4	$G_{4 \text{ in } R}$
1	2	3
10^9	$3.8 \cdot 10^{-3}$	$1.3 \cdot 10^{-3}$
10^{10}	$4.5 \cdot 10^{-2}$	$1.3 \cdot 10^{-2}$
10^{11}	$1.3 \cdot 10^{-1}$	$2.7 \cdot 10^{-2}$
10^{12}	$1.2 \cdot 10^{-1}$	$4.1 \cdot 10^{-2}$
$\dfrac{\int G_4 F(E)\,\mathrm{d}E}{\int F(E)\,\mathrm{d}E}$	$1.0 \cdot 10^{-1}$	$2.8 \cdot 10^{-2}$

The angular distribution found by BRADDICK and coworkers for the *a.p.p.* corresponds to that given by equation (A1.15) for $E = 10^{11}$ eV.

The calculation of the geometrical factors G_2 and G_3 for the events $p \wedge 2$ and $p \wedge 3$ is slightly more complicated. For instance the photograms of the type $p \wedge 2$ can be due to three different type of events:

a) The primary moves inside the solid angle of the telescope $BCDE$ and produces in Σ (with cross section σ_2) a secondary of range between 5 and 10 cm Pb. We call g_2 the corresponding geometrical factor.

b) The primary moves inside the solid angle of the telescope $BCDE$ and produces in Σ (with cross section $\sigma_3 + \sigma_4$) a secondary of range larger than 10 cm Pb emitted in such a direction that it does not discharge the counters D and E.

c) The primary moves inside the solid angle of the telescope BC but not in the solid angle of the telescope $BCDE$ and produces in Σ (with cross section σ_4) a secondary which crosses the telescope $BCDE$. We call g_2^* the corresponding geometrical factor.

Taking into account these various effects, equation (6) holds for the events $p \wedge 2$ and $p \wedge 3$ provided we put

$$G_2 = g_2 \left\{ 1 + \frac{\sigma_3 + \sigma_4}{\sigma_2} \left(1 - \frac{g_3}{g_2} \right) + \frac{\sigma_4}{\sigma_2} \frac{g_2^*}{g_2} \right\},$$

$$G_3 = g_3 \left\{ 1 + \frac{\sigma_4}{\sigma_3} \frac{g_3 - G_4 + g_3^*}{g_3} \right\}.$$

Using the numerical values

$$g_2 = 0.60\,, \quad g_2^* = 0.38\,, \quad g_3 = 0{,}59\,, \quad g_3^* = 0.10\,, \quad G_4 = 0.13\,,$$

$$\sigma_4 \sim \frac{1}{2}\,\sigma_3 \sim \frac{1}{2}\,\sigma_2\,.$$

one gets $G_2 = 0.79$, $G_3 = 0.87$.

Appendix II.

A μ-meson crossing the layer of Pb Σ can generate secondaries through 3 different processes: collision with electrons, bremsstrahlung, creation of a pair. For the cross sections corresponding to the two first phenomena we used eq. (1.7 d) and (1.37) of Rossi and Greisen [17]. Furthermore, we have assumed that the cross section for the production of pairs is equal to 1/2 that for bremsstrahlung.

The electron or gamma ray emitted in the above mentioned processes can have an energy sufficient to give rise to a shower which penetrates the layer of Pb placed above the counter-sets C, D and E.

We ask what is the probability that such a shower triggers at least one counter D and at least one counter E. Such a shower has to cross more than 35 radiation units. Therefore the initiating electron or gamma ray must have an energy such that the counter-sets B and C are certainly always crossed by many electrons.

The calculation has been done along a line quite similar to that followed by Greisen [18].

The main difference is due to the fact that instead of using for the average number of electrons present in a shower, the curves of Rossi and Greisen, we have applied the following semiempirical rule which gives results in very satisfactory agreement with the curves obtained by R. Wilson [13] with the Monte Carlo method.

We start from Heisenberg's [19] formula

$$\text{(A2.1)} \qquad \Pi(E_0, E_c, t) = \frac{\sqrt{y}-\beta}{\sqrt{t}-\alpha}\frac{1}{\sqrt{t}} \exp\left[2\sqrt{t} - a\sqrt{y} - \beta\right] \exp\left[-t\right],$$

giving the number of electrons above the critical energy E_c and we calculate the number of photons of energy between 10 and 1 MeV (absorption coefficient in Pb in radiation units 0.24).

Then we multiply equation (A1.2) by 1.5 in order to take into account the electrons below the critical energy [20] and after adding the contribution of low energy photons we normalize the final curve to the energy of the initiating electron.

Furthermore, for the detection probability of a counter for a low energy photon, we use a value of 0.05 instead of 0.02 as used by Greisen. Such a value has been deduced from the absorption coefficient of gamma rays of the considered energy and the range of the corresponding secondary electron.

[17] B. Rossi and K. Greisen: *Rev. Mod. Phys.*, **13**, 240 (1941).

[18] K. Greisen: *Phys. Rev.*, **75**, 1071 (1949).

[19] W. Heisenberg: *Kosmische Strahlung* (Berlin, 1943), cap. 2.

[20] This factor is obtained by comparing eq. (**A2**.1) with the result of H. J. Bhabha and K. Chakrabarty, *Phys Rev.*, **74**, 1352 (1948).

Using the energy spectrum (A1.21) we found that the probability that at least one counter in D and at least one counter in E is discharged, is $1 \cdot 10^{-4}$.

Such a value is about two times the value deduced from Greisen curves.

Finally we have repeated the preceding calculation, taking into account the fact that the probability of detection of a shower in E is not independent from the probability of detection in D because a low energy photon is detected when it is absorbed. The result of such a calculation is that the probability that at least one counter in D and at least one counter in E is discharged is $8 \cdot 10^{-5}$.

A similar calculation has been done assuming that the electronic shower is generated by the μ-meson 5 radiation units inside the rock (5×27 g/cm^2 = = 135 g/cm^2 = 61 cm). In this case the probability of detection in E and D is smaller than in the preceding case by a factor about 100.

RIASSUNTO

A mezzo di un sistema di contatori collegati ad un odoscopio, viene studiata la produzione di secondari penetranti, in piombo e in roccia, da parte della radiazione cosmica a 50 m di acqua equivalente. Per gli eventi interpretabili come coppie di particelle penetranti associate, si deduce una sezione d'urto totale in Pb non superiore a $(13 \pm 3) \cdot 10^{-30}$ cm^2/nucleone: questo valore è dedotto da misure di sezione d'urto differenziale rispetto al percorso dei secondari prodotti (paragrafo 4·3, tabella V). Un valore dello stesso ordine di grandezza viene dedotto per la produzione in roccia. Si mostra inoltre che gli eventi interpretabili come sciami capaci di penetrare 15 cm di Pb hanno una frequenza tale da poter essere spiegati, almeno in parte, come dovuti ad interazioni puramente elettromagnetiche. Si stabilisce pertanto un limite superiore della sezione d'urto in Pb per la produzione di sciami penetranti da parte di mesoni μ di qualche unità in 10^{-30} cm^2/nucleone (paragrafo 4·4). Infine si discutono quegli eventi che si presentano come dovuti a più particelle penetranti provenienti dalla roccia e si mostra come questi possano essere dovuti oltre che a sciami penetranti prodotti in roccia anche alle particelle penetranti presenti nelle vicinanze dell'asse di uno sciame esteso atmosferico.

Ionizzazione totale delle particelle α del polonio in argon e azoto.

G. Bertolini, M. Bettoni e A. Bisi
Istituto di Fisica Sperimentale del Politecnico - Milano

(ricevuto il 4 Agosto 1952)

Riassunto. — L'energia media w spesa da una particella del polonio per creare una coppia di ioni in argon e azoto è stata misurata con una camera a griglia. Si è trovato: $w_{argon} = 28{,}9 \pm 0{,}6$ eV, $w_{azoto} = 37{,}9 \pm 0{,}8$ eV.

1. – L'energia media w spesa da una particella α di energia determinata per creare una coppia di ioni in un gas è stata oggetto di numerose misure. Alcune di queste consistono nel determinare il numero di coppie di ioni create dalla particella in una camera di ionizzazione e in un contatore proporzionale.

Com'è noto il disaccordo fra i risultati di vari ricercatori in misure di ionizzazione è molto verosimilmente imputabile alle diverse tecniche sperimentali e al diverso grado di purezza dei gas impiegati [1] [2].

Per l'importanza che l'argon e l'azoto hanno acquistato come gas di riempimento di camere di ionizzazione e contatori, è stata misurata l'energia media w per questi gas curandone particolarmente il grado di purezza. A questo scopo è stata utilizzata una camera rapida a griglia.

2. – La camera usata è simile a quella descritta da Bunemann e Collaboratori [3].

La distanza elettrodo negativo-collettore è di 6,0 cm; quella griglia-collettore di 1,4 cm. Il volume utile è fissato del diametro del collettore, pari

[1] A. E. Taylor: *Rep. Phys. Soc. Prog. Phys.*, **15**, 49 (1952).
[2] G. C. Hanna: *Phys. Rev.*, **80**, 530 (1950).
[3] O. Bunemann, T. E. Cranshaw e J. A. Harvey: *Canad. Journal Res.*, A **27**, 191 (1948).

a 6,0 cm. La griglia, costituita da fili di acciaio armonico di 0,17 mm di diametro, ha un passo di 1,9 mm.

La camera è connessa ad un purificatore del gas in modo da realizzare una circolazione a termosifone del gas stesso. Il purificatore è un cilindro di acciaio inossidabile contenente una lega di calcio e magnesio e mantenuto ad una temperatura di 350 e 450 °C rispettivamente per l'azoto e l'argon.

La purezza dell'argon è stata controllata misurando la velocità di migrazione degli elettroni liberati nel gas dalle particelle α. Poichè il tempo di transito degli elettroni tra griglia e collettore è uguale al tempo di salita dell'impulso, la misura consiste nel determinare il tempo di salita dell'impulso con un oscillografo a traccia comandata [4].

In azoto la velocità di migrazione degli elettroni è poco sensibile alle impurità. La purezza del gas è stata allora determinata studiando l'altezza degli impulsi in funzione del tempo di circolazione. Poichè la curva ottenuta sale rapidamente ad un valore costante si è ammesso che il valore di saturazione corrispondesse alla purezza del gas.

Fig. 1. - Distribuzione spettrale delle particelle α del Po^{210}.

La sorgente di particelle α è costituita da uno strato di polonio direttamente depositato sul collettore. L'attività della sorgente era dell'ordine di 3000 disintegrazioni al minuto.

L'impulso di tensione, prodotto sull'elettrodo collettore, viene amplificato da un preamplificatore montato direttamente sulla camera e successivamente da un amplificatore. Preamplificatore e amplificatore sono del tipo Bell e Jordan [5].

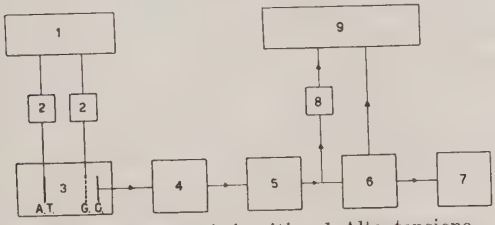

Fig. 2. - Schema dei circuiti. – 1 Alta tensione. – 2 Filtri. – 3 Camera di ionizzazione. – 4 Preamplificatore. – 5 Amplificatore. – 6 Discriminatore di impulsi. – 7 Scala di 1000. – 8 Linea di ritardo. – 9 Oscilloscopio postaccelerato.

Il tempo di salita dell'amplificatore è di 6 μs, il tempo di raccolta degli elettroni, cioè il tempo in cui la tensione del collettore sale al valore finale è di circa 5 e 4 μs rispettivamente per l'argon e l'azoto.

Lo spettro degli impulsi di uscita è stato analizzato con un

---

(4) L. Colli e U. Facchini: *Rev. Sci. Instrum.*, 282 9, (1935).
(5) W. H. Jordan e P. R. Bell: *Rev. Sci. Instrum.*, **18**, 703 (1947).

discriminatore a taglio. In queste condizioni la larghezza delle righe delle α del polonio, al semimassimo, è del 3% (fig. 1).

Lo schema di insieme dell'apparecchiatura elettronica è mostrato in fig. 2.

3. – L'argon è stato studiato da 3 a 7 atmosfere e l'azoto da 3 a 4 atmosfere. Per entrambi i gas in questo intervallo di pressione una tensione di 2 500 volt all'elettrodo negativo genera un campo sufficiente a raccogliere tutti gli elettroni formati lungo il percorso delle particelle α. La tensione di griglia non è critica; per valori superiori a 600 volt, l'altezza degli impulsi si mantiene costante entro lo 0,5%.

L'energia w è legata all'energia E delle α dalla relazione:

$$w = \frac{e}{C}\frac{A}{V}E,$$

dove e indica la carica dell'elettrone, V l'impulso di uscita, A l'amplificazione e C la capacità totale dell'elettrodo collettore e dell'ingresso del preamplificatore.

L'amplificazione A è stata misurata con un generatore di impulsi mod. 100 [6] direttamente collegato al preamplificatore. Il procedimento è corretto perchè la costante di tempo di ingresso è molto maggiore del tempo di discesa dell'amplificatore.

La determinazione della capacità C è stata effettuata misurando l'attenuazione subita da un impulso con l'inserire una capacità nota in parallelo al collettore.

Come media di 5 determinazioni si è trovato:

$$C = 28{,}2 \ \mu\mu\text{F}.$$

Per l'energia E è stato assunto il valore $E = 5{,}298$ MeV. Tale valore deve essere però corretto per tenere conto dell'autoassorbimento dello strato emittente. La correzione è stata effettuata calcolando il profilo di una riga monoenergetica nell'ipotesi che le α siano emesse isotropicamente in tutti i punti della sorgente. Questo profilo è stato poi pesato sulla distribuzione di impulsi che la catena di registrazione fornicse per gli impulsi artificiali

Si ricava così lo spostamento subito dal massimo della riga, pari nel caso in esame all'1,8%. Tenendo conto di questa correzione i valori di w risultano:

$$w_{\text{argon}} = 28{,}9 \pm 0{,}6 \ \text{eV},$$
$$w_{\text{azoto}} = 37{,}9 \pm 0{,}8 \ \text{eV}.$$

Gli errori indicati sono dovuti alle incertezze che si hanno nella misura dell'amplificazione e della capacità della camera.

(6) W. C. Elmore and M. Sands; *Electronis Experimental Tecniques* (New York, 1949) p. 323.

4. – I valori ottenuti per l'energia media w sono in accordo, come appare dalla seguente tabella, con i valori di STETTER, mentre quelli di ALDER, HUBER e METZ e quelli di DICK, FALCK-VAIRANT e RUSSEL risultano un poco inferiori.

Argon	Azoto	
24 eV	33 eV	GURNEY (7)
24,4 »	36,1 »	SCHMIEDER (8)
28,5 »	37,2 »	STETTER (9)
	33,7 ± 4%	DICK *et al.* (10)
	36,3 ± 0,4	ALDER *et al.* (11)
28,9 ± 0,6	37,9 ± 0,8	nostre misure

Le misure di STETTER, DICK *et al.*, ALDER *et al.*, sono determinazioni assolute mentre quelle di SCHMIEDER e quelle di GURNEY sono fatte relativamente all'aria e il valore di w è ricavato dal corrispondente w_{aria}.

Tutti gli sperimentatori citati misurano anche la componente ionica della ionizzazione. Il buon accordo ottenuto indica che in determinazioni di ionizzazioni totale i metodi di misura rapidi (collezione di soli elettroni) sono equivalenti ai metodi di misura lenti (collezioni di ioni ed elettroni).

Ringraziamo il prof. G. BOLLA Direttore dell'Istituto, per il costante interessamento, il dott. U. FACCHINI e l'ing. E. GATTI per le frequenti discussioni.

(7) R. W. GURNEY: *Proc. Roy. Soc. London*, **107**, 332 (1925).
(8) K. SCHMIEDER: *Ann. der Phys.*, **35**, 445 (1939).
(9) G. STETTER: *Zeits. f. Phys.*, **120**, 639 (1943).
(10) L. DICK, P. FALCK-VAIRANT e J. RUSSEL: *Helv. Phys. Acta*, **20**, 357 (1947).
(11) E. ALDER, P. HUBER e F. METZGER: *Helv. Phys. Acta*, **20**, 234 (1947).

SUMMARY

The total ionization produced by α-particles from Po^{210} has been measured in pure argon and nitrogen. Argon and nitrogen were purified by a calcium-magnesium filled convection current purifier. Electron collection has been employed, using a fast amplifier feeding an ordinary discriminator. The average energy w spent in producing a ion pair in argon and nitrogen are as follows: $w_{argon} = 28{,}9 \pm 0{,}6$ eV, $w_{nitrogen} = 37{,}9 \pm 0{,}8$ eV. Our results are in good agreement with the measurements of Stetter's laboratory.

The problem of the stability of technetium.

E. Segrè

University of California, Physics Dept. - Berkeley, Cal. U.S.A (*)

(ricevuto il 12 Settembre 1952)

Summary. (*) — Discussion, based on nuclear, geochemical and astronomical data, on the possible existence of isotopes of technetium with a period longer then 10^9 years. The only possible isotopes are Tc^{97} and Tc^{98} which, although radioactive, might have very long periods.

(*) *Editors's translation.*

Some of the nuclei found in nature even outside of the region of alpha instability are beta unstable. The oldest and most famous examples are K^{40} and Rb^{87}. In order, however, that such nuclei may exist on the earth their period must be of the order of 10^9 years at least.

In the case of technetium ($Z = 43$) it is easy to show that all its isotopes must be unstable, although some might have very long lives. Indeed for Z odd a necessary condition for stability requires that the number of neutrons N be even; this condition is of course not sufficient. The stability curve in a Z, N diagram shows that only the isotopes with $A = Z + N = 97$ or 99 could conceivably be stable, but Mo^{97} and Ru^{99} do exist in nature and are stable. From these facts it follows that Tc^{97} must decay by orbital electron capture and Tc^{99} by negatron emission.

This simple argument is supported by the experimental evidence of a Tc^{99} beta emitter with a period of $2.12 \cdot 10^5$ years [1]. For Tc^{97} the situation is a

(*) Temporarily at Brookhaven Natl. Lab., Upton N.Y.

[1] National Bureau of Standards: Circular 499 and supplements.

little less clear. A Tc^{97m} is known ([2]): the excited state is 0.096 MeV above the ground state and is presumably $p\,1/2$, but the radioactivity of the ground state has not yet been detected and its period is reported as longer than 1 000 years. Shell theory applied to this nucleus and a study of its isomerism lead to the very probable conclusion that the ground state of Tc^{97} is $g\,9/2$ whereas the ground state of Mo^{97} is $d\,5/2$ according to shell theory and some hyperfine structure measurements of ARROE ([3]). Hence the transition between ground states has $\Delta I = 2$, no parity change, but not much can be said about its energy. The presence of a $g\,7/2$ excited state of Mo^{97} 0.665 MeV above the ground state indicates that the ground state of Tc is below the excited state of Mo^{97} or at most slightly above it. Otherwise Tc^{97} would have a short life instead of a period $> 1\,000$ years as observed. Now assuming an energy of 0.66 MeV for the orbital electron capture $\Delta I = 2$ no parity change, gives a period of 10^6 years ([4]). This however is a lower limit since we have assumed the maximum energy and if the energy difference is sufficiently small the half life could be $> 10^9$ years.

We must now also consider Tc^{98} which is still doubtful in spite of several attempts to prepare it by molybdenum bombardments. On the one side it has been assigned to a positron activity with a period of 42 m ([5]), on the other side ([6]) its period has been estimated as longer than 10^3 years. Shell theory makes it likely that the spin of Tc^{98} be very high, up to 7, and hence its decay to Mo^{98} of spin 0 is highly forbidden. The situation parallels the one of K^{40} and a period $> 10^9$ years is not impossible. The argument based on shell theory is not however absolutely certain because the Nordheim ([7]) rules applied in this case to guess the spin have some exceptions.

In conclusion we see that both Tc^{97} and, more probably, Tc^{98} might have half lives long enough to persist through geological ages. All other isotopes of technetium with $92 < A < 102$ have been identified and assigned, chiefly by the careful and exacting systematic work performed by the G. E. BOYD group at Oak Ridge and by the M. L. POOL group in Ohio.

There is also some geochemical evidence which may throw light on the problem. We know now through the studies performed on technetium using its radioactive isotopes that its chemical behavior is very similar to that of

([2]) M. GOLDHABER and R. D. HILL: *Rev. of Mod. Physics* (in press).

([3]) O. H. ARROE: *Phys. Rev.*, **69**, 212 (1950).

([4]) R. E. MARSHAK: *Phys. Rev.*, **61**, 431 (1942) with empirical information brought to the author's attention by E. FEENBERG.

([5]) HOUSE, COLLIGAN, KUNDER and POOL: *Phys. Rev.*, **86**, 654 (1952).

([6]) G. E. BOYD: *Abstract of papers, 12th International Congress of Chemistry*, New York, 1951.

([7]) L. W. NORDHEIM: *Rev. Mod. Phys.*, **23**, 322 (1951).

rhenium. Among other properties, the volatility of its oxides and the ionic radii are close to those of rhenium. The geochemistry of this element has been studied in an excellent paper by I. and W. NODDACK [8] and a perusal of this paper supplemented by our present knowledge of the chemistry of technetium shows that it is reasonable to expect a close geochemical association of the two elements. Especially in the rhenium containing molybdenum ores and their derivatives one would expect to find technetium associated with rhenium.

In the analyses so far reported no technetium has been detected. No particular mention of it is contained in the paper of I. and W. NODDACK [8] in which they have used X-ray methods of analysis which are able to detect extremely small amounts of molybdenum and ruthenium down to a fraction of a part per million. Also BOYD reports [6] that in a Colorado molybdenite he has formed < 0.01 ppm Tc.

A reasonable estimate for the sensitivity of these analysis makes us think that if technetium had an abundance of 10^{-2} to 10^{-3} that of rhenium it would have been detected. On the other hand data on the abundance of the elements in the meteorites and on the earth in general show enough regularity to make it plausible [9] that technetium, if stable, would be approximately 5 times as abundant as rhenium. From this we must conclude that during geological time ($3 \cdot 10^9$ years), Tc has decayed by a factor from 500 to 5000 which puts an upper limit to $T_{1/2}$ of $3 \cdot 10^8$ years.

Recently a further piece of information has been added through the discovery in *S* stars of the spectral lines of technetium [10]. Stellar spectra of type *S* characterized by bands of zirconium oxide and by relatively strong lines of heavy metals such as barium. The atmosphere of these stars is cold (3000°) and it is extremely difficult to see how technetium could be produced in the stellar atmosphere. The hypothesis of diffusion from the interior is also unlikely and the presence of technetium in these stars is a remarkable puzzle. MERRILL has put forward 3 hypotheses: 1) Existence of a stable isotope; 2) Production of Tc by the star (no mechanism suggested); 3) That *S* type stars represent a comparatively transient phase of stellar existence.

From what we have said it is clear that a thorough search of technetium on the earth, with the objective of pushing the sensitivity of the methods used to the very limit is warranted. Fortunately the methods of radioactive tracers, of activation analysis in the pile, of optical spectroscopy and the study of the radioactivity of the samples give powerful tools which were not available

[8] I. And W. NODDACK: *Zeits. f. Phys. Chem.*, A, **154**, 207 (1931).
[9] See e.g. H. BROWN: *Rev. Mod. Phys.*, **21**, 625 (1950).
[10] P. W. MERRIL: *Science*, **115**, 484 (1952).

at the time of the search undertaken by the Noddacks and make it possible to push the sensitivity to the limit required. A desirable goal seems to be a sensitivity which would detect Tc if it were present with an abundance of 10^{-3} of that of Re in the same natural material.

RIASSUNTO

Discussione in base a dati nucleari, geochimici e astronomici sulla possibile esistenza di isotopi del tecneto con periodo superiore a 10^9 anni. I soli isotopi possibili sono Tc^{97} e Tc^{98} i quali, benchè radioattivi, potrebbero avere periodi lunghissimi.

NOTE TECNICHE

Boron Layer Scintillation Neutron Detectors.

E. Gatti, E. Germagnoli, A. Persano and E. Zimmer
Laboratori CISE - Milano

(ricevuto il 24 Luglio 1952)

Summary. — Neutron detection with layers of crystalline powder mixtures of a boron compound and of a scintillator, used in connection with a photomultiplier, has been studied. Efficiency of 6% for incident thermal neutrons and almost complete insensitivity to γ and cosmic rays is reached. Detector's geometry approaches that of an infinitely thin sheet. Pulses may be shaped so as to have less than half a microsecond rise time.

1. – Introduction.

It is often of importance, for instance in slow-neutron transmission measurements performed by means of a time-of-flight spectrometer, to use a neutron detector having a sensitive volume sharply defined and a small thickness, in order to minimize the uncertainty in the estimate of neutron velocity.

Among the methods of neutron detection hitherto fully developed, that fulfilling such a requirement seems to be the boron or lithium thick sheet ionization chamber (1). Such an ionization chamber has a maximum theoretical efficiency of 1-2% and requires high pulses amplification, moreover α-particles when reaching the sensitive volume of the chamber have a uniform energy spectrum ranging from 0 to the maximum energy corresponding to the Q of the nuclear reaction, and so if neutrons are accompanied by a strong background of γ rays, as it usually happens, the practically obtainable efficiency is considerably reduced by the necessity of discriminating against the piling-up of γ pulses.

It seemed therefore worth while to accomplish a search about the possibility of slow neutron detection by means of layers obtained by mixing crystalline powders of boron coumpounds with ZnS-Ag or ZnO, which are well known

(1) B. Rossi and H. Staub: *Ionization Chambers and Counters* (New York, 1949), pag. 186.

specific scintillators for α particles. Owing to the partial optical transparency of these layers, we relied on a higher efficiency as compared with the possible one of a layer ionization chamber.

2. – Experimental procedures.

We used in the whole run of measurements a photomultiplier RCA 5819, to which, in front of the photocathode, a lucite container was adapted. It consisted mainly of two plane surfaces between which the examined powder mixture could be sheet-shaped and lightly pressed. The experimental geometry (fig. 1) has proved to be reliable and allowed to study and change the layers readily. The neutron source (500 mg $RaBr_2$ + Be) was screened by 2.5 cm of Pb and was surrounded by a paraffin block of cubic form, 20 cm of side. A voltage of 850 volt was supplied to the phototube and conventionally distributed among the dynodes; the amplification and counting chain consisted of a cathode follower, a model 100 amplifier (we never used a gain higher than 300) an integral discriminator and a scaler.

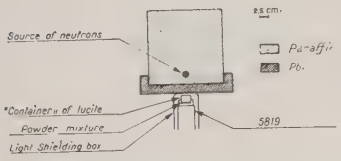

Fig. 1. – Experimental arrangement.

Every mixture was generally studied in the following way: using a known mean grain size of boron compound and scintillator, the boron content of layer was kept constant and volume percentage of scintillator was gradually increased attempting to find the percentage which gives the highest efficiency.

Curves obtained with such procedure will successively be called « saturation curves »: they are generally characterized by a rather flat maximum arising from the product of an increasing and a decreasing factor: the increasing number of grains of scintillator surrounding a boron compound grain, (what we call « saturation » of the boron compound grain) causes more α particles to fall on the scintillator and gives the increasing factor; growing optical opacity lessens pulse height and gives the decreasing factor. The latter is particularly important when boron content is high, first as the layer is optically thick, secondly as a remarkable reduction of neutron flux takes place at the face of the layer in front of the photocathode, whence the unattenuated ligth pulses are coming. Saturation curves have been generally obtained with a content of boron corresponding to $n_B\sigma_B$ ranging from 0.1 to 0.6.

A fixed composition of the mixture is now choosen and total weigth of the layer, that is $n_B\sigma_B$, is varied: « transparency curves » are obtained this way. Efficiency presents in this case an asymptotic behaviour, and keeps its value rather constant in a quite large range of $n_B\sigma_B$ values: the subsequent slow rate of decrease may be clearly ascribed to the self-shielding of neutrons.

3. – Analysis of bias curves.

In order to evaluate the effect of the limited transparency of the mixtures and to compare the measured efficiencies with those theoretically obtainable, we calculated with very rough assumptions the theoretical bias curve.

We assume: *a*) the total thickness of the layer is so large as to make it opaque to light; *b*) the grains of the boron compounds are thick in respect to the range of α particles (and consequently the energy spectrum of the emerging α particles is a continuous and constant one); *c*) the light pulses are proportional to the α's energy; *d*) the phototube, is linear. Than if A_p is the light pulse height as seen by the phototube, A is the light pulse height given by the scintillator, correspond ing to energy E of the incident particle, A_0 is the value of A_p corresponding to discriminator bias and μ is an optical attenuation coefficient of the considered layer, we may write

$$A_p = A \exp[-\mu x], \tag{1}$$

where x is the depth at which the α particle is emitted.

If we assume that the α particles are uniformly generated within the layer ($n_B \sigma_B \ll 1$) we have too

$$\mathrm{d}\bar{N} = n(A)\,\mathrm{d}x, \tag{2}$$

where $n(A)\,\mathrm{d}A$ is the number of scintillations per unit x and having height ranging from A to $A + \mathrm{d}A$. $\bar{N}$ is the number of scintillations between 0 and x per unit A.

Comparison of (1) and (2) gives

$$\frac{\mathrm{d}\bar{N}}{\mathrm{d}A_p} = \frac{n(A)}{\mu A_p},$$

and after integration between the limits A and A_0

$$\bar{N}(A_0) = \frac{n(A)}{\mu} \ln \frac{A}{A_0}.$$

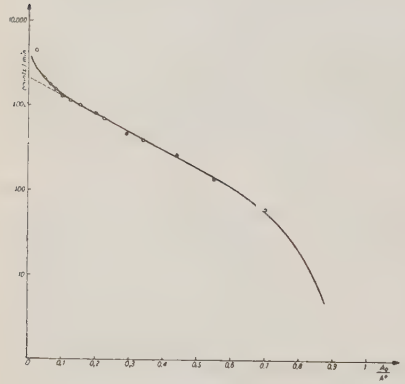

Fig. 2. – Bias curve.

Integrating again over A between A_0 and A^* (corresponding to the maximum energy of the given α's)

$$N(A_0) = \int_{A_0}^{A^*} \frac{n(A)}{\mu} \ln \frac{A}{A_0}\,\mathrm{d}A = \frac{N}{\mu}\left[\ln \frac{A^*}{A_0} + \frac{A_0}{A^*} - 1\right], \tag{3}$$

where $N = \int_0^{A^*} n(A)\,\mathrm{d}A = nA^*$ is the total number of scintillations per unit x.

The bias curve corresponding to (3) is drawn in fig. 2 together with the experimental points obtained with a layer of H_3BO_3 and ZnS. We must say that all bias curves fit very well the theoretical one even if the layer is not quite opaque.

All efficiency data are given at a bias $A_0 = 0.2A^*$.

4. – Experimental results.

We have studied mixtures containing ZnS-Ag or ZnO and one of the following boron compounds:

Compound	Specific gravity	Boron content
Amorphous boron	2.3 (?)	85-90 %
H_3BO_3	1.43	17,5 %
$Na_2B_2O_2 \cdot 10\ H_2O$	1.73	11.3 %
$Li_2B_4O_7$	2.5	25.6 %
BN	2.25	43.6 %
B_2O_3	1.844	31.0 %

ZnS-Ag was of the commercial grade for cathode-ray tubes; ZnO a very pure Merck product (> 99,9% ZnO), heated for 1-2 hours at 1000 °C, in air.

We have obtained the BN from B_2O_3 + urea: the method is described in the litterature (2) and was perfectly adequate for our purpose, though it gives a rather low yield. $Li_2B_4O_7$ was obtained from $Li_2CO_3 + H_3BO_3$ in stoichiometric proportions, by heating and melting the mixture in platinum crucible. The glassy mass crystallizes rapidly on cooling.

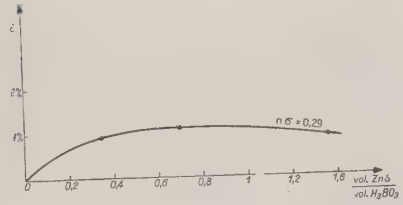

Fig. 3. – Saturation curve H_3BO_3 + ZnS.

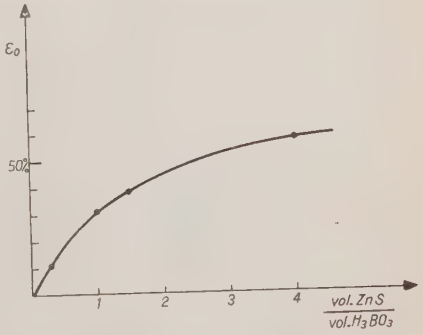

Fig. 4. – Saturation curve H_3BO_3 + ZnS.

B_2O_3 was, after preparation, disregarded in view of difficulty of grinding and keeping dry.

We had care to obtain well granulated and uniform mixtures: results about the influence of the mean diameter of grains will be reported later.

(2) G. Brauer: *Handbuch der Präparativen Anorganischen Chemie* (Stuttgart, 1952), pag. 591.

Of the two experimented phosphors, ZnS has proved more satisfactory giving pulses three times larger than ZnO; rise time of ZnS pulses is 4 μs and 2 μs for ZnO; ZnS pulses are however easily shaped with a delay line so as to have less than 0.5 μs rise time, without beeing reduced in size by more than a 3 factor. The low efficiency obtained with ZnO as scintillator is probably due to a small percentage of grains efficient as scintillator.

Let us comment the particular results of the measurements:

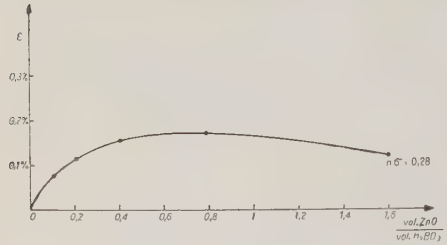

Fig. 5. – Saturation curve H_3BO_3 + ZnO.

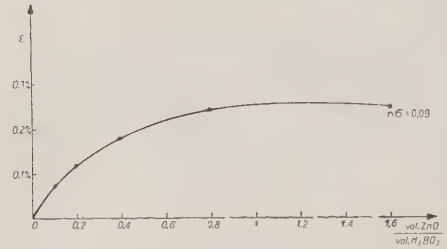

Fig. 6. – Saturation curve H_3BO_3 + ZnO.

H_3BO_3 + ZnS mixture.

A saturation curve is given in fig. 3: one can note the previously discussed effects. Fig. 4 shows a « true » saturation curve, in which volume percentage of scintillator is varied, but the transparency of the layer is kept about constant. However, every experimental point is normalized to the same number of α particles emitted within the layer. By this method the opacity effect may be disregarded and « internal efficiency », that is the ratio of counts to α particles emitted, is seen to reach a rather high asymptotic value.

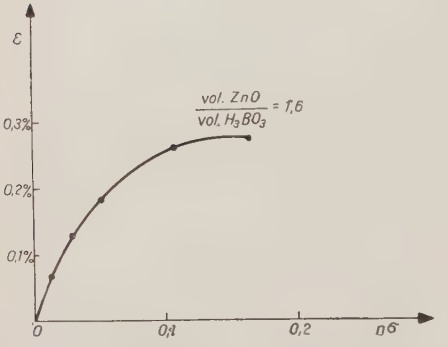

Fig. 7. – Transparency curve H_3BO_3 + ZnO.

H_3BO_3 + ZnO.

Fig. 5 is similar to fig. 3; fig. 6 shows a saturation curve with no maximum owing to the small thickness of the layer. Fig. 7 gives a transparency curve in which an asymptotic value is reached; beyond the explored value of $n_B\sigma_B$ self-absorption would lower the curve.

$Na_2B_4O_7 \cdot 10H_2O$ + ZnS or ZnO.

Notwithstanding of the good transparency, little content of boron in borax makes this compound uninteresting for our purpose: similar curves with low efficiency were taken, but are not reported.

Boron (amorphous) + ZnS.

Light is almost completely absorbed: no curves have been taken.

$Li_2B_4O_7 + ZnS$.

Figg. 8 and 9 show respectively saturation and transparency curves. This compound proves very satisfactory for transparency, large content of boron and large density, which is effective in reducing the quantity of ZnS needed to « saturate » the $Li_2B_4O_7$.

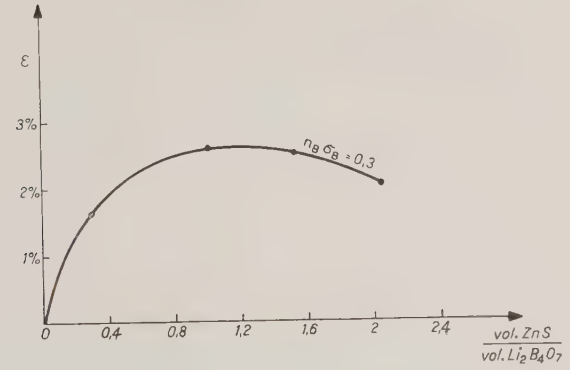

Fig. 8. – Saturation curve $Li_2B_4O_7 + ZnS$.

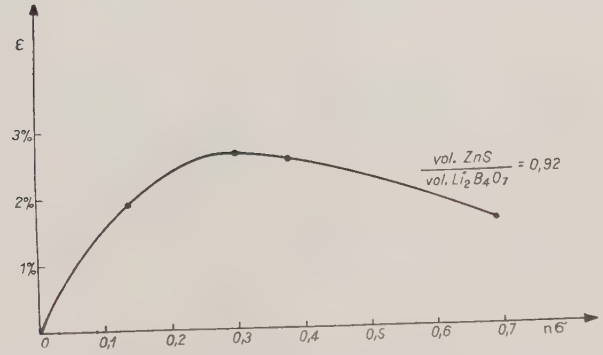

Fig. 9. – Transparency curve $Li_2B_4O_7 + ZnS$.

BN + ZnS.

BN is the richest in boron among the experienced compounds: its transparence is good and consequently it has proved to be the most efficient. In fig. 10 and 11 the two tipical curves are reported.

5. – Influence of grain size.

As the range of the α particles emitted in the $(n\,\alpha)$ reaction of boron is rather short (6 μ) in the experimented boron compounds, practically obtai-

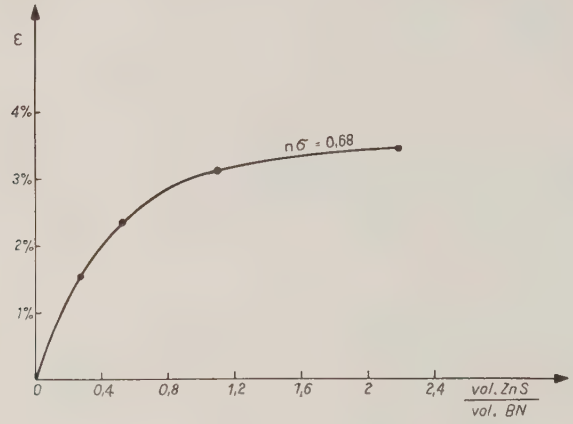

Fig. 10 – Saturation curve BN + ZnS.

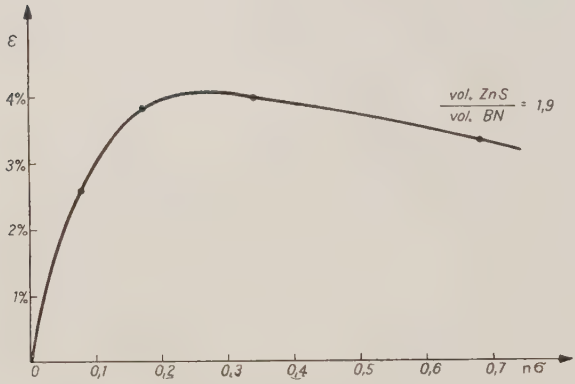

Fig. 11. – Transparency curve BN + ZnS.

nable efficiency must be strongly dependent upon the size of grains and uniformity of the mixture.

In order to test experimentally this point, a few samples of H_3BO_3 have been prepared having known and different mean size of the grains: they were carefully mixed to ZnS, whose grain size was similarly calibrated. These samples, exposed to the same neutron flux have given the counting rates

resumed in Table I. Owing to these results, all previously reported measurements were taken with the finest grain size.

TABLE I. – *Grain size effect.*

Mean grain size	Counts/min.	Mixture
0– 50 μ	2600	H_3BO_3 172 mg + ZnS 333 mg
70–150 μ	1550	»
150–180 μ	850	»
180–300 μ	680	»

6. – Absolute efficiency calibration.

The standard paraffine cavity of this laboratory which gives, with our $RaBr_2$ + Be neutron source, a known flux of neutrons [3] has allowed to determine with good accuracy the efficiency of our neutron detectors.

Thin layers of In, Rh, Ag have been exposed firstly to the known neutron flux, subsequently were introduced in the lucite container with the same geometry that was used for the mixture measurements. The ratio of the induced thermal activities, extrapolated to $n = 0$, that is, for an infinitely thin layer [3], gives the flux to which the mixtures were exposed. The accuracy of this calibration is 5%.

Of course the introduction of an absorbing mixture having some content of boron causes a drop in the measured flux: for instance we have found that experimentally the flux is reduced to 65% of his limiting value if in the container, under the neutron detector layer, is placed a 1 mm sheet of cadmium, that is a completely « dark » body for thermal neutrons. All measurements were corrected for this effect.

Efficiency for our mixture layer may be so written

$$\varepsilon = \varepsilon_0 \left(1 - \exp\left[- n_B \sigma_B(E)\right]\right),$$

where

n_B is the number of boron nuclei per cm^2,

$\sigma_B(E)$ is the capture cross section of boron at energy E

$\varepsilon_0(A_0/A^*)$ is the « internal efficiency » of the layer which gives the weighted probability over the whole layer that an α particle, generated within the mixture, gives at the phototube a pulse larger than A_0. ε_0 is therefore function of the transparency of the layer and consequently, for a given mixture, indirectly of $n_B\sigma_B$.

---

[3] A. BRACCI, U. FACCHINI and E. GERMAGNOLI: *Nuovo Cimento*, **7**, 881 (1950).

Table II summarizes the obtained results for ε and ε_0.

TABLE II. – *Maxima of efficiency for studied mixtures at a bias* $A_0/A^* = 0{,}2$ *(grain size of all components* 0-50 μ).

Mixture	$n_B\sigma_B$	ε_0	ε
H_3BO_3 172 mg + ZnS 333 mg	0,12	14,6 %	1,75%
$Li_2B_4O_7$ 300 mg + ZnS 450 mg	0,30	8,67%	2,6 %
BN 100 mg + ZnS 350 mg	0,17	22,6 %	3,84%

It is interesting to note that the ε_0 above defined is a decreasing exponential function, for a given mixture, of $n_B\sigma_B$: fig. 12. Curves of this figure are obtained from those of figg. 7, 9, 11. One clearly sees that the relatively high efficiencies obtained with thick layers of $Li_2B_4O_7$ + ZnS and BN + ZnS are, at least in part, due to the less steeper descent of ε_0 with increasing $n_B\sigma_B$.

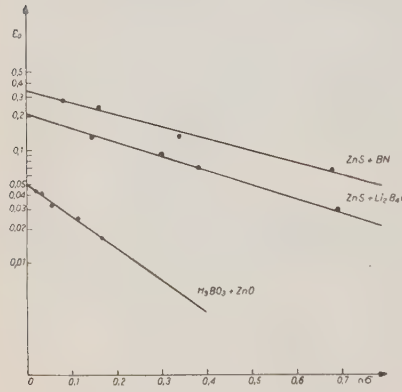

Fig. 12. – Plot of ε_0 against $n_b\sigma_B$.

7. – Conclusion.

As this report is intended only as a study of the mixed-powder layers, no serious attempt as been made to get better geometrical conditions, to get a greater sensitive surface, now of 10 cm². One temptative essay consisting placing an aluminium foil enveloping the lucite container has brought a 50% increase in efficiency, owing probably to collection of photons emerging from the upper face of the layer.

From these considerations and experimental results we think therefore that mixed-powder neutron detectors are superior for simplicity of use and preparation, and comparable as to efficiency, to BF_3 proportional counters, having moreover the advantage of an ideal geometry for some type of experiments. The comparison seems to hold even with LiI crystals and with liquid scintillators, to which has been recently pointed out [4]. Another advantage of the mixed-powder detector lies in its almost complete insensitivity to X and γ rays, which are often present in natural or artificial neutron sources, as to the cosmic background. In our case, for istance, 500 mg of Ra shielded with

[4] « Latest Development for Scintillation Counting ». *Nucleonics*, **10**, n. 3, 32 (1952).

25 mm lead at a distance of 10 cm from the mixed-powder detector did not give any count at the bias corresponding to reported figures of efficiency.

It is also of practical interest to point out that, as the pulses are of at least two orders of magnitude larger than those of phototube background, it should be possible to use the cheaper phototube 931 A.

We thank Prof. G. Bolla for his interest in the present work and Dr. A. Bracci, Dr. A. Malvicini, Dr. G. Perona for useful suggestions.

Note added in proof. — In *R.S.I.* number 6 (June 1952), pag. 264, now at disposal of the authors, a paper by W. F. Hornyak is published, about a fast neutron scintillation detector made by molding together a mixture of ZnS powder and Lucite molding powder.

RIASSUNTO (*)

Si è studiata la rivelazione dei neutroni per mezzo di strati di miscele di polveri cristalline con un sale di boro e uno scintillatore usate in unione con un fotomoltiplicatore. Si è raggiunto un rendimento del 6% per i neutroni termici incidenti, con la quasi assoluta insensibilità ai raggi α e cosmici. La geometria del rivelatore si approssima a quella di uno strato infinitamente sottile. Gli impulsi possono venir conformati in modo da ottenere un tempo di salita inferiore a mezzo microsecondo.

(*) *Traduzione a cura della Redazione.*

Un camera di ionizzazione a bassa capacità.

G. Bertolini e A. Bisi
Istituto di Fisica Sperimentale del Politecnico - Milano

(ricevuto il 4 Agosto 1952)

Riassunto. — È stata costruita una camera di ionizzazione a bassa capacità, atta a rivelare particelle α di 100 keV con un rapporto segnale/fondo dell'ordine di 5.

1. – In esperienze con camere di ionizzazione il limite inferiore delle energie misurabili è dato dal rapporto segnale/fondo. Per abbassare questo limite occorre operare su detto rapporto, sia diminuendo il rumore di fondo dell'apparecchiatura elettronica sia aumentando il segnale di uscita a parità di amplificazione.

In una camera a griglia l'impulso di tensione da classificare e registrare ha un'altezza:

$$V = \frac{q}{C} A ,$$

dove A indica l'amplificazione del sistema, q la carica generata nel gas da una particella ionizzante e raccolta dall'elettrodo collettore. La capacità C (in generale dell'ordine di 40-60 $\mu\mu$F) è costituita dalla capacità C_1 del collettore, dalla capacità C_2 della connessione tra il collettore e il preamplificatore e dalla capacità di ingresso C_3 della prima valvola del preamplificatore.

La capacità C_2 è stata eliminata ponendo la prima valvola del preamplificatore dentro la camera, con la griglia a diretto contatto con il collettore.

2. – Si è usata una camera a griglia, simile a quella descritta da Bunemann e collaboratori [1], la quale ha le stesse caratteristiche di un'altra utilizzata da noi in misure di ionizzazione totale [2].

[1] O. Bunemann, T. E. Cranshaw e J. A. Harvey: *Canad. Journ. Res.*, A **27**, 191 (1948).

[2] G. Bertolini, M. Bettoni e A. Bisi: in corso di pubblicazione.

La valvola, all'interno della camera, è alimentata attraverso quattro Kovar saldati su un bocchettone, al quale è fissato il preamplificatore. La capacità

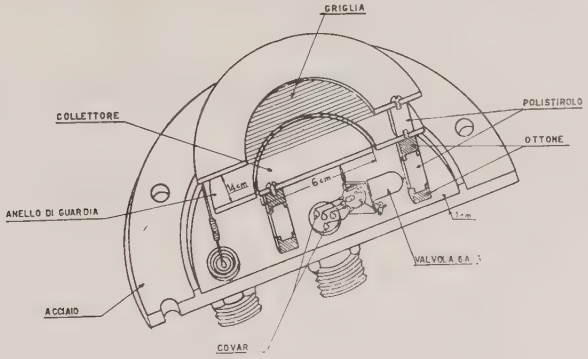

Fig. 1. – Schema della camera di ionizzazione.

della camera è stata determinata in base alla attenuazione subita da un impulso di tensione inserendo una capacità nota tra collettore e terra. L'impulso è stato inviato per induzione attraverso la griglia della camera. Si è trovato una capacità di 9,3 $\mu\mu$F.

A questo valore contribuiscono: la capacità di ingresso del primo stadio di amplificazione (~ 4 $\mu\mu$F), del collettore (~ 2 $\mu\mu$F) e della griglia verso il sostegno metallico della valvola. Con un collettore più distante dalle pareti della camera e con un sostegno isolante della valvola ci si potrebbe quindi ridurre ad una capacità di poco superiore a quella d'ingresso della valvola.

Quest'ultima è una 6 A K 5 scelta per il suo alto rapporto $g_m/C_{\text{ingr.}}$ e selezionata fra una cinquantina di tubi. Essa lavora con la griglia direttamente connessa al collettore e senza resistenza di fuga in modo da eliminare il rumore di fondo dovuto alla corrente di griglia.

Il fondo è stato misurato con un generatore di impulsi mod. 100 ([3]), ed è risultato dell'ordine di 15 microvolt all'ingresso della catena amplificatrice. Questa è costituita da un preamplificatore e da un amplificatore del tipo Bell e Jordan ([4]).

In base ai valori ottenuti per il rumore di fondo e la capacità C della camera, si può prevedere di rivelare particelle α di 100 keV con un rapporto segnale/fondo dell'ordine di 5.

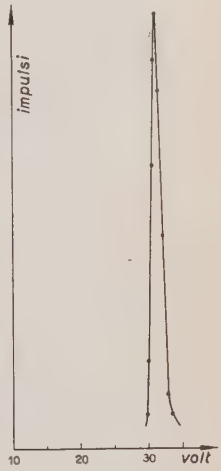

Fig. 2 - Spettro di energia di particelle α di circa 200 keV.

([3]) W. C. Elmore e M. Sands: *Electronis Experimental Techniques* (New York, 1949), p. 323.

([4]) W. H. Jordan e P. R. Bell: *Rev. Sci. Instrum.*, **18**, 703 (1947).

Come controllo sono stati studiati gli impulsi prodotti da particelle di energia dell'ordine di 200 keV. La sorgente era costituita da uno strato di polonio deposto sull'elettrodo negativo della camera e ricoperto da uno strato di mica dello spessore di 5,1 mg/cm² ([5]).

Lo spettro ottenuto è mostrato in fig. 2.

Ringraziamo il prof. G. Bolla, Direttore dell'Istituto, per il costante interessamento, l'ing. E. Gatti per i numerosi consigli e il sig. T. Mossa per l'aiuto dato per la parte elettronica.

([5]) G. T. Seaborg, J. J. Katze e W. M. Manning: *The transuranium Elements* (New York, 1949), p. 975.

SUMMARY

A grid ionization chamber of low capacity has been built, able to detect particles of 100 keV. The ratio between signal and noise is ~ 5.

LETTERE ALLA REDAZIONE

(La responsabilità scientifica degli scritti inseriti in questa rubrica è completamente lasciata dalla Direzione del periodico ai singoli autori)

The commutation laws in the theory of quantized fields.

M. Cini

Pembroke College, University of Cambridge (Inghilterra) (*)

(ricevuto il 21 Luglio 1952)

Schwinger (1) has recently shown how a consistent theory of quantized fields can be derived from a single quantum dynamical principle replacing the conventional assumptions based on analogy with classical Hamiltonian dynamics.

Peierls (2) has formulated a general rule by means of which one can obtain the commutation laws between field quantities in the Heisenberg representation at any two different space-time points.

We have investigated how Peierls' method is related to Schwinger's formulation, deriving the commutation rules for field quantities at different space-time points in the theory of quantized fields. This procedure illustrates the reason of the failure of Peierls' rule in the case of arbitrary functions of field variables.

For variables on the same surface σ we use the infinitesimal generating operator (S 2.65)

$$F = -\int_{\sigma} \delta\Pi^b \Phi^b \, \mathrm{d}\sigma \tag{1}$$

with

$$\delta\Pi^b = \varepsilon^b \delta_\sigma(x - x_0) \,, \tag{2}$$

where ε^b is a small quantity of the first order which commutes with $\Pi^a(x)$ and $\Phi^a(x)$ except when a and b both refer to half integral spin variables, in which case it anticommutes. For a general operator G on the surface σ one gets

$$-i(\zeta', \sigma|[G, F]|\zeta'', \sigma) = (\zeta', \sigma|\delta_\Pi G|\zeta'', \sigma) \,, \tag{3}$$

(*) On leave from Istituto di Fisica dell'Università, Torino.

(1) J. Schwinger: *Phys. Rev.*, **82**, 914 (1951). All symbols used in the following are the same as in Schwinger's paper which will be referred to as S.

(2) R. E. Peierls: *Report to the International Conference on fundamental particles*, Bombay 1950; *Proc. Roy. Soc.*, in the press. I am indebted to Prof. Peierls for letting me have a pre-publication copy of his work.

where $\delta_{II}G$ is the change produced in G by increasing Π^b by $\delta\Pi^b$. For $G = \Pi^a(x)$ or $G = \Phi^a(x)$ the commutation relations (S 2.81) follow immediately.

Equation (3) remains formally valid also if G is an operator of the field variables at x', on the surfaces σ'. To calculate the change in G produced by the variation $\delta\Pi^b$ performed on a different surface σ one has to investigate how the solutions of the equations of motion are affected by a variation in the boundary value of Π^b. This could be done if one had explicitly the solutions expressed in terms of boundary values, but it is also possible to alter directly the equations and derive from these the modified solutions.

The variation to be introduced in the equations is not given by (2), because this is defined only for x on σ, and we need the time dependence of it if we want to get a modification of the equations. We have to take for x' on σ' later than σ [3]

$$\delta\Pi^\beta = \varepsilon^\beta \delta_\sigma(x' - x_0) u(\sigma', \sigma) , \tag{4}$$

where $\delta_\sigma(x' - x_0)$ is now a function of the tangential component of $(x' - x_0)$ only, and $u(\sigma', \sigma)$ is a step function which is equal to one for σ' later than σ or coincident with σ, and is zero for σ' earlier than σ. It must be emphasized that (4) does *not* represent the variation induced in Π^β at point x' by the variation (2) on σ, which has to be derived from the modified equations of motion too, but represents simply the discontinuous change of Π^β on σ from Π^β to $\Pi^\beta + \varepsilon^\beta \delta_\sigma(x - x_0)$ [4]. The equations of motion become

$$\frac{\partial \mathcal{L}}{\partial \Phi^\alpha} - \partial_\mu \Pi^\alpha_\mu = \varepsilon^\beta \delta_{\alpha\beta} \delta^4(x' - x_0) . \tag{5}$$

These are the equations obtained by PEIERLS by adding a term $\lambda\Phi^\beta(x_0)$ to the total action, when λ is identified with our ε^β. If σ' is earlier than σ it is easy to see that the right hand side of (5) changes of sign.

The solutions of the modified equations to the first order in ε^β are

$$\Phi'^\alpha(x') = \Phi^\alpha(x') + \delta_{II}\Phi^\alpha(x') = \tag{6}$$

$$= \Phi^\alpha(x') + \varepsilon^\beta \left(D^{\Phi^\alpha(x')}_{\Phi^\beta(x_0)} - C^{\Phi^\alpha(x')}_{\Phi^\beta(x_0)}\right) . \qquad \begin{cases} D^\beta_\alpha \equiv 0 & \text{for } x' \text{ earlier than } x_0 \\ C^\beta_\alpha \equiv 0 & \text{for } x' \text{ later than } x_0 . \end{cases}$$

[3] It is possible to show that also the constraint variables Π^β, which are identically zero, can be given arbitrary variations (4) obtaining consistent results, and thus we need not distinguish between canonical and constraint variables.

[4] To illustrate this point we examine a simple example of particle dynamics. If the equation is $\ddot{p} + q = 0$ with $p = \dot{q}$ the solution is $q = a \exp[it] + b \exp[-it]$. Varying $p(0) = i(a - b)$ of the quantity $\delta p = \varepsilon$ the modified solution becomes $q' = q + i\varepsilon/2[\exp(-it) - \exp(it)]$. Alternatively we introduce in the equation of motion the variation $\delta p = \varepsilon u(t', t)$ obtaining the modified equation $\ddot{q}' + q' = \varepsilon\delta(t' - t)$ whose solution may be written $q' = q + \varepsilon D$ with

$$D = \frac{1}{2\pi} \int_{-\infty}^{+\infty} \frac{1}{1 - k^2} \exp[ikt] \mathrm{d}k .$$

Evaluating D from the residues at the poles $k = \pm 1$ (the contour of integration for $t > 0$ being shifted below the real axes at the poles and completed with a semicircle in the upper half of the complex k plane) one gets the preceding result. All this is a very well known application of the properties of Green's functions.

One gets from (1) (3) (4) (6)

$$[\Phi^\beta(x_0),\ \Phi^a(x_1)]_\pm = i(D^{\Phi^a}_{\Phi^\beta} - \mathcal{A}^{\Phi^a}_{\Phi^\beta}) , \tag{7}$$

where the plus or minus sign holds according to the commutation properties of ε^β previously discussed. For the commutator bracket one gets

$$D^{\Phi^a}_{\Phi^\beta} = \mathcal{A}^{\Phi^\beta}_{\Phi^a} . \tag{8}$$

For a general function of the field variables G one obtains

$$[\Phi^\beta(x_0),\ G(x_1)] = i(D^G_{\Phi^\beta} - \mathcal{A}^G_{\Phi^\beta}) , \tag{9}$$

where $D^G_{\Phi\beta}$ and $\mathcal{A}^G_{\Phi^\beta}$ are easily deduced by introducing in G the expression of Φ'^a given by (6).

Peierls has defined the function $D^{\Phi\beta}_G$ and $\mathcal{A}^{\Phi\beta}_G$ by means of the solutions

$$\Phi'^\beta(x_0) = \Phi^\beta(x_0) + \delta_G\Phi^\beta(x_0) = \tag{10}$$

$$= \Phi^\beta(x_0) + \varepsilon\,(D^{\Phi^\beta(x_0)}_{G(x_1)} - \mathcal{A}^{\Phi^\beta(x_0)}_{G(x_1)}) \qquad \begin{cases} D^\beta_G = 0 & \text{for } x_0 \text{ earlier than } x_1 \\ \mathcal{A}^\beta_G = 0 & \text{for } x_0 \text{ later than } x_1 , \end{cases}$$

of the modified equations of motion

$$\frac{\partial \mathcal{L}}{\partial \Phi} - \partial_\mu \frac{\partial \mathcal{L}}{\partial \Phi^a_\mu} = \varepsilon \left\{ \frac{\partial G}{\partial \Phi^a}\,\delta^4(x - x_1) - \partial_\mu \left(\frac{\partial G}{\partial \Phi^a_\mu}\,\delta(x - x_1) \right) \right\}, \tag{11}$$

obtained by adding the term $\varepsilon G(x_1)$ to the total action. He finds that in quantum theory the relation

$$D^{\Phi\beta}_G = \mathcal{A}^G_{\Phi\beta}, \tag{12}$$

which might have been expected to hold as a generalization of (8) is not generally valid. The reason is shown in the following.

If G is a function of the Φ^a's and of their tangential derivatives $\Phi^a_{\mu t}$'s, it commutes with the Φ^a's on the same surface and we can put

$$\Phi^{*b} = G\ ; \qquad \Phi^{*a} = \Phi^a \qquad (a \neq b) \tag{13}$$

being the new variables a complete set on σ' with the same eigenvectors of the set Φ^a. It is easy to deduce that

$$\Pi^a(x_1) = \Pi^{*b}(x_1)\,\frac{\partial G(x_1)}{\partial \Phi^a(x_1)} - \partial_{\mu t}\left(\Pi^{*b}(x_1)\,\frac{\partial G(x_1)}{\partial \Phi^a_{\mu t}(x_1)} \right). \tag{14}$$

If now Π^{*b} is varied by an amount given by (4) and the corresponding $\delta\Pi^a$ (deduced by means of (14)) is introduced in the equations of motion, one gets modified equations of the form (11). Therefore we have, making use of the infinitesimal operator (1) with the new variables replacing the old ones,

$$[G(x_1),\ \Phi^\beta(x_0)] = i(D_G^{\Phi^\beta} - \Gamma_G^{\Phi^\beta}) \tag{15}$$

and (12) holds. From the preceding derivation it is seen that the condition that G can be made diagonal on σ' together with the Φ^a's is essential. If G is a function of the normal derivatives of the Φ^a's this is not possible, and, instead of the point transformation (13) one must find a unitary transformation such that

$$\Phi^{*b} = U\Phi^b U^{-1} = G\,. \tag{16}$$

The relation (14) will no more be valid and, in general, both Π^a and Φ^a will be functions of Π^{*b}. The variation $\delta\Pi^{*b}$ will originate a change both in Π^a and Φ^a and these variations will have to be introduced in the Lagrangian equations. The modified equations will in general be different from (11) and equality (12) will no longer be satisfied.

I am indebted to Prof. PEIERLS for a very illuminating discussion, and to the British Council for the award of a scholarship.

IL NUOVO CIMENTO Vol. IX, N. 10 1 Ottobre 1952

Meson Production with Latitude Cut-Off.

Ch. Terreaux

Seminar für theoretische Physik, University of Zürich

(ricevuto il 3 Settembre 1952)

In a recent paper Cortini, Manfredini and Segrè [1] have measured the frequency of penetrating showers produced by the primary cosmic radiation with the latitude cut-off of Milan ($\sim$ 3 GeV). Comparing their results with the plural theory the authors concluded that the latter cannot agree with the experiments as the theory gave «too many small showers». The «note added in proof» by the authors (following a private letter by Prof. Heitler addressed to Prof. Amaldi) prompts me to give fuller details of the theoretical calculations when a latitude cut-off is taken into account.

The obvious reason for the discrepancy between theory and experiment alleged by the authors is that they have compared their results with calculations valid for a pure power law spectrum without cut-off at low energies as it exists more or less at mountain heights, (all the curves published by Heitler and Jánossy [2] [3] and by myself [4] refer to this case), whereas in their comparison with the theory of multiple production a cut-off was taken into account. I have extended the calculations of the frequency of penetrating showers when the incident spectrum follows a power law with a latitude cut-off at E_φ. The model and the basic assumptions used are the same as in [4]. The following observations regarding this model should be made:

(i) The total cross section Φ for meson production in a nucleon-nucleon collision is assumed to be independent of the primary energy. This is meant, of course, to include also the production of heavier mesons at high energies. Nevertheless the assumption is doubtful. It may well be that the total cross section decreases at higher energies. If, therefore, the theory gives *too many* large showers, this is no contradiction to the idea of plural production but can easily be remedied by assuming a decreasing cross section, whereas, if the number of large showers were too small, this would indicate a failure of the plural theory. A decrease of the cross section Φ for very large showers seems, indeed, to be indicated by fig. 1.

(ii) At low energies, of order Mc^2, the cross section is known to decrease rapidly. The situation is idealized by assuming that meson production vanishes

[1] G. Cortini, A. Manfredini, G. Segrè: *Nuovo Cimento*, **9**, 659 (1952).

[2] W. Heitler and L. Jánossy: *Proc. Phys. Soc.*, A **62**, 669 (1949).

[3] W. Heitler and Jánossy: *Helv. Phys. Acta*, **23**, 417 (1950).

[4] C. Terreaux: *Helv. Phys. Acta*, **24**, 551 (1951).

for $E < E_c$, say, and that Φ is constant for $E > E_c$. E_c has been determined in (4) from measurements of showers due

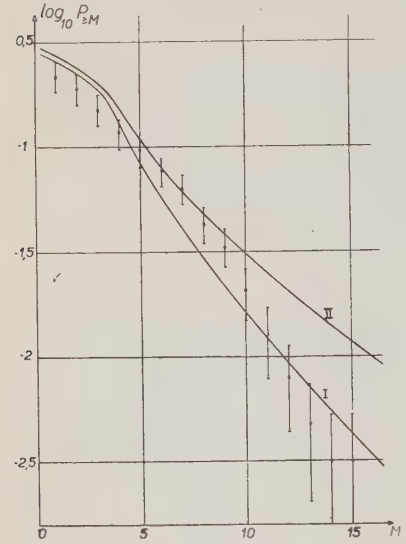

Fig. 1. – Number of penetrating showers containing at least M charged particles (20 % of which are deemed protons, 80 % mesons) produced by a primary spectrum with latitude cut-off at about 3 Gev. Exp. points of ref. (1) (photographic plates) and theoretical curves.

to a single primary energy E and it was found that $E_c = 1$–1.5 GeV. The results obtained below depend on E_φ/E_c only.

(iii) It has been explained in (3) and (4) that for the cascade process inside the nucleus, when secondary mesons occur, the close packing of the nucleons is an essential feature, and that this cascade differs considerably from the well known scheme of electron cascades. If a *fast* primary has produced a recoil nucleon, the primary and secondary both form angles so small that in the second collision the *same* nucleon (which is situated very close to the point of the first collision) is hit by the primary and recoil nucleons simultaneously. This gives rise to 2 mesons but only one further recoil nucleon. Consequently, as has been shown already in (3) and (4), and contrary to statements made by the authors of (1), the number of fast nucleons in a large shower is much smaller than the number of mesons (about 10-20%). This model is quite different from that used in the calculations of the authors of (1) and gives quite different results.

The following constants occur in the calculation (in addition to those mentioned):

σE = average energy loss of primary in a single nucleon-nucleon collision;

αE = average energy transferred to the recoil nucleon;

$\gamma = 1.1$ = potency of the primary spectrum above E_φ.

In (5) a relation between Φ and σ has been established from the known ratio of absorption (λ_a) to interaction (λ_i) mean free paths. Putting $\lambda_a/\lambda_i = 1.65$ (as found in (1) (6)) one obtains:

$$(1) \qquad Q = \Phi[1 - (1 - \sigma)^\gamma] = 1.3.$$

Since in (1) no secondary nucleons were taken into account, the numerical value of (1) is probably slightly smaller.

A variety of frequency distribution curves have been calculated with various values of Φ, α. σ, E_φ/E_c retaining, however, (1) (or a slightly smaller value), $\Phi \leqslant \pi(\hbar/\mu c)^2$ and $E_\varphi/E_c \sim$ 2,5-3.

In fig. 1 two curves are shown together with the experimental results of (1). The curves refer to the following parameters:

	Φ (in $(\hbar/\mu c)^2$)	σ	α	E_φ/E_c	Q
curve I	2,7	0,45	0,20-0,25	3	1,3
curve II	3,1	0,32	0,19	3	1,1

(5) W. HEITLER and L. JÁNOSSY: *Proc. Phys. Soc.*, A **62**, 374 (1949).
(6) H. MESSEL: *Phys. Rev.*, **83**, 26 (1951).

Both fulfil the above requirements and are therefore consistent with all other relevant experimental data extant. It is seen that I is in perfect agreement with the measurements within the statistical errors, but II can, according to what said above about a possible decrease of Φ, hardly be excluded. Not much weight should therefore be put on these particular values of the constants. Other choices of constants are also quite possible.

It is difficult to see how any argument against a predominantly plural meson production can be constructed from these measurements as the authors in [1] have tried to do. On the other hand, as has been emphasized in [2-4] the results do not preclude the occurrence of multiple processes in considerable numbers. However, the very strong dependence of the shower size on the atomic weight as found by SALANT, HORNBOSTEL, FISK and SMITH [7] and by WALKER, DULLER and SORRELS [8] certainly contradicts the idea that these showers are produced in a single collision.

I wish to thank the «Stiftung zur För derungdes Akademischen Nachwuchses» for financial assistance.

---

[7] E. O. SALANT, J. HORNBOSTEL, C. B. FISK and J. E. SMITH: *Phys. Rev.*, **79**, 184, (1950).

[8] W. D. WALKER, N. M. DULLER and J. D. SORRELS: *Phys. Rev.*, **86**, 865 (1952).

Pion Production and Charge Independence.

A. Gamba

Istituto di Fisica dell'Università - Torino

(ricevuto il 12 Settembre 1952)

The assumption of charge independence in reactions involving nucleons and pions is equivalent to assigning an isotopic spin 1/2 to the nucleon and an isotopic spin 1 to the pion, together with the assumption that the total isotopic spin T is a constant of the motion (1). This is a very satisfying feature of the theory, since a convenient formalism is provided to simplify the calculations. With this method Messiah (2) and Luttinger (3) have independently derived the cross sections for the production of a single pion in the reaction $p + d$.

It seems worth while, to investigate the relative cross sections for the production of two or three pions in a single nucleon-nucleon collision. The results of these calculations might provide further tests of the charge independence hypothesis, by comparison with experiment, when more powerfull accelerating machines will be available. There may be some interest in these calculations also in another connection, as was pointed out to me by prof. Wataghin (4). If ζ and τ mesons are composite particles, build up with two and three pions respectively, when these particles will be artificially produced, we may possibly deduce their isotopic spin state.

For completeness we give also the well known results for a single pion production. One can easily verify in particular the general theorem of Watson (reference (1)) that in a nucleon-nucleon collision the number of charged pions produced is twice the number of neutral ones at any order of multiplicity.

1 pion production.

There are three possible isotopic spin states, which are completely characterized by the total isotopic spin T (of the two nucleons plus the pion) and T_N (total isotopic spin of the two nucleons only). The three states are ($T = 0$, $T_N = 1$);

(1) W. Heitler: *Proc. Roy. Irish Acad.*, **51**, 33 (1946); K. M. Watson and K. K. Brueckner: *Phys. Rev.*, **83**, 1 (1951); K. M. Watson: *Phys. Rev.*, **85**, 852 (1952).
(2) A. M. L. Messiah: *Phys. Rev.*, **86**, 430 (1952).
(3) J. M. Luttinger: *Phys. Rev.*, **86**, 571 (1952).
(4) G. Wataghin: private communication.

($T = 1$, $T_N = 0$); ($T = 1$, $T_N = 1$). Let A, B, C be the relative contributions of these states to each reaction. The cross sections are then as follows:

$$\sigma(p + p \to p + p + \pi^0) = \sigma(n + n \to n + n + \pi^0) = \frac{1}{2} C ,$$

$$\sigma(p + p \to p + n + \pi^+) = \sigma(n + n \to p + n + \pi^-) = B + \frac{1}{2} C ,$$

$$\sigma(p + n \to p + p + \pi^-) = \sigma(p + n \to n + n + \pi^+) = \frac{1}{3} A + \frac{1}{2} C ,$$

$$\sigma(p + n \to p + n + \pi^0) = \frac{1}{3} A + B .$$

2 pion production.

The possible states are characterized by the total isotopic spin T (of the two nucleons plus the two pions), by T_N (total isotopic spin of the two nucleons) and T_π total isotopic spin of the two pions). We have six states ($T = 0$, $T_N = 0$, $T_\pi = 0$); ($T = 0$, $T_N = 1$, $T_\pi = 1$); ($T = 1$, $T_N = 0$, $T_\pi = 1$); ($T = 1$, $T_N = 1$, $T_\pi = 0$); ($T = 1$, $T_N = 1$, $T_\pi = 1$); ($T = 1$, $T_N = 1$, $T_\pi = 2$), whose relative contributions are indicated with A, B, C, D, E, F respectively. Then we have for the cross sections:

$$\sigma(p + p \to p + p + \pi^+ + \pi^-) = \sigma(n + n \to n + n + \pi^+ + \pi^-) = \frac{2}{3} D + \frac{1}{2} E ,$$

$$\sigma(p + p \to p + p + 2\pi^0) = \sigma(n + n \to n + n + 2\pi^0) = \frac{1}{3} D + \frac{1}{7} F ,$$

$$\sigma(p + p \to p + n + \pi^+ + \pi^0) = \sigma(n + n \to p + n + \pi^0 + \pi^-) = C + \frac{1}{2} E + \frac{2}{7} F ,$$

$$\sigma(p + p \to n + n + 2\pi^+) = \sigma(n + n \to p + p + 2\pi^-) = \frac{4}{7} F ,$$

$$\sigma(p + n \to p + p + \pi^0 + \pi^-) = \sigma(p + n \to n + n + \pi^+ + \pi^0) = \frac{1}{3} B + \frac{1}{2} E + \frac{2}{7} F .$$

$$\sigma(p + n \to p + n + \pi^+ + \pi^-) = \frac{2}{3} A + \frac{1}{3} B + C + \frac{2}{3} D + \frac{2}{7} F ,$$

$$\sigma(p + n \to p + n + 2\pi^0) = \frac{1}{3} A + \frac{1}{3} D + \frac{1}{7} F .$$

3 pion production.

Notations as in the preceding section. It must only be added that two states $T_\pi = 1$ exist, one of which belongs to the one dimensional symmetrical representation of the permutation group of the three pions ($T_\pi = 1$ (symm.)), and the other to the two dimensional representation of the same group ($T_\pi = 1$ (two dim.)). For $T_\pi = 0$ (antisymm.) and $T_\pi = 2$ (two dim.) a single state exists. The possible states are then nine ($T = 0$, $T_N = 0$, $T_\pi = 0$); ($T = 0$, $T_N = 1$, $T_\pi = 1$ (symm.)); ($T = 0$, $T_N = 1$, $T_\pi = 1$ (two dim.)); ($T = 1$, $T_N = 1$, $T_\pi = 0$); ($T = 1$, $T_N = 0$, $T_\pi = 1$ symm.)); ($T = 1$, $T_N = 0$, $T_\pi = 1$ (two dim.)); ($T = 1$, $T_N = 1$, $T_\pi = 1$ (symm.)); ($T = 1$, $T_N = 1$, $T_\pi = 1$ (two dim.)); ($T = 1$, $T_N = 1$, $T_\pi = 2$), whose contributions are A, B, C, D, E, F, G, H, K respectively. We obtain:

$$\sigma(p+p\to p+p+\pi^+ +\pi^0+\pi^-) = \sigma(n+n\to n+n+\pi^+ +\pi^0+\pi^-) = D+\frac{1}{5}G+\frac{1}{2}H+\frac{1}{4}K,$$

$$\sigma(p+p\to p+p+3\pi^0) \qquad = \sigma(n+n\to n+n+3\pi^0) \qquad = \frac{3}{10}G,$$

$$\sigma(p+p\to p+n+2\pi^+ +\pi^-) \quad = \sigma(n+n\to p+n+\pi^+ +2\pi^-) \quad = \frac{4}{5}E+\frac{1}{2}F+\frac{2}{5}G+\frac{1}{4}H+\frac{3}{8}K,$$

$$\sigma(p+p\to p+n+\pi^+ +2\pi^0) \quad = \sigma(n+n\to p+n+2\pi^0+\pi^-) \quad = \frac{1}{5}E+\frac{1}{2}F+\frac{1}{10}G+\frac{1}{4}H,$$

$$\sigma(p+p\to n+n+2\pi^+ +\pi^0) \quad = \sigma(n+n\to p+p+\pi^0+2\pi^-) \quad = \frac{3}{8}K,$$

$$\sigma(p+n\to p+p+\pi^+ +2\pi^-) \quad = \sigma(p+n\to n+n+2\pi^+ +\pi^-) \quad = \frac{4}{15}B+\frac{1}{6}C+\frac{2}{5}G+\frac{1}{4}H,$$

$$\sigma(p+n\to p+p+2\pi^0+\pi^-) \quad = \sigma(p+n\to n+n+\pi^+ +2\pi^0) \quad = \frac{1}{15}B+\frac{1}{6}C+\frac{1}{10}G+\frac{1}{4}H+\frac{3}{8}K,$$

$$\sigma(p+n\to p+n+\pi^+ +\pi^0+\pi^-) = A+\frac{2}{51}B+\frac{1}{3}C+D+\frac{2}{5}E+F+\frac{1}{4}K,$$

$$\sigma(p+n\to p+n+3\pi^0) \qquad = \frac{1}{5}B+\frac{3}{5}E.$$

LIBRI RICEVUTI E RECENSIONI

C. D. Rochester and I. G. Wilson – *Cloud chamber Photographs of the Cosmic Radiation.* – Un vol. di VII+128 pagg. con 129 figure. Pergamon Press. Ltd. – London 1952.

Lo studio delle particelle elementari costituisce l'argomento centrale delle ricerche sperimentali e teoriche della fisica dei nostri giorni.

Il rapido e incessante sviluppo delle nostre conoscenze sulle proprietà e sulla natura di queste particelle, che ha caratterizzato le ricerche di questi ultimi venti anni, è in buona parte dovuto all'impiego di due tecniche particolari: quella della camera ad espansione (detta comunemente camera di Wilson) e quella delle emulsioni fotografiche. È essenzialmente all'avvento di queste due tecniche che si deve fra l'altro la scoperta stessa della maggior parte delle particelle elementari finora conosciute.

È infatti grazie alla camera ad espansione che il fisico è arrivato alla scoperta dell'elettrone positivo, del neutrone, del mesone μ, del neutretto e recentemente di quel tipo di mesone pesante noto nella letteratura col nome di mesone V. D'altra parte la tecnica delle emulsioni fotografiche, in quelle che si sogliono chiamare le lastre nucleari, ha invece portato alla scoperta del mesone π e recentemente a quella della maggior parte dei cosiddetti mesoni pesanti, quali il mesone K, il mesone τ, il mesone Z.

G. D. Rochester e I. G. Wilson dell'Istituto di Fisica della Università di Manchester, due specialisti di fama mondiale nell'impiego della tecnica della camera ad espansione, hanno raccolto in un pregevole ed elegante atlante il fior fiore del materiale ottenuto con detta macchina nei vari laboratori del mondo specializzati in questo campo di ricerche.

Le 129 fotografie, contenute nell'atlante, sono raggruppate in cinque sezioni e sono illustrate da didascalie talvolta ampie le quali fanno sì che l'atlante possa servire come guida a chi voglia rendersi conto delle possibilità di questa tecnica meravigliosa per le ricerche fisiche e come introduzione allo studio delle particelle elementari per il fisico non specializzato.

Nella prima sezione sono studiate le caratteristiche delle tracce in dipendenza del modo di operare e delle condizioni sperimentali. Nella seconda è presentata una raccolta di tracce elettroniche e di sciami dovuti al ben noto processo della cascata elettromagnetica. La terza sezione è dedicata al mesone μ e al suo processo di disintegrazione. La quarta alle disintegrazioni nucleari e allo studio delle particelle che in queste si producono. L'ultima sezione costituisce la documentazione dell'esistenza delle particelle V.

La bellezza delle fotografie, nitidamente riprodotte, è sempre tale da suscitare l'ammirazione pure nel profano e da invitare ad un meditato esame anche il fisico non specializzato in questo attraente campo di ricerche.

Infine non è senza soddisfazione che il lettore italiano, scorrendo questa raccolta di tutto ciò che di meglio è stato ottenuto colla camera ad espansione, constaterà come la fisica del nostro Paese non sia affatto assente ma anzi sia degnamente rappresentata da quattro splendide fotografie eseguite da valenti ricercatori (Lovati, Mura, Salvini e Tagliaferri) dell'Istituto di Fisica dell'Università di Milano.

P. Caldirola

On the energy range relation for fast Muons in Rock.

M. MANDÒ and L. RONCHI jr.

Il Nuovo Cimento, **9**, 517 (1952).

Addendum. – Prof. COCCONI informs us that the results quoted in the footnotes ([26]) and ([33]) of our paper as « COCCONI and others » should have been quotes as « BARRET, BOLLINGER, COCCONI, EISENBERG and GREISEN: *Rev. of Mod. Phys.*, in the press ». We also beg the reader to refer to this paper for the final conclusions of the above mentioned authors, whose preliminary results were only known by us at the time of writing.

Direttore responsabile: G. POLVANI Tipografia Compositori - Bologna

Questo fascicolo è stato licenziato dai torchi il 23-IX-1951